Alma Mater Studiorum – Università di Bologna

DOTTORATO DI RICERCA IN

Scienze della Terra

Ciclo XXIV

Settore Concorsuale di afferenza: 04/A2

Settore Scientifico disciplinare: GEO/03 GEOLOGIA STRUTTURALE

TITOLO TESI

Characterization of fold-related fractures in the carbonate rocks of the *Cingoli* anticline, northern Apennines, Italy

Presentata da: **Dott. Lorenzo PETRACCHINI**

Coordinatore Dottorato

Prof. Roberto Barbieri

Relatore

Dott. Marco Antonellini

Co-Relatori

Dott.. Davide Scrocca
Dott. Andrea Billi

Esame finale anno 2013

‘*Life is short and the earth is complex’*

Abstract

Thrust fault-related folds in carbonate rocks are characterized by deformation accommodated by different structures, such as joints, faults, pressure solution seams, and deformation bands. Defining the development of fracture systems related to the folding process is significant both for theoretical and practical purposes. Fracture systems are useful constrains in order to understand the kinematical evolution of the fold. Furthermore, understanding the relationships between folding and fracturing provides a noteworthy contribution for reconstructing the geodynamic and the structural evolution of the studied area. Moreover, as fold-related fractures influence fluid flow through rocks, fracture systems are relevant for energy production (geothermal studies, methane and CO_2 , storage and hydrocarbon exploration), environmental and social issues (pollutant distribution, aquifer characterization).

The PhD project shows results of a study carried out in a multilayer carbonate anticline characterized by different mechanical properties. The aim of this study is to understand the factors which influence the fracture formation and to define their temporal sequence during the folding process.

The studied are is located in the Cingoli anticline (Northern Apennines), which is characterized by a pelagic multilayer characterized by sequences with different mechanical stratigraphies. A multi-scale analysis has been made in several outcrops located in different structural positions.

This project shows that the conceptual sketches proposed in literature and the strain distribution models outline well the geometrical orientation of most of the set of fractures observed in the Cingoli anticline. On the other hand, the present work suggests the relevance of the mechanical stratigraphy in particular controlling the type of fractures formed (e.g. pressure solution seams, joints or shear fractures) and their subsequent evolution.

Through a multi-scale analysis, and on the basis of the temporal relationship between fracture sets and their orientation respect layering, I also suggest a conceptual model for fracture systems formation.

Riassunto

Le anticlinali carbonatiche presentano un'intensa fratturazione indotta dalla deformazione durante il piegamento. Caratterizzare e comprendere lo sviluppo dei sistemi di fratture collegati al processo plicativo risulta essere di notevole interesse sia da un punto di vista scientifico che applicativo. I sistemi di fratture forniscono un contributo fondamentale per la comprensione dell'evoluzione cinematica della pieghe, inoltre, la comprensione delle relazioni tra sistemi di fratture e pieghe può contribuire a definire l'evoluzione strutturale dell'area di studio. Da un punto di vista applicativo è ormai noto come i sistemi di fratture incidono enormemente sulla circolazione dei fluidi. Di conseguenza la loro definizione trova un'applicazione importante nel settore energetico (flussi geotermici, stoccaggio gas e CO_2, esplorazione petrolifera), ambientale (dispersione di inquinanti nel sottosuolo), e sociale (caratterizzazione degli acquiferi ecc.).

La tesi di Dottorato presenta uno studio sull'analisi e la caratterizzazione di sistemi di fratture in un'anticlinale carbonatica caratterizzata da un multistrato con diverse caratteristiche meccaniche. Il progetto di Dottorato si pone l'obiettivo di comprendere i fattori che maggiormente influenzano le proprietà dei sistemi di fratture e di definire la loro evoluzione nel tempo.

A tal fine è stata analizzata l'anticlinale di Cingoli (Appennino settentrionale) che espone una serie di interessanti affioramenti in calcari pelagici. Attraverso analisi a diverse scale di osservazione sono stati quindi caratterizzati i sistemi di fratture in affioramenti posizionati lungo tutta l'anticlinale e in diverse posizioni strutturali.

Nel lavoro è stato osservato e discusso come la posizione strutturale e soprattutto la stratigrafia meccanica influiscono sulla formazione dei sistemi di fratture. In particolare è stato osservato come i modelli proposti in letteratura sintetizzano e schematizzano bene l'assetto geometrico di alcune fratture osservate a Cingoli. In questo lavoro, però, si è evidenziato come la stratigrafia meccanica ha un ruolo decisivo soprattutto per quanto riguarda la tipologia meccanica di fratture.

Table of Content

1. General Introduction

1.1 Problem Definition and Aim of the Project

Fold-related fractures are significant structures affecting rock sequences during the folding process (e.g. Price, 1966; Stearns, 1964 and 1968; Price and Cosgrove, 1990; Nelson, 2001). Understanding those variables which control the fracture patterns has considerable implications both for academic studies and for applied purposes.

The fractures intensity, their orientations, and the type of structures formed (i.e. joints, faults, pressure solution seams, deformation bands) influence the fluid flow (e.g. Engelder and Scholz, 1981; Antonellini and Aydin, 1994; Caine et al., 1996; Sibson, 1996; Nelson, 2001; Aydin, 2000; La Pointe et al., 2002; Billi, 2005; Agosta et al., 2007 and 2009). In particular, the types of structures formed during folding produce different impact on the fluid flow: pressure solution seams (PSSs), if no changes in stress conditions occur after their formation, act as barriers; joints represent good conduits; faults may facilitate or inhibit the fluid flow according to the fault compartment (Caine et. al., 1996). Former works proposed models and schemes in order to identify and predict the orientation, the distribution and the density of fractures systems (e.g. Price, 1966; Stearns, 1964 and 1968; Friedman, 1969; Price and Cosgrove, 1990; Hudlestone et al, 1996; Fischer and Jackson, 1999). Many of these models are based on the indisputable observation that the fractures systems are related to the state of stress at the time of their formation. For this reason many works relate the fractures properties (in particular the orientation and density) to the mechanism and to the kinematics evolution through which the fold develops (e.g. Price, 1966; Stearns, 1964 and 1968; Friedman, 1969; Stearns and Friedman, 1972; Hudlestone et al, 1996; Couples et al., 1998; Fischer and Jackson, 1999). However, many works suggest that the mechanical stratigraphy, the properties of rocks and other local factors (e.g. environmental conditions, local stress perturbation etc.) are important variables which influence in particular the type of fractures formed (i.e. joints, PSSs, faults etc.) and their dimensions (e.g. Jaeger and Cook, 1979; Segall and Pollard, 1980; Marshak and Engelder, 1985; Corbett et al., 1987; Protzman and Mitra, 1990; Narr and Suppe, 1991; Antonellini and Aydin, 1994; Caputo, 1995; Gross, 1995; Fischer and Jackson, 1999; Mollema and Antonellini, 1999; Bai and Pollard, 2000; Chester, 2003; Di Naccio et al., 2005; Caputo, 2005; Antonellini et al., 2008; Aydin et al., 2010; Rustichelli et al., 2012).

Hence, as the mechanical stratigraphy and the properties of rocks influence the type of fractures and, as a consequence, the fluid flow, it is fundamental to clearly assess and predict

the relationships between fractures systems and mechanical properties of the rocks involved in the folding process.

Furthermore, it has been observed that connection and shearing of previous structures (e.g. joints, PSSs or deformation band) may lead to the formation of longer faults which play a primary role for fluid flow (Engelder and Marshak, 1985; Antonellini et al., 1994; Peacock and Sanderson, 1995; Willemse et al., 1997; Salvini et al., 1999; Billi et al., 2003; Graham et al. 2003; Tondi et al., 2006; Aydin et al., 2010; Agosta et al., 2009). Therefore, it is fundamental to better understand the architecture and growth mechanism of these conductive structures and to define their relationship with the folding process and the previously formed fractures systems .

The aim of this project is to analyse the influence that mechanical stratigraphy and rock properties exert on the fractures systems and, in particular, to evaluate the relationship between mechanical stratigraphy and the type of fractures formed in the folding process. Furthermore, detail fractures analysis at different scale of observation have been carried out in order to better understand the growth of through-going faults from former structures (e.g. PSSs). The aim is to offer a detailed structural analysis and coherent genetic model of structures that are potentially fluid-conductive fractures.

1.2 Layout of the thesis

This thesis shows results of a study carried out in the *Cingoli* anticline, northern Apennines. This thrust fault-related fold provides several sites to investigate relationships among fracturing, mechanical stratigraphy and folding process. Fractures systems characterization have been made in outcrops located in different structural positions (i.e. backlimb, hinge and forelimb) and characterized by different mechanical properties.

The thesis consists of three sections.

- **Geological setting and structural framework**: This section exposes the regional geological context of the studied area (northern Apennines), it describes the stratigraphy, the structural framework and the suggested tectonic evolution of the *Cingoli* anticline. The previous works concerning the *Cingoli* anticline are here reviewed.
- **Fold-related fractures: the role of mechanical stratigraphy and rock properties:** This section shows the main results of the fractures analysis carried out in different sites of the *Cingoli* anticline. A review of the previous works concerning fold-related fractures and the folding processes, and some theoretical aspects are reviewed. For each site the fractures systems have been analysed at different scales observations and presented through detailed mappings. Type of fractures (i.e. mode of fracture formation), attitude, orientation relative to bedding surfaces (high angle to bedding or low angle to bedding), mechanical confinement (stratabound or non-stratabound) and termination relationships represent the key data sets collected in the field. The results are finally analysed in term of mechanical stratigraphy differences among sites and of structural position. The results have been finally compared with schemes and model presented in previous work.

  This manuscript is currently in preparation for publications.
- **Fault development through fractured pelagic carbonates of the *Cingoli* anticline, Italy: possible analog for subsurface fluid-conductive fractures:** This section reports the results of analyses made on pelagic micrites cropping out in two sites located in the anticline backlimb. In this work it is suggested a conceptual model for fault nucleation and growth that envisions studied faults as late-stage structures, which formed by incorporating and connecting segments of bedding surfaces and early developed PSSs. The conceptual model is discussed in terms of fault and fracture permeability, highlighting the possible role exerted by the documented structures on subsurface fluid

flow. Note that some data collected and some figures have been already exposed in the previous chapter. This manuscript has been accepted for publication in *Journal of Structural Geology* and is currently *in press*.

REFERENCES

Agosta, F., Prasad, M., Aydin, A., 2007. Physical properties of carbonate fault rocks, Fucino basin (Central Italy): implications for fault seal in platform carbonates. Geofluids 7, 19-32.

Agosta, F., Alessandroni, M., Tondi, E., Aydin, A., 2009. Oblique-slip normal faulting along the northern edge of the Majella anticline: inferences on hydrocarbon migration and accumulation. Journal of Structural Geology 31, 690-774.

Antonellini, M., Aydin, A., 1994. Effect of faulting on fluid flow in porous sandstones: petrophysical properties. American Association of Petroleum Geologists Bulletin 78, 355-377.

Antonellini, M., Tondi, E., Agosta, F., Aydin, A., Cello, G., 2008. Failure modes in basin carbonates and their impact on fault development, Majella Mountain, central Italy. Marine and Petroleum Geology 25, 1074-1096.

Aydin, A., 2000. Fractures, faults, and hydrocarbon entrapment, migration and flow. Marine and Petroleum Geology 17, 797-814.

Aydin, A., Antonellini, M., Tondi, E., Agosta, F., 2010. Deformation along the leading edge of the Majella thrust sheet in central Italy. Journal of Structural Geology 32, 1291-1304.

Bai, T., Pollard, D.D., 2000. Fracture spacing in layered rocks: a new explanation based on the stress transition. Journal of Structural Geology 22, 43-57.

Billi, A., Salvini, F., Storti, F., 2003. The damage zone-fault core transition in carbonate rocks: implications for fault growth, structure, and permeability. Journal of Structural Geology 25, 1779-1794.

Billi, A., 2005. Attributes and influence on fluid flow of fractures in foreland carbonates of southern Italy. Journal of Structural Geology 27, 1630-1643.

Caine, J.S., Evans, J.P., Forster, C.B., 1996. Fault zone architecture and permeability structure. Geology 24, 1025-1028.

Caputo, R., 1995. Evolution of orthogonal sets of coeval extension joints. Terra Nova 7, 479-490.

Caputo, R., 2005. Stress variability and brittle tectonic structures. Earth-Science Reviews, 70, 103-127.

Chester, J.S., 2003. Mechanical stratigraphy and fault-fold interaction, Absaroka thrust sheet, Salt River Range, Wyoming. Journal of Structural Geology 25, 1171-1192.

Corbett, K., Friedman, M., Spang, J., 1987. Fracture development and mechanical stratigraphy of Austin Chalk, Texas. AAPG Bull. 71, 17-28.

Couples, G., D., Lewis, H., Tanner, P.W.G., 1998. Strain partitioning during flexural-slip folding. In: Coward M.P., Daltaban, T.S., Johnson, H. (eds) Structural Geology in reservoir characterization. Geological Society, London, Special Publications, 127, 149-165.

Di Naccio, D., Boncio, P., Cirilli, S., Casaglia, F., Morettini, E., Lavecchia G., Brozzetti, F., 2005. Role of mechanical stratigraphy on fracture development in carbonate reservoirs: insights from

outcropping shallow water carbonates in the Umbria-Marche Apenninens, Italy. Journal of Volc. and Geoth. Research.

Engelder, T., Scholz, C., 1981. Fluid flow along very smooth joints at effective pressure up to 200 megapascals. In: Carter, N.L. (Ed.), Mechanical Behaviour of Crustal Rock. AGU Geophysical Monograph Series 24, 147-152.

Engelder, T., Marshak, S., 1985. Disjunctive cleavage formed at shallow depths in sedimentary rocks. Journal of Structural Geology, 7, 327-342.

Fischer, M.P., Jackson, P.B., 1999. Stratigraphic controls on deformation patterns in fault-related folds: a detachment fold example from the Sierra Madre Oriental, northeast Mexico. Journal of Structural Geology 21, 613-633.

Friedman, M., 1969. Structural analysis of fractures in cores from the Saticoy Field, Ventura Co., California. AAPG Bullettin 53, 367-389.

Graham Wall, B.R., Antonellini, M., Aydin, A., 2003. Formation and growth of normal faults in carbonates within a compressive environment. Geology 31, 11-14.

Gross, M.R., 1995. Fracture partitioning-failure mode as a function of lithology in the Monterey Formation of coastal California. Geological Society of America Bullettin 10, 779-792.

Hudlestone, P.J., Treagus, S.H., Lan, L., 1996. Flexural flow folding: Does it occur in nature? Geology 24, 203-206.

Jaeger, J.C., Cook, N.G.W., 1979. Fundamentals of rock mechanics, 3rd edn. Chapmann and Hall, London, 593 pp.

La Pointe, P., Hermanson, J., Parney, R., Eiben, T., Dunleavy, M., Steele, K., Whitney, J., Eubanks, D., Straub, R., 2002. 3-D reservoirs and stochastic fracture network modelling for enhanced oil recovery, Circle Ridge Phosphoria/Tensleep Reservoir, Wind River Reservation, Arapho and Shoshone Tribes, Wyoming. DOE: DE-FG26-00BC15190.

Marshak, S., Engelder, T., 1985. Development of cleavage in limestones of a fold-thrust belt in eastern New York. Journal of Structural Geology 7, 345-359.

Mollema, P.N., Antonellini, M., 1999. Development of strike-slip faults in the dolomites of the Sella Group, northern Italy. Journal of Structural Geology 21, 271-292.

Narr, W., Suppe, J. 1991. Joint spacing in sedimentary rocks. Journal of Structural Geology 13, 1037-1048.

Nelson, R.A., 2001. Geologic Analysis of Naturally Fractured Reservoir, 2nd edition, Gulf Professional Publishing, Houston.

Peacock, D.C.P., Sanderson, D.J., 1995. Pull-apart, shear fractures, and pressure solution. Tectonophysics 241, 1-13.

Price, N.J. 1966. Fault and joint development in brittle and semi-brittle rocks. Pergamon, Oxford, 176 pp.

Price, N.J., Cosgrove, J.W., 1990. Analysis of geological structures. Cambridge University Press, Cambridge, 502 pp.

Protzman, G.M., Mitra, G., 1990. Strain fabric associated with the Meade thrust sheet: Implications for cross-section balancing. Journal of Structural Geology 12, 403–417.

Rustichelli, A., Tondi, E., Agosta, F., Cilona, A., Giorgioni, M., 2012. Development and distribution of bed-parallel compaction bands and pressure solution seams in carbonates (Bolognano Fm., Majella Mountain, Italy). Journal of Structural Geology 37, 181-199.

Salvini, F., Billi, A, Wise, D.U., 1999. Strike-slip fault-propagation cleavage in carbonate rocks: the Mattinata fault zone. Journal of Structural Geology 21, 1731-1749.

Segall, P., Pollard, D.D., 1980. The mechanics of discontinuous faults, Journal of Geophysical Research 85, 4337-4350.

Sibson, R.H., 1996. Structural permeability of fluid-driven fault-fractures meshes. Journal of Structural Geology 18, 1031-1042.

Stearns, D.W., 1964. Macrofracture patterns on Teton Anticline, N.W. Montana (Eos). Trans A.G.U., 45, 107

Stearns, D.W., 1968. Certain aspects of fractures in naturally deformed rocks. Rock mechanics seminar. R.E. Riecker, 97-118. Terr. Sci. Lab., Bedford, Mass.

Stearns, D.W., Friedman, M., 1972. Reservoirs in fractured rocks. AAPG Memoir 16, 82-100.

Tondi, E., Antonellini, M., Aydin, A., Marchegiani, L., Cello, G., 2006. The roles of deformation bands and pressure solution seams in fault development in carbonate grainstone of the Majella Mountain, Italy. Journal of Structural Geology 28, 376-391.

Willemse, E.J.M., Peacock, D.C.P., Aydin, A., 1997. Nucleation and growth of strike-slip faults in limestones from Somerset, U.K. Journal of Structural Geology 19, 1461-1477.

2. Geological Setting and Structural Framework

2.1 Introduction

The *Cingoli* anticline is located in the inner foothills of the northern Apennines fold-and-thrust-belt of the Marche region and it is part of the footwall of the main external thrust of the Apennine chain (i.e. the *Sibillini* thrust; Figs. 2.1 and 2.2a). This part of the Apennines developed with an eastward piggy-back thrusting sequence during Miocene-Pliocene time (e.g. Bally et al., 1986; Calamita and Deiana, 1986; Bosellini A., 2004). The studied anticline, in particular, has developed since late Messinian time, involving a Mesozoic-Cenozoic sedimentary sequence (Calamita et al., 1990; Menichetti, 1991; Deiana et al., 2002; Mazzoli et al., 2002; Fig. 2.2b and c) and it is formed by the characteristic litostratigraphy of the *Umbria-Marche* sedimentary sequence (e.g. Carloni, 1964; Calamita et al., 1990, 1999; Menichetti, 1991; Marchegiani et al., 1999; Deiana et al., 2002; Mazzoli et al., 2002; Fig. 2.2).

In these last decades many regional studies have been undertaken so as to define the stratigraphy and the geodynamic evolution of the central-northern Apennines. Since the 1980s, field data have been integrated both with seismic reflection profiles and well data in order to better analyze the structural evolution of the Apennines fold-and-thrust-belt (e.g. Centamore and Deiana, 1986; Bally et al., 1986; Barchi, 1991; Anelli et al., 1994; Barchi et al., 1998a and 1998b; Calamita et al., 1990, Scrocca et al., 2003). Besides being involved in those regional works, various authors analyze in detail the *Cingoli* anticline area (Carloni 1960 and 1964; Ciancetti and Nanni, 1989; Calamita et al., 1990; Menichetti, 1991; Marchegiani et al., 1999; Deiana et al., 2002; Mazzoli et al., 2002). This section exposes a synthesis of the previous works undertaken in the area of the *Cingoli* anticline in order to set the regional geological context (northern Apennines), to describe the stratigraphic sequence of the anticline and finally to illustrate the structural framework and the suggested tectonic evolution.

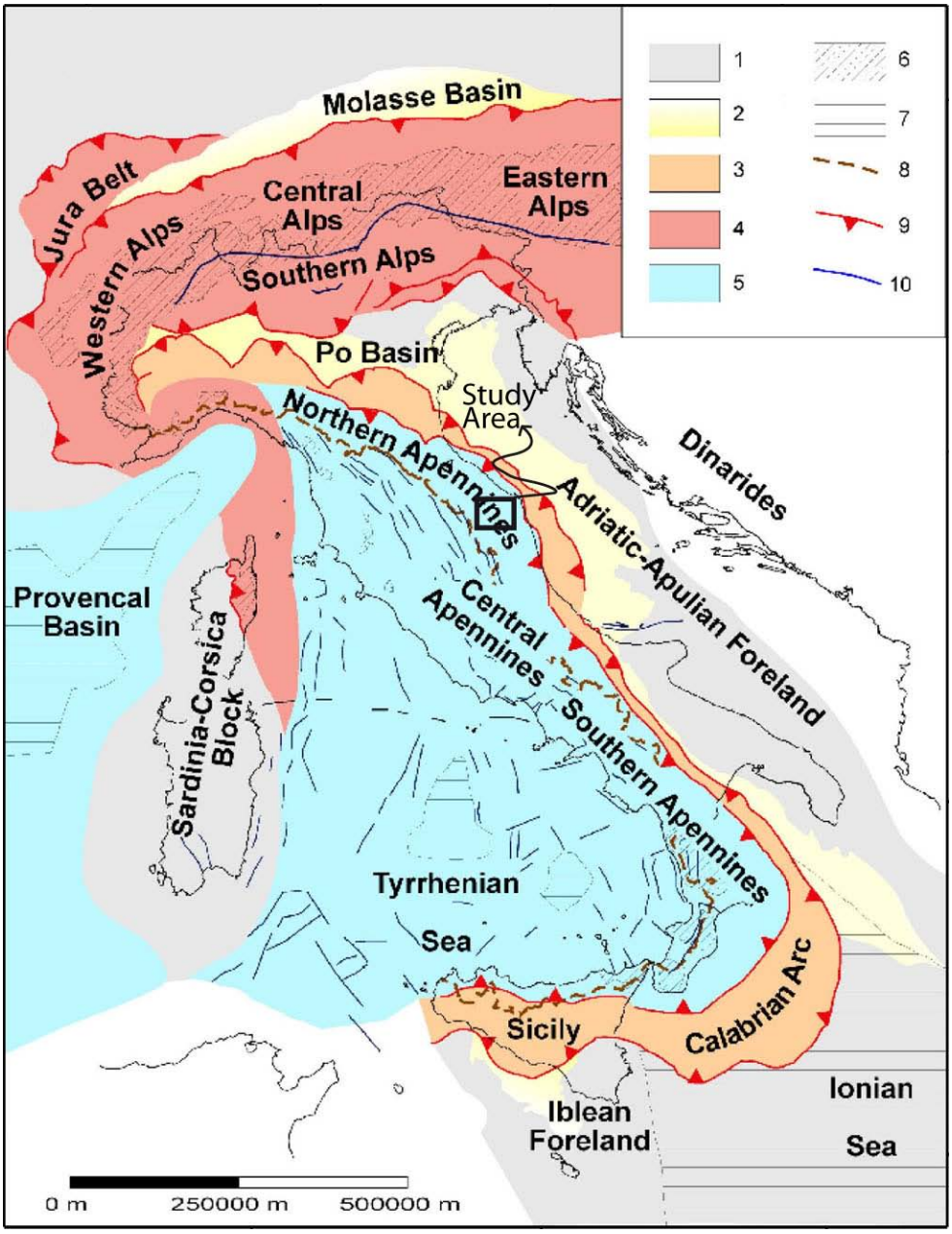

Fig. 2.1: Tectonic map of Italy (after Scrocca et alii, 2003).

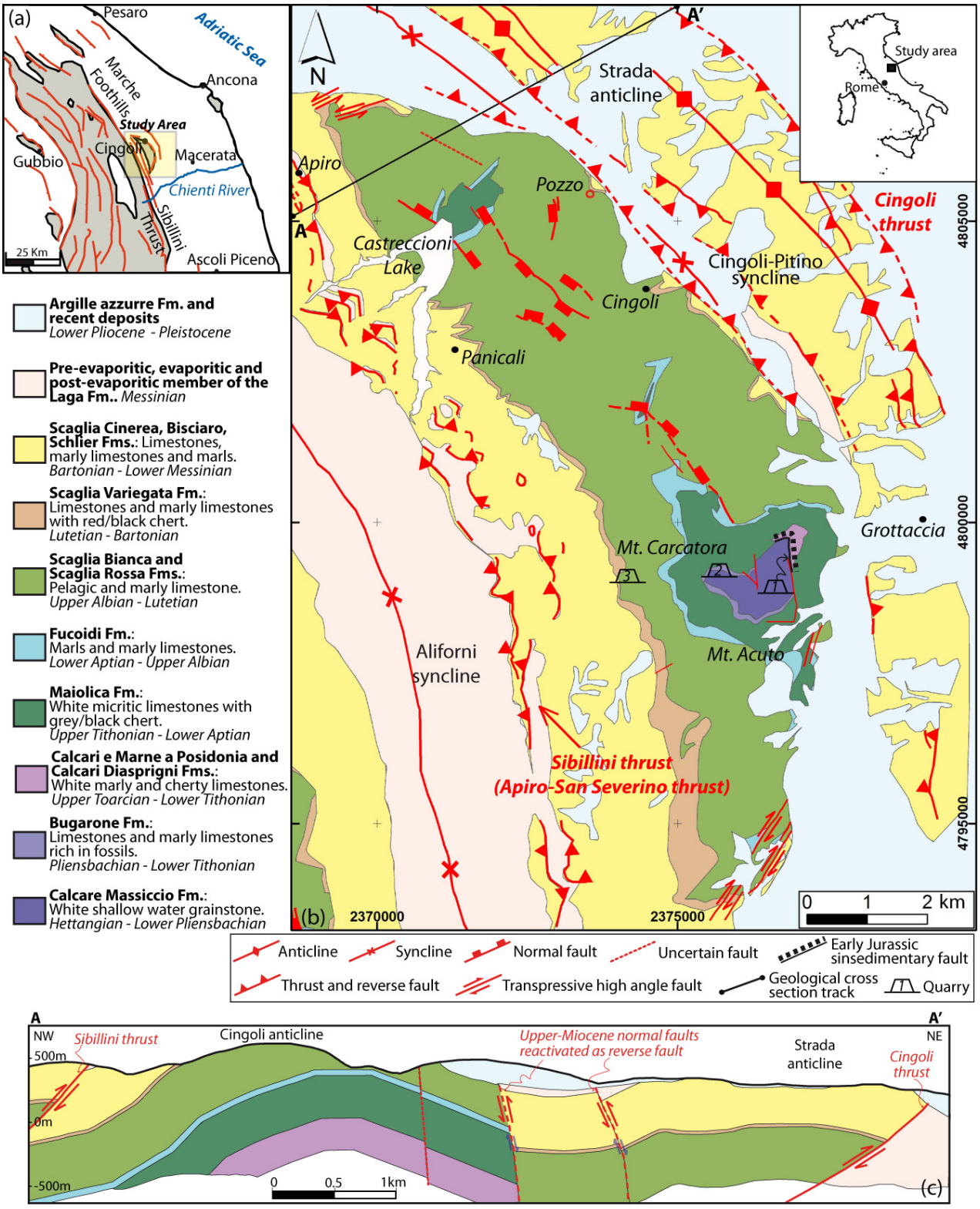

Fig. 2.2: (a) Location of the study area. The *Cingoli* anticline is in the foothills of the northern Apennines fold and thrust belt, *Umbria-Marche* area, Italy. (b) Simplified geo-structural map of the *Cingoli* anticline area (modified after Servizio Geologico d'Italia, 2003 - Coordinate System: Gauss Boaga, Est - Roma 1940). (c) Geological cross-section through the northern sector of the *Cingoli* anticline, based on confidential seismic reflection profile and previous studies (Mazzoli et al. 2002; Deiana et al., 2002; Servizio Geologico d'Italia, 2003).

2.2 Geology of the Northern Apennines

The *Umbria-Marche* domain is part of the northern Apennines fold-and-thrust-belt which is the result of the westward subduction of the Adria continental plate beneath the Corsica-Sardinia block (Doglioni et al., 1999; Mazzoli et al., 2002; Carminati et al., 2004; Fig. 2.1). This sector of the Italian peninsula represents an arched belt characterized by NE-verging folds and related thrusts (Menichetti, 1991; Calamita et al., 1999; Calamita et al., 2007). This area is the result of three important deformation phases: the Lower Jurassic continental rifting during the Tethys Ocean formation, the Apennine orogenic process of the Upper Miocene-Pliocene and the most recent Tyrrhenian extensional phases (Bally et al., 1986; Montanari et al., 1989; La Vecchia, 1982; Bosellini, 2004).

The sedimentary sequence of the northern Apennines is strongly influenced by its tectonic evolution. The basement is generally covered by conglomerates of the *Verrucano* Fm., followed by the Upper Triassic evaporitic sediments of the *Burano* Fm., up to 2000m in thickness, made of dolomites, anhydrite, and chalk. The *Burano* Fm. is an evidence of the ongoing subsidence and it is the base of the carbonate-dominated sequence of the Adria plate (La Vecchia,1982; Mazzoli et al., 2002; Marino and Santantonio, 2010). During Early Jurassic the area is dominated by wide regional carbonate platforms leading to the deposition of shallow-water carbonates of the *Calcare Massiccio* Fm. (Channel et al., 1977; La Vecchia, 1982; Calamita and Deiana, 1986; Di Francesco et al., 2010). The *Umbria-Marche* platform during the late Hettangian-Sinemurian time underwent an extensional regime and the region was dissected into faulted blocks with the formations of basins (graben) and structural highs, the Pelagic Carbonate Platform (PCP *sensu* Santantonio, 1993 and 1994; Fig. 2.3). The resulting sedimentation reflects the morphology of the area with the deposition of a “complete” pelagic sequence in the deeper basins and a condensed/reduced sedimentation on the PCPs (Colacicchi et al., 1970; Centamore et al., 1971; Santantonio, 1993 and 1994; Di Francesco et al., 2010; Fig. 2.3). This jagged paleo-topography, typical of many Jurassic sedimentary sequences of the western Mediterranean (Marchegiani, 1999 and literature therein), produces heteropies of facies and lateral variation of thickness up to the Lower Cretaceous when, with the deposition of the *Maiolica* Fm., the topography was finally levelled off. Deposition of fine-grained pelagic limestones, marly limestones and chert persists until the Eocene (i.e. *Scaglia* Fms.; Di Francesco et al., 2010) overlied by hemipelagic succession of Eocene-Miocene time (i.e. *Scaglia Cinerea*, *Bisciaro* and *Schlier* Fms). The hemipelagic succession are younger to east and they are interpreted as a

foreland ramp sequence (Marchegiani et al., 1999; Deiana et al., 2002). With the approaching orogenetic front since Oligocene time, the northern Apennines were involved into the foreland fold-and-thrust belt and synorogenic and post-orogenic siliciclastic turbidites sequences were deposited. These sequences filled piggy-back and foredeep basins and their relative temporal deposition shows a progressive migration of the orogenic process from west to east. The orogenic process reaches the *Umbria-Marche* region during the lower Miocene (Calamita et al., 1990; Menichetti, 1991; Calamita et al., 1994). Nowadays the foreland of the Apennine orogen is in the Adriatic sea where the compression is still active (e.g. La Vecchia, 1982; Montone et al., 1999; Scrocca, 2006). As far as the *Cingoli* anticline area is concerned, the actual tectonic regime is not so clear. The *Cingoli* fold is located between the foreland to the east, characterized by a compressional stress regime, and the *Umbria-Marche* domain to the west where there are evidence of an extensional tectonic (Montone et al, 1999, 2004 and 2012) According to Chiarabba et al. (2005), however, the *Cingoli* anticline is located in the area still characterized by a compressive stress regime. From the Pleistocene to the actual, in the inner sector of the northern Apennines, the Tyrrhenian back-arc extension acts on the former structures with a NE-SW extension direction, generating the well-known neo-tectonic activity of the area (La Vecchia, 1982; Calamita and Deiana, 1986; Menichetti, 1991; Montone et al., 1999; Chiarabba et al., 2005).

As far as the basement tectonics is concerned, during the last decades many studies have been carried out and various interpretation have been done. Magnetic maps of the *Umbria-Marche* sector, which do not show particular anomalies, suggest that the magnetic basement is not involved in the orogenic process (Arisi Rota and Fichera, 1985) and Bally et al. (1986) propose a basement gently dipping to the west with the *Burano* Fm. as a basal décollement localized at 5 km depth in the Adriatic Sea and dipping up to 12-14 km in the Umbria Region. Other works, on the contrary, suggest a basement involved in the Tertiary deformation, which seems to be confirmed by the seismic profiles interpretation of the CROP project (Ghisetti et al., 1993; Barchi et al., 1998b; Coward et al., 1999; Mazzoli et al., 2002; Fantoni and Franciosi, 2009).

Hence the northern Apennines and its *Umbria-Marche* sector represent the effects of a sequence of geological deformation phases. In particular, the structural and morphological framework with the characteristic NE verging fold-and-thrust belts is the consequence of the westward subduction of the Adria continental plate beneath the Corsica-Sardinia block with its sedimentary succession disharmonically deformed respect to the basement along the main

regional décollement (i.e., the *Burano* Fm.) and along other decoupling surfaces as the Messinian evaporites, the *Scaglia Cinerea* Fm., the *Marne a Fucoidi* Fm. and *Rosso Ammonitico* Fm. (Bally et al., 1986).

The above mentioned deformation events represent the main processes that affected the northern Apennines and the *Umbria-Marche* sectors during their geological history. In addition to these important deformation events, other tectonics events occurred in the area with a regional or even local impact on the stratigraphy, structural and evolutionary style. These secondary processes will be discussed in the following sections.

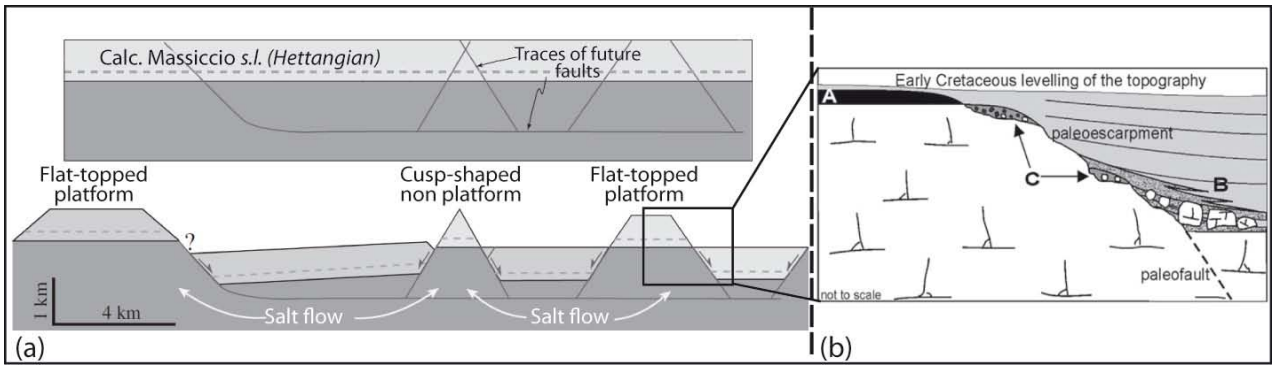

Fig. 2.3: (a) Sketch showing the structural evolution of the Umbria-Marche sector during the Lower Jurassic rifting (modified after Santantonio and Carminati, 2010). After the extension the region was dissected by normal faults with the formation of basin areas and structural highs, the latter characterized by different shape. The structural high of the *Cingoli* anticline shows characteristic of a flat-topped platform. (b) Model of carbonate sedimentation after the Jurassic rifting (after Marino et al., 2010). The structural high is characterized by a reduced pelagic succession (Bugarone Fm.; A), basin area is interested by a "complete" succession (B) and by a composite succession with condensed and silicoclastic sediments covered by pelagic carbonates of the "complete" succession (C).

2.3 Stratigraphy of the *Cingoli* Anticline

The lithostratigraphy of the *Cingoli* anticline and the surrounding area represents a typical example of the *Umbria-Marche* succession (Fig. 2.4).

Carloni (1960 and 1964) provides a first insight of the Meso-Cenozoic sedimentary succession outcropping in the study area as well as of the foredeep and recent deposits in the surrounding basinal area. In the last two decades, other authors published several works on the stratigraphy of the *Cingoli* anticline and they suggested a model for the structural evolution and the main deformation processes affecting the *Cingoli* anticline (Ciancetti and Nanni, 1989; Calamita et al., 1990; Menichetti, 1991; Calamita et al., 1999; Marchegiani et al., 1999; Deiana et al., 2002; Mazzoli et al., 2002). This section presents a brief review of these former works.

The Permian-Triassic portion of the *Umbria-Marche* succession (*Verrucano* and *Burano* Fms.) does not outcrop in the *Cingoli* anticline. The oldest exposed deposits are the massive early Liassic shallow water limestones of the *Calcare Massiccio* Fm. cropping out in the core of the *Cingoli* anticline and well-exposed in two active quarries (Fig. 2.2b). The *Calcare Massiccio* Fm. appears deeply fractured with clear evidence of karst phenomena, especially along N-S oriented fractures (Fig. 2.5). As the *Burano* Fm. is not outcropping, the *Calcare Massiccio* thickness is unknown. The maximum thickness outcropping is visible in one of the two quarries (Quarry 1 in Fig. 2.2 and Fig. 2.5) and is approximately 300 m. The mean thickness of the *Calcare Massiccio* reported in literature is generally of 800 m (Calamita and Deiana, 1986) but it can exceed 1 km (Santantonio and Carminati, 2010 and references therein). The *Calcare Massiccio* Fm. is followed by the deposition of pelagic sediments distinguished in “condensed” and “complete” sequences (Santantonio, 1993 and 1994 and references therein; Marchegiani et al., 1999). These sequences are a record of the early Jurassic extensional tectonics (rifting), which leads to the formation of a complex submarine topography with tectonically controlled basins and structural highs. In the *Umbria-Marche* region the contacts between the *Calcare Massiccio* Fm. and the younger pelagic “complete” sequence are mainly controlled by early Jurassic NNE and NW-striking normal faults (Marchegiani et al., 1999). This complex deposition environment is well shown also in the core of the *Cingoli* anticline and especially in one of the quarry where the paleo-Jurassic border of the structural high crops out (Quarry 1 in Fig. 2.2 and in Fig. 2.6). As a matter of fact the structural lineament visible in the quarry, at least its higher sector, would be better considered as a normal fault almost parallel to the paleo-escarpment surface but with an higher dip-angle. Indeed the limit between the shallow water sediments of

the *Calcare Massiccio* Fm. and the basinal units is often characterized by non-cohesive fault breccias and clay. Furthermore, the angle between the bedding of the *Calcare Massiccio* Fm. and this structural feature is too high to be considered as a paleo-escarpment (Figs. 2.5 and 2.6). Besides this structural analysis the quarry clearly shows the old paleo-topography with the "complete" succession in the basin pinching out against the structural high (the north-eastern part in Fig. 2.5), and the structural high of the *Calcare Massiccio* Fm. (the south-western part in Fig. 2.5) with the "condensed" sequence at the top of it and outcropping in a western quarry (quarry 2 in Fig. 2.2).

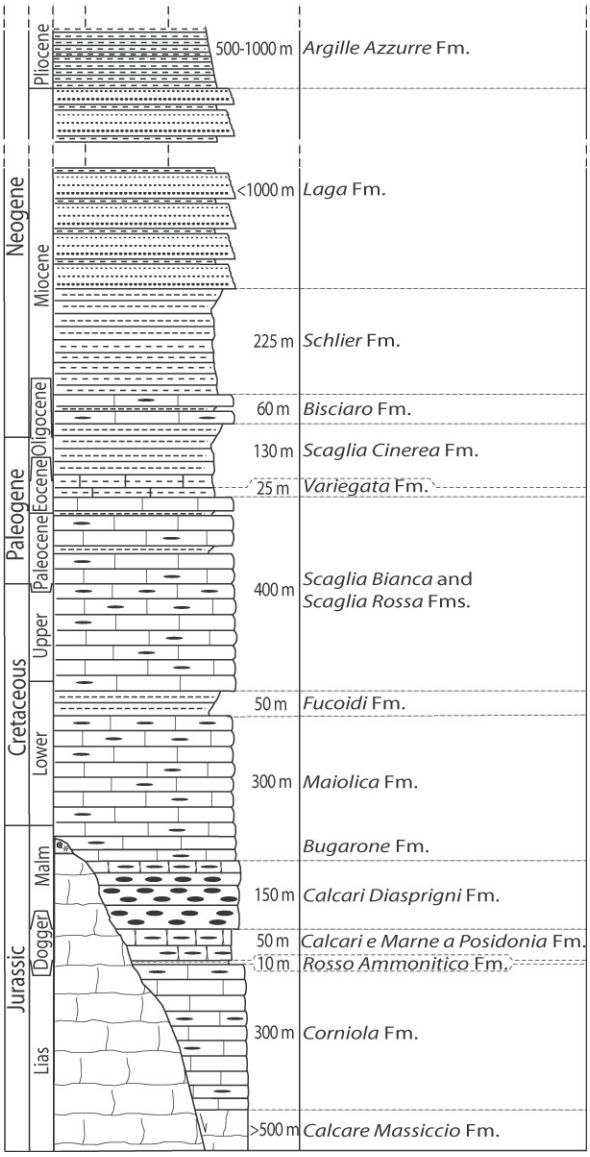

Fig. 2.4: Stratigraphic succession of the *Umbria-Marche* area (modified after Di Francesco et al., 2010). Thickness of the formations for the lower part of the sequence up to *Scaglia Cinerea* Fm. refers to measured sections in the *Cingoli* anticline area, whereas the thicknesses of the upper formations derive from literature data.

The “condensed” sedimentary sequence, which is developed over the early Jurassic structural highs, consists of grey stratified limestones, nodular limestones, and marls of the *Bugarone* Fm. (Lower Pliesbachian-Lower Tithonian; Santantonio, 1993; Santantonio et al., 1996). During the same time span, a pelagic sedimentary sequence was deposited in progressively deeper basins, consisting of grey biomicritic limestones of the *Corniola* Fm. (Lower Sinemurian-Lower Toarcian), limestones and red nodular marls of the *Rosso Ammonitico* Fm. (Toarcian), thinly-bedded limestones with cherts and marls of the *Calcari a Posidonia* Fm. (Toarcian p.p.-Lower Bajocian p.p.), and grey-greenish cherty limestones of the *Calcari Diasprigni* Fm. (Upper Bajocian-Lower Tithonian; Galluzzo and Santantonio, 2002). Marchegiani et al. (1999) recognize, nearby the edge of the intrabasinal high, a composite succession (*sensu* Centamore et al., 1971) with nodular limestones of the *Bugarone* Fm. overlain by pelagic limestone of the “complete” succession. This composite succession could suggest a gradual assimilation of the area within the basin (Marchegiani et al., 1999) or could represent patches of epi-escarpment deposits of the “condensed” succession subsequently on-lapped by sediments of the basinal units (Di Francesco et al., 2010; Fig. 2.3b). A rather homogeneous pelagic depositional environment characterized the Tithonian to early Messinian period. From the Tithonian to almost all of the Lower Cretaceous (till to the Lower Aptian), the micrites of the *Maiolica* Fm. were deposited in the area filling up the paleo-topography formed in the Lower Jurassic. After the *Maiolica* Fm., shales and marls pertaining to the *Marne a Fucoidi* Fm. (Lower Aptian-Upper Albian), and fine-grained pelagic limestones, marly limestones, and chert of the *Scaglia Bianca*, *Scaglia Rossa*, and *Scaglia Variegata* Fms. (late Albian till mid-Eocene) were deposited. Between Oligocene and early Messinian time, the area was characterized by the deposition of hemipelagic marly limestones pertaining to the *Scaglia Cinerea* Fm., *Bisciaro* Fm., and *Schlier* Fm., which are interpreted as a foreland ramp sequence deposited during the formation of the lithosphere flexure due to the incoming subduction process (Deiana et al., 2002; Mazzoli et al., 2002). The subsequent siliciclastic deposits fill the foredeep and thrust-top basins and are younger from west, in the *Aliforni* Basin, to the east, in the internal foothill basin on the eastside of the *Cingoli* structure (Fig. 2.2a). These Messinian turbidites show a different stratigraphy on both sides of the *Cingoli* anticline. In the *Aliforni* basin, a lightly cemented sandy unit with intercalations of marly clay, the *Apiro* Fm. of Carloni (1964), overlies the *Schlier* Fm. and could be equivalent to the pre-evaporitic *Laga* Fm. outcropping south of here (Ciancetti and Nanni, 1989; Deiana et al., 2002; Mazzoli et al., 2002). The middle Messinian *Gessoso-Solfifera* Fm. lies over this sandy unit and is followed by the

equivalent post-evaporitic member of the *Laga* Fm. represented here by the *San Donato* Fm., a pelitic and sandy unit, and by the Upper Messinian *Colombacci* Fm. On the other hand, in eastern side of the *Cingoli* anticline the pre-evaporitic member of the *Laga* Fm. is missing and the *Schlier* is directly covered by the *Gessoso-Solfifera* Fm. overlain by a peculiar and local facies of conglomerates and grit, the *Avenale* Fm. in Carloni (1964), heteropic with the *Colombacci* Fm. of the Upper Messinian. This latter unit is made of a variety of clasts, mainly black cherts, probably deriving from the *Maiolica* Fm. and *Scaglia* Fms. of the *Cingoli* anticline (Carloni, 1964; Calamita et al., 1990). The study area was finally affected by the main orogenic phase at the end of the deposition of the *Gessoso-Solfifera* Fm. (mid-Messinian time). The contractional deformation progressively propagated toward east activating new faults. Lastly, the early Pliocene *Argille Azzurre* Fm. (marine clays) overlapped the thrust front of the *Cingoli* anticline.

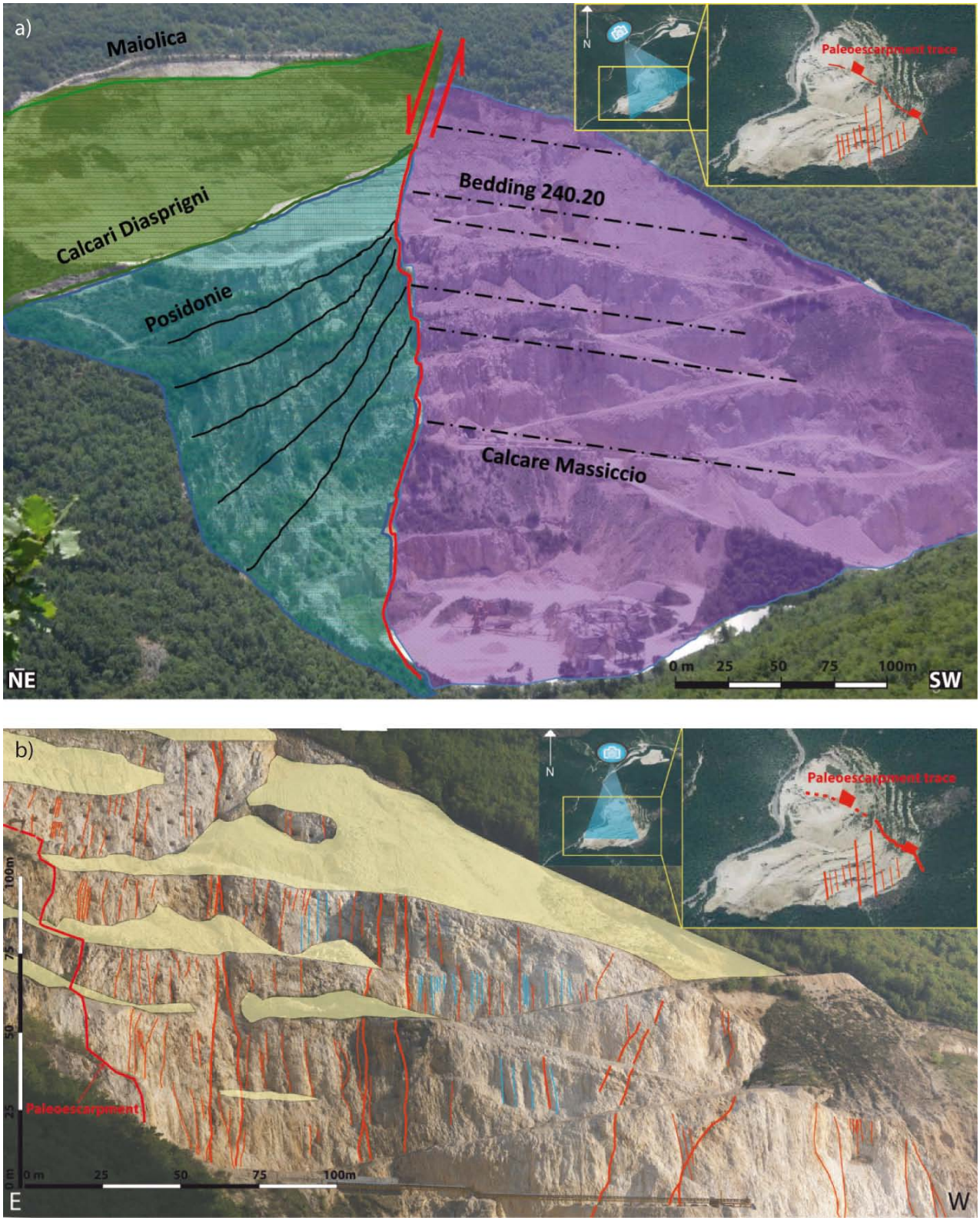

Fig. 2.5: Picture and related line drawing of Quarry 1 in the core of the *Cingoli* anticline. (a) The picture shows the pelagic "complete" sequence pinching out on the *Calcare Massiccio* Fm. along the reactivated paleo-escarpment (see text for more details). (b) Line drawing (in red) of the main fractures in the *Calcare Massiccio* side of the quarry, in light blue the traces left by the explosions.

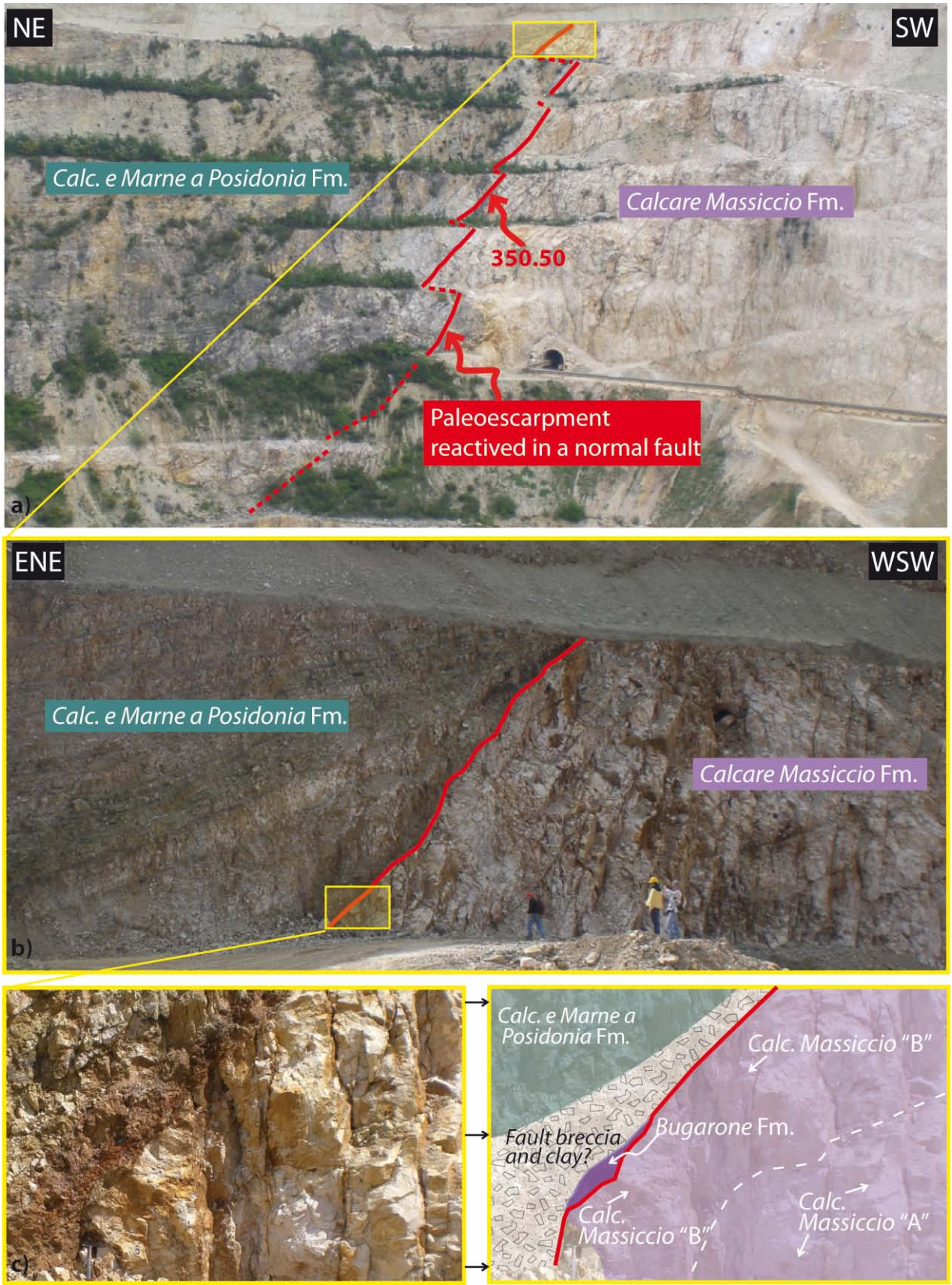

Fig. 2.6: Picture showing the paleo-escarpment of the structural high in Quarry 1. Breccias and clay present along the surface dividing the pelagic succession from the *Calcare Massiccio* Fm., suggest that the paleo-escarpment has been reactivated as a normal fault. *Calcare Massiccio* "A" is characterized by shallow water deposits riches in benthic fauna while *Calcare Massiccio* "B" represents the drowning succession (sensu Marino and Santantonio, 2010) with both benthic- and planktonic-fauna.

2.4 Structural Framework and Tectonic Evolution

The *Cingoli* anticline is a NE verging asymmetrical anticline with gently dipping limbs and a narrow flat hinge area (Fig. 2.2c). It is characterized by a NW-SE oriented fold axis curving to approximately N-S in the southern part of the fold. The anticline is confined by E-W-striking, left-lateral, transpressional faults, in the North (here called *Apiro* fault), and by NNE-SSW-striking right-lateral faults in the South (Fig. 2.2b).

The core of the anticline is made up by the Lower Jurassic paleo-escarpment cut by a younger normal fault almost parallel to the former fault direction. The Meso-Cenozoic succession is dislocated by several NW-SE oriented faults. These faults generally show a dip-slip shear with a total displacement from tens to hundred meters (Menichetti, 1991) and, since no facies or thickness variation in the sediments cut by the fault is observed (at least up to the Upper Eocene deposits), they can be considered as post-Eocene faults related to a break-up of the crest hinge during the folding process or to the extensional pre-thrusting Miocene activity that will be discussed further in this paragraph. Mesoscopic NW-SE extensional faults acting after the Jurassic rifting and during the so-called passive-margin phase of the *Umbria-Marche* have been detected by many authors and few of those structures have been recognized in the field (Ciancetti and Nanni, 1989; Montanari et al., 1989; Marchegiani et al.; 1999 among many others). This post-rifting tectonic activity is well-documented, by stratigraphic and structural data, also in other area of the central-northern Apennine indicating the persistence of an extensional regime even during the passive margin phase usually considered a stable stage (Marchegiani et al., 1999 and literature therein). The faults related to this deformation stage have generally three main trends: NE-SW, NW-SE and NNW-SSE. Marchegiani et al. (1999) have documented, in the central sector of the *Cingoli* anticline, a thickening of more than 150 m within the *Scaglia Rossa* Fm. and they suggest that this differential thickening is due to the reactivation of Jurassic faults. As suggested by Marchegiani et al. (1997 and 1999), the lateral thickness changes involving post-Lower-Jurassic-rifting sediments could be in part explained by differential compaction. In fact, subsidence curves of various stratigraphic sections in different area of the *Umbria-Marche* region show a relative sharp dropping of the basin area in the Upper Cretaceous compared to a more gradual drop of the structural highs (Marchegiani et al., 1999; Fig. 2.7). Thermal subsidence or differential compaction should have acted almost constantly during time both in the structural highs and basin areas. The sudden fall of the basin

areas during the Upper Cretaceous-Early Paleogene respect to the intra-basinal highs suggest that subsidence is of tectonic origin.

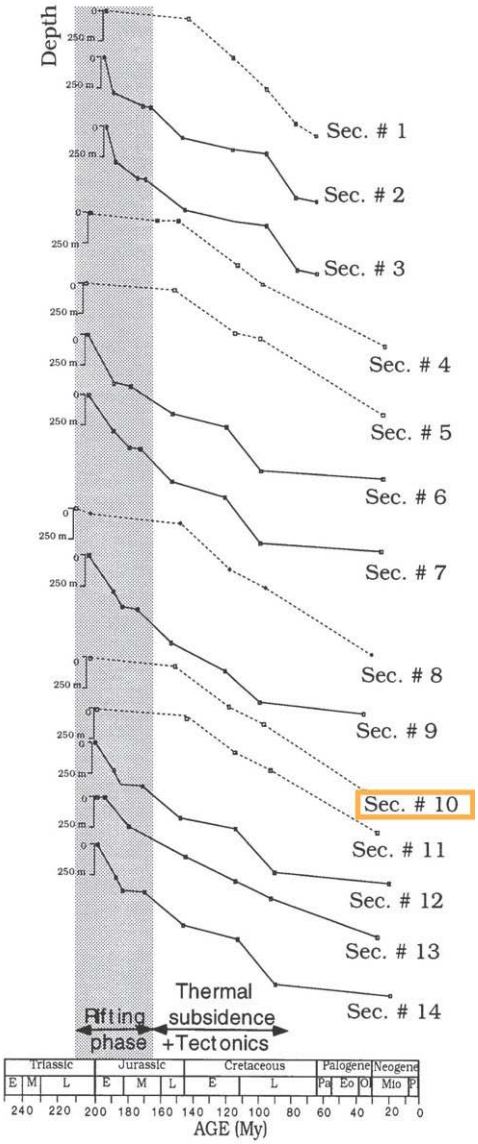

Fig. 2.7: Subsidence curves for different sections along the Umbria-Marche area (after Marchegiani et al., 1999). Solid lines represent curves characterizing "complete" successions whereas dashed lines structural highs. The solid lines present a sharp subsidence during the Cretaceous-early Paleogene in contrast with the smoother curves characterizing the structural highs. Section 10 represents the structural high of the Cingoli anticline.

In order to better analyse the post-rift tectonic evolution of the *Cingoli* anticline and to constrain the structural and sedimentary elements therein, it is useful to outline the main structures in the neighbourhood of the Meso-Cenozoic outcropping anticline. The main tectonic feature recognized to the west of the studied fold is the *Apiro-San Severino* thrust (Fig. 2.2b), which represents the northern sector of the *Sibillini* thrust (Calamita et al., 1990; Deiana et al., 2002; Mazzoli et al., 2002). The *Apiro-San Severino* thrust and its related splays are clearly shown by older-on-younger tectonic contacts between the *Schlier* Fm. and the pre-evaporitic

member of the *Laga* Fm. and the *Gessoso-Solfifera* Fm. The thrust, which carries on its top the *Aliforni* syncline, cored by Messinian deposits, has a NNW-SSE direction in the northern sector and, likewise the *Cingoli* anticline, it rotates to a N-S trend in the South. The thrust is buried in the North by Lower Pliocene deposits suggesting that the activity is antecedent to their deposition. The *San Donato* Fm. (Upper Messinian) within the *Aliforni* syncline shows growth strata suggesting that the initial compressive activity could have affected the area during the late Messinian, just after deposition of the *Gessoso-Solfifera* Fm. (Deiana et al., 2002). The eastern side of the *Cingoli* anticline is formed by a narrow syncline characterized by the *Argille Azzure* Fm. of the Lower Pliocene lying with an unconformable contact on the *Gessoso-Solfifera* Fm. and on the heteropic local unit of the *Colombacci* Fm. (i.e. *Avenale* Fm.). The stratigraphic contact between the *Avenale* Fm. and the *Sc. Cinerea* Fm. is a critical point for the structural evolution of the *Cingoli* anticline and, as discussed further in this paragraph, it may be due to a pre-thrusting tectonic activity. Going in an eastern direction, the *Strada* anticline crops out. It is characterized by the *Schlier* Fm. and shows a trend similar to the *Cingoli* anticline. At the front of the *Strada* anticline there is the easternmost thrust related to the *Cingoli* anticline and it is currently covered by Pliocene deposits. The *Schlier* Fm. of the *Strada* fold are cut by a series of thrust-related splays and the western contact with the Pliocene deposits and the unit of the *Laga* Fm. are generally of tectonic origin.

Many authors recognize a pre-thrusting normal faulting during the Upper Miocene in the *Umbria-Marche* Apennines (Mazzoli et al., 2002; Deiana et al., 2002 and references therein) and some authors have associated these normal faults with the flexure of the Adria plate foreland (see reference in Deiana et al., 2002). This activity and its sedimentary implications are critically analysed and discussed in former works (Mazzoli et al., 2002; Deiana et al., 2002 and references therein) and they are not discussed in this present work. However, it is relevant to highlight that this extensional tectonic activity occurs at the front of the *Sibillini* thrust and of the *Cingoli* anticline and it plays a crucial role in the deposition of the siliciclastic turbidites series. The structures related to this pre-thrusting tectonics show a direction almost similar to the fold axes and are characterized by steep planar surfaces. Stratigraphic and sedimentologic analysis lead to consider the onset of this extensional tectonic activity at a pre-Messinian time and its termination before the *Gessoso-Solfifera* Fm. sedimentation (Deiana et al., 2002). The unconformable contacts in the eastern side of the *Cingoli* anticline is probably the result of two normal faults related to the pre-thrusting extensional tectonics previously discussed and afterwards reactivated as back-thrusts (Deiana et al., 2002; Fig. 2.2c).

According to the structural framework discussed above, the evolution of the *Cingoli* anticline occurs through a series of tectonic events. The first tectonic event is related to the Jurassic rifting which dismembers the carbonate platform in structural high and basin areas. The subsequent sedimentation reflects this paleo-topography with the deposition of a "complete" pelagic sequence in the deeper basin and a condensed sedimentation on the structural highs. This complex paleo-topography is levelled off with the deposition of the *Maiolica* Fm. After the main-rift phase, the area undergoes a further extensional tectonic activity, acting in particular since the Upper Cretaceous up to the Paleogene and it leads to a thickness variation, in particular of the *Scaglia Rossa* Fm. An additional important extensional tectonic activity, interpreted as a result of the flexure of the foreland lithosphere, occurs presumably in the upper Miocene until the deposition of the *Gessoso-Solfifera* Fm. (Deiana et al., 2002). As suggested by the growth of strata in the *San Donato* Fm. within the *Aliforni* syncline and by the conglomerate facies overlying the evaporitic series in the eastern side of the *Cingoli* anticline, the area is finally affected by the main orogenic event at the end of the deposition of the *Gessosso-Solfifera* Fm. The foredeep sequences show an eastern propagation of the orogenic process until the early Pliocene when the *Argille Azzurre* Fm. overlies the thrust front of the *Cingoli* anticline.

REFERENCES

Anelli, L., Gorza, M., Pieri, M., Rota, M., 1994. Subsurface well data in the northern Apennines (Italy). Mem. Soc. Geol. 48, 461-471.

Arisi Rota, F., Fichera, R., 1985. Magnetic interpretation connected to "geo-magnetic provinces": The italian case history. Preprint 47th Meeting European Association of Exploration Geophysicists.

Bally, A.W., Burbi, L., Cooper, C., Ghelardoni, R., 1986. Balanced sections and seismic reflection profiles across the Central Apennines. Mem. Soc. Geol. It. 35, 257-310.

Barchi, M.R., 1991. Integration of a seismic profile with surface and subsurface geology in a cross-section through the Umbria-Marche Apennines. Boll. Soc. Geol. It. 110, 469-479.

Barchi, M.R. Minelli, G., Pialli, G., 1998a. The CROP 03 profile: a synthesis of results on deep structures of the northern Apennines. Mem. Soc. Geol. It. 52, 383-400.

Barchi, M.R., De Feyter, A., Magnani, M.B., Minelli, G., Pialli, G., Sotera, B.M, 1998b. The structural style of the Umbria-Marche fold and thrust belt. Mem. Soc. Geol. It. 52, 557-578.

Bosellini, A., 2004. The western passive margin of Adria and its carbonate platforms. In: Crescenti, V., Calamita, F., Cantalamessa, G., Centamore, E., Deiana, G., Dramis, F., Micarelli, A., Pieruccini, U., Potetti, M., Romano, A., 1978. Dati preliminari sulla neotettonica dei fogli 132 (Norcia), 124 (Macerata), 115 (Città di Castello). C.N.R. Prog. Fin. Geod. Pubbl. 251, 179-215.

Calamita, F., Daiana, G., 1986. Geodinamica dell'Appennino umbro-marchigiano. Mem. Soc. Geol. It. 35, 311-316.

Calamita, F., Cello, G., Invernizzi, C., Paltrinieri, W., 1990. Stile strutturale e cronologia della deformazione lungo la traversa M.S. Vicino – Polverigi (Appennino marchigiano esterno). Studi Geologici Camerti, Volume Speciale, 69-86.

Calamita, F., Cello, G., Deiana, G., Paltrinieri, W., 1994. Structural styles, cronology rates of deformation, and time-space relationships in the Umbria-Marche thrust system (central Apennines, Italy). Tectonics 13, 873-881.

Calamita, F., Coltorti, M., Pieruccini, P., Pizzi, A., 1999. Evoluzione strutturale e morfogenesi plio-quaternaria dell'Appennino umbro-marchigiano tra il preappennino umbro e la costa adriatica. Boll. Soc. Geol. It. 118, 125-139.

Calamita F., Patruno, S., Pomposo, G., Tavarnelli, E., 2007. Geometria e cinematica delle anticlinali dell'Appennino centrale esterno: il ruolo delle faglie dirette giurassi che. Rend. Soc. Geol. It. 4, 167-169.

Carloni G.C., 1960. Il nucleo dell'anticlinale di Cingoli (Macerata). Giorn. di Geol. 28, s. 2a, 113-122.

Carloni G.C., 1964. La Geologia dei dintorni di Cingoli (Appennino Marchigiano). Giorn. di Geol. 32, 365-401.

Carminati, E., Doglioni, C., Scrocca, D., 2004. Alps vs Apennines. In: Crescenti, V., D'Offizi, S., Merlino, S., Sacchi, L. (Eds.), Geology of Italy, Special Volume of the Italian Geological Society for the IGC 32 Florence - 2004, Società Geologica Italiana, 141-151.

Centamore, E., Chiocchini, D., Deiana, G., Micarelli, A., Pieruccini, U., 1971. Contributo alla conoscenza del Giurassico dell'Appennino umbro-marchegiano. Studi Geologici Camerti 1, 7-89.

Centamore, E., Deiana, G., 1986. La Geologia delle Marche. Studi Geologici Camerti, Volume Speciale, 145 pp.

Channel, J.E.T., D'Argenio, B., Horwath, F., 1977. Adria the African Promontory in Mesozoic mediterranean paleogeography. Earth-Sci. Rev. 15, 213-292.

Chiarabba, C., Jovane, L., Di Stefano, R., 2005. A new view of Italian seismicity usinf 20 years of instrumental recordings. Tectonophysics 395, 251-268.

Ciancetti, G., Nanni, T., 1989. Note sulla Geologia dell'anticlinale di Monte Acuto di Cingoli (Marche). Boll. Soc. Geol. It. 108, 553-564.

Colacicchi, R., Passeri, L., Pialli, G., 1970. Nuovi dati sul Giurese umbro-marchigiano ed ipotesi per un suo inquadramento regionale. Mem. Soc. Geol. It. 9, 839-874.

Coward, M.P., De Donatis, M., Mazzoli, S., Paltrinieri, W., Wezel, F.C., 1999. Frontal part of the northern Apennines fold and thrust belt in the Romagna-Marche area (Italy): Shallow and deep structural styles. Tectonics 18, 559-574.

Deiana, G., Cello, G., Chiocchini, M., Galdenzi, S., Mazzoli, S., Pistolesi, E., Potetti, M., Romano, A., Turco, E., Principi, M., 2002. Tectonic evolution of the external zones of the Umbria-Marche Apennines in the Monte San Vicino-Cingoli area. Boll. Soc. Geol. It., Volume Speciale 1, 229-238.

Di Francesco, L., Fabbi, S., Santantonio, M., Bigi, S., Poblet, J., 2010. Contribution of different kinematic models and a complex Jurassic stratigraphy in the construction of a forward model for the Montagna dei Fiori fault-related fold (Central Apennines, Italy). Geological Journal 45, 489-505.

Doglioni, C., Gueguen, E., Harabaglia, P., Mongelli, F., 1999. On the origin of W-directed subduction zones and applications to the western Mediterranean. Geological Society Special Publication 156, 541-561.

Fantoni, R., Franciosi, R., 2009. Mesozoic extension and Cenozoic compression in Po Plain and Adriatic foreland. Rendiconti online Soc. Geol. It. 9, 28-31.

Galluzzo, F., Santantonio, M. 2002. The Sabina Plateau: a new element in the Mesozoic palaeogeography of Central Apennines. Tectonic Studies Group Meeting, 1997. Boll. Soc. Geol. It., Volume Speciale 1, 561–588.

Ghisetti, F., Barchi, M., Bally, A. W., Moretti, I., and Vezzani, L., 1993. Conflicting balanced structural sections across the Central Apennines (Italy): problems and implications, in: Spencer, A. M. (Ed.): Generation, Accumulation and Production of Europe's Hydrocarbons III, Special Publication of the European Association of Petroleum Geoscientists 3, 219–231.

La Vecchia, G., 1982. Confronto fra due sistemi a pieghe: l'Appennino umbro-marchigiano ed il Giura franco-svizzero. Boll. Soc. Geol. It. 101, 69-76.

Marchegiani, L., Deiana, G., Tondi, E., 1997. Tettonica pre-orogenica in Appennino centrale. Studi Geologici Camerti 14, 211-228.

Marchegiani, L., Bertotti, G., Cello, G., Deiana, G., Mazzoli, S., Tondi, E., 1999. Pre-orogenic tectonics in the Umbria-Marche sector of the Afro-Adriatic continental margin. Tectonophysics 315, 123-143.

Marino, M., Santantonio, M., 2010. Understanding the geological record of carbonate platform drowing across rifted Tethyan margins: Example from the Lower Jurassic of the Apennines and Sicily (Italy). Sedimentary Geology 225, 116 -137.

Mazzoli, S., Deiana, G., Galdenzi, S., Cello, G., 2002. Miocene fault-controlled sedimentation and thrust propagation in the previously faulted external zones of the Umbria-Marche Apennines, Italy. EGU Stephan Mueller Special Publication Series 1, 195-209.

Menichetti, M., 1991. La sezione geologica Cingoli-M. Maggio-Tevere nell'Appennino umbro-marchigiano: analisi cinematica e strutturale. Studi Geologici Camerti Volume Speciale 1, 315-328.

Montanari, A., Chan, L.S., Alvarez, W., 1989. Synsedimentary tectonics in the late Cretaceous – early Tertiary pelagic basino f the northern Apennines, Italy. Controls on Carbonate Platform and Basin development, SEPM Special Pubblication 44, 379-399.

Montone, P., Amato, A., Pondrelli, S., 1999. Active stress map of Italy. Journal of Geophysical Research 104, 25595-25610.

Montone, P, Mariucci, M. T., Pondrelli, S., Amato, A., 2004. An improve stress map for Italy and surrounding regions (central Mediterranean). Journal of Geophysical Research 109, B10410, doi: 10.1029/2003JB002703

Montone, P., Mariucci, M. T., Pierdominici, S., 2012. The Italian present-day stress map. Geophysical Journal International 189, 705-716.

Santantonio, M., 1993. Facies association and evolution of pelagic carbonate platform/basin systems: example from the italian Jurassic. Sedimentology 40, 1039-1067.

Santantonio, M., 1994. Pelagic carbonate platforms in the geologic record: their classification, and sedimentary and paleotectonic evolution. America Association of Petroleum Geologists Bullettin 78, 122-141.

Santantonio, M., Galluzzo, F., Gill, G. 1996. Anatomy and paleobathymetry of a Jurassic pelagic carbonate platform/basin system, Rossa Mts, Central Apennines (Italy). Geological Implications. Palaeopelagos 6, 123–169.

Santantonio, M, Carminati, E., 2010. Jurassic rifting evolution of the Apennines and southern Alps (Italy): Parallels and differences. Geological Society of America Bulletin, doi: 10.1130/B30104.1.

Scrocca, D., Doglioni, C., Innocenti, F., Manetti, P., Mazzotti, P., Bertelli, L., Burbi, L., D'offizi, S., 2003. CROP Atlas: seismic reflection profiles of the Italian crust. Memorie Descrittive della Carta Geologica d'Italia 62.

Scrocca, 2006. Thrust front segmentation induced by differential slab retreat in the Apennines (Italy). Terra Nova 18, 154–161.

Servizio Geologica d'Italia, 2003. Tolentino. Servizio Geologico d'Italia, Carta Geologica d'Italia 1:50,000, sheet 302, Rome.

3. Fold–Related Fractures: The Role of Mechanical Stratigraphy and Rock Properties

3.1 Introduction

Thrust fault-related folds are generally characterized by intense fracturing and faulting generation (Nelson, 2001). Understanding and predicting the distribution, orientation and the type of fold-related fractures is of a great importance both for academic and applied purposes.

Folding processes are influenced by many factors such as the mechanism and kinematic of folding processes, the presence of pre-existing structures, the rheology, and the environmental conditions (Ramberg, 1963; Suppe, 1985; Couples et al., 1998; Fischer and Jackson, 1999; Bellahsen et al., 2006, Evans and Fischer, 2012). As the pattern of fold-related fractures systems are conditioned by the stress and strain distribution at the time of their formation (Billings, 1972; Jaeger and Cook, 1976; Hancock, 1985; Couples et al., 1998; Cooke et al., 1999; Fischer and Wilkerson, 2000; Nelson, 2001; La Pointe et al., 2002), understanding the relationships between folding and fracturing provides a noteworthy contribution for reconstructing the geodynamic and structural evolution of the studied area (e.g. Fischer and Wilkerson, 2000; Bellahsen et al., 2006, Tavani et al. 2006, Tavani et al., 2011). For instance, through analysis of the fracture systems associated to the local stress/strain distribution, it is possible to unravel if the fold hinge has migrated or not, to suggest the presence of pre-existing fractures or consider a fold lateral growth (e.g. Fischer and Wilkerson, 2000; Bergbauer and Pollard, 2004; Bellhasen et al., 2006; Savage et al., 2010).

Furthermore, the features of fractures systems, in particular the geometry, the density and the type of fractures, influence the fluid flow through rocks (e.g. Engelder and Scholz, 1981; Antonellini and Aydin, 1994; Caine et al., 1996; Sibson, 1996; Jones et al., 1998; Nelson, 2001; Aydin, 2000; La Pointe et al., 2002; Billi, 2005; Agosta et al. 2009, Faulkner et al., 2010) and their characterization is significant for many applied fields. Joints, veins, pressure solution seams (PSSs), deformation bands (DBs), faults are all structures normally generated during folding (Price, 1966; Stearns, 1964 and 1968; Friedman, 1969; Stearns and Friedman, 1972; Price and Cosgrove, 1990; Tavani et al., 2006; Agosta et al., 2009; Tavani et al., 2008, Tavani et al., 2011). Each of these structures shows a different impact on fluid flow. PSSs are ductile compressive structures and generally with a thin clay-rich material on their surfaces so, if no changes in the state of stress occurs, they inhibit fluid flow (Agosta et al. 2009). Joints form conduits for fluid flow whereas DBs are structures with reduce porosity and they inhibit fluid flow. Faults may act as barriers or carriers in relation to the fault compartment (fault core or damage zone; Caine et al., 1996) and to the mechanical characteristics of the hosting rock

(Agosta et al., 2010 and reference therein). Hence, revealing the mechanical type of structures formed during folding is as important as predicting their geometries.

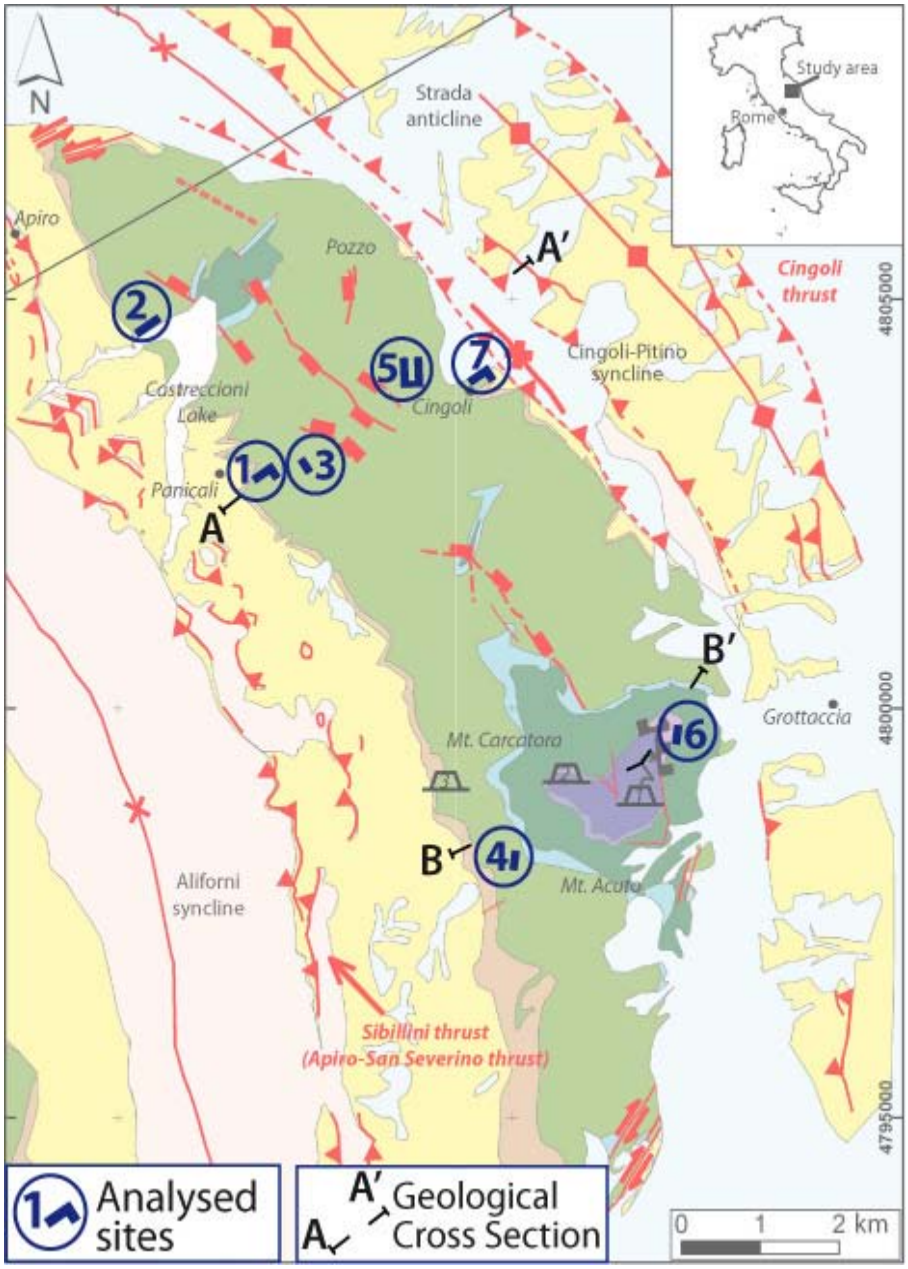

Fig. 3.1: Geological map of the Cingoli anticline showing the analysed sites and the traces of two geological profiles

The features of fold-related structures depend on the kinematic and the mechanism of folding processes, but former works suggest that mechanical stratigraphy, local stress perturbation (e.g. presence of former fractures), and rheology are also important variables which affect the fractures properties (e.g. mechanical type of fractures, density, dimension and so on; e.g. Jaeger and Cook, 1979; Segall and Pollard, 1980; Marshak and Engelder, 1985; Corbett et al., 1987; Woodward and Rutherford, 1989; Protzman and Mitra, 1990; Narr and Suppe, 1991; Antonellini and Aydin, 1994; Caputo, 1995; Gross et al., 1995; Fischer and Jackson,

1999; Cooke et al., 1999; Mollema and Antonellini, 1999; Bai and Pollard, 2000; Chester, 2003; Di Naccio et al., 2005; Caputo, 2005; Antonellini et al., 2008; Aydin et al., 2010; Rustichelli et al., 2012). An integrated study taking in account the kinematic evolution of the fold, the structural settings and the mechanical properties of the analysed sequence should be considered to predict and analyse the fracture patterns related to folding.

This work presents results of a study carried out in the *Cingoli* anticline, a thrust-related fold in the northern Apennines, which provides an ideal opportunity to investigate relationships among fracturing and mechanical stratigraphy relative to the structural setting (and evolution) of the fold (Figs. 3.1 and 3.2). The aim of this work is to examine how mechanical stratigraphy

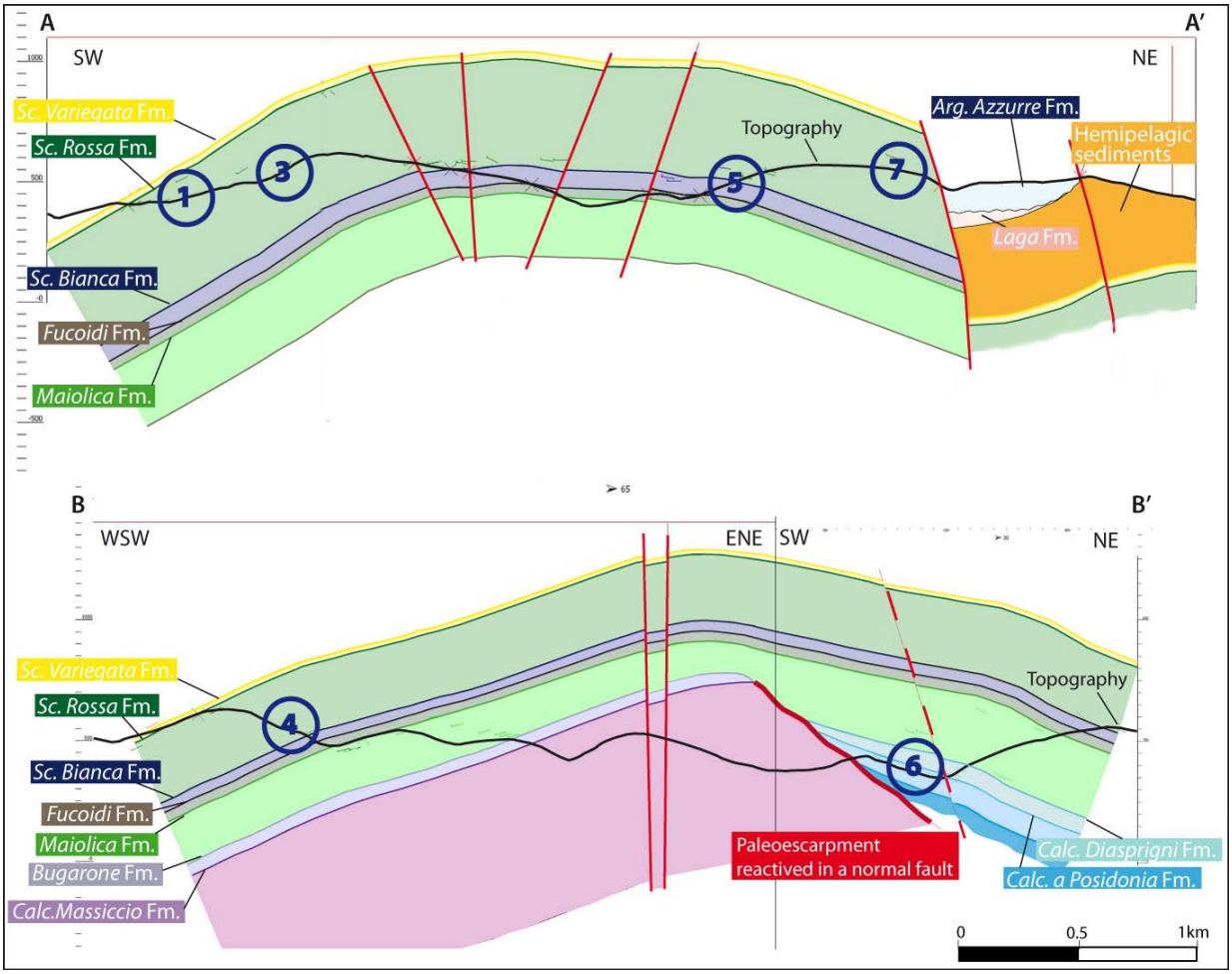

Fig. 3.2: Geological cross sections of the Cingoli anticline close to the studied sites (see Fig. 3.1 for sections localization).

influences the fracture features and in particular their geometry and their mechanical type (i.e. PSSs, joints, faults etc), and, therefore, how the mechanical stratigraphy may have an influence on both the fluid flow and the strain distribution during the folding process. Furthermore, the results of this work are compared with fracturing models exposed in literature, which only in part consider the relevance of the mechanical properties of the folded sequence.

In order to collect and compare data in various structural settings of the fold structure, seven sites in different structural positions of the studied area have been analysed (Figs. 3.1 and 3.2). Although they are mostly within the *Scaglia* Fms. (only one is in the *Calcare a Posidonia* Fm.) the sites show different stratigraphic patterns: thinly bedded limestones with chert interlayers, thinly bedded limestones with marl interlayers and bedded limestones with neither cherts nor marl layers characterize these outcrops. Fractures systems patterns (e.g. attitude, mode of fracture formation, orientation relative to bedding surfaces, cross-cutting relationship etc.) represent the key data sets collected in the field and they are presented through detailed mappings at different observation scales.

3.2 Previous Studies on Folding Processes and Fold-Related Fractures

This work refers to the definition of fracture used by Aydin (2000), which considers a fracture as a "structure defined by two surfaces or a zone across with a displacement discontinuity occurs". With this definition a further classification can be made by analyzing the mode of fracture and the relative movement between the couple of surfaces (or zone) and the propagation front (Pollard and Aydin, 1988; Aydin, 2000):

- Mode I: opening mode. The displacement is perpendicular to the fracture surface.
- Mode II: shear mode. The shearing displacement of the fracture surfaces is perpendicular to the fracture front.
- Mode III: shear mode. The shearing displacement is parallel to the propagation front.
- Anti-mode I: contractional mode. This mode refers to structures where the sense of motion is perpendicular to the surfaces of the structure but with an opposite sense of motion compared to Mode I (i.e. pressure solution seams and compaction bands). These features are defined as ductile structures and hence they should not be considered as proper fractures. As discussed in this section, anti-mode I structures are important features formed during folding and they affect fluid flow and the deformation process. Furthermore, if the stress state changes in time, anti-mode I may open or shear displacement may occur on their surfaces. For these reasons, although not properly correct, I consider these structures as fractures.

In this work, when the type of fractures formation is not expressed, fracture refers as a generic term including pressure solution seam (PSS), sheared PSS, joint, sheared joint and faults (Pollard and Aydin, 1988).

Schultz and Fossen (2008) expose a further and relevant feature for fracture classification. Field evidences show that displacement, in the sense of Pollard and Aydin (1988), is not always sharp as in a joint or in those faults characterized by well-defined slip surface. Some fractures do not show a discontinuous and sharp change in mechanical properties between well-defined surfaces, but on the contrary, they show an almost continuous change within a relative thin zone (Aydin, 1978; Antonellini and Aydin, 1994 and 1995; Agosta et al., 2009; Rustichelli et al., 2012). These structures are defined "table structural discontinuities" (Schultz and Fossen, 2008) or "weak discontinuities" (Aydin et al., 2006) in contrast with the "sharp discontinuities" (Schultz and Fossen, 2008) or "strong discontinuities" (Aydin et al., 2006).

The geometries of natural fractures systems can be related to the state of stress (and the related strain) at the time of their formation (Billings, 1972; Jaeger and Cook, 1979; Friedman and Sowers, 1970, Hancock, 1985; Caputo, 1995; Couples et al., 1998; Cooke et al., 1999; Fischer and Wilkerson, 2000; Nelson, 2001; La Pointe et al., 2002). The mechanism of folding (e.g. bending, buckling, flexural slip, flexural flow, etc.; Ramberg, 1963 and Suppe, 1985) and folding kinematics (e.g. hinge migration, cylindrical vs. non-cylindrical fold shape, lateral growth of the fold; Storti and Salvini, 1996; Fischer and Wilkerson; 2000; Savage et al., 2010) are processes which strongly affect the stress and strain distribution and, as a consequence, the fracture patterns (Couples et al., 1998; Fischer and Jackson, 1999; Fischer and Wilkerson, 2000; Salvini and Storti 2001; Sanders et al., 2004 among many others). Furthermore, as presented in many former works, the mechanical type of fractures and their shape (e.g. length) are also strongly conditioned by the mechanical properties and the stratigraphy of the deformed sequence (Corbett et al., 1987; Gross, 1993; Gross, 1995; Cooke et al., 1999; Mollema and Antonellini, 1999; Gillespie et al., 1999; Fischer and Jackson, 1999; Graham et al., 2003; Di Naccio et al., 2005; Bellahsen et al., 2006, Graham et al., 2006; Antonellini et al., 2008; Aydin et al., 2010; Rustichelli et al., 2012).

It is possible to discriminate fractures systems due to regional stress from those related to local (folding) processes on the basis of geometrical relationships among fold axis orientation, attitude of joints, and their trend in unfolded strata (see Hancock, 1985). According to these authors, bed-perpendicular joints, which show different orientation in the fold, are pre-folding (i.e. regional) if they acquire similar orientation once the strata have been unfolded. On the contrary, joints showing symmetry respect to the fold axis (i.e. normal or parallel) are ascribed to be of syn-folding origin (Stearns and Friedman, 1972; Hancock, 1985). Bellahsen et al. (2006) interpret fractures oriented parallel or perpendicular to bedding strike as syn-folding because their geometries do not change once the bed has been unfolded.

As mentioned before and in order to predict fractures geometries, several models have been proposed to define the stress state and the strain distribution during the folding process (Ramsay, 1967; Billings, 1972; Hills, 1972; Ramsay and Huber, 1987; Couples et al., 1998). A first important discrimination derives from the physical process responsible of the fold formation. Buckling and bending represent the main folding mechanisms recognized in literature (Suppe, 1985). Buckling refers to rock sequences, which deflect perpendicular to layering under a compressive force applied parallel to the layers direction (Fig. 3.3a). Bending refers to the perpendicular deflection of rock layers in response to perpendicular applied forces (i.e. diapirs

and laccoliths; Fig. 3.3a). A third mechanism is the passive amplification, which occurs when a pre-existing curved structure (sedimentary or tectonic) grows due to the homogeneous strain of rock volume (Suppe, 1985). Several former works suggest different strain distribution models through which the fold may evolve. The two end-member models proposed in literature are the tangential longitudinal strain (TLS) and the flexural flow (Fig. 3.3b; Billings, 1972; Ramsay, 1967; Ramsay and Hubert, 1987; Twiss and Moores, 1992; Hudlestone et al., 1996; Couples et al., 1998; Fischer and Jackson, 1999; Frehner, 2011; Evans and Fischer, 2012). In TLS model the strain is both perpendicular and parallel to layering with extension and contraction respectively in the outer and in the inner side of the hinge zone (Fig. 3.3b-I). Through this model, a finite neutral surface is formed within the layer and its curvature is related to the strain distribution, hence high strain occurs in the hinge and little or even no strain along the limbs. Note that in TLS model the thickness remains constant and there is not distortion within the folded layer. Recent studies based on numerical modelling suggest that the neutral surface is not continuous through the fold but, on the contrary, they suggest an inward migration of a discontinuous neutral surface with fold tightening (Frehner, 2011). In the flexural-flow the deformation is distributed continuously in the layers and the strain occurs through layer-parallel simple shear, hence there is not presence of orthogonally-flexed layers (Fig. 3.3b-II). In contrast with TLS model, the strain is particularly intense along the limbs and small in the hinge area. The flexural flow deformation occurs in layer of rock characterized by a planar anisotropy in viscosity (Hudleston et al., 1996). Hudleston et al. (1996) presented experimental data, which demonstrate that it is not possible to obtain in nature parallel buckle folds through flexural flow model as many of the common rocks do not reach the adequate anisotropy needed for the flexural flow model development. On the other hand, the same authors suggest that a multilayer sequence with a repetition of weak and stiff layers can reproduce a deformation pattern with the overall structures similar to those derived through the flexural flow model (Fig. 3.3b-III). With a multilayer sequence, the anisotropy derives from the different viscosity of the two rocks, which deform in two different ways: the weaker layers undergo to a layer-parallel simple shear whereas the stiffer layers deform through a TLS model. Finally, the flexural slip model is proposed for a multilayer sequence where the shear occurs along discrete surfaces, normally the bedding planes (Fig. 3.3b-IV). Through this model, each competent layer deforms according to the TLS model. Couples et al. (1998) propose a model of stress distribution during folding based on photo-elastic analysis, mathematical modelling, and experimental studies. According to this model in a single layer subjected to flexure the principal stresses are normal

or parallel to layering just close to the folds hinges whereas the rest of the folds are characterized by oblique-to-layer stresses directions. However, the strain distribution along the limbs related to the stress state proposed by Couples et al. (1998) are similar to those expected in flexural flow and in the multilayer of Hudleston et al. (1996; Fig. 3.3b-II and –III).

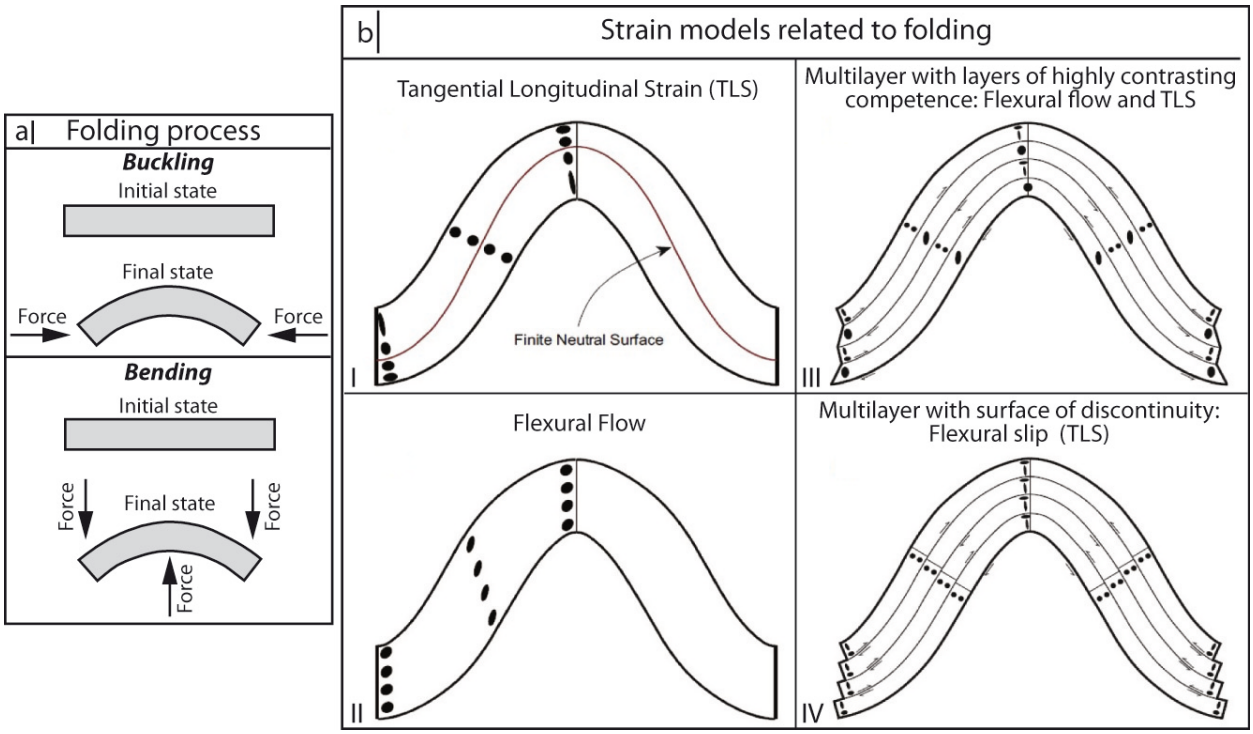

Fig. 3.3: (a) Mechanism of folding: buckling and bending. (b) Strain deformation models during folding (modified after Hudleston and Lan, 1993). I and II represents the two most common models proposed in literature for a single and isolated bent layer; III and IV are models for multilayer sequence characterized respectively by bedding-parallel shear and bedding-parallel slip.

As observed by Fischer and Jackson (1999), a single strain pattern could not be the only model through which the fold develops but, on the contrary, different mechanical units deform through different models. Furthermore, different folding model can act in the same mechanical unit through time. The folding process (i.e. buckling and bending) and the associated fold evolution model (TLS, flexural flow, flexural slip etc) are important variables affecting fracture system patterns.

The most used classifications of fold-related fractures present in literature (Price, 1966; Stearns, 1964 and 1968; Friedman, 1969; Stearns and Friedman, 1972 and Price and Cosgrove, 1990) are based on analysis carried out in laboratory tests and on the concept that these fractures are strongly related to the local stress state (Nelson, 2001). The base for these schemes is the observation that shear fractures form at an acute angle respect to the maximum compressive principal stress directions and at an obtuse angle respect to the minimum compressive principal stress directions, whereas extension fractures form perpendicular to the minimum compressive principal stress directions and parallel to the maximum and

intermediate compressive principal stress (Price, 1966; Stearns, 1964 and 1968; Friedman, 1969; Stearns and Friedman, 1972). At the present, it has been demonstrated that structures geometries and types depend also on the confinement stresses, on the material properties and on the existence or not of pre-existing structures (Jaeger and Cook, 1979; Pollard and Segall, 1987; Caputo, 1995). Price (1966) and Stearns (1964 and 1967) developed a conceptual model describing the orientation of fold-related fractures; Price and Cosgrove (1990) schematize these previous works, adding some observations, as followed (Fig. 3.4):

- Extensional fractures form perpendicular and parallel to fold axes and almost vertical respect to bedding (T fractures in Fig. 3.4c of Price et al., 1966; and fractures in Fig. 3.3f).
- Shear fractures form both vertical and at low angle to bedding and both oblique, parallel and perpendicular to fold axes (R fractures in Fig. 3.4c of Price et al., 1966 and fractures in Fig.3.4g and h). According to the state of stress, normal, reverse, strike-slip and oblique-slip faults may form. Price and Cosgrove (1990) noted that the most frequent shear fractures are strike or oblique slip faults.

Note that with these analysis no anti-mode I fractures are mentioned.

These fold-related fractures development mostly concerns the deformation occurring in the central portion of the fold; away from the hinge zone the deformation seems to be related to slip along bedding surfaces (Price and Cosgrove, 1990).

The schematic models proposed by Price (1966) and Stearns (1964 and 1967) have been subjected to some critical reviews. For instance, Bellahsen et al. (2006) observed that in these schemes the temporal evolution of the fold is not considered, and they note that the presence of pre-existing fractures and the effects of primary faults have not been taken into account. Furthermore, it is relevant to underline that the different folding mechanism and different strain deformation models proposed in literature (see before) should be considered as important variables for fractures formations.

Couples et al. (1998) suggests that strain deformation due to flexure may act only in the hinge zone (where fractures in Fig. 3.4h may form) whereas layers in planar limbs do not experience flexure but they are characterized by layer-parallel slip (or shear). They hence propose that planar limbs can be characterized by parallel to hinge fractures at an oblique angle to bedding formed due to a bedding-plane slip process. In order to explain the vertical fractures, both parallel, perpendicular and oblique to fold axes presented in the Price and Stearns scheme, Couples et al. (1998) propose the so called “inchworm fashion” movement (or

patchy bedding-plane slip), where the shear is localized at time only in some portion of the sheet with subsequent activation of other portions.

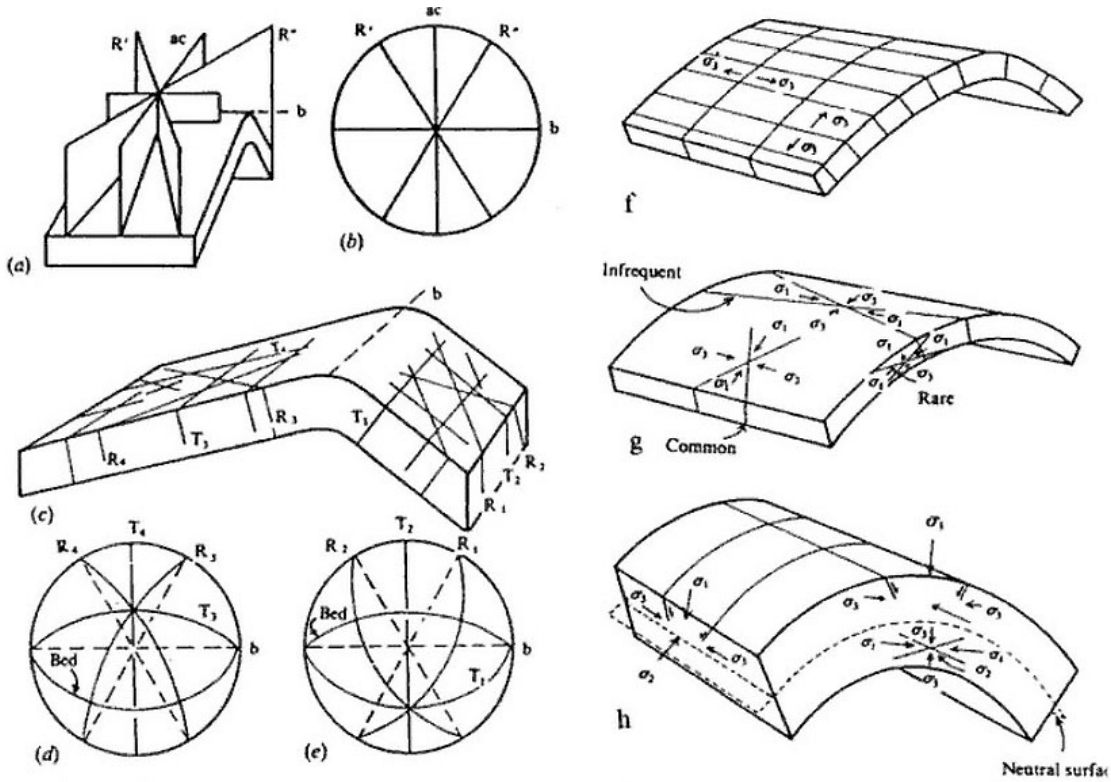

Fig. 3.4: (a-e) Fractures schemes and relative stereonets proposed by Price et al., 1966). (f-h) Fracture schemes of former studies summarized in Price and Cosgrove, 1990.

Fischer and Jackson (1999) outline the relationship between mechanism of folding (i.e. buckling and bending), strain distribution models (i.e. TLS, flexural flow and flexural slip) and fractures formation. In particular they observe that for folds characterized by layer-parallel shortening (i.e. fold due to buckling) and experiencing TLS deformation, fractures perpendicular to fold axes form in the fold limbs whereas fractures parallel to fold axes characterize the hinge zone. The stronger the layer-parallel shortening is, the narrower the area characterized by fractures parallel to axes is. Buckling folds deforming under flexural flow deformation are, instead, characterized by perpendicular to fold axes fractures both in the hinge and the fold limbs, whereas folds deformed through flexural slip develop TLS features in layers between the slip surfaces and they are hence characterized by both parallel to fold axes fractures (in the hinge zone) and perpendicular to fold axes fractures (in the fold limbs).

Fischer and Wilkerson (2000) interpreted the extensional fracture normal to the fold axis as the product of layer-parallel shortening, the extensional fracture parallel to the fold axis due to the outer arc extension and the conjugate shear fractures due to layer-parallel shortening. Furthermore, they suggest that joints oblique to the fold axis may be induced by fold-related

strain (e.g. due to lateral fold growth) and their orientation depends on the structural position respect to the fold.

The presented literature concerning fold-related fractures deals in particular with extension fractures and faults, but as carbonate rocks are prone to dissolution (Stockdale, 1922 and 1926; Bathurst, 1971; Alvarez et al., 1976), pressure solution seams (PSSs) should be further considered as important deformation mechanisms (Rutter, 1983; Engelder and Marshak, 1985). In fact, tectonic deformation may induce PSSs formation both perpendicular and oblique to bedding (Park and Schot, 1968; Railsback and Andrews, 1995; Ebner et al., 2010) and it is widely observed that shearing of PSSs are responsible for fault development and hence they should be considered as important features controlling the overall deformation during a tectonic event (Alvarez et al., 1978; Engelder and Marshak, 1985; Peacock and Sanderson, 1995; Willemse et al., 1997; Salvini et al., 1999; Billi et al., 2003; Graham et al. 2003; Tondi et al., 2006; Antonellini et al., 2008; Agosta et al., 2009; Aydin et al., 2010; Petracchini et al., 2012 *in press*). PSSs and DBs have been also observed in folds and it has been suggested that these structures are strongly connected with the early and on-going stages of the folding process (Marshak and Engelder, 1985; Tavani et al., 2006; Agosta et al, 2009; Tavani et al., 2008; Tavani et al., 2011, Aydin et al., 2010; Evans and Fischer, 2012). Perpendicular to bedding PSSs have been observed in several anticline and they usually form two sets of fractures at right angle to each other. These two PSSs sets are considered to be pre-tilting fractures (Allmendinger, 1982, Mitra et al., 1984; Protzam and Mitra, 1990; Aydin et al., 2010; Agosta et al., 2009). Tavani et al. (2006) consider the longitudinal-to-fold axis PSSs at high angle to bedding as syn-folding structures. The authors suggest that these PSSs are formed during the early stage of fold nucleation due to layer-parallel shortening. According to Agosta et al. (2009), the two PSSs sets at right angle to each other and showing mutual cross-cutting relationships may be explained through a systematic “swap” of the greatest and least principle stress axes as Caputo (1995) proposed for orthogonal cross joints. In addition, PSSs oblique to bedding have been recognized in different folds and their genesis has been related to folding process (Marshak and Engelder, 1985; Tavani et al., 2006; Agosta et al., 2009). Marshak and Engelder (1985) consider the oblique PSSs as a consequence of mechanical rotation of early structures or a consequence of a different local stress field due to the beds tilting. In some previous work, the PSSs at an oblique angle to bedding are considered as tail PSSs forming in the contractional quadrants relative to a shearing (flexural slip) bedding surface (Rispoli, 1981; Willemse et al., 1997; Graham et al., 2003; Agosta and Aydin, 2006, Antonellini et al., 2008).

Furthermore, in order to understand and predict fold-related fractures it is relevant to consider that the fracture geometry, density and the mechanical type of structures (i.e PSSs, joints, faults) are also related to many others factors as local stress perturbation, facies, diagenesis, and mechanical properties of rocks (e.g. Jaeger and Cook, 1979; Marshak and Engelder, 1985; Caputo, 1995; Fischer and Jackson, 1999; Di Naccio et al, 2005; Graham, 2006; Bellahsen et al., 2006; Antonellini et al. 2008, Gross et al. 2012).

For these reasons, the schemes proposed in literature should be considered a simplification of more complex systems, which can, in turn, be correlated to environmental conditions, and local properties of the sequence involved in folding process.

3.3 Composite Materials

Composite materials have been made in the human history for several purposes; ancient societies, imitating nature, combined heterogeneous materials in order to take advantage of the best properties of dissimilar constituents (Roylance, 2008). Examples of actual composites are steel-belted tires, plywood with alternate fibers directions, concrete and concrete with steel rods (Hosford, 2005). Composite materials have been made in order to provide goods with mechanical properties otherwise unavailable (i.e. boats, airplanes, spacecrafts, insulating materials etc.). Combination of properties from different materials permits to obtain, for example, goods with stiff, strong and lightweight characteristics at the same time.

In the mechanics of materials, composites refer to a matrix reinforced with particles, fibers, or laminae (Hosford, 2005; Roylance, 2008). The physical concept is that the particles, fibers, or laminae with high strength and stiffness are impregnated into a component (i.e. the matrix) which transfers the loads to the reinforcing materials. In this way, the composites acquire good properties even if the matrix may dilute the properties of the reinforcing materials to some degrees (Roylance, 2008).

In this work the theoretical concepts developed to made artificial composites are used in order to explain some of the natural evidences observed through this study.

3.3.1 Theory

Consider a block made up of two different materials, α and β, where α represents the lamina of reinforcing material and β the matrix (Fig. 3.5). Defining X_α and X_β the thicknesses of α and β; $X_\alpha+X_\beta$ the slab of a single lamina; $N(X_\alpha+X_\beta)$ the total length of the slab; L the width and depth of the block, we have that the volume fractions of each phase are:

$$\boxed{V_\alpha = \frac{X_\alpha}{X_\alpha+X_\beta}} \; ; \; \boxed{V_\beta = \frac{X_\beta}{X_\alpha+X_\beta}}$$

It is possible to study the behaviour of a composite analysing two end-member cases.

The first case is when the external force applied is perpendicular to the lamina direction (Fig. 3.5). In this case the stress applied on each phase is the same, as $\sigma = \frac{F}{L^2}$ (i.e. equal stress condition), but the strains are different. If X is not too small compared to L and assuming that the strains of each phase are equivalent to those that would be formed during compression for the single component, the deformation of α and β are respectively:

$$\varepsilon_\alpha = \frac{\Delta X_\alpha}{X_\alpha} \rightarrow \Delta X_\alpha = \varepsilon_\alpha \cdot X_\alpha$$

$$\varepsilon_\beta = \frac{\Delta X_\beta}{X_\beta} \rightarrow \Delta X_\beta = \varepsilon_\beta \cdot X_\beta$$

Hence, the total deformation of the composite is:

$$\Delta X_c = N\Delta X_\alpha + N\Delta X_\beta$$

and the composite strain is:

$$\varepsilon_c = \frac{\Delta X_c}{N \cdot (X_\alpha + X_\beta)} = \frac{[\Delta X_\alpha + \Delta X_\beta]}{X_\alpha + X_\beta} = \frac{\Delta X_\alpha}{X_\alpha + X_\beta} + \frac{\Delta X_\beta}{X_\alpha + X_\beta} = \frac{\varepsilon_\alpha \cdot X_\alpha}{X_\alpha + X_\beta} + \frac{\varepsilon_\beta \cdot X_\beta}{X_\alpha + X_\beta} = V_\alpha \cdot \varepsilon_\alpha + V_\beta \cdot \varepsilon_\beta$$

This equation shows that the composite strain is a volumetric average of the strains of the two phases.

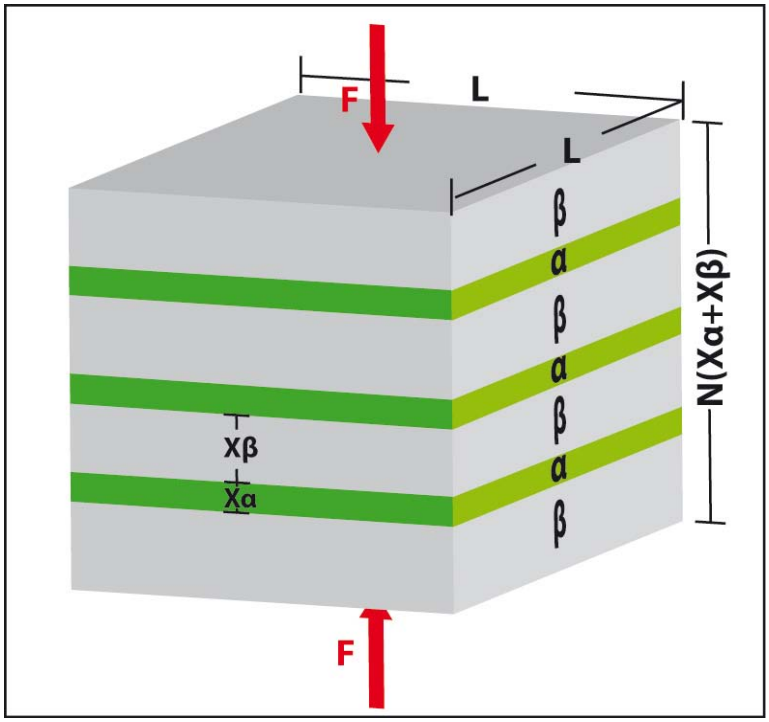

Fig. 3.5: Schematic block of a composite experiencing a perpendicular to lamination external forces. α and β represent single laminae with different Young's modulus, Xα and Xβ are the slab of a single lamina, N(Xα+Xβ) the total length of the slab, L is the height and depth of the block, and F is the applied force.

Considering an elastic deformation for both phases (i.e. $\varepsilon_\alpha = \frac{\sigma_\alpha}{E_\alpha}$; $\varepsilon_\beta = \frac{\sigma_\beta}{E_\beta}$) and, in this specific case, the stress applied on the composite equals to those applied to each phase (i.e. $\sigma_c = \sigma_\alpha = \sigma_\beta$), the composite strain takes the form:

$$\varepsilon_c = \sigma\left(\frac{V_\alpha}{E_\alpha} + \frac{V_\beta}{E_\beta}\right)$$

As the Young's modulus for composite (composite modulus) is $\varepsilon_c = \frac{\sigma}{E_c}$, we have

$$E_c = \frac{\sigma}{\varepsilon_c} = \frac{\sigma}{\sigma \cdot \left(\frac{V_\alpha}{E_\alpha} + \frac{V_\beta}{E_\beta}\right)} = \frac{E_\alpha \cdot E_\beta}{V_\alpha \cdot E_\beta + V_\beta \cdot E_\alpha} \quad [1]$$

This equation represents the mechanical behaviour of a composite, characterized by linear elastic deformation, when both phases experience equal stress, that is when the force applied is perpendicular to the lamination direction (in this case $(L \cdot L)$ face; Fig. 3.5)

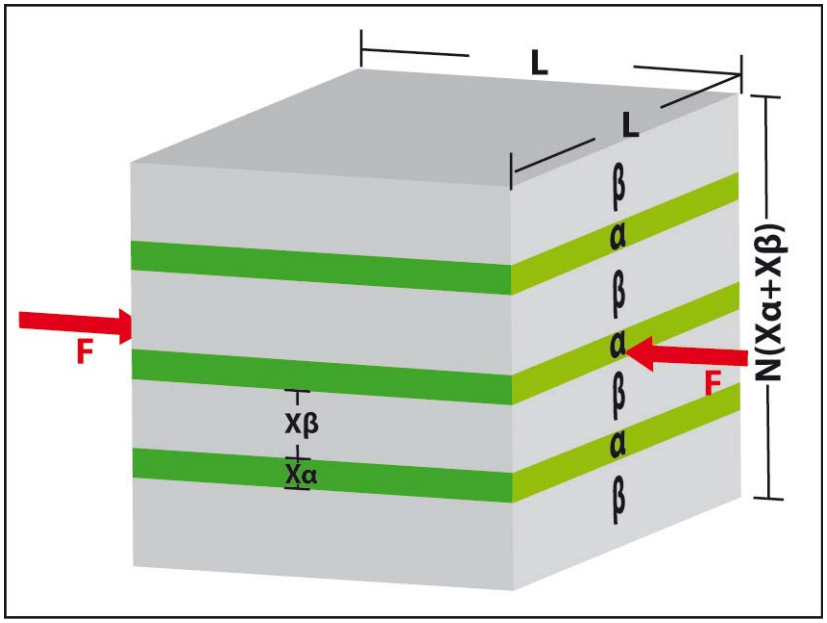

Fig. 3.6: Schematic block of a composite experiencing a parallel to lamination external forces. α and β represent single laminae with different Young's modulus, Xα and Xβ are the slab of a single lamina, N(Xα+Xβ) the total length of the slab, L is the height and depth of the block, and F is the applied force.

In the second case, the applied external force is parallel to the lamina direction (Fig. 3.6). In this configuration the strains of both phases and of the composite are equal (i.e. equal strain condition) but, on the contrary, the external force is partitioned unequally between the two phases.

The total external force applied is equal to the sum of the forces on each phase: $F = F_\alpha + F_\beta$ and each stress phase is respectively:

$$\sigma_\alpha = \frac{F_\alpha}{NX_\alpha \cdot L} \rightarrow F_\alpha = \sigma_\alpha \cdot NX_\alpha \cdot L$$

$$\sigma_\beta = \frac{F_\beta}{NX_\beta \cdot L} \rightarrow F_\beta = \sigma_\beta \cdot NX_\beta \cdot L$$

Hence, the total external force applied on the composite is:

$$F = NL\left(\sigma_\alpha \cdot X_\alpha + \sigma_\beta \cdot X_\beta\right)$$

The composite stress (σ_c) is equal to the applied external force divided for the cross-sectional area transverse to the force direction:

$$\boxed{\sigma_c = \frac{F}{NL(X_\alpha + X_\beta)} = \frac{NL(\sigma_\alpha \cdot X_\alpha + \sigma_\beta \cdot X_\beta)}{NL(X_\alpha + X_\beta)} = \frac{\sigma_\alpha \cdot X_\alpha}{X_\alpha + X_\beta} + \frac{\sigma_\beta \cdot X_\beta}{X_\alpha + X_\beta}}$$

This equation is the most followed rule by composites as the lamellae geometry is usually made in order to consider valid the equal-strain approximation.

That the equal-strain condition is useful to provide reinforcement can be illustrated for the simple case in which both phase are elastic (i.e. $E_c = \frac{\sigma_c}{\varepsilon}$; $E_\alpha = \frac{\sigma_\alpha}{\varepsilon}$; $E_\beta = \frac{\sigma_\beta}{\varepsilon}$). For this condition, the composite modulus (E_c) is equal to:

$$\boxed{E_c \cdot \varepsilon = \frac{E_\alpha \cdot \varepsilon \cdot X_\alpha}{X_\alpha + X_\beta} + \frac{E_\beta \cdot \varepsilon \cdot X_\beta}{X_\alpha + X_\beta} = E_\alpha \cdot V_\alpha + E_\beta \cdot V_\beta} \qquad [2]$$

Note the difference between this equation with the corresponding one for the first case.

Considering $F_\alpha = \sigma_\alpha \cdot NX_\alpha \cdot L$ and $F_\beta = \sigma_\beta \cdot NX_\beta \cdot L$, the forces ratio born by the two phases for a linear elastic deformation is equal to:

:

$$\boxed{\frac{F_\alpha}{F_\beta} = \frac{\sigma_\alpha \cdot X_\alpha}{\sigma_\beta \cdot X_\beta}} = \frac{E_\alpha \cdot \varepsilon \cdot X_\alpha}{E_\beta \cdot \varepsilon \cdot X_\beta} = \boxed{\frac{E_\alpha \cdot X_\alpha}{E_\beta \cdot X_\beta}} = \frac{E_\alpha \cdot V_\alpha \cdot (X_\alpha + X_\beta)}{E_\beta \cdot V_\beta \cdot (X_\alpha + X_\beta)} \quad \rightarrow \quad \boxed{\frac{F_\alpha}{F_\beta} = \frac{E_\alpha \cdot V_\alpha}{E_\beta \cdot V_\beta}} \qquad [3]$$

Fig. 3.7 is a diagram of F_α/F_β ratio as a function of V_α, which is considered the stiffer phase. In equal-strain condition, F_α/F_β ratio is directly proportional to V_α and to the ratio of the Young's modulus of the two phases (i.e. E_α/E_β).

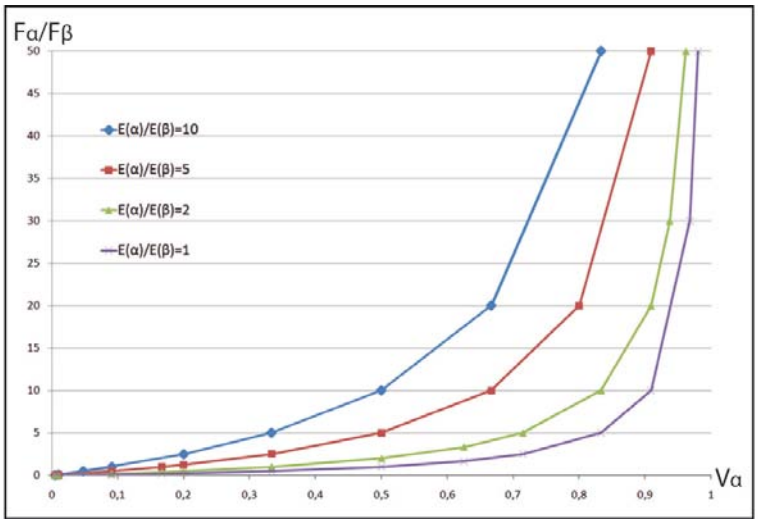

Fig. 3.7: Diagram of the Fα/Fβ ratio as a function of Vα, for different Eα/Eβ value.

Plotting the composite modulus as a function of V_α, it is possible to analyse how the stiffer lamina affects the mechanical behaviour of the composite (Fig. 3.8). The diagram of Fig. 3.8 shows the linear relationship between the composite modulus and both the percentage of the stiffer laminae in the composite and the E_α/E_β ratio.

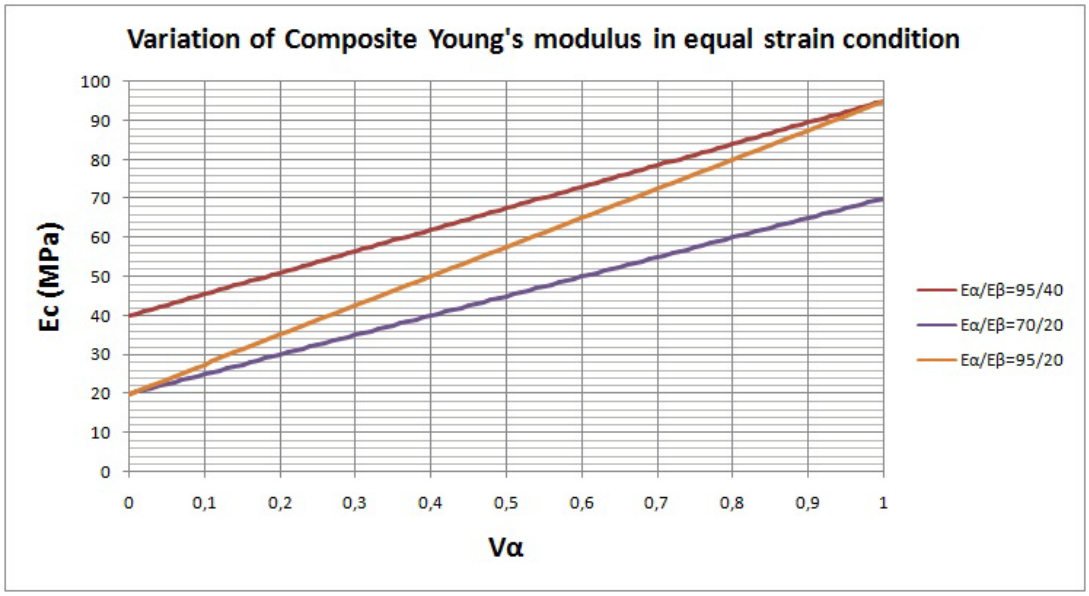

Fig. 3.8: Diagram of the E_c as a function of Vα and for three different values of EαEβ ratio. Note that even for low percentage of the stiffer laminae, the composite modulus increase notably. Eα and Eβ represent typical dynamic Young's modulus for chert and limestone.

This diagram is made using some of the most common values of dynamic Young's modulus characterizing limestone and chert samples (Schmidt, 1975; Lama and Vutukuri, 1978; Beauchamp and Purdy, 1986; West, 1994; Gross, 1995; Wyllie, D.C., 2005; Baldi et al. 2007). The diagram shows that the bigger the percentage of the stiffer laminae in the composite is, the more the composite tends to the stiffer modulus. The bigger the E_α/E_β ratio is, the more quickly the composite modulus increases (compare the two trends with $E_\alpha/E_\beta = 95/20$, and $E_\alpha/E_\beta = 70/20$). It is important to note that for lower values of V_α, the composite modulus increases notably: with V_α = 0.1 and $E_\alpha/E_\beta = 70/20$, the composite modulus is 25% bigger than the modulus characterizing only the matrix (i.e. only limestone) it increases from 20 MPa to 25 MPa; with V_α = 0.1 and $E_\alpha/E_\beta = 95/20$, the composite modulus is 40% bigger than limestone one, it increases from 20 MPa to 28 MPa.

Furthermore, it has been observed that mechanical properties (e.g. Young's modulus) of the composites depend on the orientation between stress and laminae direction (Raylance, 2008). For instance, it has been demonstrated that in unidirectional aligned laminae the Young's modulus drops rapidly for off-axis loading (Raylance, 2008).

In the discussion section, the behaviour of composites will be used in order to analyse geological evidences observed in the field.

3.4 Methods

In this work seven sites (road cuts exposures, quarries, and excavations for house foundations) have been analysed in the Cingoli anticline representing data in different structural settings of the fold structure (Fig. 3.1); outcrops in backlimb, hinge and forelimb have been studied, but whereas four sites are representative of the backlimb, just one and two are, respectively, located in the hinge and in the forelimb. The lack of sites in the hinge and in the forelimb was due to difficulties in finding good exposures within these two structural settings. In particular, the hinge corresponds to a topographic relief, which is usually characterized by rounded woods covered crests without outcrops or road-cuts. Some sites are characterized by more than one wall (e.g. site 1, 5 and 7), often oriented either perpendicular or parallel to the anticline axis (hence at right angle to each other) offering a 3D view of the fractures. Exposures of bedding surfaces are also present in site 1. In order to avoid additional local perturbation of stress, the studied sites are far away from major tectonic structures (large-displacement faults).

Fractures systems characterization have been made through different scales observations and presented through detailed mappings. Several line drawings have been made for each site at the macro- and mesoscale and the reported fractures have been accurately analysed in the field. Type of fractures (i.e. mode of fracture formation), attitude, orientation relative to bedding surfaces (high angle to bedding or low angle to bedding), mechanical confinement (stratabound or non-stratabound) and termination relationships represent the key data sets collected in the field. Some fractures have also been observed in thin-sections, cut perpendicular to the fracture trend, in order to better identify the mechanism and mode for their formation. We consider as high angle to bedding (HAB) those structures that form an angle with bedding greater than 75° (between 75° and 90°) and as low angle to bedding (LAB) those structures forming an angle to bedding smaller than 75°. This threshold angle was chosen on the basis of geomechanical considerations, which predict closure and opening fracture formations, respectively in the compressional and extensional quadrants, at 72° to a sheared discontinuity (i.e. flexural slip planes in this case) (Pollard and Aydin, 1988). Attitude data, expressed in degrees as dip direction/dip (e.g. 245°/30° to indicate that the fracture plane dips towards N245° with a dip angle of 30°), have been collected both through scanlines and from random measurements. Since the affiliation of fractures to a specific set was determined not only on the basis of fracture attitude (i.e. fracture parallelism) but considering also the mode of fracture formation, a first discrimination of fractures sets has been made directly in the field.

Stereonets showing lower hemisphere equal area projection of fractures poles have then confirmed the sets affiliations of fractures. Fig. 3.2 shows two geological profiles, which are parallel to the tectonic transport direction and crossing 6 of the 7 studied sites. Plotting the sites on the geological profiles it is possible to identify and compare the structural and stratigraphic position of the studied outcrops. Literature data, in particular attitude data provided by the *Regione Marche – Servizio Ambiente e Paesaggio* and the geological map at 1:50000 scale developed within the CARG Marche Project (Sheet 302 *Tolentino*), have been used for the geological profiles. However, to obtain a more homogeneous dataset along the structure and to clarify some relevant aspects to better constrain the outcropping stratigraphic succession, an original geological survey has been undertaken in particular along the calcareous outcropping succession. The north-eastern side of A-A' profile derives from Deiana et al. (2002) and Mazzoli et al. (2002) interpretation, whereas the carbonate side of A-A' profile and all B-B' profile derives from personal interpretation (Fig. 3.2). The software Move™ of the Midland Valley has been used to build up the geological cross sections.

In sites 4, 5 and 6 I have made some detailed stratigraphic logs to better characterize the thickness (and volumetric) proportion between chert and limestone beds.

Furthermore, X-ray powder diffraction analysis of three samples collected in site 5 have been made in order to compare materials present on bedding surfaces and on oblique to bedding structures with the (residual) hosting rock (i.e. limestone of the *Scaglia Bianca* Fm.) as to define the origin of these material.

3.5 Results

3.5.1 Backlimb

SITE 1: Site 1 is located in the backlimb of the *Cingoli* anticline, close to the *Panicali* locality (Fig. 3.1). Site 1 consists of two sub-vertical walls (outcrop T1 and T2) oriented at right angles to each other, and approximately perpendicular and parallel to the *Cingoli* anticline axis. Site 1 also includes a bedding-parallel pavement which has been studied to better understand the three-dimensional distribution of fractures. The T1 outcrop is oriented SW-NE, approximately 30 m-long, and 3 m-high. The T2 outcrop is NW-SE oriented, about 15 m-long, and 1.5 m-high. The dimensions of the bedding-parallel pavement are 30 by 40 cm.

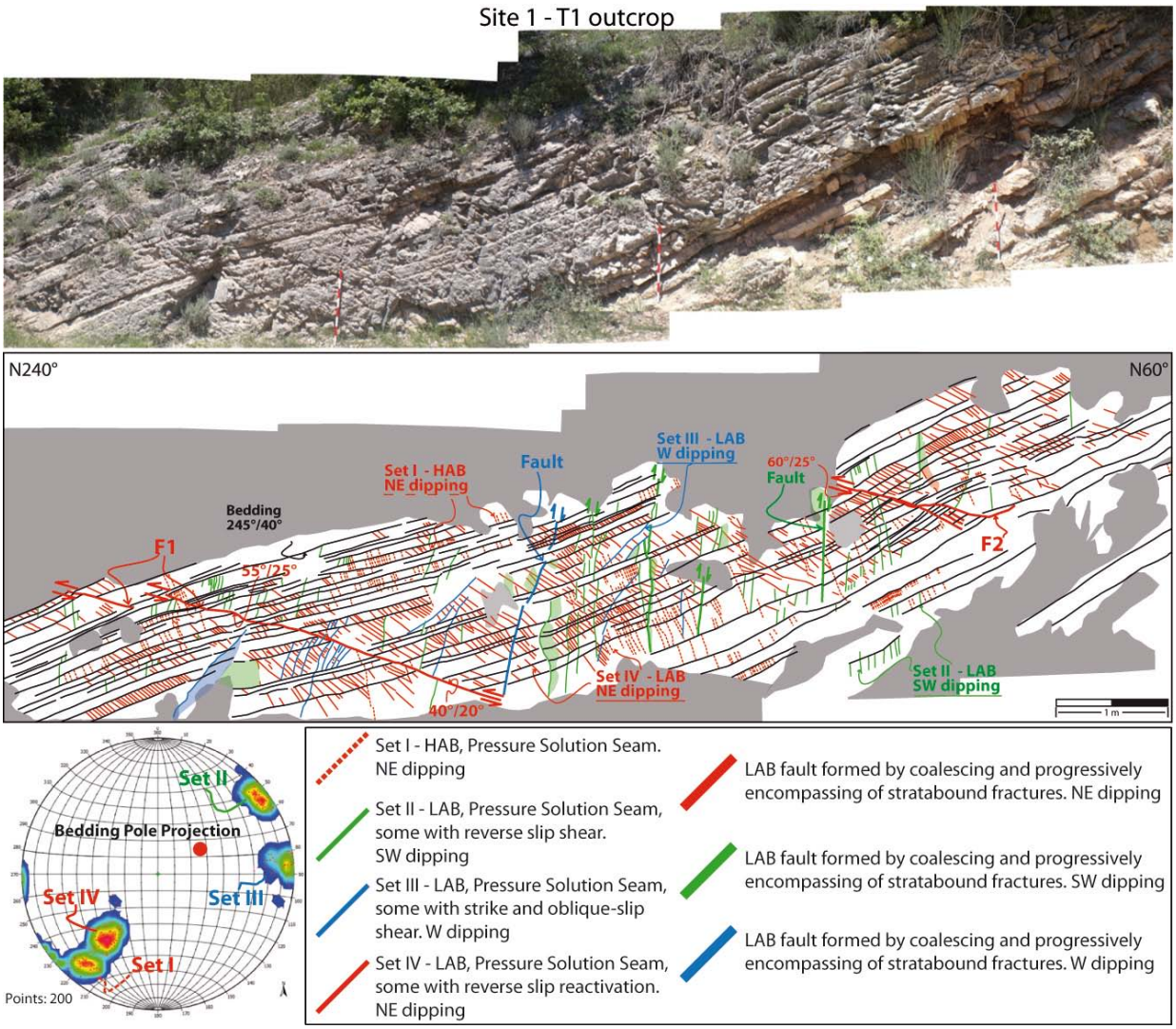

Fig. 3.9: Photomosaic and related line drawing of T1 outcrop in site 1. Note lower hemisphere equal area projection of PSSs poles. Four sets of pressure solution seams (PSSs) characterize the outcrop whereas no mode I fractures sets (or at least so persistent and quantitatively important) have been observed. Note two reverse NE-dipping faults (F1 and F2) cutting through the fractured strata. Attitude data are expressed in dip azimuth/dip form; HAB: high angle to bedding; LAB: low angle to bedding.

The outcrops of site 1 show the upper part of the *Scaglia Rossa* Fm., which is here characterized by thinly-bedded reddish limestones and marly limestones without chert, and by a clay content higher than in the lower portion of this formation (Figs. 3.9 and 3.10). Bedding

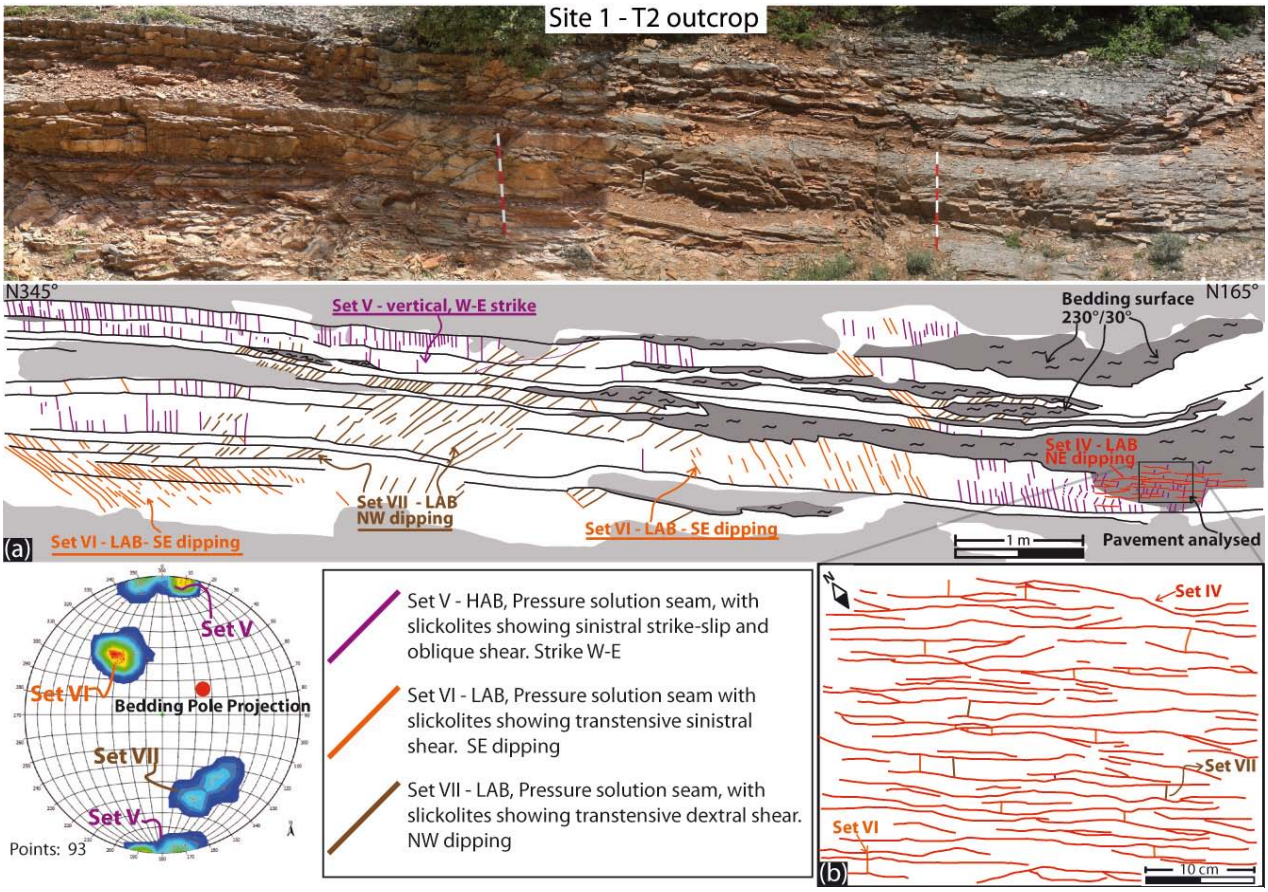

Fig. 3. 10: : (a) Photomosaic and related line drawings of the T2 outcrop in site 1. Note lower hemisphere equal area projection of PSSs poles. Three sets of pressure solution seams (PSSs) characterize the outcrop whereas no mode I fractures sets (or at least so persistent and quantitatively important) have been observed. (b) Fracture mapping on a small portion of a bed-parallel pavement 30 by 40 cm. Attitude data are expressed in dip azimuth/dip form; HAB: high angle to bedding; LAB: low angle to bedding.

surfaces are defined by PSSs with a mean orientation of 235°/30°. Carbonate beds are generally 10-50 cm thick; thinner (up to 5 cm thick) layers of marls and marly limestones are also present at different levels. Slickenlines and other kinematic markers present on several bedding surfaces, particularly where marl interlayers occur, are consistent with a flexural slip mainly along a NE-SW trend.

The T1 and T2 outcrops are characterized by strata-bound PSSs spaced between 1 and 10 cm (i.e. this spacing refers to the distance between two adjacent fractures pertaining to the same set) whereas there is not a significant presence of mode I fractures. Marl layers constitute the mechanical discontinuity against which all PSSs sets abut. When these layers are absent, some PSSs cut across the bedding surfaces. A few longer through-going faults are also exposed along the T1 outcrop (Fig. 3.9).

Fracture sets are described below following a temporal criterion (from the oldest to the youngest sets), which was determined by careful observation of their abutting and crosscutting relationships. In the T1 outcrop, we recognized four main sets of fractures (Figs. 3.9 and Fig. 3.11):

Set I: Set I is characterized by HAB (85°-90°) PSSs with toothed surfaces, iron oxides stains and clay residues. Field and thin-section observations show clear evidence of dissolution along these surfaces (Fig. 3.11a-d). The stylolite peaks are generally perpendicular to the PSSs planes (Fig. 3.11b and d), which are mostly stratabound and with a mean attitude of 39°/72° (see stereonet in Fig. 3.9). PSSs of Set I do not show evidence of shear displacement (Fig. 3.11a) and usually have their tips right along the bedding surfaces, particularly along the contact between carbonate beds and the thin marl layers.

Set II: Fractures of this set consist of LAB (55°) PSSs (Fig. 3.11e-h), with a mean attitude of 234°/84° (see stereonet in Fig. 3.9). Some of these PSSs abut or veer towards those of Set I (Fig. 3.12c), indicating that Set I is older than Set II. Exceptions to this rule are occasionally observed (Fig. 3.12c). Fractures of Set II do not generally show evidence of shear displacement except in a few cases, where some dip-slip reverse (or sub-vertical) offsets were observed (Fig. 3.11f).

Set III: This set is formed by LAB (<60°) PSSs, oriented 270°/77°. Some of these surfaces show evidence of younger left-lateral strike-slip offsets (Fig. 3.11i and j). For this reason, some fractures of Set III cut across bedding surfaces and are generally longer than most stratabound fractures forming the background fabric of the T1 outcrop. Fractures of Set III are not as well developed as fractures of other sets occurring in the T1 outcrop.

Set IV: Fractures of this set are the most frequent and pervasive in the T1 outcrop (Fig. 3.9). They consist of LAB (c. 60°) PSSs (Fig. 3.11k, m and n), which are generally strata-bound and with a mean attitude of 40°/38°. Field and thin-section observations show that stylolite peaks are perpendicular to the PSSs surfaces. Occasionally, these fractures show evidence of dip-slip reverse offsets (Fig. 3.11l). Fractures of Set IV normally terminate against or veer towards fractures of Set I, Set II, and Set III (Fig. 3.12).

The T1 outcrop exposes two reverse, LAB faults that cut through the fractured carbonate beds (see F1 and F2 in Fig. 3.9). The F1 and F2 faults are roughly parallel to Set IV, and characterized by an offset of between 10 and 20 cm. Slickenlines along these faults show dip-slip kinematics nearly parallel to the outcrop and indicate, together with other kinematic indicators, a reverse sense of motion. The two fault zones consist of a segmented slip surface surrounded by a damage zone as thick as 10 cm, containing fractures and, in places, coarse

breccia. Small, sub-vertical, LAB faults further deform the rock volume between the F1 and F2 faults. These minor faults strike parallel to fractures of Set II, and are characterized by offsets smaller than 5 cm.

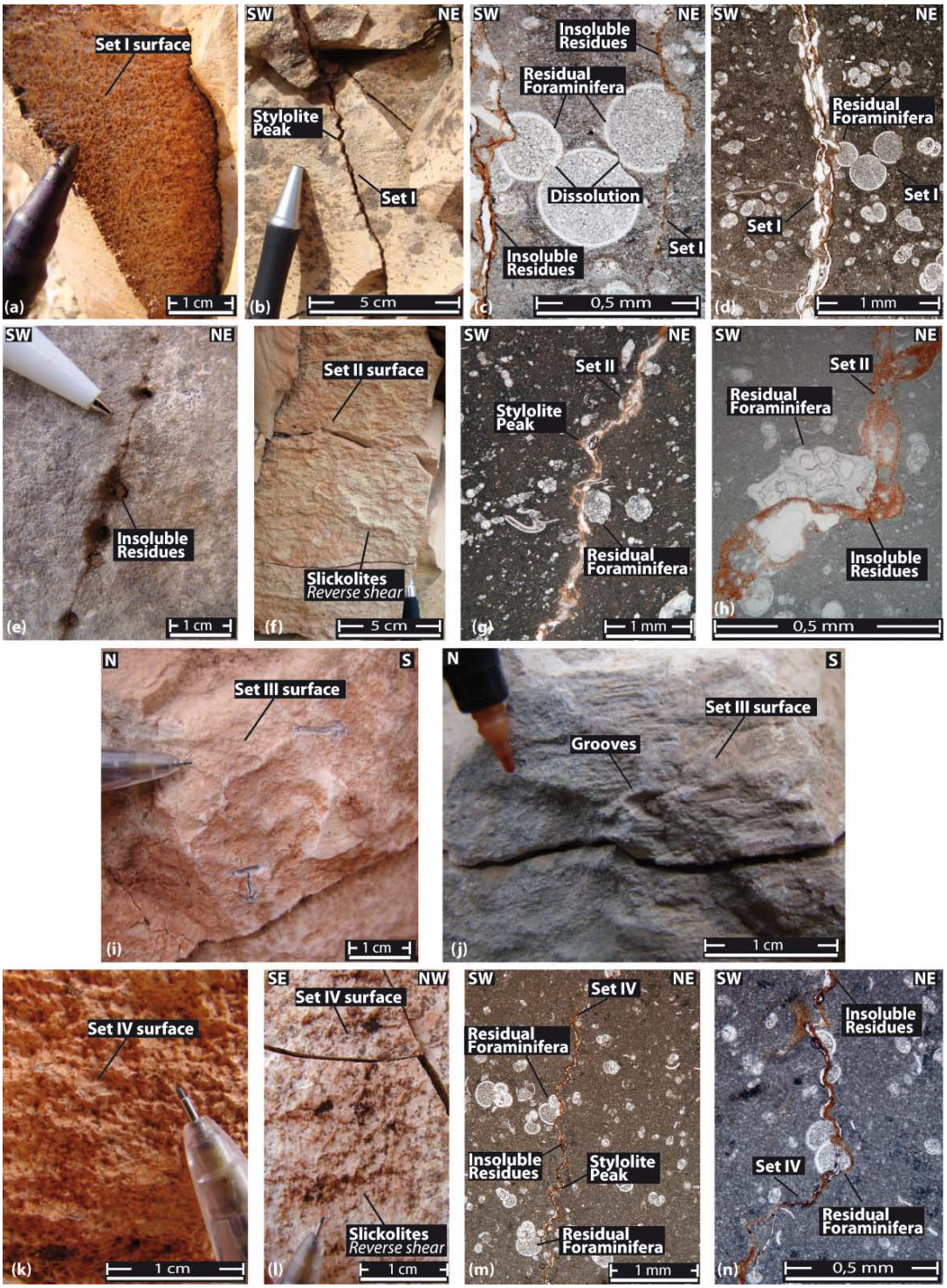

Fig. 3.11: Microscopic and mesoscopic photographs of PSSs from Set I, Set II, Set III, and Set IV. (a) Pressure solution seam (PSS) surface of Set I. Set I surfaces are usually characterized by clay residues and by peaks normal to the pressure solution plane. (b) Set I PSS profile showing stylolite peaks. (c) and (d) Set I PSSs (thin-sections) accompanied by partially dissolved shells belonging to planktonic foraminifera. (e) Set II PSS profile accompanied by insoluble residues. (f) Set II PSS surface characterized by slickolites consistent with a reverse dip-slip displacement. (g) and (h) Set II PSSs (thin-sections) with partially dissolved shells belonging to planktonic Foraminifera. (i) and (j) Set III surfaces. This set is generally characterized by PSSs with smooth peaks and, more often, with slickolites and grooves showing a left-lateral strike-slip offset. (k) Set IV PSS surface. Set IV surfaces are usually characterized by clay residues and by perpendicular stylolite peaks. (l) Set II PSS surface characterized by slickolites consistent with a reverse dip-slip offset. (m) and (n) Set II PSSs (thin-sections) accompanied by partially dissolved shells belonging to planktonic Foraminifera.

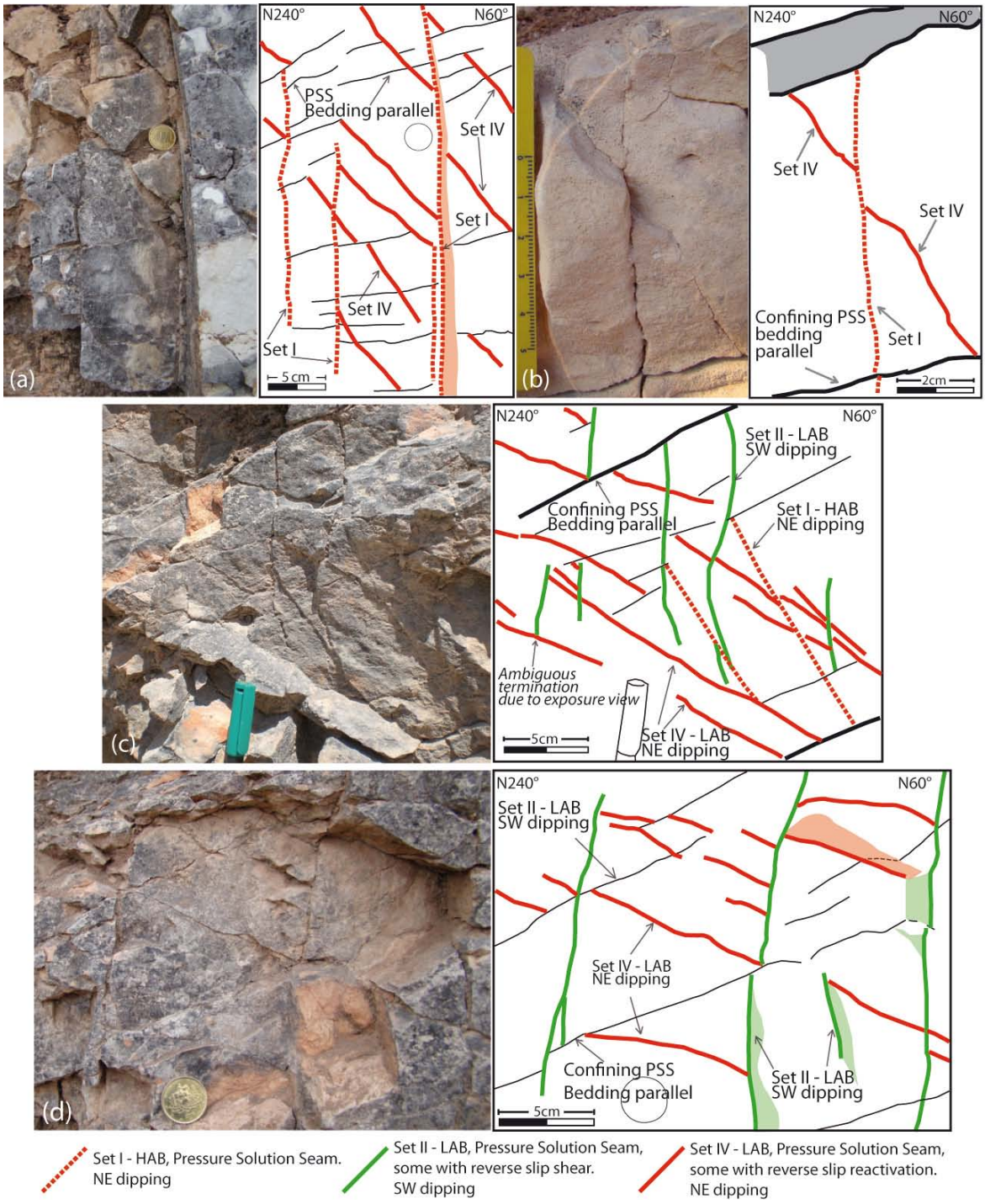

Fig. 3.12: Photographs and related line drawings showing crosscutting and abutting relationships among the most pervasive pressure solution seams (PSSs) of the T1 outcrop in site 1. (a) and (b) PSSs of Set IV terminating against PSSs of Set I. (c) PSSs of Set IV terminating against PSSs of Set I and Set II. Note also that two PSSs of Set II terminate against PSSs of Set I. (d) PSSs of Set IV terminating against PSSs of Set II. HAB: high angle to bedding; LAB: low angle to bedding.

In the T2 outcrop, we recognized three main sets of fractures (Fig. 3.10):

Set V: This set is formed by strata-bound, sub-vertical, HAB, E-W striking PSSs (Fig. 3.13a). Only a few of these PSSs cut through the bedding. Fractures of Set V show slightly toothed surfaces, with iron oxides and clay residues. Some of these surfaces (the ones that are non-strata-bound) are characterized by left-lateral oblique- to strike-slip small offsets (Fig. 3.13b).

Sets VI and VII: These sets consist of LAB PSSs but with important shear features; they are oriented respectively 145°/45° and 328°/54°, hence nearly perpendicular to the fold axis (see stereonet in Fig. 3.10). These PSSs are strata-bound and generally characterized by wrinkled surfaces and clay residues (Fig. 3.13c and e). Sets VI and VII show frequent evidence of transtensional kinematics (Fig. 3.13d and f).

A small bedding-parallel pavement located at the base of the T2 outcrop (Fig. 3.10) documents the abutting relationships between fracture sets. This pavement shows that fractures of Sets VI and VII are confined by the longer fractures of Set IV, which is, therefore, older than Sets VI and VII (Fig. 3.10b).

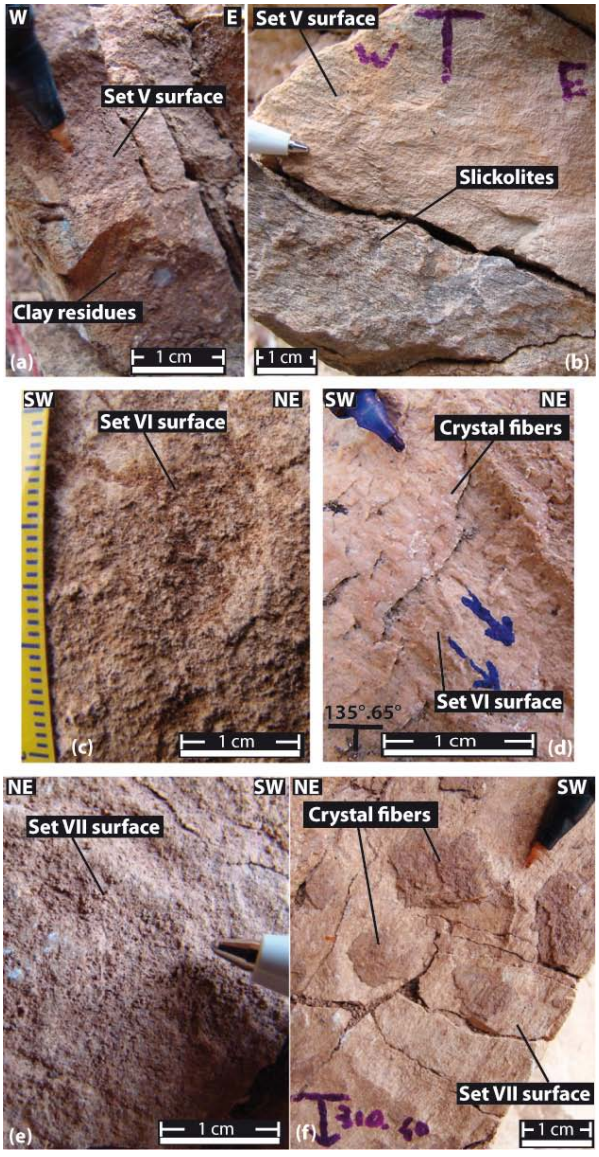

Fig. 3.13: Mesoscopic photographs at different scales of fractures from Sets V, VI, and VII. (a) Pressure solution seam (PSS) from Set V. Set V surfaces are usually characterized by clay residues and by smooth perpendicular stylolite peaks. (b) PSS surface from Set V showing slickolites consistent with transtensive offset. (c) PSS surface from Set VI. (d) Surface from Set VI characterized by crystal (calcite) fibers consistent with a left-lateral transtensive offset. (e) PSS surface from Set VII. (d) Surface from Set VII characterized by crystal (calcite) fibers and grooves consistent with a right-lateral transtensive offset.

SITE 2: Site 2 is located close to the *Castriccioni* Lake in the north of the *Cingoli* anticline (Fig. 3.1) and it is characterized by a SW-NE oriented wall (Fig. 3.14). Site 2 exposes the *Scaglia Rossa* Fm. which is here characterized by reddish limestones with thicker beds compared to the *Scaglia* Fm. of site 1. The carbonates beds are from 0.1 to 1 m in thickness and there are not marl or chert levels. The bedding surfaces usually coincide with PSSs associated with thin and nodular remnants of dissolved limestones. The bedding orientation measured in site 2 is 230°/30°, which is approximately parallel (the bedding strike) to the *Cingoli* anticline axis. Slickenlines and other kinematic markers present over several bedding surfaces show that bedding underwent to flexural slip along the NE-SW trend.

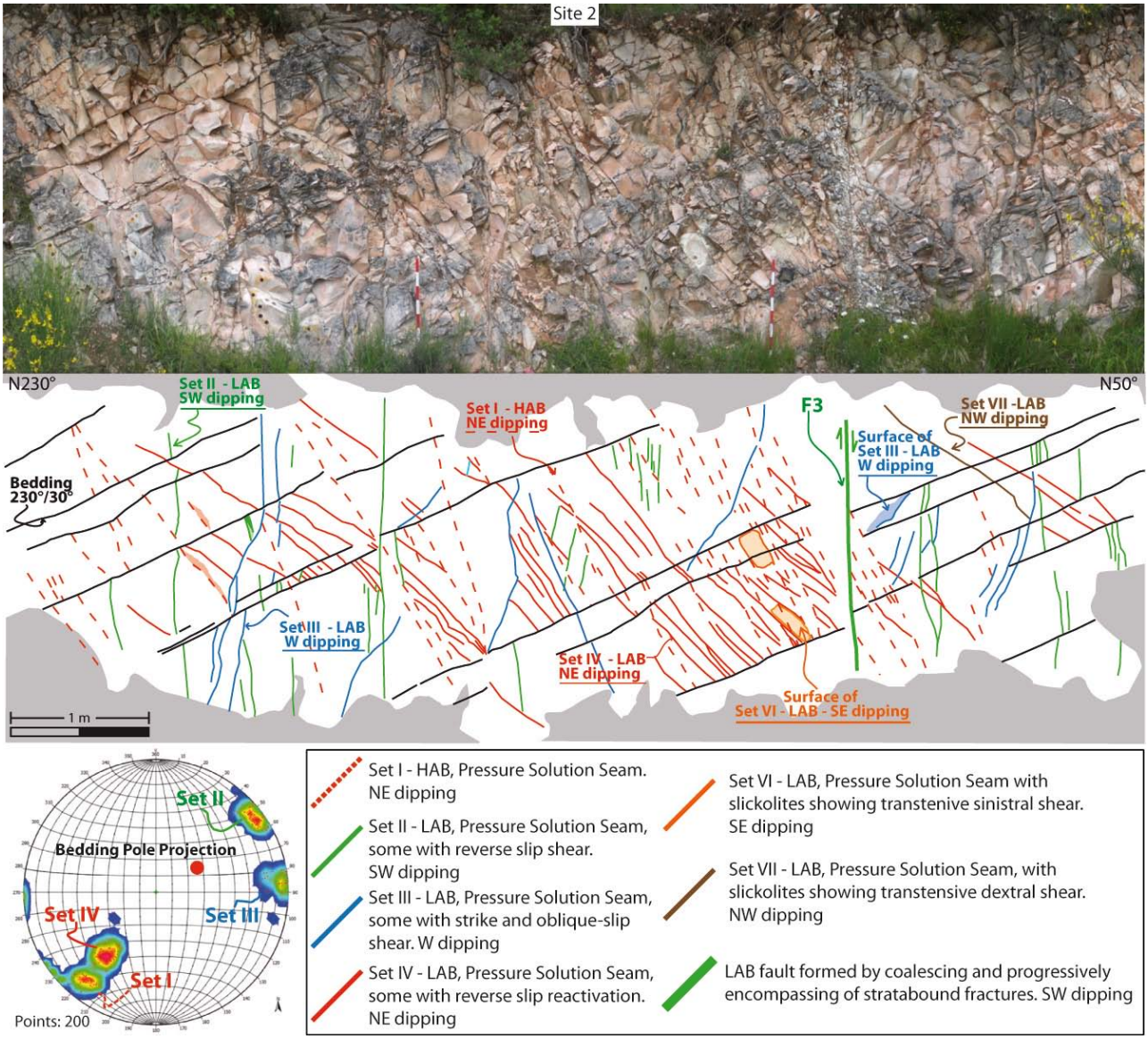

Fig. 3.14: Photomosaic and related line drawing of site 2. Note lower hemisphere equal area projection of PSSs poles. The outcrop shows Pressure Solution Seams (PSSs) similar to those observed in site 1. PSSs of Sets I, II, III, and IV have been mapped. Note, on the right side, the presence of a sub-vertical fault (F3) cutting through the fractured carbonate strata. Attitude data are expressed in dip azimuth/dip form; HAB: high angle to bedding; LAB: low angle to bedding.

As observed in site 1, this studied area does not show mode I fractures but it is prevalently characterized by PSSs pertaining to Sets I, II, III, and IV observed in site 1 (Fig. 3.14). Fractures of Sets V, VI, and VII are also present, but poorly exposed, because of their orientation parallel to the studied wall. In particular, site 2 is intensely deformed by PSSs of Set IV, whereas PSSs of Sets I, II, and III are less common. PSSs of Set IV are strata-bound, LAB, and usually confined by PSSs of Sets I, II, and III. PSSs of Set I and II are rare. It is interesting to note, however, that some PSSs of Set II are non-strata-bound, longer than most fractures observed in the outcrop, and characterized by evidence of dip-slip shear offset. Similarly, to what happens for Set II, also PSSs of Set III are poorly developed in the T3 outcrop and they are often characterized by evidence of dip-slip shear offset (Fig. 3.14).

On the northeastern side of the T3 outcrop, a 220°/88° oriented sub-vertical fault occurs (see F3 in Fig. 3.14). Slickenlines are dip-slip (pitch angle is about 90°) along the fault plane and kinematic indicators indicate a sub-vertical reverse offset of about 12 cm. The F3 fault surface is rather continuous for a length of almost 2 m (except in the upper portion) and it is characterized by the absence of a fault core.

SITE 3: Site 3 is located along an unpaved road between the town of *Cingoli* and the *Panicali* locality (Fig. 3.1). This road is flanked by a 3 m-high wall of *Scaglia Rossa* Fm. and several E-W oriented portions of the outcrop have been analysed (Fig. 3.15). The site shows highly fractured whitish micritic limestone of the *Scaglia Rossa* Fm. with bed surfaces characterized by PSSs with a very thin residual material on it (<1 mm). The mean attitude of the bedding surface is 250°/30°. In this site, the *Scaglia Rossa* Fm. does not contain chert or marly beds and it appears more massive and stiffer compared to what observed in particular in site 1. The walls are characterized by a frequent repetition of continuous and discontinuos bedding parallel PSSs. These PSSs are in same case the mechanical confinement boundary for all the other structures observed in the site but sometimes they seem subsequent to structures at HAB (compare Fig. 3.15b with c). Where visible, the limestone beds are from 5 to 20 cm in thickness. The studied walls are mainly characterized by HAB fractures, both strata- and non-strata-bound, and by some LAB sets of fractures. It has been difficult, in this site, to define the mechanical type of fractures but many of the fractures look like PSSs and slickolites. In particular, the wall are strongly deformed by the presence of HAB, strata- and non-strata-bound fractures with a mean attitude of 55°/63° (PSS1 Set). The faces of the PSS1 set do not show well-developed stylolites but they are wrinkled with iron oxides residues. These PSSs are generally bed-confined (Fig.

3.15c) but in some portion of the outcrop they are very long and without strata-confinement (Fig. 3.15a and b). Some of the fractures of PSS1 set show reverse motion.

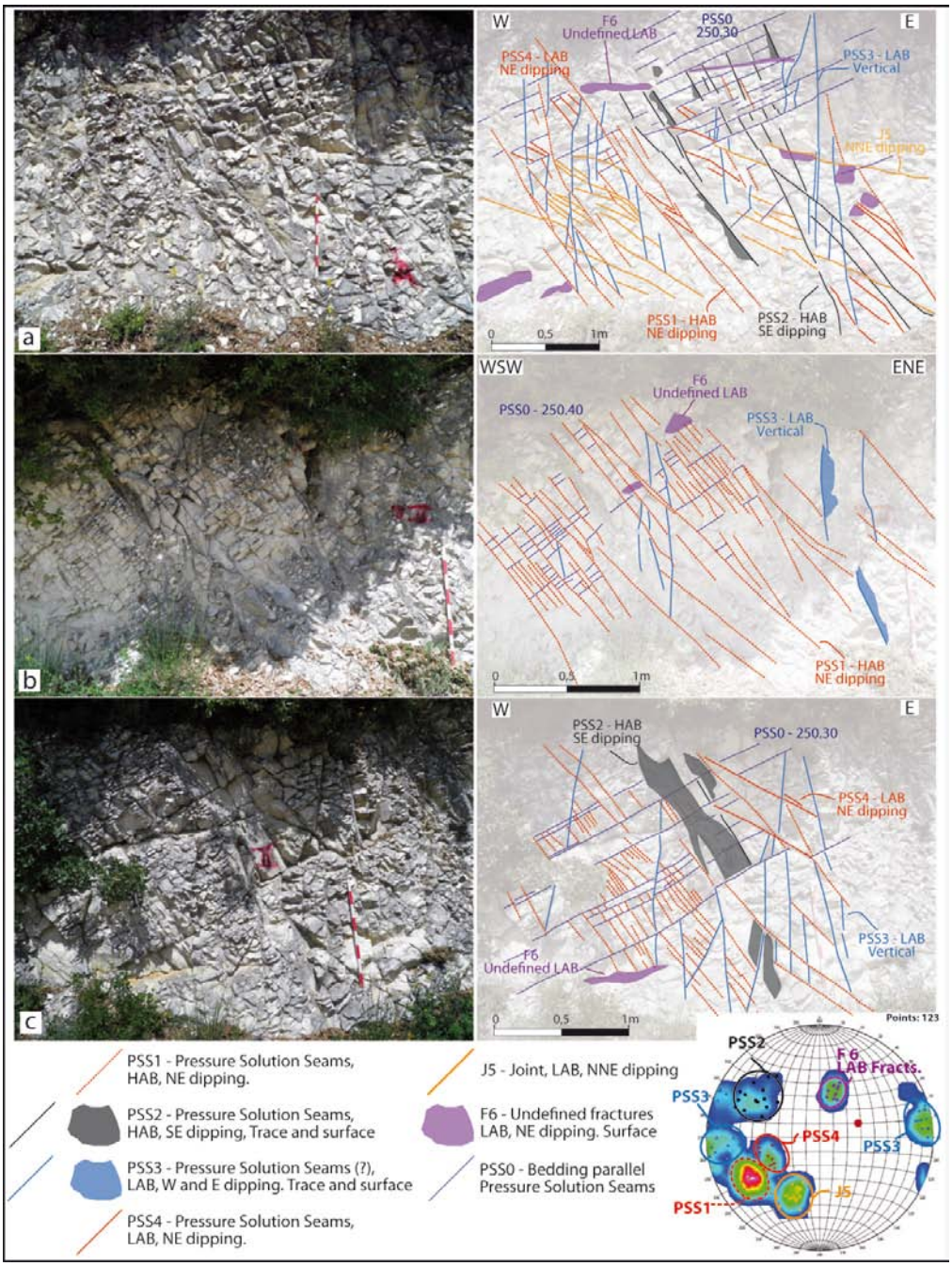

Fig. 3.15: Photographs and related line drawings of site 3 showing the principal sets of fractures. Note stereonets - lower hemisphere equal area projection of fractures poles. Site 3 is characterized by micritic limestones without chert and marly layers. Bedding parallel PSSs act as weak mechanical confinement surfaces hence an intense non-stratabound fracturing, characterized by PSSs both HAB and LAB, involves the walls. (a) The HAB PSS1 and PSS2 sets are non-stratabound but sometimes they abut against bedding parallel surfaces. LAB sets of fractures generally abut against PSS1 and PSS2 sets. (b) Bedding parallel PSSs are sometimes confined between fractures of PSS1 set which is generally non-stratabound. (c) When the bedding surfaces are well developed, PSS1 set is characterized by stratabound fractures.

The PSS2 set is formed by other HAB PSSs with a mean attitude of 120°/57°. They are not frequent as the PSS1 set of fractures and they are both strata- and non-stratabound. Some of these fractures show strike-slip and dextral transtensive movement. Site 3 is characterized even by LAB sets (Fig. 3.15): PSS3 set are vertical, N-S oriented, and they are generally observed in all walls of the exposure. It is difficult to ascertain accurately their mechanical type but their faces show evidence of pressure solution processes. These fractures are non-stratabound but sometimes abut against bedding parallel PSSs, and on PSS1 and PSS2 set fractures (Figs. 3.15 and 3.16).

PSS4 set are LAB, strata- and non-strata-bound PSSs with a mean attitude of 70°/40°. They abut against the PSS3 set and they are not so frequent (Figs. 3.15 and Fig. 3.16b).

Joints of J5 set are generally confined between fractures of PSS1, PSS2 and PSS3 sets but sometimes they can cut through these sets. They have a general attitude of 24°/50° and sometimes they show dip-slip movement (Fig. 3.16a and b).

Finally, site 3 is characterized by very LAB surfaces formed by undefined fractures types showing an intense fluid flow circulation observed through a reddish patina probably due to oxidation phenomena. These fractures (F6) show a mean attitude of 200°/36°.

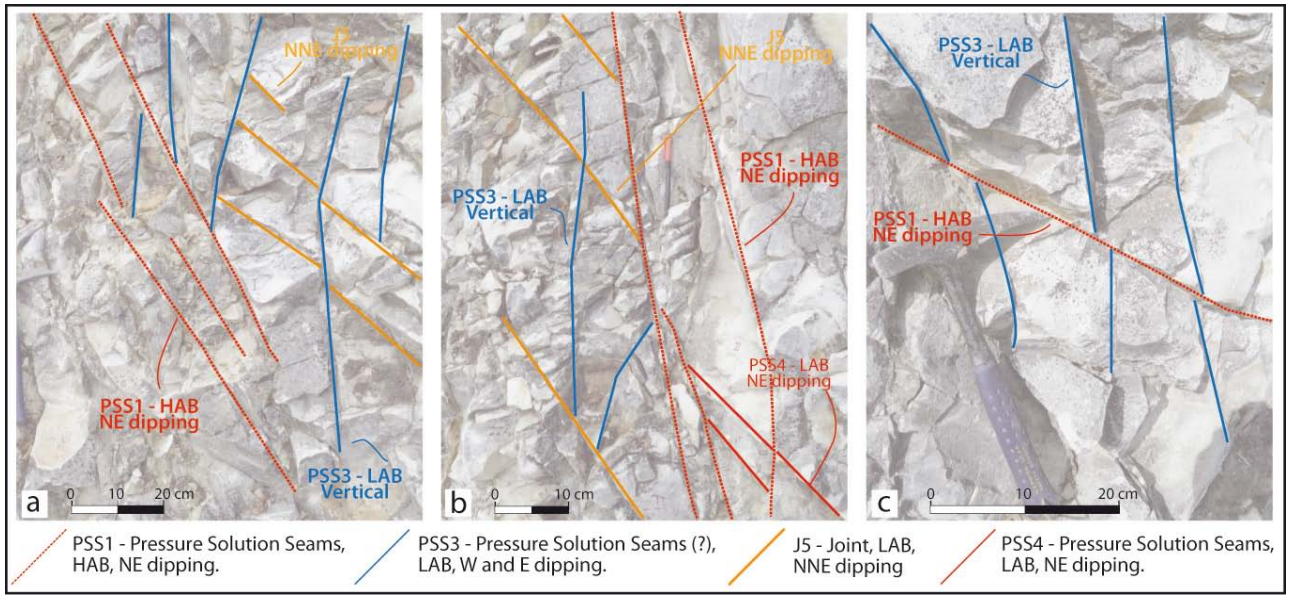

Fig. 3.16: : Close-up photographs and related line drawings of site 3 showing the reciprocal crosscutting relationship between some fractures sets.

SITE 4: Site 4 is the southernmost outcrop studied along the *Cingoli* anticline and it is located SW with respect to the core of the anticline (Fig. 3.1). Site 4 is in a small quarry with a NS oriented wall, approximately 80 m-long, and with a short northern side perpendicular to the longer one (Fig. 3.17a). *Scaglia* Fms. and the black shales of the *Bonarelli* level outcrop in site 4 (Fig. 3.17a and b). The upper Cenomanian bituminous shales are 1 m in thickness and they crop out only in the northern side of the quarry. White and light reddish thinly bedded micritic limestones with grey chert layers (*Sc. Bianca* Fm.) characterize the outcrop up to 10 m above the *Bonarelli* black shale (Fig. 3.17c). The upper part of the quarry is made up of reddish thinly bedded micritic limestone with reddish chert layers of the *Scaglia Rossa* Fm. (Fig. 3.17d).

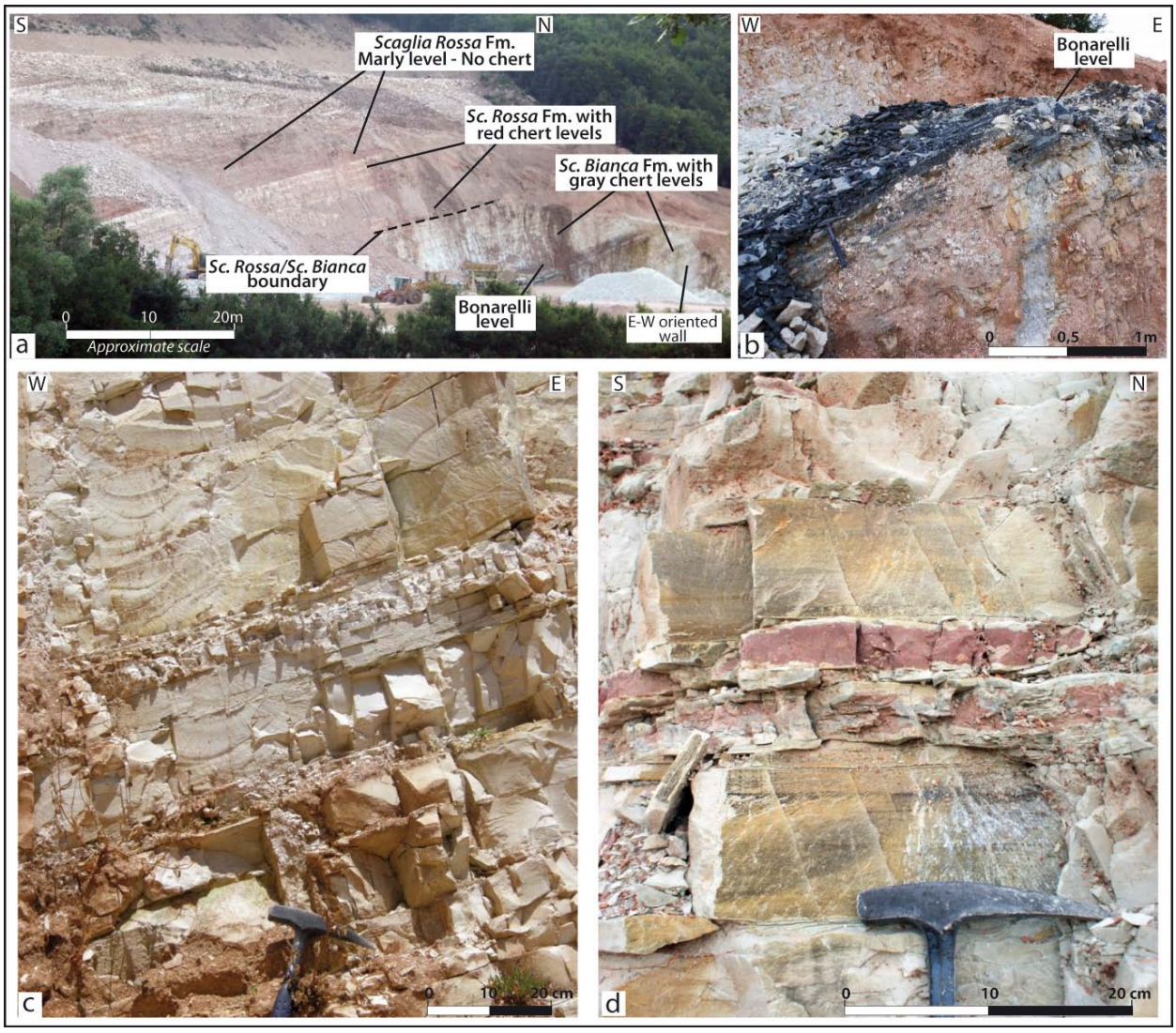

Fig. 3.17: (a) Photograph of site 4. The studied area is within a quarry and it is located to SW respect to the core anticline. The site is characterized by NS oriented wall, 80 m long, and by a E-W oriented smaller wall in the north side. The outcrop is characterized by micritic limestones with grey chert layers of the Scaglia Bianca Fm., where the Bonarelli level crops out, and by the micritic limestone with reddish chert of the Scaglia Rossa Fm. Furthermore the upper part of the Scaglia Rossa Fm. is without chert layers and it is characterized by thin marl levels. (b) Photograph of the Bonarelli level within the Scaglia Bianca Fm. characteristic of the Upper Cenomanian. (c) Photograph of the Scaglia Bianca Fm. with thinly bedded micritic limestones with grey chert layers (d) Photograph of the Scaglia Rossa Fm. with thinly bedded micritic limestones with reddish chert layers.

Note that the distinction between *Scaglia Rossa* and *Scaglia Bianca* Fms. has been made only according to the chert colour: reddish chert characterizes the *Scaglia Rossa* Fm., whereas grey/black/dark-blue colours are typical of the *Scaglia Bianca* Fm. Bed surfaces have a mean attitude of 245°/30°and they are generally characterized by PSSs sometimes with a very thin residual material (<1 mm), probably clay. The carbonate beds are from 2 to 20 cm in thickness (Fig. 3.17c and d). In this outcrop the *Scaglia* Fms. do not show marly levels with the exception for the higher part of the wall where micritic carbonate layers alternate with thin schist-like marl layers and where there are no chert levels (Fig. 3.18a). Three stratigraphic logs made within the *Scaglia Rossa* Fm. with chert layers show that the chert represents 11% of the total thickness (Fig. 3.19).

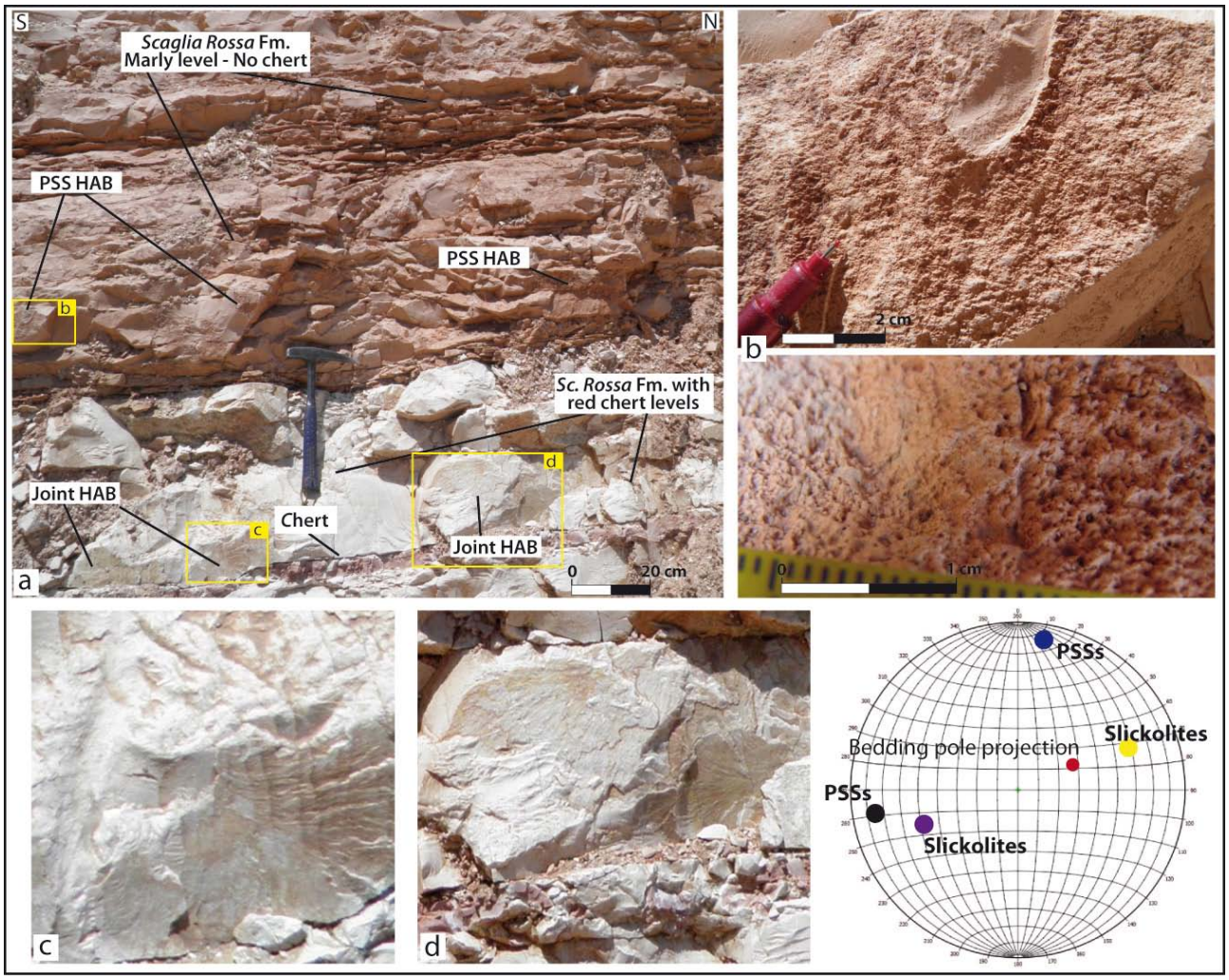

Fig. 3.18: (a) Close-up photograph in site 4 of the boundary between the Scaglia Rossa Fm. with chert layers (the lower portion) and the schistose-like marl layers without chert (the upper portion). Note the presence of joints in the cherty Scaglia Rossa Fm. and of PSSs in the marly portion. The PSSs are almost parallel to the joints in the lower part. (b) Two close-up photographs of the PSSs characterizing the Scaglia Rossa Fm. with marl layers. (c) and (d) Two close-up photographs of the joints characterizing the Scaglia Rossa Fm. with chert layers. Note stereonets - lower hemisphere equal area projection of fractures poles - only for the marly Scaglia Rossa Fm. Note that the stereonet for the marly portion is only representative of few structures observed.

The fracture systems characterizing the *Scaglia Bianca* and *Rossa* Fms. with chert layers are similar. The two formations are characterized by mainly mode I fractures (i.e. joints and veins) and subordinately by slickolites (Fig. 3.20). In particular this site is characterized by two persistent sets of joints: the J1 set is formed by HAB strata-bound joints with mean attitude of 70°/72° (Fig. 3.20a-c); the J2 set is characterized by HAB strata-bound joints and veins with mean attitude of 165°/87° (Fig. 3.20c-e). Hence, J1 and J2 sets are respectively parallel and perpendicular to bedding strike. The J1 set does not show shear and the fractures faces show clear evidences of mode I opening with hackle and rib marks, plumose structures and manganese dendrites (Fig. 3.20a-c). The J2 set shows the distinctive elements of mode I fractures (i.e. hackle and rib marks) but some of these joints show a subsequent reactivation with an oblique sinistral (with normal component) shear as shown by slickenlines (i.e. calcite fibers and grooves; Fig. 3.20d-e). Some of the fractures belonging to this set are even represented by veins (Fig. 3.20c). It has not been observed a well defined cross-cutting relationship between J1 and J2 sets: fractures of these sets reciprocally abut or cross-cut each other showing in this way a configuration similar to that one described in Caputo (1995) and called “fracture grid-lock” (see also Hancock et al., 1987). Note that site 4 does not show any wide bedding parallel surface and the cross-cutting relationships between J1 and J2 sets have been made on vertical exposures, it is hence possible that the observation made before (i.e. the “fracture grid-lock” feature of J1 and J2 sets) could be misleading. These two sets are the most pervasive fractures observed in site 4 and their spacing is from 2 to 5 cm. Other secondary fractures have been recognized in the portion of the quarry with *Scaglia* Fms. with chert layers and they can be divided in other three sets: LAB strata-bound veins (i.e. V3 set) with mean attitude of 210°/70° (Fig. 3.20f); HAB dextral transtensive slickolites (S4) with mean attitude of 66°/50° (Fig. 3.20g and h); and sub-vertical veins (V5 set) with mean attitude of 110°/86°, which always abut against S4 set faces (Fig. 3.20g). Note that in the unrotated stereonet the fractures of S4 set appears as LAB but rotating horizontally the bedding plane these slickolites appear as HAB, furthermore, it is not clear their sense of motion, it seems that they underwent to a reverse or dextral transpressive sense.

On the contrary the *Scaglia Rossa* Fm. with schist-like marl layers and without chert (i.e. the higher portion of the quarry) does not show the same intensive jointing observed in the lower part of the *Scaglia* Fms. with chert. This portion of the outcrop shows evidences of PSSs and slickolites both HAB and LAB (Fig. 3.18b). Due to the difficulties to reach the outcrop, it has been impossible to make an accurate analyses of this portion of the quarry, thus the data

should be considered not representative of all fractures outcropping. After rotating the bedding plane to the horizontal, two sets of fractures HAB can be distinguished: the PSSs with mean attitude of 80°/75° and almost parallel to the J1 set, and the slickolites at 70°/50°parallel to the S4 slickolites in the lower portion of the quarry (see stereonets in Fig. 3.18). Furthermore, this part of the quarry shows other HAB PSSs dipping towards S and few LAB slickolites at 250°/60° (see stereonets in Fig. 3.18). Some mode I fractures are still recognizable but, compared with the lower part of *Scaglia* Fms., they are rare and not so persistent.

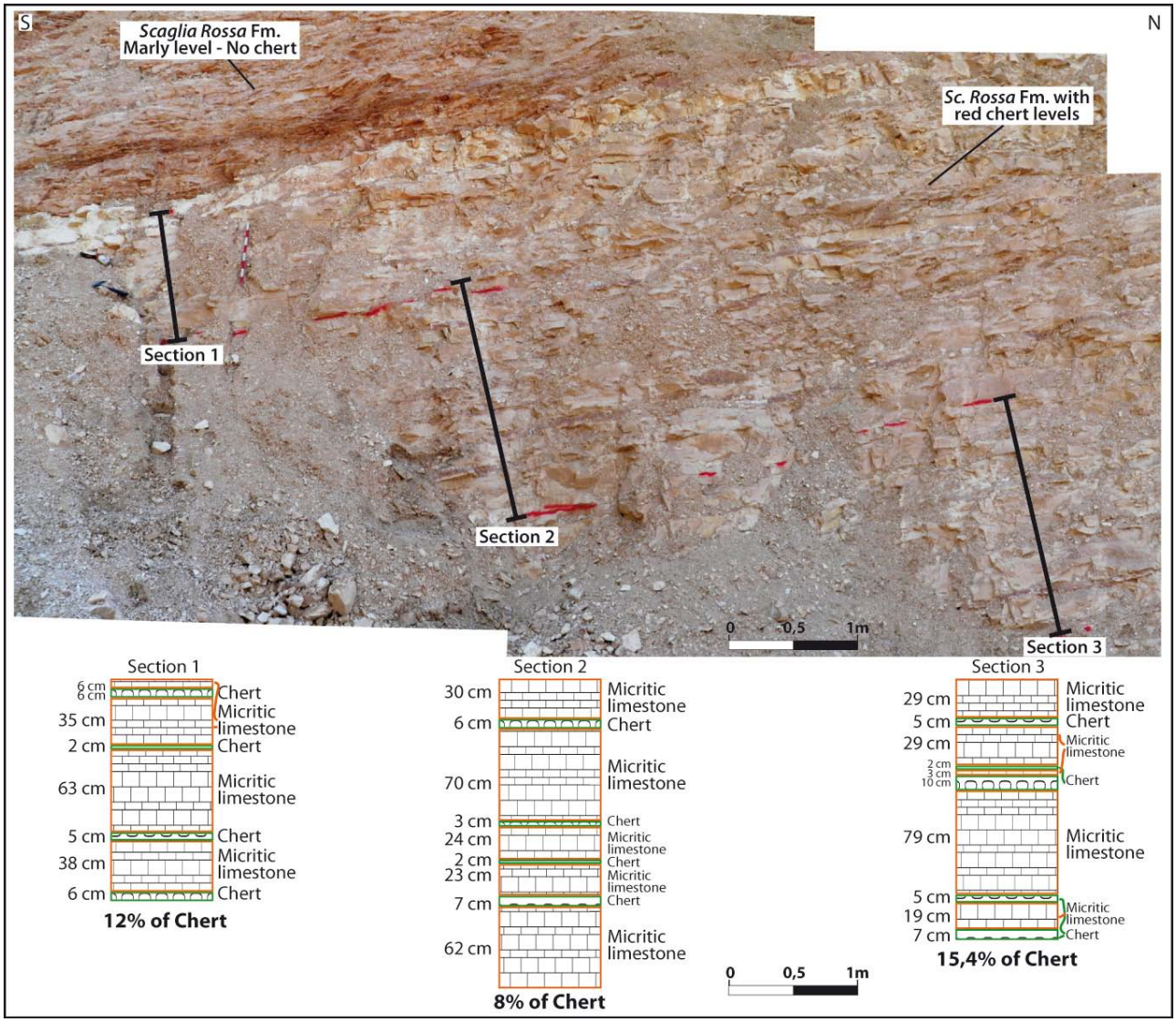

Fig. 3.19: Photograph and related stratigraphic sections measured on the NS oriented wall of site 4. The chert layers represent the 11% of the total thickness.

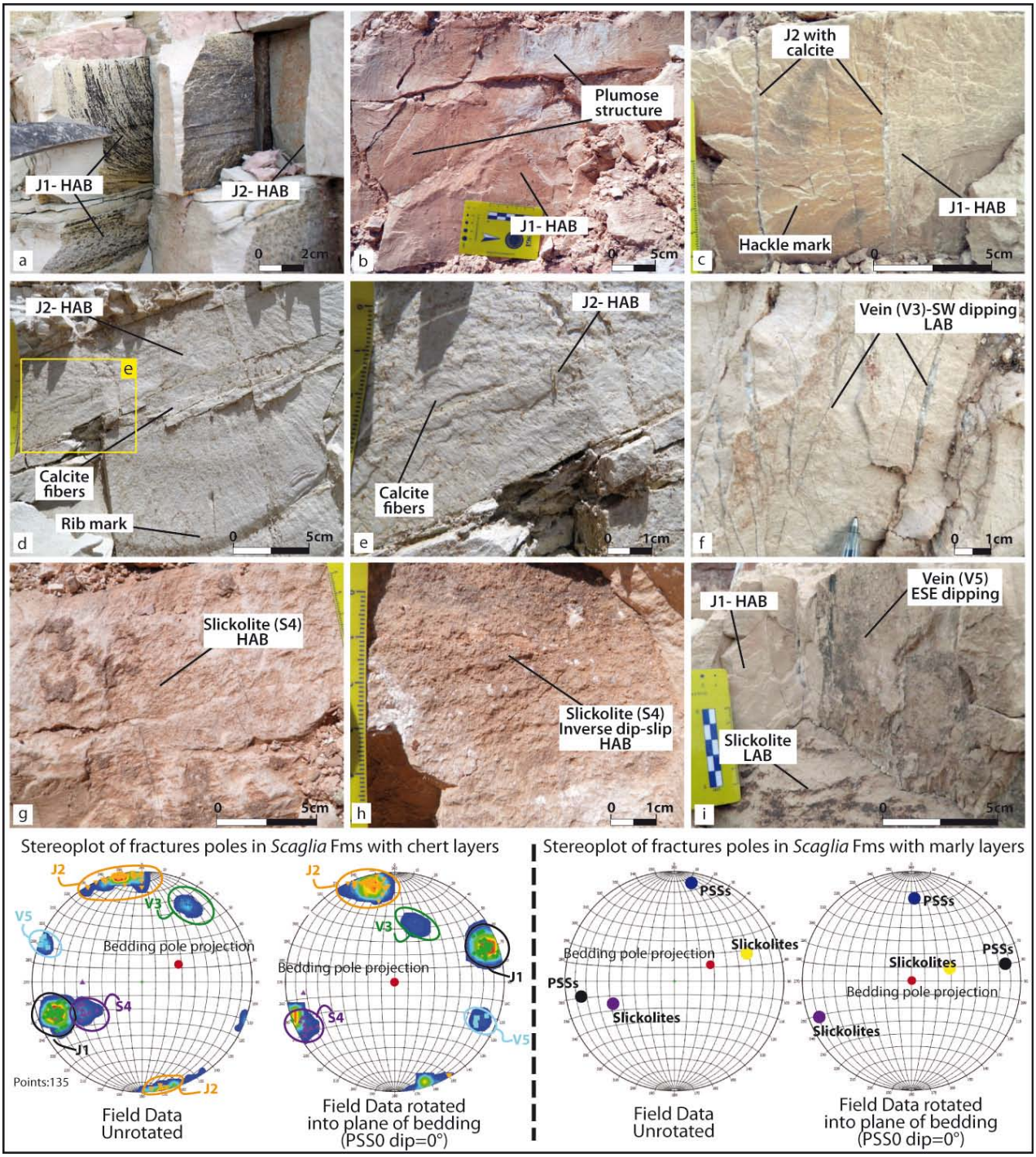

Fig. 3.20: Mesoscopic photographs of the structures observed in site 4. Note stereonets - lower hemisphere equal area projection of fractures poles - both for the cherty Scaglia Fms. and for the marly Scaglia Rossa Fm. Note that the stereonet for the marly portion is only representative of few structures observed. The rotated stereonets show the fractures attitude respect to bedding turned horizontal. (a) Close-up photograph of HAB joints of J1 set with manganese dendrites. (b) Close-up photograph of HAB joints of J1 set showing plumose structures. (c) Close-up photograph of HAB joints of J1 set showing hackle marks and sections of J2 set with calcite inclusions. (d) Close-up photograph of HAB joints of J2 set showing hackle and rib marks with slickenlines. (e) Detail of photograph (d) showing calcite fibers on J2 set indicating a sinistral transtensive shear. (f) Close-up photograph of LAB veins (V3 set). (g) and (h) Photographs of HAB slickolites showing dextral transtensive shear and reverse dip-slip shear. (i) Photograph of vein abutting on S4 slickolite. HAB: high angle to bedding; LAB: low angle to bedding; PSS0: Bedding parallel pressure solution seam.

3.5.2 Hinge

SITE 5: Site 5 is located in the national shooting range of *Cingoli*, 500 m to the NW of the village (Fig. 3.1). This site consists of three walls; two of the three walls are approximately 150 m-long and NS oriented whereas the southern wall is perpendicular to the formers (EW oriented) and 20 m-long (Fig. 3.21). White micrite characterize the outcrop (Figs. 3.22 and 3.23). The carbonate beds are from 6 to 50 cm in thickness and slightly dipping towards NNE (e.g. 25°/10°) or almost horizontal. I suggest to consider this site representative of the hinge of the *Cingoli* anticline due to the almost horizontal beds but it could be even considered as the transition between hinge and forelimb as shown in (Fig. 3.2). The bedding surfaces, called PSS0, are well-defined and formed by PSSs with iron oxides residues and a greenish fine-grained material which is from less than 1 mm to 6 mm thick. The micrite beds alternate with parallel to bedding, and almost continuous, dark-blue chert layers up to 8 cm in thickness (Figs. 3.22 and 3.23). Chert lenses and nodules are also present. As observed for site 4, the chert colour (i.e. dark-blue) generally distinguishes the *Scaglia Bianca* Fm. from the *Scaglia Rossa* Fm., which is generally characterized by red chert. Two stratigraphic logs made on the eastern wall of this site show that the chert percentage is 5% and 8% (Fig. 3.24). The greenish material observed on the bedding surfaces is always present around the chert, on the layers, nodules, and lenses. The bedding surfaces do not show shear and the columns are well preserved and perpendicular to the bedding surfaces.

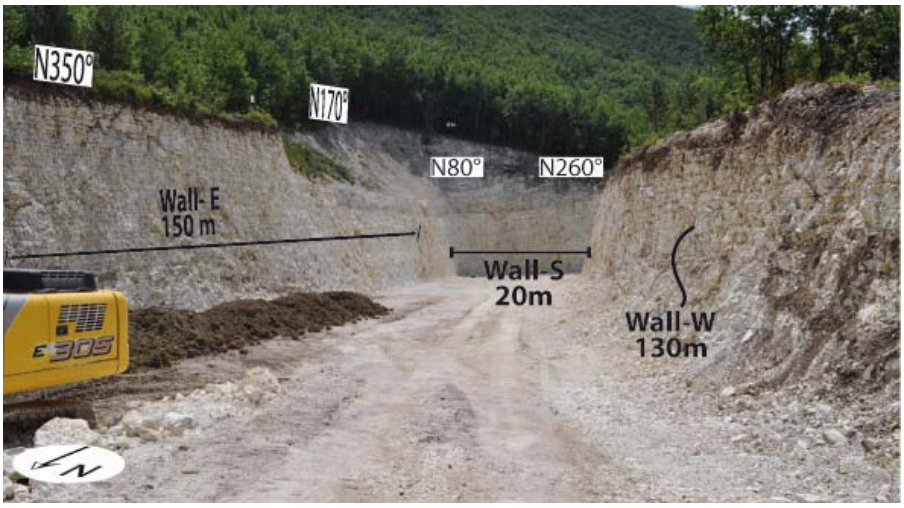

Fig. 3.21: Photograph of site 5. The studied area is located within the national shooting range of Cingoli and it is characterized by three walls: two N-S oriented (approximately 150 m-long) and one E-W oriented (20 m-long).

In this site two detailed analysis have been carried out, one along the southern wall (S-Wall) and the other on the eastern one (E-Wall). Along the southern wall, a detailed line drawing at different scales has been done for a length of 8 m along the outcrop (Figs. 3.22 and 3.23). The fractures distinguished in this wall, but observed also in the entire site, are mainly joints. They are recognized by their typical faces characterized by hackle and rib marks, and by the lack or the rare presence of iron oxides or other residues on fracture faces (Fig. 3.25). Four main sets of joints have been distinguished (see stereonet in Fig. 3.22). The J1 and J2 sets are joints at HAB, with a mean attitude respectively of 215°/75° and of 300°/85°, therefore parallel and orthogonal to the bedding strike. These two strata-bound joint sets are the most important and persistent systems in the site. The J1 set is characterized by pure mode I features (see hackle and rib marks, and manganese dendrites in Fig. 3.25a) but often shows strike-slip or oblique dextral shear (with a normal component) on the fracture faces which are characterized by calcite fibers or striae (Fig. 3.25b). Joints of J2 set do not show shear and they terminate on the J1 faces (Fig. 3.25c). J3 set is characterized by LAB strata-bound joints with a mean attitude of 235°/60° (Fig. 3.25d). This set of joints (i.e. J3) is not observed in the entire site but it seems to be concentrated in some characteristics areas. Fig. 3.22 shows that J3 joints are localised close to or terminate against longer surfaces. Joints of the J3 set form an angle of 70° with the surfaces of the structures against which they abut and they are generally mechanically confined within chert or PSS0 layers (see the right side of Fig. 3.22b). Another relevant fracture set observed in the site, but not visible in the S-Wall, is characterized by LAB strata-bound joints (i.e. J4 set) with a mean attitude of 20°/74°. They usually abut against J3. The J4 joints somewhere produce offset along the bedding surfaces. Some LAB PSSs are also observed in the S-Wall and in the entire site but they are not as pervasive as the joint sets. They are characterized by orange/reddish surfaces with iron oxides residues and with the same greenish material that lies on the bedding surfaces. The PSS1 set is recognized in the S-Wall (Fig. 3.22) and is characterized by stylolite surfaces with a mean attitude of 120°/53°. Other PSSs have been distinguished and they are generally LAB and dipping towards NW and S.

Furthermore, the S-Wall contains longer structures that show two main trends: the most pervasive set dips towards SE, hence parallel to the PSS1, and the other set dips towards NE (Fig. 3.22).

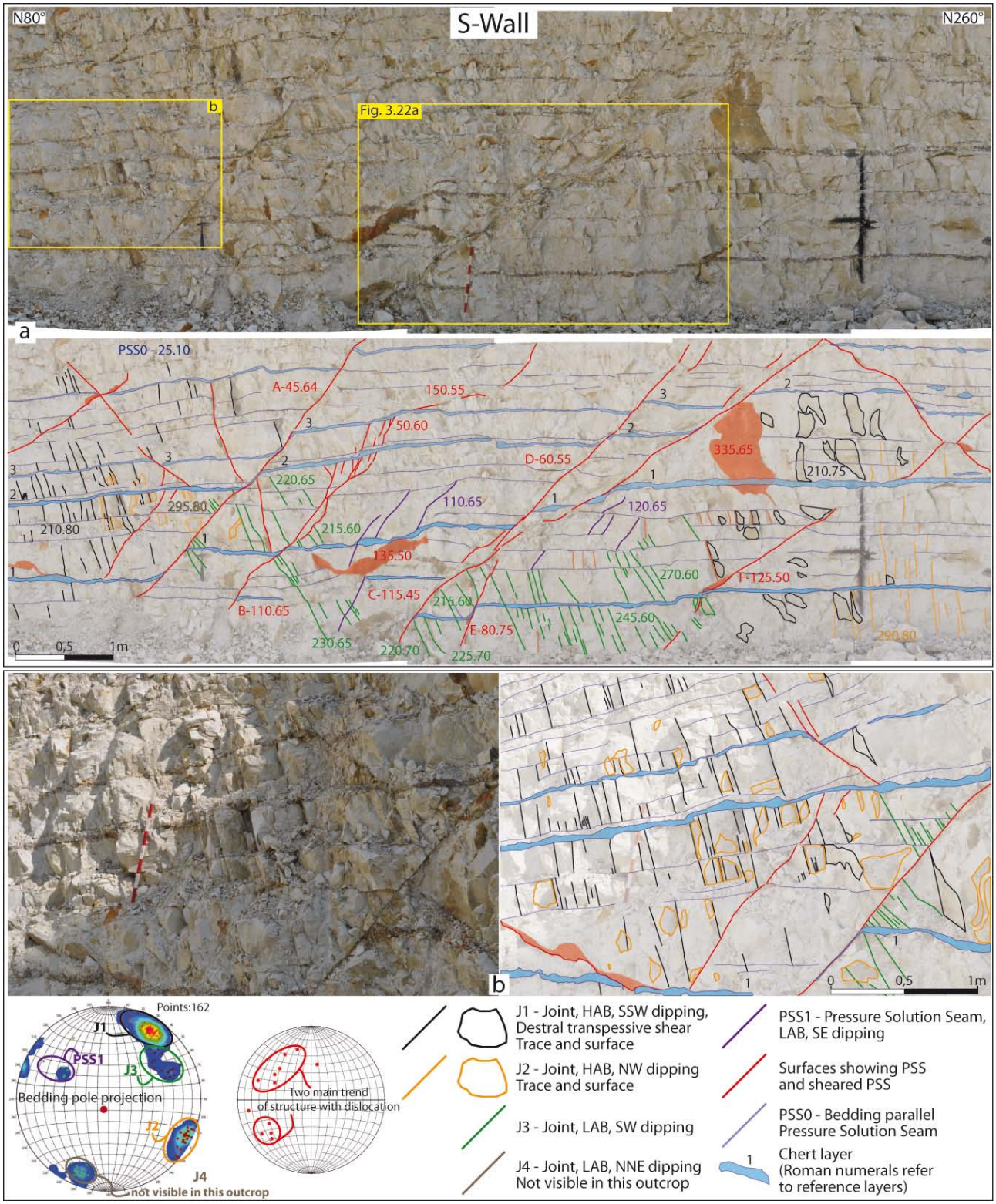

Fig. 3.22: (a) Photomosaic and related line drawing of S-Wall in site 5 showing the principal sets of fractures and longer structures with evident displacement. Note stereonets - lower hemisphere equal area projection of joints, PSSs and other structures poles. Site 5 is characterized by at least 4 sets of mode I fractures (i.e. joints): J1 and J2 are HAB stratabound joints whereas J3 and J4 are LAB stratabound joints. PSSs have been recognized on the S-Wall but they are rare compared with the joint systems. PSS1 set is LAB and stratabound. Other stratabound PSSs have been observed in site 5; they are all LAB and they dip towards NW and S. The longer structures (in red) generate an evident displacement but on their surfaces there are evidences of pressure solution processes and shear. Attitude data are expressed in dip azimuth/dip form. (b) Photograph and related line drawing of a portion of S-Wall. Note on the right side of the pictures the J3 set which abut on the surface with shear. The angle between J3 and sheared surfaces is 70°. HAB: high angle to bedding; LAB: low angle to bedding; PSS0: Bedding parallel pressure solution seam.

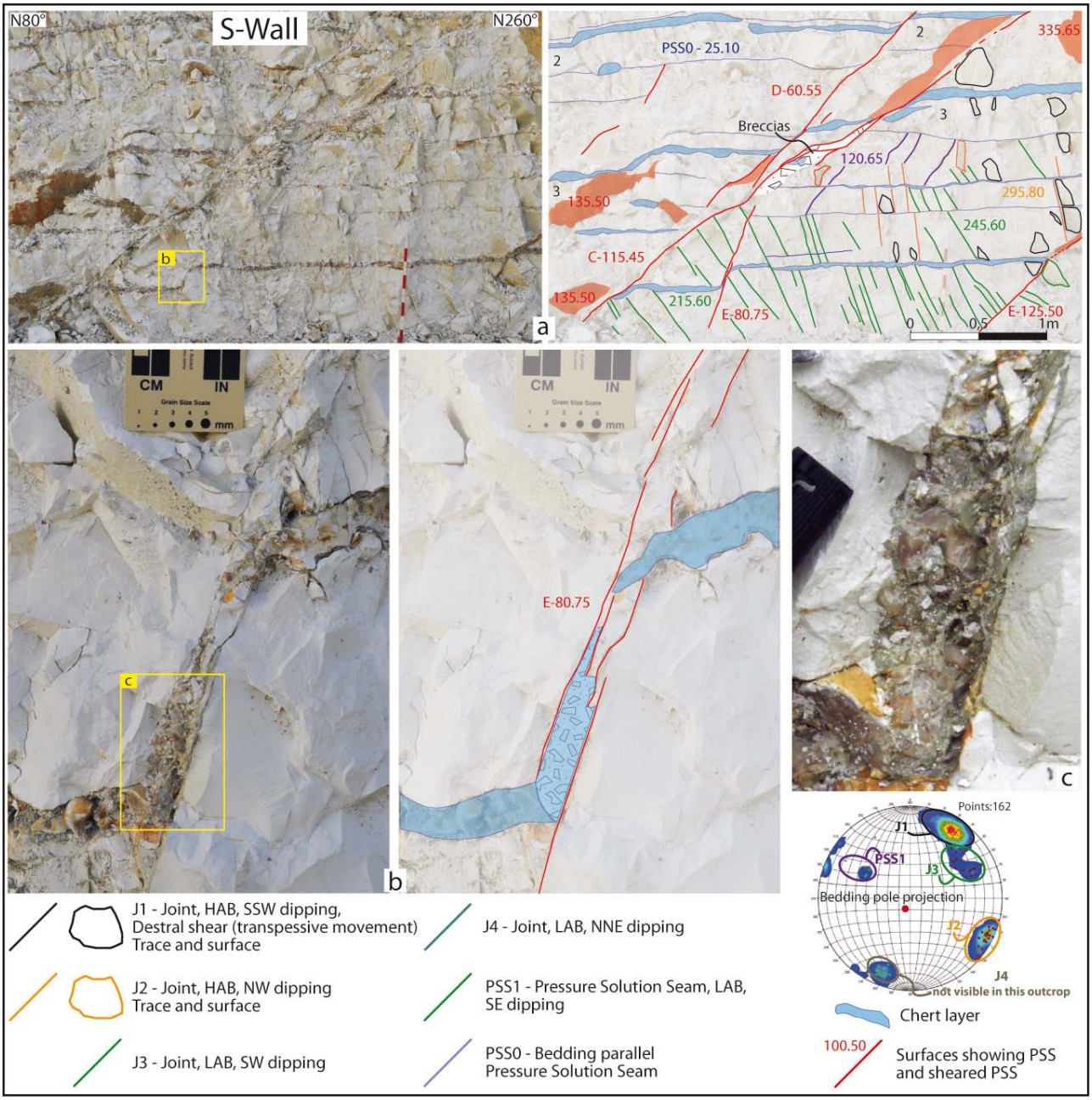

Fig. 3.23: (a) Photograph and related line drawing of a portion of S-Wall. Structure C is the only surfaces showing displacement where breccias occur. Generally all the structures generating displacement are characterized by well defined surfaces, without breccias and gouge, and with evidence of pressure solution processes. (b) and (c) Close-up photographs and related line drawing of S-Wall. Note that the chert layer is spread on the surface and it is completely crumbled in small clasts. Some veins may occur but pressure solution processes are well visible along the surfaces. Attitude data are expressed in dip azimuth/dip form. HAB: high angle to bedding; LAB: low angle to bedding; PSS0: Bedding parallel pressure solution seam.

These structures generate an offset from few centimetres up to 40 cm. The faces of these structures show features that display different mechanical origins. Columns, orange iron oxides residues and greenish material, similar to that one observed along the bedding surfaces, which is up to 5 mm in thickness and sometimes includes small chert clasts, characterize the surfaces of the offsetting structures, hence suggesting an anti-mode I mechanism. At the same time, the faces are characterized by slickolites, calcite fibers, and grooves showing dip-slip movement (in

particular B and D structures in Fig. 3.22) and. Furthermore, some calcite veins are also present along these surfaces. Small breccia pockets have been observed only along structures C in the S-Wall (Fig. 3.23a), whereas all other structures have well-defined surfaces. Another peculiar feature is the deformation style of the chert layers. Fig. 3.23b shows a chert layer deformed along one of these offsetting structures (Figs. 3.22 and 3.23a). In this site, chert layers do not show a sharp offset but they seem to be bent along the surface. When the displacement occurs, as in Fig.3.23, the chert is spread on the surface of the offsetting structures and it is completely crumbled in small clasts. Note that in Fig. 3.23c the surfaces where the chert is spread have evidence of pressure solution and the chert layer is completely crumbled and mixed with limestone clasts and veins of unknown material.

The site is also characterized by HAB strike-slip faults. A sinistral NW-SE oriented strike-slip fault is observed on the E-Wall (see the right side of Fig. 3.26) with breccia zones up to 50 cm in thickness. This fault is visible also in the western side. Other smaller faults are observed in the site and they show normal and strike-slip movement.

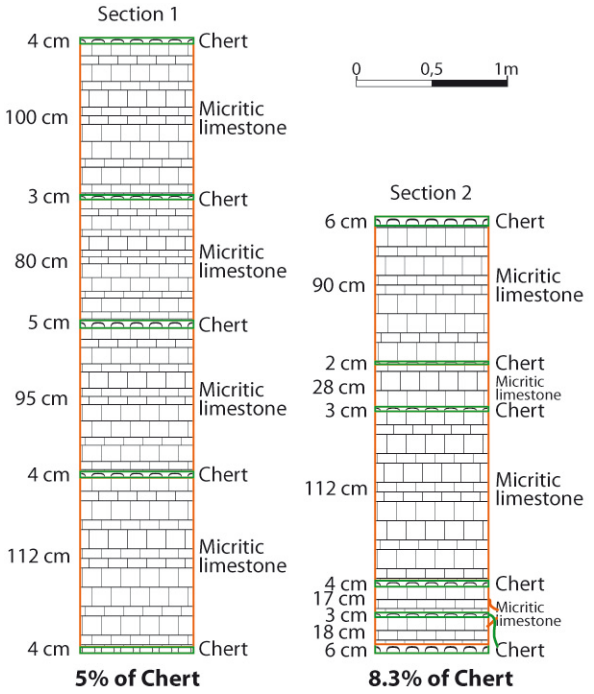

Fig. 3.24: Two stratigraphic sections measured on E-Wall of site 5. The chert layers represent respectively the 5% and 8% of the total thickness.

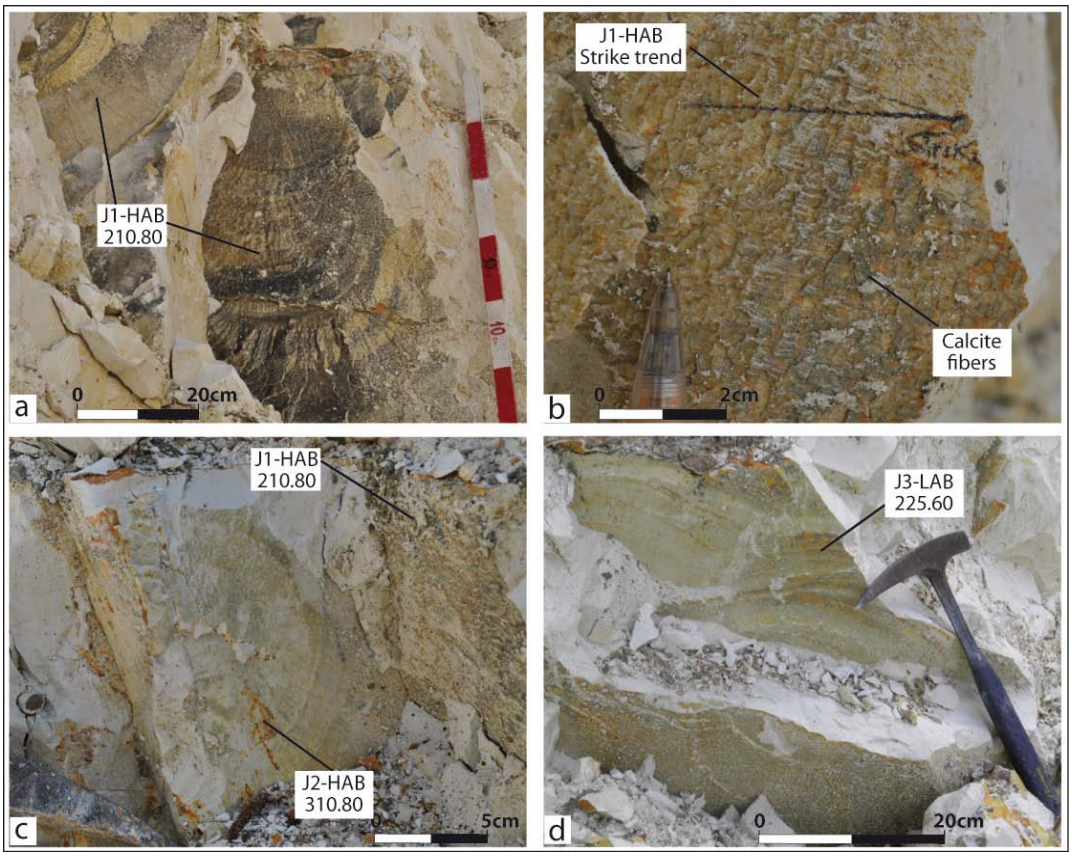

Fig. 3.25: Mesoscopic photographs of joint surfaces. Note the presence of hackle marks, ribs marks and manganese dendrites in (a), (c) and (d). (b) Some joints of J1 set are characterized by dextral transtensive shear. (c) J2 set usually abut on joints of J1 set. Attitude data are expressed in dip azimuth/dip form. HAB: high angle to bedding; LAB: low angle to bedding.

In order to better analyse the offsetting LAB structures observed in the S-Wall, a further detailed analysis on similar structures has been carried out on the E-Wall. An accurate line drawing has been drafted to characterize the geometrical pattern of these structures, their relative temporal formation, and the apparent offset of the bedding and chert layers. All structures generating offset (i.e. all the structures distinguished by lower-case letter in Fig. 3.26) have been carefully examined. Two important LAB trends, respectively SE and NNW dipping, can be distinguished (Fig. 3.26). NNW dipping structures seem to be confined in or abut against other set of structures. All structures analysed are formed by a series of structures joined together or slightly separated along the bedding surfaces or along the chert layers. The faces of these structures are mainly characterized by pressure solution with columns, orange iron oxides stains, and with a greenish material on their surfaces (Figs. 3.27a-b and 3.28a). Other segments, despite their belonging to the same structures, show sheared faces with slickolites, calcite fibers and striae (Fig. 3.27c and d). Finally, there are segments characterized by an almost white and planar surface sometimes with small breccia pockets and veins. An

oblique sinistral shear (with a normal component) characterizes most of those surfaces, but dip-slip and oblique dextral (with a normal component) shear is manifest too. These structures usually terminate on the chert layers or on the PSSs of the bedding surfaces (i.e. PSS0) but, sometimes, they terminate within the calcareous beds even without important mechanical discontinuity (Fig. 3.28c). Fig. 3.28b shows one of these structures (on the left side of the photograph) which produce 3 cm of offset on the PSS0 but abuts against the chert layer without crossing it. In the same figure there are other small and strata-bound fractures, with the same trend of the former one, which produce a slight bending of the chert and PSS0 layers without any detectable offset. Where both SE and the NNW dipping structures are present, a variation in thicknesses is observed (Fig. 3.28b and c). The greenish fine-grained material on the bedding surfaces is not really cut by the offsetting structures but it seems to be bent (not smeared) along the offsetting structures. Furthermore, the surfaces where this kind of offset occurs, show pressure solution processes with columns perpendicular to the surfaces itself (Fig. 3.28d). In few structures, usually more at HAB than the other features, the greenish material is really displaced, in other terms the fine-grained material is cut by the offsetting structure. Where this occurs, there are veins along the sheared surface. On the contrary, the chert layers show different amount of offset: no offset at all (Fig. 3.27e), a small offset with the chert layers slightly deformed (Fig. 3.27f), a much greater offset with the chert layers still not displaced but crumbled in small clasts (Fig. 3.27g) and a much important offset with the chert layer completely dislocated and "smeared" on the surface showing pressure solution processes (Figs. 3.27h and 3.28a). The structures where the offset occurs are even characterized by thick calcite inclusion (up to 2 cm in thickness) and by cataclasite with calcareous clasts in a calcite cement.

Furthermore the fine-grained greenish materials observed both on the bedding surfaces and on the offsetting structures have been sampled for X-ray powder diffraction analysis together with the micrite sample. The micrite sample has been attacked in laboratory with hydrochloric acid in order to analyse the insoluble residual. Fig. 3.29 shows the results of the X-ray powder diffraction analysis of the three sample which show characteristics peaks of quartz, illite, k-feldspar, montmorillonite, and calcite (Fig. 3.29).

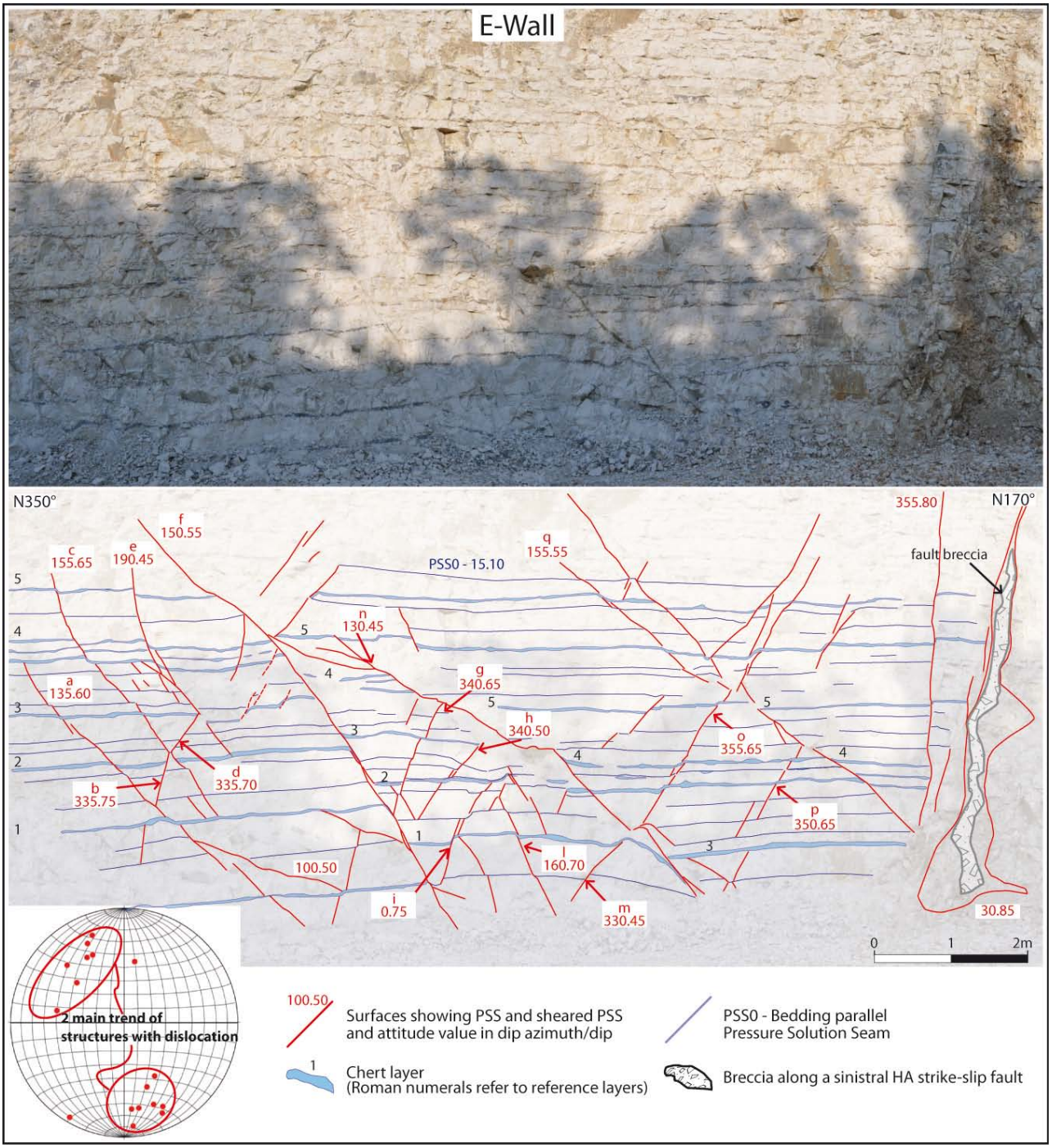

Fig. 3.26: Photomosaic and related line drawing of E-Wall in site 5 showing the structures with evident displacement. Note stereonet - lower hemisphere equal area projection of the structures poles. Two important LAB trends characterized the wall, one SE and the other NNW dipping. All the structures distinguished by lower-case letter have been carefully examined: mechanical type of surfaces (i.e. mode I, anti-mode I etc), presence or not of residues, kinematical indicators, displacement measurements and so on. Note that NNW oriented structures generally abut to or are confined within SW trend. A sinistral strike-slip fault with breccia is showed on the left side of the photograph. Attitude data are expressed in dip azimuth/dip form. HAB: high angle to bedding; LAB: low angle to bedding; PSS0: Bedding parallel pressure solution seam.

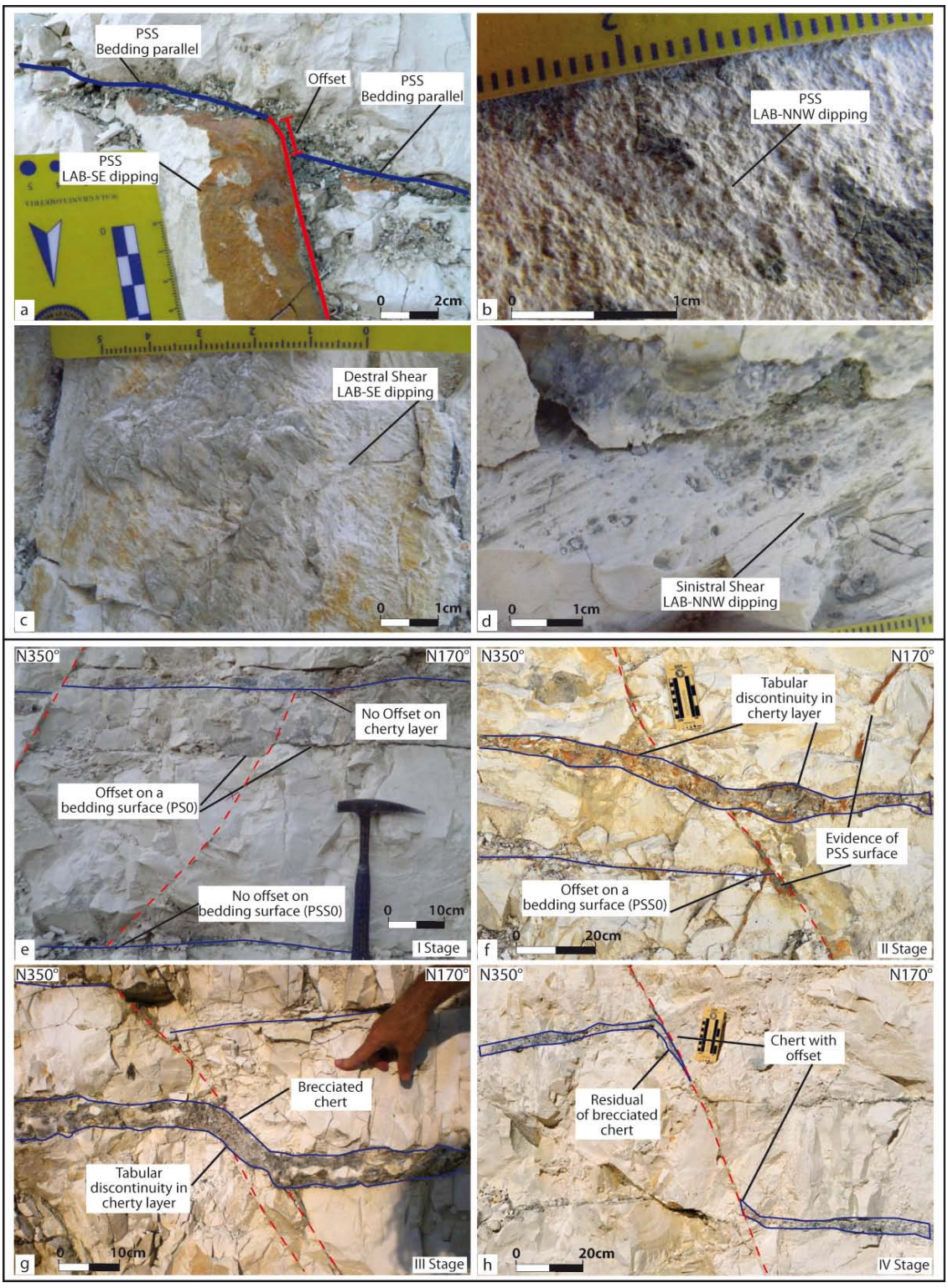

Fig. 3.27: Mesoscopic photographs of the structures observed in E-Wall. a-d: close-up view of structures surfaces; e-h: section view of the structures. (a) Photograph of the surface of a SE dipping structures. Note the offset generated by the structures and the orange iron oxides residues with the greenish fine-grained material. (b) Close-up photograph of the surface dipping towards NNW, small columns and the greenish fine-grained material are present. (c) Close-up photograph of the SE dipping structures showing slickolites and calcite fibers. (d) Close-up photograph of the NNW dipping structure surfaces showing slickolites. (e) Photograph of structure showing no chert dislocation but PSS0 displacement. (f) Initial deformation of chert layer, no displacement but a gently fold characterizes the chert. (g) The chert layer is still continuous but the displacement is evident and the chert is now crumbled. (h) Final step with the chert layer dislocated and spread on the surface. The chert is totally crumbled and there are presences of vein and other fragments (see Fig. 3.29a and b). HAB: high angle to bedding; LAB: low angle to bedding; PSS0: Bedding parallel pressure solution seam.

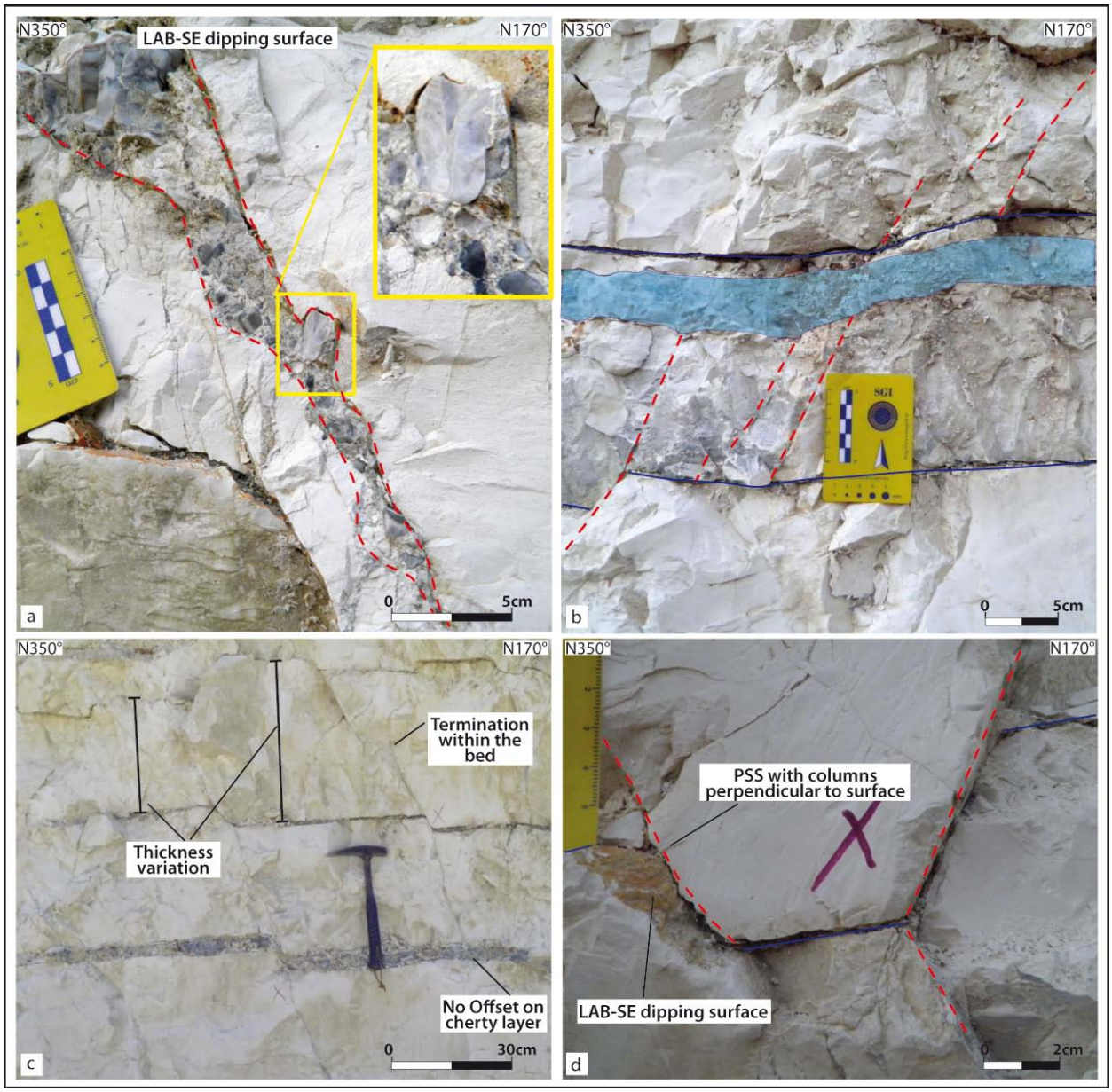

Fig. 3.28: (a) Close-up photograph of Fig. 3.27h. The chert layer is completely crumbled in clasts. Note the bigger clast with PSS on its border. (b) Close-up photograph of a portion of E-Wall showing one of the longer structures (on the left side of the photograph) which produce 3 cm of dislocation on the PSS0 but abutting on the chert layer without generating any offset. Other small and stratabound fractures, with the same trend of the former one, produce a slight bending of the chert and PSS0 layers without any observable offset. (c) Mesoscopic photograph of a portion of E-Wall. Note that some structures terminate within the strata whereas other structures abut on chert or PSS0 layers. The photograph shows variation in thickness of calcareous beds. (d) Close up photograph of the two trends of structures with displacement. Note the PSS characterizing the SE dipping structures with columns perpendicular to the surface. LAB: low angle to bedding; PSS0: Bedding parallel pressure solution seam

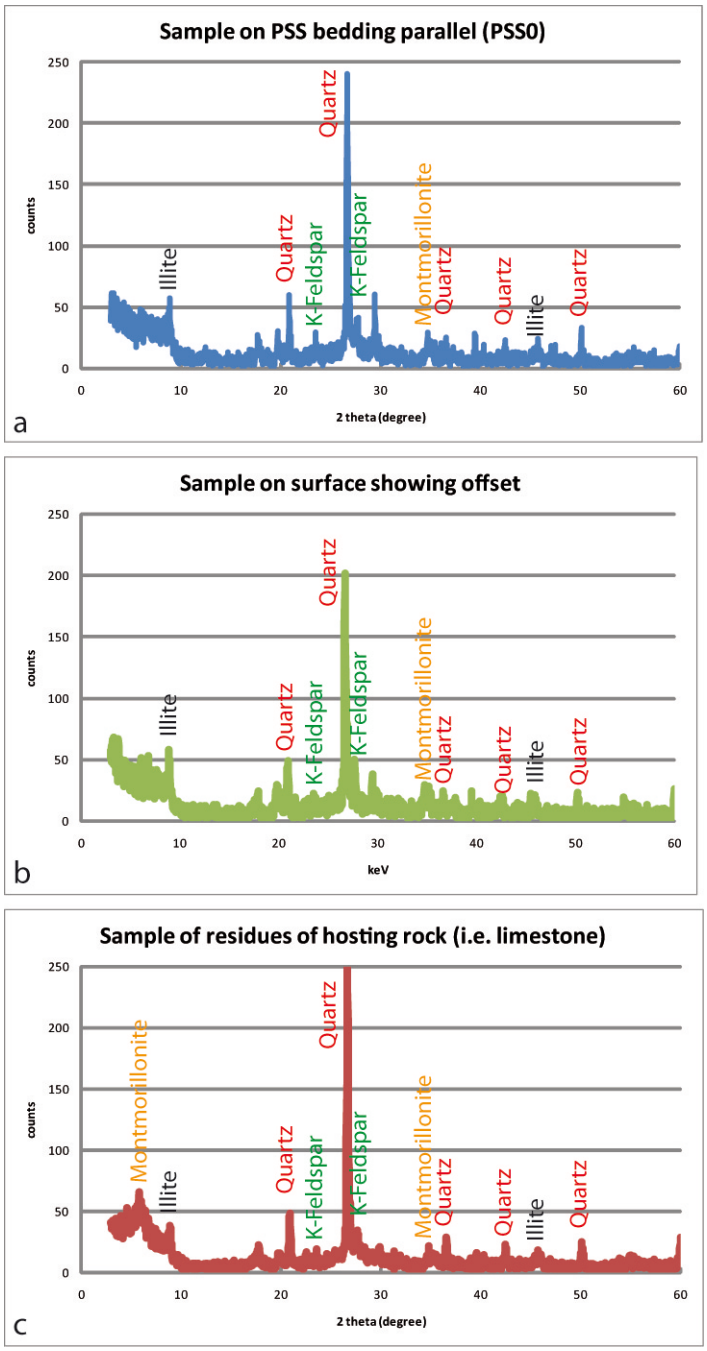

Fig. 3.29: X-ray powder diffraction graphs of three samples in site 5: the first is the residual material on PSS0, the second represents the diffractogram of residual material on the offsetting structures and the third is relative to the residual material after acid attack on the limestone. The three diffractogram are similar.

3.5.3 Forelimb

SITE 6: Site 6 is located within Quarry 1 (Fig. 3.1) where the paleo-Jurassic border of the structural high crops out showing the contact between the *Calcare Massiccio* Fm. and the younger pelagic complete sequence (see Figs. 2.5 and 2.6 in Chapter 2). The outcrop studied is approximately 200 m to the north of the paleo-escarpment (basin-ward) and it consists of a EW-oriented-50-m-long wall. The outcrop is within the *Calcari a Posidonia* Fm. and it is characterized by an rhythmic sequence between thinly-bedded pelagic limestones and grey-purplish cherts; very thin marl levels alternate with chert and micrite (Fig. 3.30a). Beds are from 2 cm up to 30 cm in thickness and they have a mean attitude of 15°/20°, which is similar to the paleo-escarpment orientation. The thicker chert beds alternate with thin carbonate levels (Fig. 3.30b).

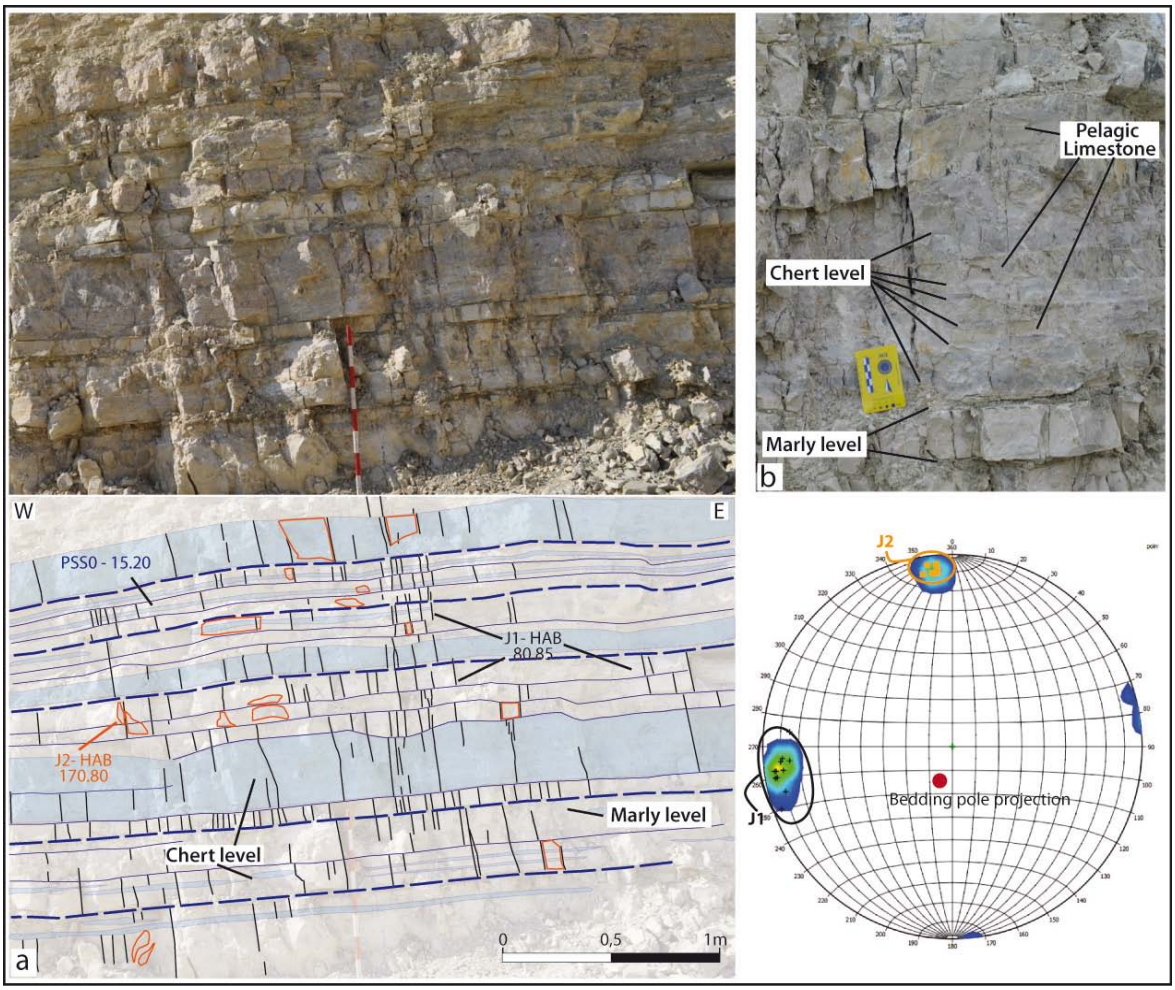

Fig. 3.30: (a) Photograph and related line drawing of EW oriented wall in site 6 showing the principal sets of fractures. Note stereonets - lower hemisphere equal area projection of joint poles. Site 6 is characterized in particular by 2 sets of mode I fractures (i.e. joints): J1 and J2 are HAB stratabound joints respectively NS and EW oriented. Note the presence of a more intense NS jointing in the centre of the photograph. Attitude data are expressed in dip azimuth/dip form. HAB: high angle to bedding; PSS0: Bedding parallel pressure solution seam. (b) Close-up photograph of a chert bed showing the thin repetition of chert and carbonate layers.

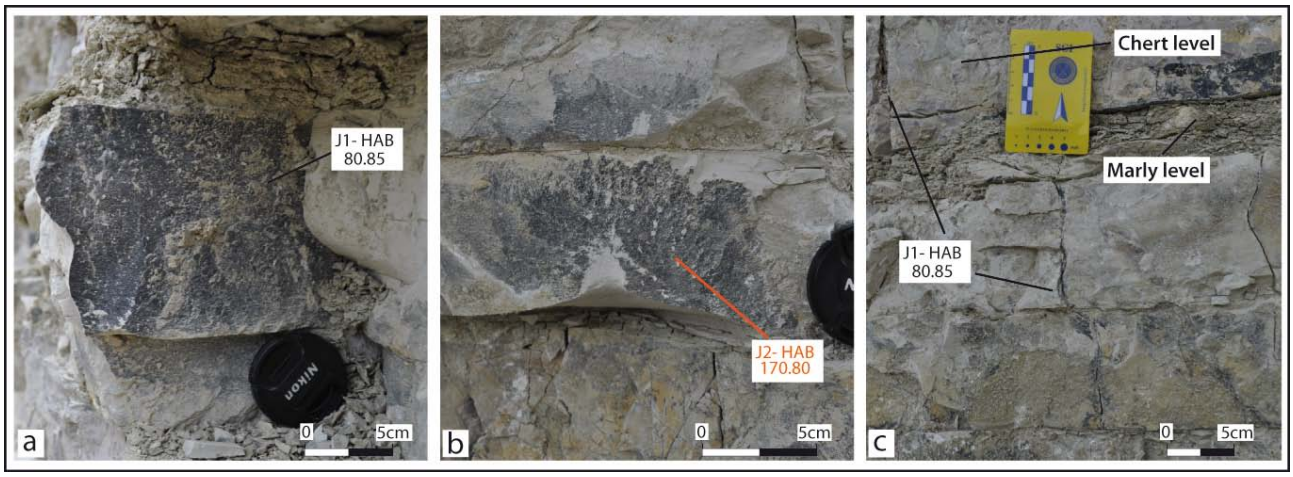

Fig. 3.31: (a) and (b) Mesoscopic photographs of joint surfaces. Note the presence of hackle marks and manganese dendrites. (c) Joints develop both in chert and carbonate beds whereas marl layers form a mechanical confinement. Note that joints developed in two different beds may join. Attitude data are expressed in dip azimuth/dip form. HAB: high angle to bedding.

In this site, a detailed analysis on the fracture system has been carried out showing the presence of persistent strata-bound mode I fractures. In particular two sets characterize the outcrop: a NS oriented HAB set of joints (J1 set) with a mean attitude of 83°/80° and a EW oriented HAB set of joints (J2 set) with a mean attitude of 170°/82° (Fig. 3.30a). Both sets show on their surfaces hackle marks and manganese dendrites (Fig. 3.31a and b) and they are present in limestone as well as within the chert beds (Fig. 3.31c). These joints are generally strata-bound but joints from different beds can merge forming a longer non-strata-bound mode I fracture (Fig. 3.31c). The outcrop shows area of intense NS oriented fracturing with a concentration of joints of J1 set (Fig. 3.32a). These NS oriented trend of deformation coincides with some faults observed in the site. In particular, there are evidences of two vertical dip-slip NS oriented faults which show different degree of displacements. One fault is characterized by an offset of 5 cm and by breccia zones up to 10 cm in thickness (Fig. 3.32b), the other fault has a very thick damage zone, up to 15 m in thickness, which can be divided in an inner intense damage zone and an outer 1 m-thick less deformed damage zone (Fig. 3.32c). Furthermore it is observed that this NS oriented trend of deformation control the overall strain of the *Calcari a Posidonia* Fm. and also of the *Calcare Massiccio* Fm. (Fig. 3.32d). Both the formations are characterized by a persistent NS oriented fracturing system, which often evolves in so-called fracture corridors, and fault zones (Fig. 3.32d).

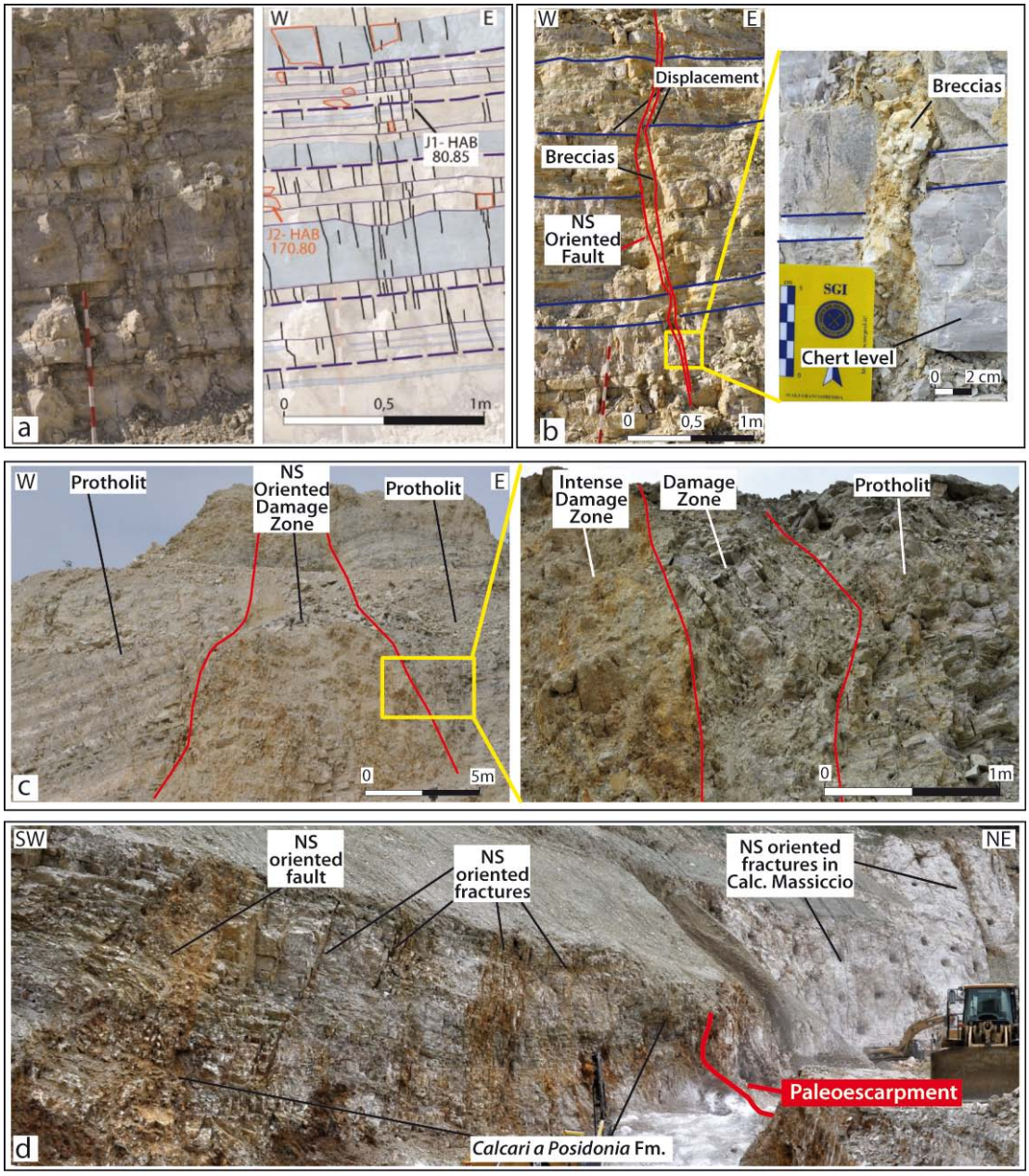

Fig. 3.32: (a) Photograph and related line drawing of a portion of the EW oriented wall showing an area of intense NS oriented fracturing with a concentration of J1 set fractures. (b) Photograph of a small NS oriented dip-slip vertical fault with 5 cm of offset and close-up photograph of the related breccia. (c) Photograph of a portion of the wall in site 6 showing a NS oriented fault with 15 m of damage zone. The close-up view shows two different damage zones: the inner zone has an intense degree of deformation and it is followed, towards the protholite direction, by a less deformed 1m thick zone. (d) Photograph of the main face of the quarry where the paleoescarpment crops out showing the contact between the Calcare Massiccio Fm. and the Calcari a Posidonia Fm. Note that the NS oriented fractures and faults are persistent in the quarry and they characterize the Calcare Massiccio Fm. too. Attitude data are expressed in dip azimuth/dip form. HAB: high angle to bedding.

SITE 7: Site 7 is located in the *Cingoli* town within an artificial excavation for the foundation of an house (Fig. 3.1). This site consists of two walls oriented at right angle to each other and approximately perpendicular and parallel to the *Cingoli* anticline axis (Fig. 3.33). Wall 1 is SW-NE oriented and it is 18 m-long whereas Wall 2 is NW-SE oriented and 14 m-long (Fig. 3.33). Site 7 is within the *Scaglia Rossa* Fm. which is here characterized by thinly-bedded creamy/grey limestones, marly limestones and thin marl/clay layers (Figs. 3.34 and 3.35). In this site the *Scaglia Rossa* Fm. does not contain chert beds. The limestone and marly limestone beds are from 1 to 15 cm in thickness whereas the marl/clay layers are up to 1 cm in thickness. This site shows a higher clay content compared to the other studied sites. Bedding surfaces have a mean attitude of 50°/20° and they are defined and formed by pressure solution seams (PSSs) with iron oxides and clay residues; these PSSs are defined as PSS0.

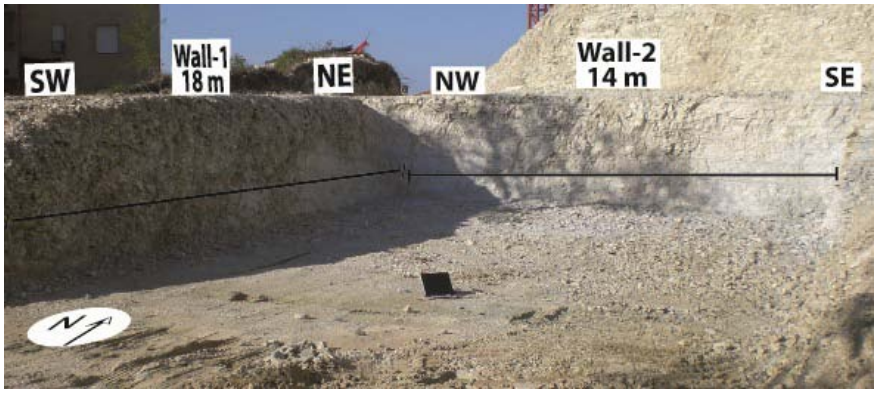

Fig. 3.33: Photograph of site 7. The studied area is located in the Cingoli town within an artificial excavation for house buildings. The site is characterized by two walls: Wall 1 is SW-NE oriented (18 m-long); Wall 2 is NW-SE (14 m-long).

In this site two detailed analysis have been carried out, one for each wall (Figs. 3.34 and 3.35).

Along Wall 1, a detailed line drawing at different scale has been done (Fig. 3.34). Wall 1 is characterized both by strata-bound and non-strata-bound fractures, and it shows prevalently HAB fractures and few, generally non-strata-bound, LAB fractures. It has been difficult to distinguish the mechanical type of fractures. Generally PSSs and slickolites are most pervasive fractures recognized in site 7, few joints and veins have been observed but they do not represent systematic characterizing features. Fig. 3.34a shows W-dipping, LAB faults producing a maximum offset of 30 cm, but there are fractures showing the same trend and pattern of these LAB faults without offset generation (e.g. F4). Some of these LAB faults abut against the marl/clay layers (Figs. 3.34a and Fig. 3.37a). The faults surfaces show oblique dextral shear (with a normal component) characterized by slickenlines such as grooves and calcite fibers (Fig. 3.36e). Some of the faults faces present slickolites and pressure solution processes. Only two of

these LAB faults present breccias (note F2 and F3 faults in Fig. 3.34a) whereas the others are generally formed by sharp surfaces.

Fig. 3.34: (a) Photomosaic and related line drawing of Wall 1 in site 7 showing the principal sets of fractures and faults with evident displacement. Note stereonets - lower hemisphere equal area projection of PSSs, slickolites and faults poles. Site 7 is characterized by W dipping, transtensive, LAB faults with a maximum offset of 30 cm and by other non-stratabound, N-NE dipping, LAB PSSs and slickolites (S5 set) which sometimes produce centimetric offset with a dextral transtensive shear. (b) Photograph and related line drawing of a portion of Wall 1. The outcrop is characterized by at least 4 set of fractures mainly PSSs and slickolites (i.e. PSS1, PSS2, S3 and S4). Attitude data are expressed in dip azimuth/dip form. HAB: high angle to bedding; LAB: low angle to bedding; PSS0: Bedding parallel pressure solution seam.

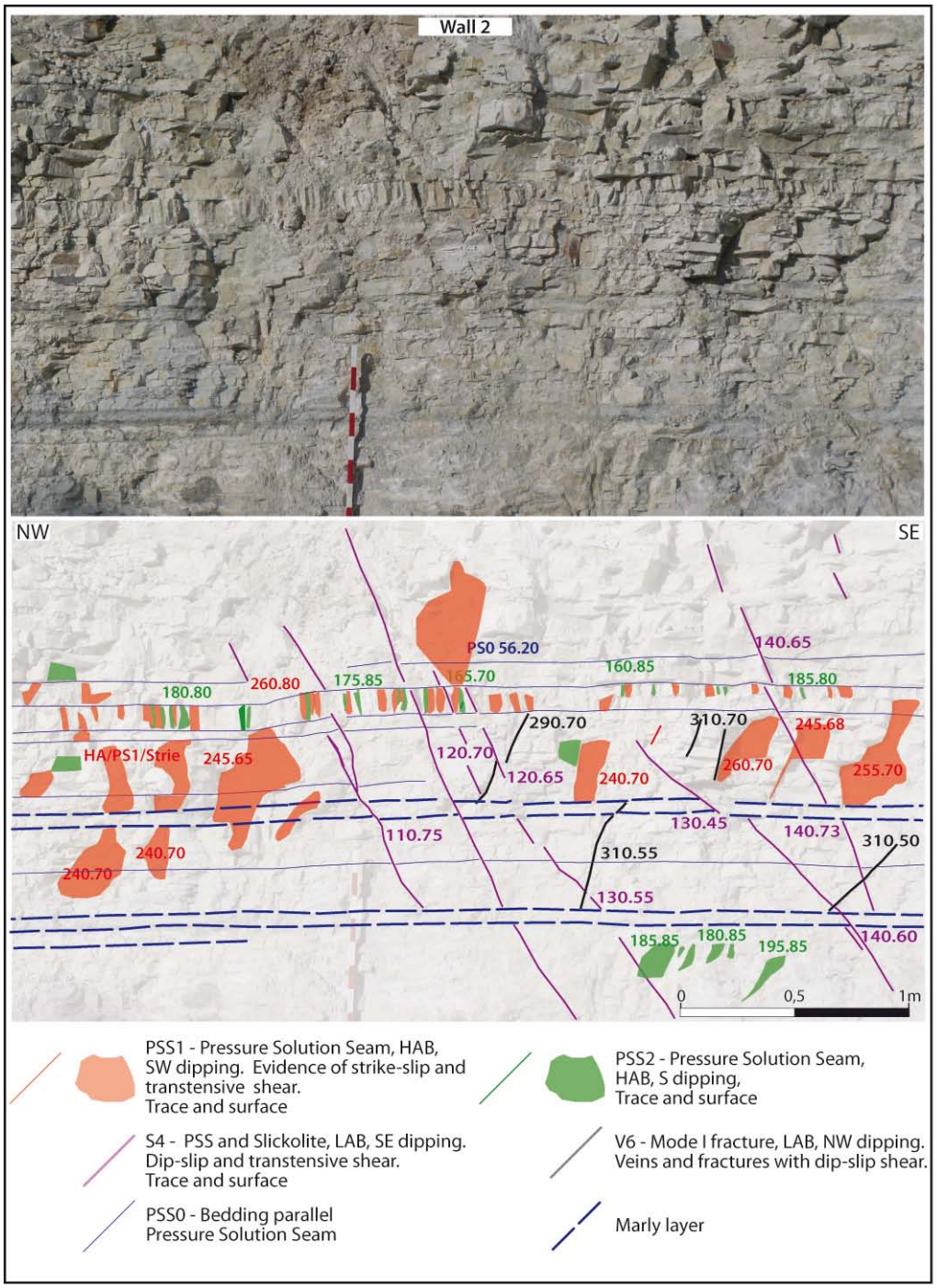

Fig. 3.35: Photomosaic and related line drawing of Wall 2 in site 7. This wall shows the same fractures sets of Wall 1. Wall 2 permit to observe the non-stratabound pattern of S4 set fractures and the offset which they produce. Some rare mode I fractures characterize Wall 2. They dip towards NW of 65° and they are veins and joints some with dip-slip shear. Attitude data are expressed in dip azimuth/dip form. HAB: high angle to bedding; LAB: low angle to bedding; PSS0: Bedding parallel pressure solution seam.

Other long fractures are mainly slickolites and subordinately PSSs characterizing the S5 set; they have a mean attitude of 20°/50° and in some cases they produce an offset in the order of centimetres showing an oblique dextral shear (with a normal component; Figs. 3.34a-b and 3.36h). These fractures abut against marl layers and they show a reciprocal ambiguous cross-

cutting relationship with the LAB faults (Figs. 3.34a and 3.37b). It is relevant to note that the S5 set fractures are mainly formed by a series of small strands slightly dislocated along the bedding surfaces which give the perception of a continuous structure (compare Figs. 3.34 and 3.37).

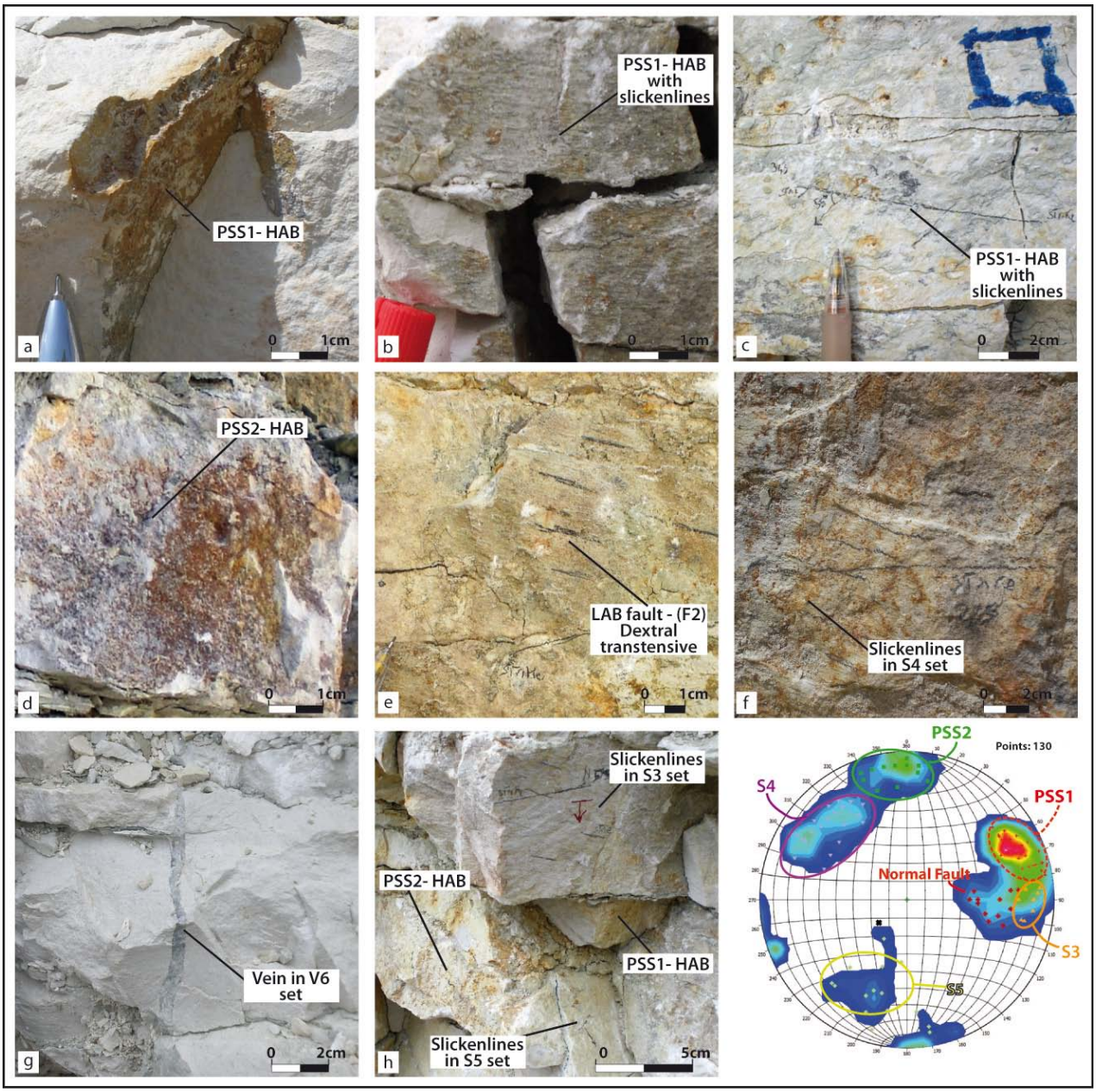

Fig. 3.36: Mesoscopic photographs at different scales of some fractures sets observed in site 7. (a) Pressure solution seam (PSS) of PSS1 set. (b) Face of a fracture of PSS1 set with slicknelines showing strike-slip shear. (c) Face of a fracture of PSS1 set with slickenlines showing dextral transtensive shear. (d) Pressure solution seam (PSS) of PSS2 set. (e) Face of one of the LAB faults showing dextral transtensive shear. (f) Face of a fracture of S4 set with slickenlines. (g) Vein of V6 set. (h) Photograph showing the three HAB fractures of PSS1, PSS2 and S3 sets and a shearing surface of S5 set fracture.

A closer analysis allows for other fractures to be distinguished in Wall 1 (Figs. 3.34b). The PSS1 set fractures are HAB, strata-bound PSSs with a mean attitude of 245°/65°. The fractures faces show evidence of pressure solution processes with columns, iron oxides and clay residues

(Fig. 3.36a). Some fractures of this set show shear both strike-slip and oblique dextral (Fig. 3.36b and c). The PSS2 set fractures are HAB, strata-bound PSSs with a mean attitude of 175°/70° (Fig. 3.36d). These fractures do not show evidence of shear. The S3 set fractures are LAB, strata-bound slickolites with a mean attitude of 270°/70°. They show evidence of oblique (with a normal component) shear (Fig. 3.36h). The S4 set fractures area LAB, both strata-bound and non-strata-bound PSSs and slickolites with a mean attitude of 130°/60°. They show evidence of oblique (with a normal component) shear (Fig. 3.36f). Due to the outcrop orientation the crosscutting relationships of these fractures sets has not been detected.

The fractures sets characterizing Wall 2 are similar to those described in Wall 1 (Fig. 3.35). In this wall the fractures of the S4 set are longer, non-strata-bound and they abut only against thicker marl/clay layers, they show clear evidence of shear with an offset of a few centimetres. Some veins are also observed: the V6 set are LAB, mode I fractures with a mean attitude of 300°/65° (Figs. 3.35 and 3.26g).

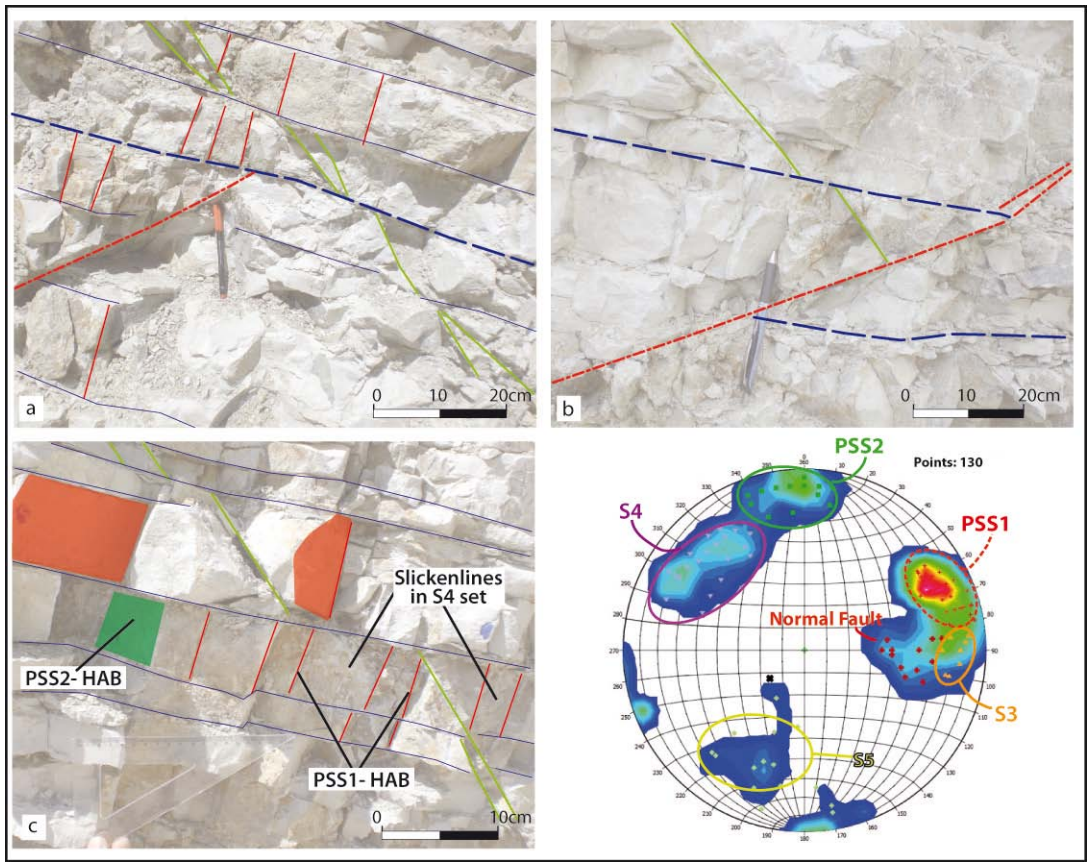

Fig. 3.37: (a) Photograph and related line drawing showing the LAB fault abutting on the marl/clay layers and some strands of Set 5 fractures. (b) Photograph and related line drawing showing the S5 fractures abutting both on a marl layer and on the LAB fault. (c) Photograph and related line drawing showing some strands of set 5 fractures and the HAB fractures of PSS1 and PSS2. HAB: high angle to bedding; LAB: low angle to bedding; PSS0: Bedding parallel pressure solution seam.

3.6 Discussion

The *Cingoli* anticline provides useful sites to investigate relationships among fracturing, mechanical stratigraphy and folding process. The seven outcrops studied are located in different structural positions related to fold structure (i.e. backlimb, hinge and forelimb) and characterized by the *Scaglia* Fms. and *Calcari a Posidonia* Fm. at different stratigraphic positions and with different mechanical properties (Figs. 3.1 and 3.2).

The results of fracture system analysis presented in this work suggest that almost all fractures affecting the anticline are related to the folding process. The data collected show patterns similar to the fracture schemes predicted by former works. In particular, the geometry of fractures related to the structural position in the fold is almost similar to those predicted in literature. The *Cingoli* anticline is characterized by high angle to bedding fractures parallel and perpendicular to fold axes, and by several oblique-to-fold-axes fractures, most of them showing shear on their surfaces. Field data, on the other hand, suggest that some fractures features are not predicted by the schemes proposed in literature and that many properties of fold-related fractures are influenced by local factors and especially by rock properties and the mechanical stratigraphy. In particular, results show that the mechanical type of fractures (i.e. joint, PSS, fault etc.), their dimensions and the evolution during folding of fracture system are a function primarily of mechanical stratigraphy.

Fig. 3.38 shows the orientations and type of fractures in relation with the structural position and the mechanical stratigraphy. Results show that some sites are mainly deformed through anti-mode I structures (i.e. PSSs), whereas other outcrops are affected by mode I fractures (i.e. joints). It is relevant to note that sites in the same structural position are affected by different sets of fractures and by different type of fractures (e.g. compare sites from 1 to 4), it is hence reasonable to suppose that this difference arise from factors related to local variation in term of rock properties and mechanical stratigraphy and not to folding process. It is important to note that the most important difference between sites characterized by joints and those characterized by PSSs is the presence of chert layers in outcrops where anti-mode I fractures are absent.

In literature it is observed that calcareous rocks are prone to dissolution and that HAB PSSs are common structures formed in the early stage of the folding process due to layer-parallel shortening (Stockdale, 1922 and 1926; Alvarez et al., 1976; Allmendinger, 1982; Mitra et al.,

1984; Engelder and Marshak, 1985; Tavani et al., 2006; Tavani et al., 2008; Agosta et al., 2009; Aydin et al., 2010; Tavani et al., 2011; Evans and Fischer, 2012).

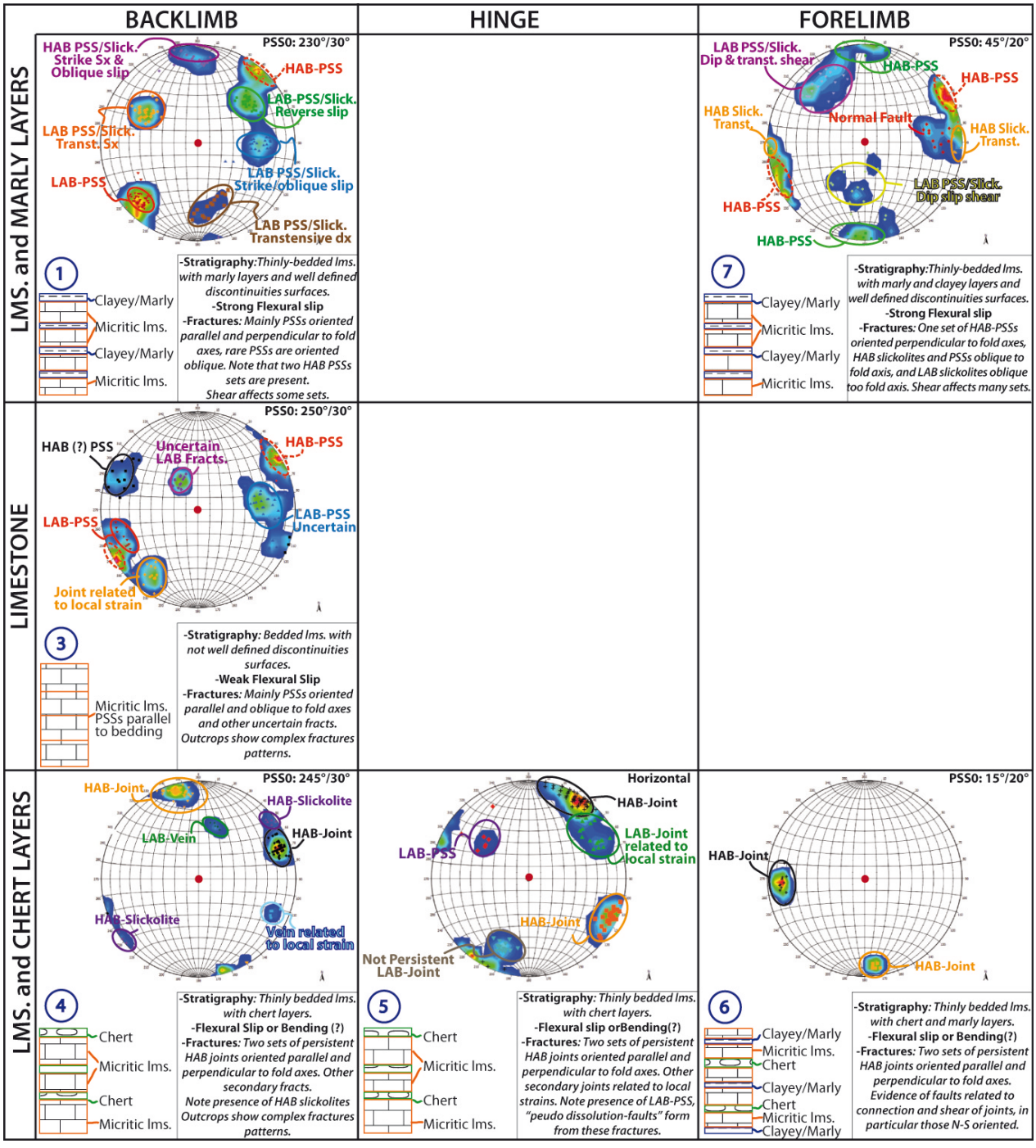

Fig. 3.38: Rotated stereonets - lower hemisphere equal area projection of fractures poles of the studied sites in relation with the structural position and the mechanical stratigraphy.

Some of the studied sites show this deformation pattern but others do not. Theoretically, as the HAB PSSs are formed before tilting and during the first stage of folding, we should find these structures everywhere around the fold. Why these PSSs are not observed in some sites? As already noted, it is not due to structural setting as site 4 is in the same structural position of

sites 1 and 2, and it is not due to the presence of local syntectonic or pre-folding structures. Other reasons should be considered to explain this distinction.

In order to explain the differences observed in these outcrops, I propose to consider the sequence of thinly bedded micrite and chert layers similar to a composite material where the chert is the stiff lamina and the micrite is the matrix. During the first phases of folding, characterized by a stress applied parallel to the laminae direction (the compressional NE-SW oriented stress), the ratio of the forces applied on the two phases of composites, as observe in the theory section (relationship [3]; Fig. 3.7), is:

$$\boxed{\frac{F_\alpha}{F_\beta} = \frac{E_\alpha \cdot V_\alpha}{E_\beta \cdot V_\beta}}$$

and the composite modulus is directly proportional to the percentage of the stiffer phase (i.e. chert) and to the E_α / E_β ratio (Fig. 3.8). Fig. 3.39 shows the effects of the stiffer laminae (i.e. chert layers) on the mechanical behaviour of the composite. In a rock sequence made only of limestone beds, the slope of the "stress vs. strain" curve depends on the Young's modulus of the limestone (the green line in Fig. 3.39). In this condition, the limestone, at a certain stress value, passes from elastic to plastic behaviour and the PSSs start to nucleate. On the other hand, the composite is characterized by different mechanical properties, with an overall Young's modulus higher than that relative to the limestone sequence (the blue line in Fig. 3.39). It is important to keep in mind that we are considering the stress applied parallel to the laminae direction (i.e. the chert layers) and so we are in equal strain condition, which means that the PSSs should nucleate at the same strain value. According to this analysis and as showed in Fig. 3.39, to reach the PSSs nucleation, the composite requires a higher stress value than that relative to the limestone rocks. I suggest that at the early stage of the folding process, the layer-parallel shortening provides the required stress for the nucleation of PSSs in those sequence characterized only by limestone beds, or limestone with marly layers, but this stress is not enough for the formation of PSSs in a sequence characterized by limestone and chert, which behaves as a composite material. Following this analysis, the PSSs formation during the early stages of folding is strongly influenced by the mechanical properties of the sequence, and in particular, if the chert layers are present PSSs formation may be inhibited.

Field observations strengthen this consideration. Fig. 3.18a shows the contact between the *Scaglia Rossa* Fm. with chert layers, in the lower part of the figure (note the continuous reddish chert layers at the bottom of the picture), and the reddish *Scaglia Rossa* Fm. without chert layers and with thin marl interlayers, in the upper part of the figure. The different mechanism

of fractures formation is evident. The *Scaglia Rossa* Fm. with chert layers is characterized mainly by joints (Fig 3.18c and d) whereas the *Scaglia Rossa* Fm. with marl interlayers shows mainly evidence of PSSs.

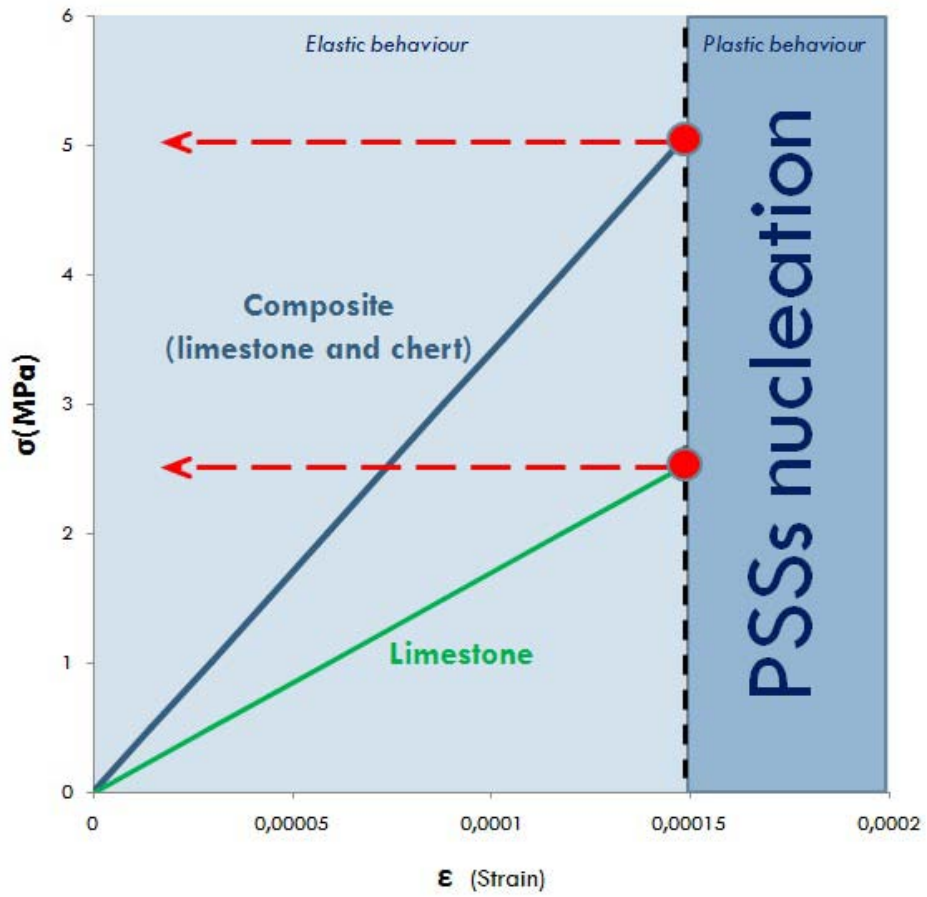

Fig. 3.39: Diagram showing the effects of the stiffer laminae (i.e. chert layers) on the mechanical behaviour of the composite. To reach the PSSs nucleation, the composite requires an higher stress value than that one relative to a limestone rocks.

Note that the partitioning of the stress between chert and limestone phases is strongly influenced by the angle between the stress direction and the laminae orientation. If stress direction is not parallel to the laminae, the partitioning of the stress changes and the limestone may reach the minimum value of stress for the onset of PSSs. Hence, it is reasonable to observe some LAB PSSs and slickolites in site 4 and 5, and interpret them as structures formed after the beds tilting.

If we analyse in detail the sites where the PSSs are the dominant mechanism it is possible to observe a further significant implication due to the different mechanical stratigraphy. Fractures in these sites are mainly HAB and LAB PSSs, and slickolites. The sites, except for site 7, are all in the backlimb of the *Cingoli* anticline and close to each other, so it could be assumed that the rocks should have been exposed to the same locale stress/strain distribution (Figs. 3.1 and 3.2), hence differences between the sites should be related to other factors. HAB PSSs with trend parallel to the fold axis (i.e. NW-SE) characterize all these sites. These PSSs could be compared,

as they do not abut against other fracture, to those PSSs developed due to the layer-parallel-shortening at the onset of anticline development (Engelder and Marshak, 1985; Tavani et al., 2006; Tavani et al., 2008; Agosta et al., 2009; Aydin et al., 2010; Tavani et al., 2011; Evans and Fischer, 2012). These sites are also characterized by HAB PSSs oblique to the fold axes, which further experienced shear displacement. Note that it has been impossible to observe the cross-cutting relationship with the former HAB PSSs. HAB PSSs oblique to fold axes are not so common in literature and it is difficult to suggest their formation mechanism. A preliminary hypothesis to explain these latter structures is that, at the beginning of the folding process, local anisotropies such as pre-existing tectonic and sedimentary structures may have locally driven non-cylindrical processes. Stress orientation may have been hence locally influenced by these anisotropies changing in this its regional trajectory (i.e. SW-NE). It should also be considered that the studied marly limestones are extremely prone to pressure solution as previously demonstrated (Stockdale, 1922 and 1926; Alvarez et al., 1976; Allmendinger, 1982; Mitra et al., 1984; Engelder and Marshak, 1985). Therefore, the occurrence of pressure solution seams may in some cases be the effect of local, small, tectonic loads.

Almost all the sites without chert layers show a significant presence of LAB PSSs, except for site 3, which is characterized mainly by HAB PSSs. In the literature (Rispoli, 1981; Willemse er al., 1997; Graham et al., 2003; Agosta and Aydin, 2006, Antonellini et al., 2008) some PSSs observed at an oblique angle to bedding have been considered as tail PSSs forming in the contractional quadrants relative to shearing (flexural slip) along another surface (bedding or pre-existing joints or PSSs). As flexural slip has been observed along bedding surfaces, the mechanism proposed in literature could explain those LAB PSSs formed due to a top-to-the-crest layer parallel shear normal to the fold axis (e.g. Fischer and Jackson, 1999; Tavani et al., 2011). Moreover, the observed late-stage LAB PSSs (dipping toward the hinge) and associated back-thrust (hanginwall-to-the-hinterland) are incompatible with the earlier stage structures (PSSs dipping toward the hinterland) and hence with a top-to-the-crest flexural slip. These late-stage structures (i.e PSSs dipping toward the hinge) suggest a kinematic change during the folding process probably due to the increasing of the frictional resistance and the subsequent change in the accommodation process (similarly to what Mitra, 2002, suggests for the formation of the back-thrusts). Moreover, several works suggest the presence of a buried back-thrust to the west of the studied area (Calamita et al., 1990; Menichetti, 1991; Fantoni and Franciosi, 2009) which could, hence, represents an evidence of the kinematic change of the fold evolution.

The interpretation of LAB PSSs sets oblique to the fold axes is rather complicated; these sets, in fact, imply pressure solution processes with compression axis almost oblique (and not parallel) to the direction of the main tectonic transport. It is reasonable to suppose that the fold limbs are not perfectly planar and, as suggested by the "inchworm fashion" movement of Couples et al (1998), the flexural slip could involve only part of the sheet at a time, transferring subsequently the shear on other patches of the layers. Hence, it is possible to suggest a general movement of the flexural slip top-to-the-crest but, in localised patches of the limb, for instance those characterized by anomalies in curvature or by pre-existing structures, the flexural slip could act oblique or even longitudinal to the main shear direction, explaining in this way the oblique and perpendicular to fold axis PSSs sets. Further data or a better theoretical understanding are necessary to fully interpret the development of these fracture sets during the folding process.

In any case, as above mentioned, the inclination of the marly limestone of the *Scaglia* Fms. to form PSSs (Stockdale, 1922 and 1926; Alvarez et al., 1976; Allmendinger, 1982; Mitra et al., 1984; Engelder and Marshak, 1985) lead to register any changing in the stress orientation (due for instance to pre-existing structures, sedimentary features, changes in curvature of the limbs etc.). It is hence important to discriminate those structures related to the folding process and those to local factors. The knowledge of these local structures is significant as they influence both fluid flow and the general accommodation of deformation (e.g. late-stage thrust).

What clearly emerges from the data collected in those sites characterized by PSSs is that the flexural slip is probably one of the main principal mechanism for the formation of anti-mode I structures. Hence, those sites characterized by alternating layers of highly contrasting competence or by well defined surfaces of discontinuity should be characterized by HAB and LAB PSSs. The results shown in this work seem to confirm this hypothesis, in fact the only site characterized mainly by HAB PSSs and just few LAB PSSs is site 3 where no marl layers are present and where the parallel to bedding surfaces are often discontinuous. According to this consideration, the mechanical stratigraphy plays hence another fundamental role for the fracture system characterization.

Hence, it is difficult to explain all the variability of fractures observed in those outcrops characterized by thinly bedded limestones and limestones with marly interlayers through the strain models proposed in literature, in particular the flexural slip model (Fig. 3.4b-IV). Local factors and the influence of mechanical stratigraphy play a leading role for the pattern of the fracture system formed during folding, in particular for what concerns the type of fracture

generated. On the contrary, the sites with chert layers and characterized by HAB joints show geometries similar to the scheme proposed in literature and predicted through the strain distribution models (Figs. 3.3 and 3.4). These sites are mainly characterized by joints perpendicular and parallel to the fold axis which have been already observed in literature (Price, 1966; Stearns, 1964 and 1968; Stearns and Friedman, 1972; Price and Cosgrove, 1990; Zhao and Jacobi, 1997; Couples et al., 1998; Fischer and Jackson, 1999; Fischer and Wilkerson, 2000; Salvini and Storti, 2001; Billi and Salvini, 2003; Tavani et al., 2006; Bellahsen et al., 2006; Tavani et al., 2008; Antonellini et al. 2008). The perpendicular to fold axes joints are considered to develop due to the layer parallel shortening during the first stage of folding process (e.g. Fischer and Jackson, 1999; Tavani et al., 2006; Tavani et al., 2008; Tavani et al., 2011) whereas, the parallel to fold axes joint observed in the hinge area could be due to the outer arc extension (Price, 1966; Stearns, 1964 and 1968; Stearns and Friedman, 1972; Price and Cosgrove, 1990; Fischer and Jackson, 1999; Fischer and Wilkerson, 2000; Bellahsen et al., 2006). On the other hand, it is rather complex to explain those joints parallel to fold axes and exposed along the anticline limbs. These joints seem to be coeval with the joints perpendicular to fold axes. This system of two sets of coeval joints looks like the so called “fracture grid-lock” described by Hancock et al. (1987) and Caputo et al. (1995). Caputo et al. (1995) observed that this pattern could be related to a local perturbation of the stress field due to the formation of opening fractures, which produces a “swap” between the two principal stress components. The continuous repetition of this mechanism through time lead to the formation of the so called “fracture grid-lock”. However, this mechanism is not applicable for the HAB joints observed in the *Cingoli* anticline. In fact, under a compressive tectonic regime ($\sigma_3 = \sigma_z$) the fractures pattern deriving from this mechanism should show a set perpendicular to fold axes and the other set almost horizontal. I suggest considering these joints parallel to fold axes as fractures due to local curvatures of the layers already present during the early stage of the fold formation and similar to the joints described in Bellahsen et al. (2006). It is important to note that the cross-cutting relationships between J1 and J2 sets have been made only on vertical exposures, the sites do not show any wide outcropping bedding parallel surface, and so it is possible that the observation made is misleading.

Furthermore, within this work an intriguing mechanism is suggested for the formation of some LAB offsetting structures observed in site 5. This site is characterized mainly by joints but, LAB offsetting structures have been observed (Fig. 3.22 and 3.26). These structures are formed by a series of segments, which show mainly pressure solution processes on their surfaces and

which are joined together, or slightly separated along the bedding surfaces or along the chert layers. A mechanism for the formation of these structures is here exposed. The first consideration is that limestones are prone to pressure solution but chert layers, on the contrary, are less sensitive to the applied stresses. During contraction and formation of oblique PSSs (few LAB PSSs have been observed in the site), the carbonate rock tends to dissolve with volume reduction and chert layers start to bend (Fig. 3.27e and f). As dissolution and volume reduction progresses, the chert layers form a tabular discontinuity characterized, due to the brittleness of chert, by breccias (Fig. 3.27g). If the dissolution continues, the chert layers break up and a slipping surface is formed (Fig. 3.27h). Since the volume reduction is high, veins and small faults create in order to compensate for material loss. Once that some of these PSSs are joined together, a well-defined surface is formed and along this surface slip may occur (Fig. 3.27c and d). This mechanism of deformation is supported by many field observations. The surfaces of these structures show columns, orange iron oxides, and they are characterized by a thin (residual?) greenish material (Figs. 3.23, 3.27a and b, and Fig. 3.28a and d). The presence of two LAB PSSs, which dip towards opposite direction and which are not formed at the same time, could explain the variation in thicknesses of the limestone beds (Fig. 3.28c). Furthermore, the offset shown in bedding parallel layers but not in the confining chert layers (Fig. 3.28a) represent other field evidences. The X-ray powder diffraction analysis of the greenish material sampled along the bedding surfaces and along the offsetting structures compared with those relative to the residual of the host rock (i.e. calcareous material) show that the samples are almost identical with peaks of quartz, illite, k-feldspar, montmorillonite and calcite (Fig. 3.22). The only difference is the absence of calcite minerals in the limestone sample, but it is due because the sample has been attacked with hydrochloric acid. These analysis show that both the material on the bedding surfaces and on the offsetting structures derives from the dissolution of the limestones.

These field and laboratory observations could suggest that the long offsetting structures are not proper faults but they represent surfaces of dissolution connected together. With the progress of pressure solution these structures may appear as faults. Considering these structures as “dissolution pseudo-faults” some problems may arises in particular in order to explain the stress distribution which could have been acted for their formation. Further detailed analysis should be made and a better theoretical understanding of this process is necessary.

3.7 Conclusions

This work suggests that the mechanical stratigraphy of the sequence involved in the folding process influence the formation of fold-related fractures. The schemes and model proposed in literature are useful to predict the geometries of the fracture systems but the mechanical type of fractures and their dimension are strongly influenced by local properties.

In particular it has been observed that the deformation of limestone with chert layers could be compared to the deformation acting on fiber composites. Chert layers act, during the early stage of folding when the compressive stress is almost bedding parallel, as a stiff lamina, which is embedded in a weak limestone matrix. In this way, a partitioning of stress occurred and the chert layers bear the greatest stress. For this reason, the stress on the limestone beds do not reach the supposed value for the onset of stylolitization as observed by the absence of pre-folding HAB PSS. For this reason, these sequences are mainly characterized by joints whereas, PSSs affect sequence without the stiffer phase (i.e. chert) and hence prone to dissolution.

Furthermore, it has been observed that sequences characterized by weaker layers (i.e. limestone beds with thin marl layers) are characterized by intense flexural slip. With the flexural slip several PSSs, especially at LAB, may form during the folding process. Those sites (in particular site 3) without important mechanical discontinuities, and hence without significant flexural slip, show the formation of HAB PSSs whereas the LAB PSSs is not well developed. As the mechanical layering is not so persistent, these sites are mainly characterized by non-stratabound PSSs.

Furthermore, the pressure solution processes may lead to the formation of long and almost continuous offsetting structures, called “dissolution pseudo-faults”. These pseudo-faults derive from connection of LAB pressure solution segments. The surfaces of these segments are characterized by evidence of pressure solution processes even if, due to the volume loss, veins, joints, and slip surfaces may contribute to the deformation within the volume of rock next to these structures

Recognizing and predicting the differences due to the mechanical stratigraphy is of great importance in particular for fluid flow. This study suggests that within a unique fold, and even within the same formation, different mechanical units can be characterized by different fluid flow. Sequence characterized by limestones with chert layers could be deformed mainly through mode I structures which form conduits for fluid flow, whereas limestones sequence without marl layers are deformed mainly through antimode-I fractures which inhibit fluid flow.

This work refers to local observations along an anticline in the northern Apennines, but the sequence observed (i.e the *Scaglia* Fms.) is a widespread sequence characterizing all the Tethys Ocean. Hence, what observed in the *Cingoli* anticline, once further studies strengthen the analysis shown in this work, could be of great relevance not only at the local scale.

REFERENCES

Agosta, F., Aydin, A., 2006. Architecture and deformation mechanism of a basin-bounding normal fault in Mesozoic platform carbonates, Central Italy. Journal of Structural Geology 28, 2445–2467.

Agosta, F., Alessandroni, M., Tondi, E., Aydin, A., 2009. Oblique-slip normal faulting along the northern edge of the Majella anticline: inferences on hydrocarbon migration and accumulation. Journal of Structural Geology 31, 690-774.

Agosta, F. Alessandroni, M., Antonellini, M., Tondi., E., Giorgioni, M., 2010. From fracture to flow: a field-based quantitative analysis of an outcropping carbonate reservoir. Tectonophysics 490, 197-213.

Allmendinger, R.W., 1982. Analysis of microstructures in the Meade plate of the Idaho–Wyoming foreland thrust belt, U.S.A.. Tectonophysics 85, 221-251.

Alvarez, W., Engelder, T., Lowrie, W., 1976. Formation of spaced cleavage and folds in brittle limestone by dissolution. Geology 4, 698-701

Alvarez, W., Engelder, T., Geiser, P.A., 1978. Classification of solution cleavage in pelagic limestones. Geology 6, 263-266.

Antonellini, M., Aydin, A., 1994. Effect of faulting on fluid flow in porous sandstones: petrophysical properties. American Association of Petroleum Geologists Bulletin 78, 355-377.

Antonellini M., Aydin A., 1995. Effect of faulting on fluid flow in porous sandstones: geometry and spatial distribution. AAPG Bulletin, 79 (5), 642–671.

Antonellini, M., Tondi, E., Agosta, F., Aydin, A., Cello, G., 2008. Failure modes in basin carbonates and their impact on fault development, Majella Mountain, central Italy. Marine and Petroleum Geology 25, 1074-1096.

Aydin A., 1978. Small faults formed as deformation bands in sandstone. Pure and Applied. Geophysics, 116, 913–930.

Aydin, A., 2000. Fractures, faults, and hydrocarbon entrapment, migration and flow. Marine and Petroleum Geology 17, 797-814.

Aydin, A., Borja, R. I. Eichhubl P., 2006. Geological and mathematical framework for failure modes in granular rock: Journal of Structural Geology 28, 83–98.

Aydin, A., Antonellini, M., Tondi, E., Agosta, F., 2010. Deformation along the leading edge of the Majella thrust sheet in central Italy. Journal of Structural Geology 32, 1291-1304.

Bai, T., Pollard, D.D., 2000. Fracture spacing in layered rocks: a new explanation based on the stress transition. Journal of Structural Geology 22, 43-57.

Baldi, A.M., Fuoco, S., Nucolussi P.P., 2007. Lo scavo della galleria stradale di Martignano (Trento): previsioni e riscontri:il ruolo delle indagini geofisiche. AGI Padova.

Bathrust, R.G.C., 1971. Carbonate Sediments and their diagenesis. Amsterdam, London, New York, Elsevier, pp. 620.

Beauchamp, E.K., Purdy, B.A., 1986. Decrease in fracture toughness of chert by heat treatment. Journ. Of Material Science 21, 1963-1966.

Bellahsen, N., Fiore, P., Pollard, D.D., 2006. The role of fractures in the structural interpretation of Sheep Mountain Anticline, Wyoming. Journal of Structural Geology 28, 850-867.

Bergbauer, S., Pollard, D.D., 2004. A new conceptual fold-fracture model including prefolding joints, based on field data from the Emigrant Gap Anticline, Wyoming. Geol. Soc. Of American Bull. 116, 294-307.

Billi, A., Salvini, F., Storti, F., 2003. The damage zone-fault core transition in carbonate rocks: implications for fault growth, structure, and permeability. Journal of Structural Geology 25, 1779-1794.

Billi, A., 2005. Attributes and influence on fluid flow of fractures in foreland carbonates of southern Italy. Journal of Structural Geology 27, 1630-1643.

Billings, M.P., 1972. Structural Geology, 3rd edn. Prentice-Hall, Englewood Cliffs, New Jersey.

Caine, J.S., Evans, J.P., Forster, C.B., 1996. Fault zone architecture and permeability structure. Geology 24, 1025-1028.

Calamita, F., Cello, G., Invernizzi, C., Paltrinieri, W., 1990. Stile strutturale e cronologia della deformazione lungo la traversa M.S. Vicino – Polverigi (Appennino marchigiano esterno). Studi Geologici Camerti, Volume Speciale, 69-86.

Caputo, R., 1995. Evolution of orthogonal sets of coeval extension joints. Terra Nova 7, 479-490.

Caputo, R., 2005. Stress variability and brittle tectonic structures. Earth-Science Reviews 70, 103-127.

Chester, J.S., 2003. Mechanical stratigraphy and fault-fold interaction, Absaroka thrust sheet, Salt River Range, Wyoming. Journal of Structural Geology 25, 1171-1192.

Cooke, M.L., Mollema, P.N., Pollard, D.D., Aydin, A., 1999. Interlayer slip and joint localization in the East Kaibab Monocline, Utah: field evidence and results from numerical modeling. In: Cosgrove, J. W., Ameen, M.S. (eds). Forced Folds and Fractures. Geological Society, London, Special Publications 169, 23-49.

Corbett, K., Friedman, M., Spang, J., 1987. Fracture development and mechanical stratigraphy of Austin Chalk, Texas. AAPG Bull. 71, 17-28.

Couples, G., D., Lewis, H., Tanner, P.W.G., 1998. Strain partitioning during flexural-slip folding. In: Coward M.P., Daltaban, T.S., Johnson, H. (eds.). Structural Geology in reservoir characterization. Geological Society, London, Special Pubblications 127, 149-165.

Deiana, G., Cello, G., Chiocchini, M., Galdenzi, S., Mazzoli, S., Pistolesi, E., Potetti, M., Romano, A., Turco, E., Principi, M., 2002. Tectonic evolution of the external zones of the Umbria-Marche Apennines in the Monte San Vicino-Cingoli area. Boll. Soc. Geol. It., Volume Speciale 1, 229-238.

Di Naccio, D., Boncio, P., Cirilli, S., Casaglia, F., Morettini, E., Lavecchia G., Brozzetti, F., 2005. Role of mechanical stratigraphy on fracture development in carbonate reservoirs: insights from outcropping shallow water carbonates in the Umbria-Marche Apenninens, Italy. Journ. Of Volc. and Geoth. Research.

Ebner, M., Koehn, D., Toussaint, R., Renard, F., Schmittbuhl, J., 2009. Stress sensitivity of stylolite morphology. Earth and Planetary Science Letters 277, 394-398.

Ebner, M., Toussaint, R., Schmittbuhl, J., Koehn, D., Bons, P., 2010. Anisotropic scaling of tectonic stylolites: A fossilized signature of the stress field?. Journal Of Geophysical Research 115, B06403, doi:10.1029/2009JB006649.

Engelder, T., Scholz, C., 1981. Fluid flow along very smooth joints at effective pressure up to 200 megapascals. In: Carter, N.L. (Ed.), Mechanical Behaviour of Crustal Rock. AGU Geophysical Monograph Series 24, 147-152.

Engelder, T., Marshak, S., 1985. Disjunctive cleavage formed at shallow depths in sedimentary rocks. Journal of Structural Geology, 7, 327-342.

Evans, M.A., Fischer, M.P., On the distribution of fluids in folds: A review of controlling factors and processes, Journal of Structural Geology (2012), http://dx.doi.org/10.1016/j.jsg.2012.08.003.

Fantoni, R., Franciosi, R., 2009. Mesozoic extension and Cenozoic compression in Po Plain and Adriatic foreland. Rendiconti online Soc. Geol. It. 9, 28-31.

Faulkner, D.R., Jackson, C.A.L., Lunn, R.J., Schlische, R.W., Shipton, Z.K., Wibberley, C.A.J., Withjack, M.O., 2010. A review of recent developments concerning the structure, mechanics and fluid flow properties of fault zones. Journal of Structural Geology 32, 1557-1575.

Fischer, M.P., Jackson, P.B., 1999. Stratigraphic controls on deformation patterns in fault-related folds: a detachment fold example from the Sierra Madre Oriental, northeast Mexico. Journal of Structural Geology 21, 613-633.

Fischer, M.A., Wilkerson, M.S., 2000. Predicting the orientation of joints from fold shape: results of pseudo-three-dimensional modeling and curvature analysis. Geology 14, 451-460.

Frehner, M., 2011. The neutral lines in buckle folds. Journal of Structural Geology 33, 1501-1508.

Friedman, M., 1969. Structural analysis of fractures in cores from the Saticoy Field, Ventura Co., California. AAPG Bullettin 53, 367-389.

Friedman, M., Sowers, G. M., 1970. Petrofabrics: a critical review. Canadian Journal of Earth Sciences 7, 477-497.

Gillespie, P.A., Johnston, J.D., Loriga, M.A., Mccaffrey, K.J.W., Walsh, J.J. & Watterson, J., 1999. Influence of layering on vein systematics in line samples. In: Mccaffrey, K.J.W., Lonergan, L.L., Wilkinson, J.J. (eds.), Fractures, Fluid Flow and Mineralization. Geological Society, London, Special Publications 155, 35-56.

Graham Wall, B.R., Antonellini, M., Aydin, A., 2003. Formation and growth of normal faults in carbonates within a compressive environment. Geology 31, 11-14.

Graham-Wall, B., Girgacea, R., Mesonjesi, A., Aydin, A., 2006. Evolution of fluid pathways through fracture controlled faults in carbonates of the Albanides foldthrust belt. American Association of Petroleum Geologists Bulletin 90, 1227–1249.

Gross, M.R., 1993b. The effects of mechanical stratigraphy on failure mode and fracture spacing in the Monterey Formation of coastal California. PhD Thesis, Pennsylvania State University, USA.

Gross, M.R., 1995. Fracture partitioning-failure mode as a function of lithology in the Monterey Formation of coastal California. Geological Society of America Bullettin 10, 779-792.

Gross, M.R., Bahat, D., Becker, A., 2012. Relations between jointing and faulting based on fracture-spacing ratios and fault-slip profiles: A new method to estimate strain in layered rocks. Geology 25, 887-890.

Hancock, P.L., 1985. Brittle microtectonics: principles and practice. Journal of Structural Geology 7, 437-457.

Hancock P.L., Al-Kadhi A., Barka, A.A., Bevan, T.G., 1987. Aspects of ana-lysing brittle structures, Ann. Tectonicue 1, 519.

Hills, E.S., 1972. Elements of Structural Geology, Second edition. Chapman and Hall, London.

Hosford, W. F., 2005. Mechanical behavior of materials. Cambridge University Press, New York, pp.425.

Hudleston, P.J., Lan, L., 1993. Information from fold shapes. Journal of Structural Geology 15, 253-264.

Hudlestone, P.J., Treagus, S.H., Lan, L., 1996. Flexural flow folding: Does it occur in nature? Geology 24, 203-206.

Jaeger, J.C., Cook, N.G.W., 1979. Fundamentals of rock mechanics, 3rd edition. Chapmann and Hall, London, 593 pp.

Jones, G., Fischer, Q.J., Knipe, R.J., 1998. Faulting, fault sealing and fluid flow in hydrocarbon reservoirs. Geol. Soc. Lond. Spec. Pubbl. 147.

Lama, R. D., Vutukuri, V. S., 1978. Handbook on mechanical properties of rocks-testing techniques and results. Vol. 3. 495 pp.

La Pointe P., Hermanson J., Parney R., Eiben T., Dunleavy M., Steele K., Whitney J., Eubanks D. & Straub R., 2002. 3-D reservoirs and stochastic fracture network modelling for enhanced oil recovery, Circle Ridge Phosphoria/Tensleep Reservoir, Wind River Reservation, Arapho and Shoshone Tribes, Wyoming. DOE: DE-FG26-00BC15190.

Marshak, S., Engelder, T., 1985. Development of cleavage in limestones of a fold-thrust belt in eastern New York. Journal of Structural Geology 7, 345-359.

Mazzoli, S., Deiana, G., Galdenzi, S., Cello, G., 2002. Miocene fault-controlled sedimentation and thrust propagation in the previously faulted external zones of the Umbria-Marche Apennines, Italy. EGU Stephan Mueller Special Publication Series 1, 195-209.

Menichetti, M., 1991. La sezione geologica Cingoli-M. Maggio-Tevere nell'Appennino umbro-marchigiano: analisi cinematica e strutturale. Studi Geologici Camerti Volume Speciale 1, 315-328.

Mitra, G., Yonkee, W.A., Gentry, D.J., 1984. Solution cleavages and its relationship to major structures in the Idaho–Utah–Wyoming thrust belt. Geology 12, 354–358.

Mollema, P.N., Antonellini, M., 1999. Development of strike-slip faults in the dolomites of the Sella Group, northern Italy. Journal of Structural Geology 21, 271-292.

Narr, W., Suppe, J. 1991. Joint spacing in sedimentary rocks. Journal of Structural Geology 13, 1037-1048.

Nelson, R.A., 2001. Geologic Analysis of Naturally Fractured Reservoir, 2nd edition, Gulf Professional Publishing, Houston.

Parck, W.C., Schot, E.H., 1968. Stylolites: their nature and origin. Journ. Sediment. Petrol. 38, 175-191.

Peacock, D.C.P., Sanderson, D.J., 1995. Pull-apart, shear fractures, and pressure solution. Tectonophysics 241, 1-13.

Petracchini, L. Antonellini, M., Billi, A., Scrocca, D., Fault development through fracture pelagic carbonates of the Cingoli anticline, Italy: Possible analog for subsurface fluid-conductive fractures. Journal of Structural Geology (2012). *In press*

Pollard, D.D., Aydin, A., 1988. Progress in understanding jointing over the past century. Geological Society of American Bulletin 100, 1181-1204.

Pollard, D.D., Segall, P., 1987. Theoretical displacements and stresses near fractures in rock: with applications to faults, joints, veins, dikes and solution surfaces. In: B. A., Atkinson (ed.), Fracture mechanics of rock: London, Academic Press, 277–349.

Price, N.J., 1966. Fault and joint development in brittle and semi-brittle rocks. Pergamon, Oxford, 176 pp.

Price, N.J., Cosgrove, J.W., 1990. Analysis of geological structures. Cambridge University Press, Cambridge, 502 pp.

Protzman, G. M., Mitra, G., 1990. Strain fabric associated with the Meade thrust sheet: Implications for cross-section balancing: Journal of Structural Geology 12, 403–417.

Railsback, B.L., Andrews, L.M., 1995. Tectonic stylolites in the 'undeformed' Cumberland Plateau of southern Tennessee, Journ. Struct. Geol. 17, 911–915. doi:10.1016/0191-8141(94)00127-L.

Ramberg, H., 1963. Strain distribution and geometry of folds. Bulletin of the Geological Institute of the University of Uppsala 42, 1-20.

Ramsay, J.G. 1967. Folding and Fracturing of Rocks. McGraw-Hill.

Ramsay, J.G., Huber, M.I., 1987. The Techniques of Modern Structural Geology. Volume 2. Folds and Fractures. Academic, New York.

Rispoli, R., 1981. Stress fields about strike-slip faults inferred from stylolites and tension gashes: Tectonophysics, 75, 29-36.

Roylance, D., 2008.Mechanical properties of materials.

Rustichelli, A., Tondi, E., Agosta, F., Cilona, A., Giorgioni, M., 2012. Development and distribution of bed-parallel compaction bands and pressure solution seams in carbonates (Bolognano Fm., Majella Mountain, Italy). Journal of Structural Geology 37, 181-199.

Rutter, E.H., 1983. Pressure solution in nature, theory and experiment. Journ. Geol. Soc. London 140, 725-740.

Salvini, F., Billi, A, Wise, D.U., 1999. Strike-slip fault-propagation cleavage in carbonate rocks: the Mattinata fault zone. Journal of Structural Geology 21, 1731-1749.

Salvini, F., Storti, F. , 2001. The distribution of deformation in parallel fault-related folds with migrating axial surfaces: comparison between fault-propagation and fault-bend folding. Journal of Structural Geology 23, 25-32.

Sanders, C., Bonora, M., Richards, D., Kozlowski, E., Sylwan, C., Cohen, M, 2004. Kinematic structural restorations and discrete fracture modeling of a thrust trap: a case study from the Tarija Basin, Argentina. Marine and Petroleum Geology 21, 845–855

Savage, H.M., Shackleton, J.R. Cooke, M.L., Riedel, J.J. 2010. Insights into fold growth using fold-related joint patterns and mechanical stratigraphy. Journal of Structural Geology 32, 1466-1475.

Schultz A., Fossen H., 2008. Terminology for structural discontinuities. AAPG Bullettin, 92 (7), 853-867.

Schmidt. R.A., 1975. Experimental mechanics, 161-167.

Segall, P., Pollard, D.D., 1980. The mechanics of discontinuous faults, Journal of Geophysical Research 85, 4337-4350.

Servizio Geologica d'Italia, 2003. Tolentino. Servizio Geologico d'Italia, Carta Geologica d'Italia 1:50,000, sheet 302, Rome.

Sibson, R.H., 1996. Structural permeability of fluid-driven fault-fractures meshes. Journal of Structural Geology 18, 1031-1042.

Stearns, D.W., 1964. Macrofracture patterns on Teton Anticline, N.W. Montana (Eos). Trans A.G.U., 45, 107

Stearns, D.W., 1968. Certain aspects of fractures in naturally deformed rocks. Rock mechanics seminar. R.E. Riecker, 97-118. Terr. Sci. Lab., Bedford, Mass.

Stearns, D.W., Friedman, M., 1972. Reservoirs in fractured rocks. AAPG Memoir 16, 82-100.

Storti, F., Salvini, F., 1996. Progressive rollover fault-propagation folding: a possible kinematic mechanism to generate regional-scale recumbent folds in shallow foreland belts. AAPG Bull. 80, 174-193

Stockdale, B., 1922. Stylolites: Their Nature and Origin, IX. Indiana University Studies, pp. 97.

Stockdale, P.B., 1926. The stratigraphic significance of solution in rocks. Journal Geology 34, 399-414.

Suppe, J., 1985. Principles of Structural Geology, Prentice-Hall, Englewood Cliffs, NJ, 537 pp.

Tada, R., Siever, R., 1989. Pressure solution during diagenesis. Annal review Earth Planet. Sci. 17, 89-118.

Tavani, S., Storti, F., Fernànedz, O., Muñoz, J.A., Salvini, F., 2006. 3-D deformation pattern analysis and evolution of the Añisclo anticline, southern Pyrenees. Journal of Structural Geology 28, 695-712.

Tavani, S., Storti, F., Salvini, F., Toscano, C., 2008. Stratigraphic versus structural control on the deformation pattern associated with the evolution of the Mt. Catria anticline, Italy. Journal of Structural Geology 30, 664-681.

Tavani, S., Mencos, J., Bausà, J., Muñoz, J.A., 2011. The fracture pattern of the Sant Corneli Bóixols oblique inversion anticline (Spanish Pyrenees). Journal of Structural Geology 33, 1662-1680, doi:10.1016/j.jsg.2011.08.007.

Tondi, E., Antonellini, M., Aydin, A., Marchegiani, L., Cello, G., 2006. The roles of deformation bands and pressure solution seams in fault development in carbonate grainstone of the Majella Mountain, Italy. Journal of Structural Geology 28, 376-391.

Twiss, R.J., Moores, E.M., 1992. Structural Geology. New York, Freeman and Company, 532pp.

West, T.R., 1994. Geology applied to engineering: Englewood Cliffs, N.J., Prentice Hall, 560 pp.

Wyllie, D.C. (1999) Foundations on Rock, 2nd edn, Taylor and Francis Press, Boca Raton, FL, pp. 345–347.

Willemse, E.J.M., Peacock, D.C.P., Aydin, A., 1997. Nucleation and growth of strike-slip faults in limestones from Somerset, U.K. Journal of Structural Geology 19, 1461-1477.

Woodward, N.B., Rutherford, E. Jr, 1989. Structural lithic units in external orogenic zones. Tectonophysics 158, 247–267.

Zhao, M., Jacobi, R.D., 1997. Formation of regional cross-fold joints in the northern Appalachian Plateau. Journal of Structural Geology 19, 817-834.

Zoback, M.D., Barton, C.A., Brudy, M., Castillo, D.A., Finkbeiner, T., Grollimund, B.R:, Moos, D.B., Peska, P., Ward, C.D., Wirput, D.J., 2003. Determination of stress orientation and magnitude in deep wells. Rock Mechanics and Mining Sciences 40, 1049-1076.

4. Fault Development Through Fractured Pelagic Carbonates of the *Cingoli* Anticline, Italy: Possible Analog for Subsurface Fluid-Conductive Fractures

Lorenzo Petracchini, Marco Antonellini, Andrea Billi, Davide Scrocca

Published in: *Journal of Structural Geology*, *Volume 45*, *December 2012*, *Pages 21-37*

4.1 Introduction

Faults have a significant impact on fluid flow through rocks, as they may act as barriers, carriers, or combined barrier-carrier systems through the different fault zone compartments (Engelder and Scholz, 1981; Cooper, 1992; Antonellini and Aydin, 1994; Sibson, 1996; Caine et al., 1996 and 2003; Odling et al., 1999; Salvini et al., 1999; Aydin, 2000; Billi, 2005; Micarelli et al., 2006; Agosta et al., 2007; Billi et al., 2008; Agosta et al., 2009 among many others). These complex structures represent an important target in environmental, industrial, and economic studies and activities such as groundwater, hydrocarbon and geothermal exploitation, waste disposal, CO_2 storage, and assessment of pollutant dispersion in aquifers (e.g., Brusseau, 1994; Gudmundsson, 2000; Nelson, 2001; Caine and Tomusiak, 2003). In the hydrocarbon industry, fractured carbonate reservoir development is a very challenging task (e.g., properly deviating wells or determining the fractures that are open and those that are closed) due to the complexity of fracture patterns and their related permeability structure (e.g., Peacock and Sanderson, 1995; Willemse et al., 1997; Mollema and Antonellini, 1999; Antonellini and Mollema, 2000; Billi and Salvini, 2001; Graham et al., 2003; Billi et al., 2003; Mazzoli and Di Bucci, 2003; Tondi et al., 2006; Antonellini et al., 2008; Agosta et al., 2010; Aydin et al., 2010; Guerriero et al., 2011). Recent works documented that fluid movements in fractured reservoirs are mainly controlled by a limited number of through-going conductive fractures (or fracture swarms), whereas the surrounding cloud of smaller fractures has a smaller influence on fluid flow (Lonergan et al., 2007; Ozkaya et al., 2007; Wennberg et al., 2007; Akbar and Montaron, 2008; Singh et al., 2008; Questiaux et al., 2010; Souque et al., 2011). The different contribution to fluid flow of the aforementioned structures is known from flowmeter data from producing wells (Ozkaya and Minton, 2007). What is less well known, in contrast, is the architecture and growth mechanisms of the subsurface conductive fractures (or fracture swarms). As these fractures are important for fluid flow in fractured carbonate reservoirs, possible exposed analogs (i.e., conceivably assumed as such; e.g., Wennberg et al., 2007) must be studied to improve the current knowledge of conductive-fractures at reservoir depths and, consequently, develop reliable flow models.

In this paper, we study small faults cutting fractured carbonate beds (i.e., marly limestone forming the late Cretaceous-Eocene *Scaglia Rossa* Formation) exposed in the backlimb of the Cingoli anticline, northern Apennines, Italy (Fig. 4.1).

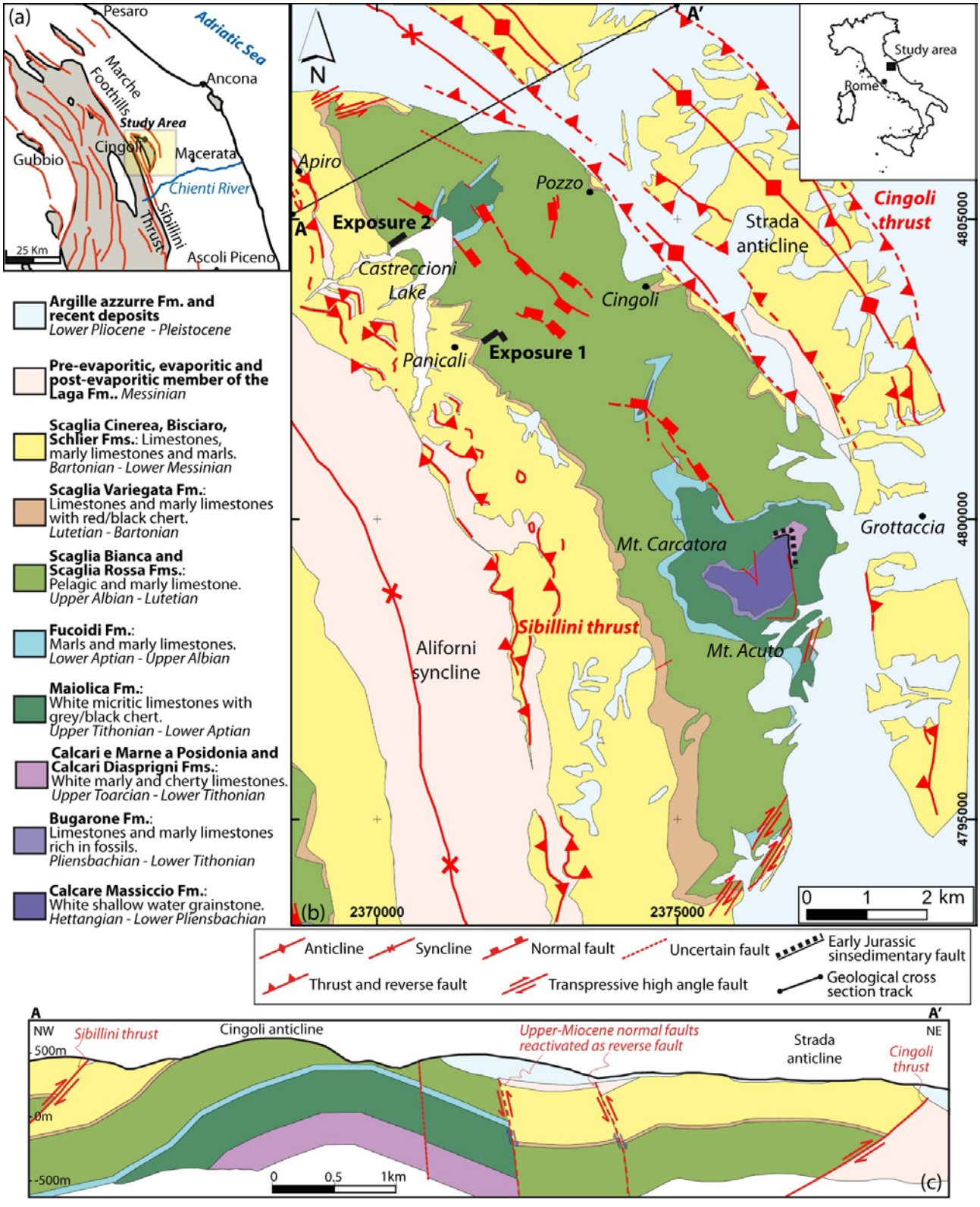

Fig. 4.1: (a) Location of the study area. The Cingoli anticline is in the foothills of the northern Apennines fold and thrust belt, Umbria-Marche area, Italy. (b) Simplified geo-structural map of the Cingoli anticline area (modified after Servizio Geologico d'Italia, 2003 - Coordinate System: Gauss Boaga, Est - Roma 1940). The exposures studied in this paper are located in the northern sector of the anticline backlimb, within the Scaglia Rossa Fm. (c) Geological cross-section through the northern sector of the Cingoli anticline, based on a seismic reflection profile and previous studies (Mazzoli et al. 2002; Deiana et al., 2002; Servizio Geologico d'Italia, 2003).

Fractured anticlines are well-known natural traps for fluids (e.g., Nelson, 2001; Fischer et al., 2009). Due to their connected geometry and architecture, we assume that the faults and associated fractures that we observed in this study may be considered as analogs of conductive fractures in subsurface carbonate rocks. Understanding their growth mechanisms is, therefore, of theoretical and applied relevance. The assumption is speculative as the architecture of conductive fractures at reservoir depths is substantially unknown due to the limited resolution of subsurface investigation methods (below seismic resolution). Our main aim is, however, to offer a detailed structural analysis and coherent genetic model of structures that are potentially fluid-conductive fractures, particularly when compared with the small, stratabound, and poorly-connected fractures forming the background fabric in the carbonate host rock. The presented case history is also interesting, among other reasons, for the presence of close hydrocarbon fields characterized by similar anticlinal structures in the same sedimentary sequence (i.e., the Po Plain and the Adriatic foreland; Pieri and Mattavelli, 1986; Mattavelli et al., 1993; Casero, 2004).

4.2 Methods

This work focuses on two exposures located in the Cingoli anticline backlimb (Fig. 4.1). The studied exposures allow for a 3D view of fractures, with natural cross sections oriented either perpendicular or parallel to the anticline axis. Additional exposures of bedding surfaces are also present (Fig. 4.2). The localities of the exposures are far away from major tectonic structures (large-displacement faults).

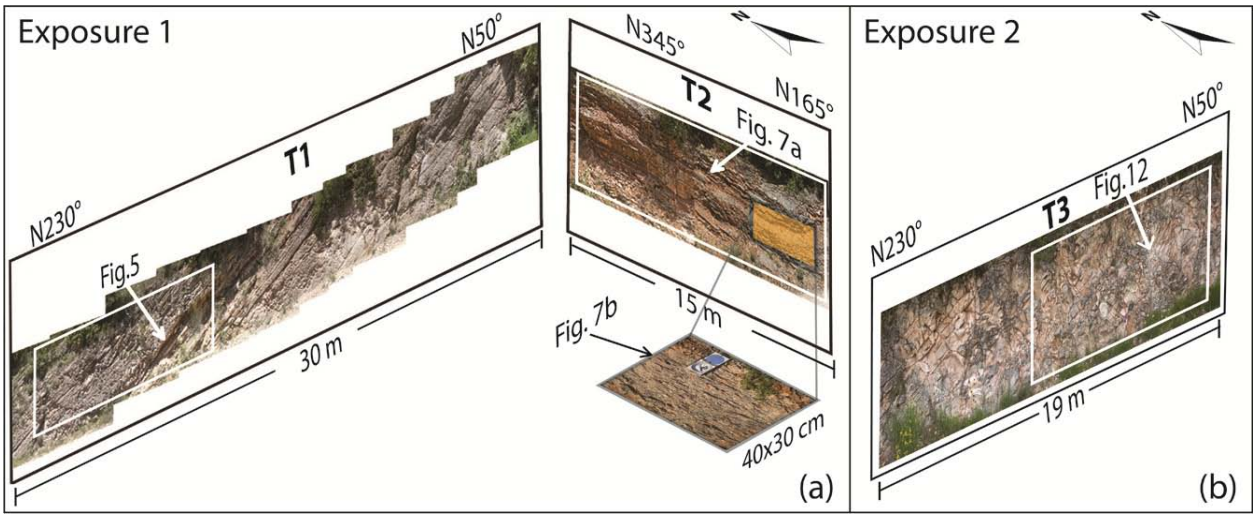

Fig. 4.2: Schematic 3D-view of the studied exposures. (a) Exposure 1 is characterized by two outcrops, T1 and T2, which are perpendicular and parallel, respectively, to the Cingoli anticline axis. Note in outcrop T2 a bedding-parallel pavement (30 by 40 cm) that was mapped at the 1:1 scale to study fracture relationships. (b) Exposure 2 is characterized by a single outcrop (T3) perpendicular to the anticline axis.

In this paper, we use fractures as a generic term including pressure solution seams, sheared pressure solution seams, joints, and faults (Pollard and Aydin, 1988). In the Cingoli anticline, fractures are characterized by a typical background pattern (e.g., Tavani et al., 2010) mainly consisting of closely-spaced stratabound pressure solution seams (PSSs), which can be nearly perpendicular or at low angles to bedding. We consider as high angle to bedding (HAB) those structures that form an angle with bedding greater than 75° (between 75° and 90°) and as low angle to bedding (LAB) those structures forming an angle to bedding smaller than 75°. This threshold angle was chosen on the basis of geomechanical considerations, which predict closure and opening fracture formations, respectively in the compressional and extensional quadrants, at 72° to a sheared discontinuity (i.e. flexural slip planes) (Pollard and Aydin, 1988).

The background fabric of fractures is, in places, crosscut by through-going faults and associated fractures. In the following sections, we focus our attention on the geometry and development of these faults.

The data presented in this work derive from field surveys and detailed mapping of the studied exposures. In particular, we mapped the fractured exposures, reporting each fracture on photomosaics at 1:1 to 1:20 scale and verifying the fracture type directly in the field. We paid particular attention to the following issues:

(1) Type of fractures (i.e., PSSs, sheared PSSs, joints, or faults);

(2) Orientation of fractures and their orientation relative to bedding surfaces;

(3) Fracture confinement (stratabound vs. non-stratabound);

(4) Fracture abutting and crosscutting relationships;

(5) Evolution of fractures (e.g., from PSSs to sheared PSSs);

(6) Geometric, tectonic, and temporal relationships between through-going faults, bedding surfaces, and the background fabric of fractures.

We also studied the fractured carbonates in thin-sections by using an optical microscope to identify the fracture type and origin (e.g., PSSs, sheared PSSs, faults). Fracture attitude data are henceforth expressed in degrees as dip direction/dip (e.g., 245°/ 30° to indicate that the fracture plane dips toward N245° with a dip angle of 30°). The main characteristics of fracture sets recognized in Exposures 1 and 2 are reported in the synoptic view of Fig. 4.3.

Set	Type	Orientation	Mech. Confinement	Angle to bed.	Kinematics	Abutting
I	PSS	NE dipping	Strata-bound	HAB	NO	No abutting
II	PSS	SW dipping	Strata-bound	LAB	Reverse	Ambiguous
III	PSS	W dipping	Strata-bound	LAB	Sinistral Strike Slip	Abut on Set I
IV	PSS	NE dipping	Strata-bound	LAB	Reverse	Abut on Set I-II-III
V	PSS	N & S dip., subvert.	Strata-bound	HAB	Oblique/Strike Slip	?
VI	PSS	SE dipping	Strata-bound	LAB	Transtensional - Sx	Abut on Set IV
VII	PSS	NW dipping	Strata-bound	LAB	Transtensional - Sx	Abut on Set IV

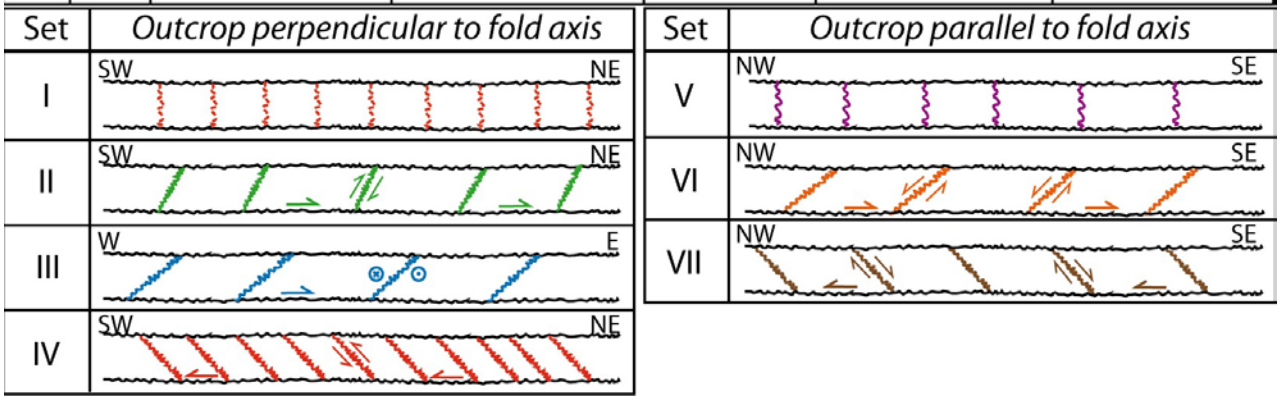

Fig. 4.3: Synopsis of all observed fracture sets and main attributes. PSS: pressure solution seam; HAB: high angle to bedding (75-90°); LAB: low angle to bedding (< 75°).

4.3 Results

4.3.1 Exposure 1

Exposure 1 consists of two sub-vertical outcrops (T1 and T2) oriented at right angles to each other, and approximately perpendicular and parallel to the Cingoli anticline axis (Figs. 4.1 and 4.2a). Exposure 1 also includes a bedding-parallel pavement that we characterized to better understand the three-dimensional distribution of fractures (Fig. 4.2a). The T1 outcrop is SW-NE oriented, approximately 30 m-long, and 3 m-high. The T2 outcrop is NW-SE oriented, about 15 m-long, and 1.5 m-high. The dimensions of the bedding-parallel pavement is 30 by 40 cm.

Outcrops of Exposure 1 show the upper part of the Scaglia Rossa Fm., which is here characterized by thinly-bedded reddish limestones and marly limestones without chert, and by clay content higher than in the lower portion of this formation (Figs. 4.4, 4.5 and 4.6). Along the T1 and T2 outcrops (Figs. 4.4 and 4.5), bedding surfaces are defined by PSSs with a general orientation of 235°/30°. Carbonate beds are generally 10-50 cm thick; thinner (up to 5 cm thick) layers of marls and marly limestones may also be present at different levels. Slickenlines and other kinematic markers present on several bedding surfaces, particularly where marly interlayers occur, are consistent with a flexural slip mainly along a NE-SW trend.

The T1 and T2 outcrops are characterized by stratabound PSSs spaced between 1 and 10 cm (i.e., this spacing refers to the distance between two adjacent fractures pertaining to the same set). Marly layers constitute the mechanical discontinuity against which all PSSs sets abut. When these layers are absent, some PSSs cut across the bedding surfaces. A few longer through-going faults are also exposed along the T1 outcrop (Figs. 4.4 and 4.5).

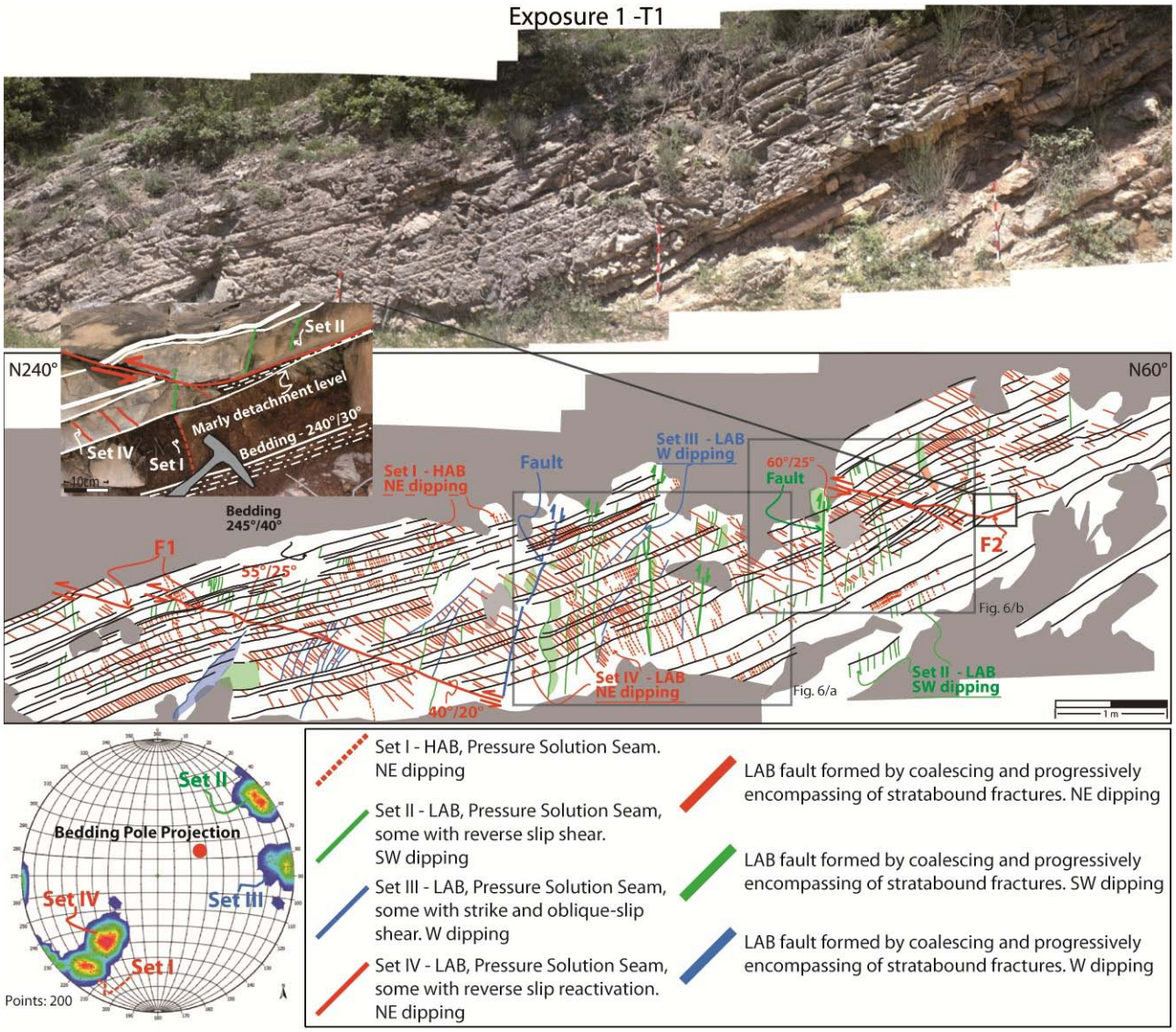

Fig. 4.4: Photomosaic and related line drawing of T1 outcrop in Exposure 1. Four sets of pressure solution seams (PSSs) are identified (see lower hemisphere equal area projection of PSSs poles and their density contours). Note two reverse NE-dipping faults (F1 and F2) cutting through the fractured strata. In the small photograph, a detail from the F2 fault is displayed, showing a marly layer acting as a detachment level, along which fault movement occurred. Attitude data are expressed in dip azimuth/dip form; HAB: high angle to bedding; LAB: low angle to bedding.

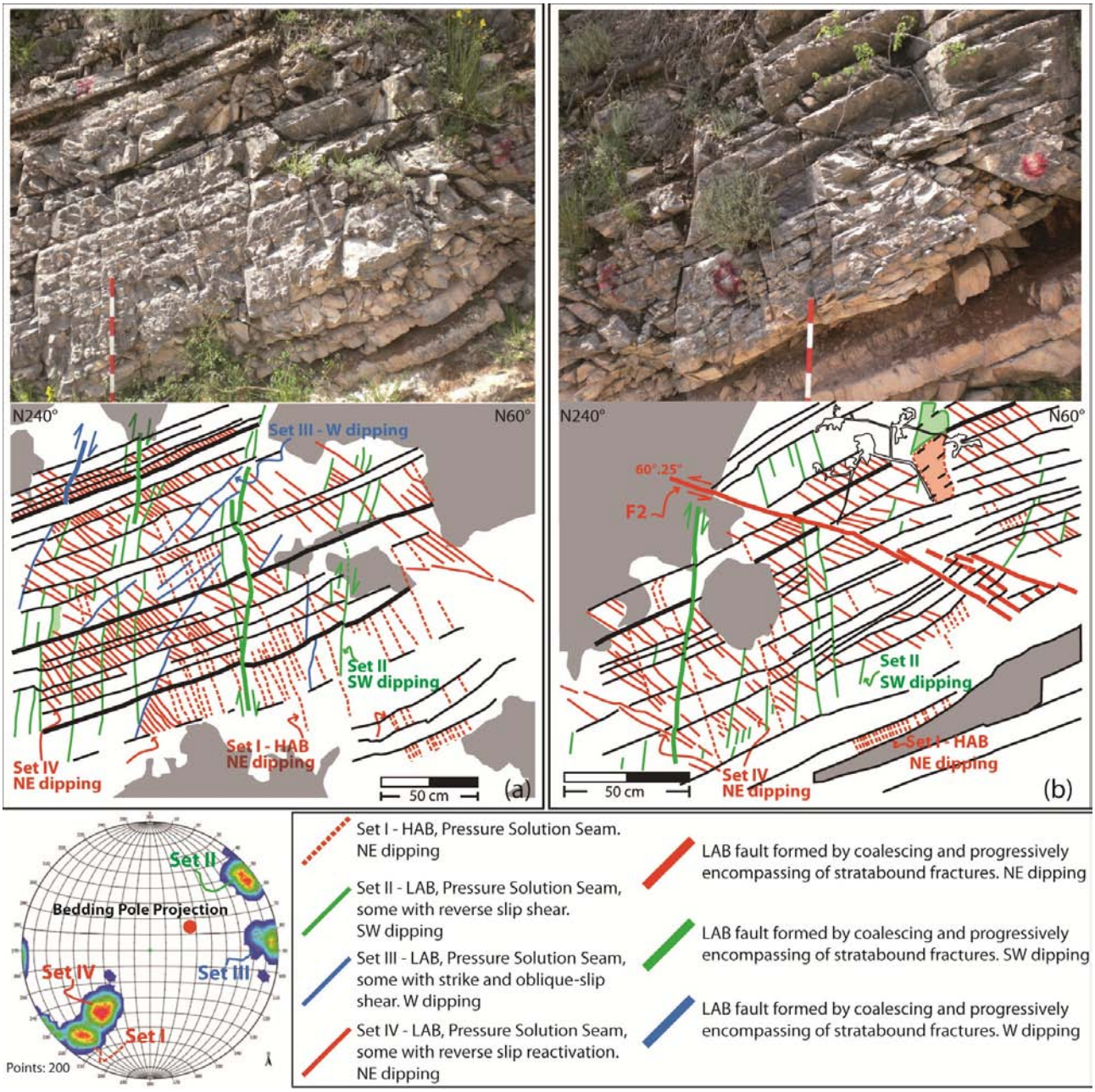

Fig. 4.5: Photomosaic and related line drawings of portions of the T1 outcrop in Exposure 1, showing the geometric relationships between sets of pressure solution seams (PSSs; see lower hemisphere equal area projection of PSSs poles and their density contours) and faults. Attitude data are expressed in dip azimuth/dip form; HAB: high angle to bedding; LAB: low angle to bedding.

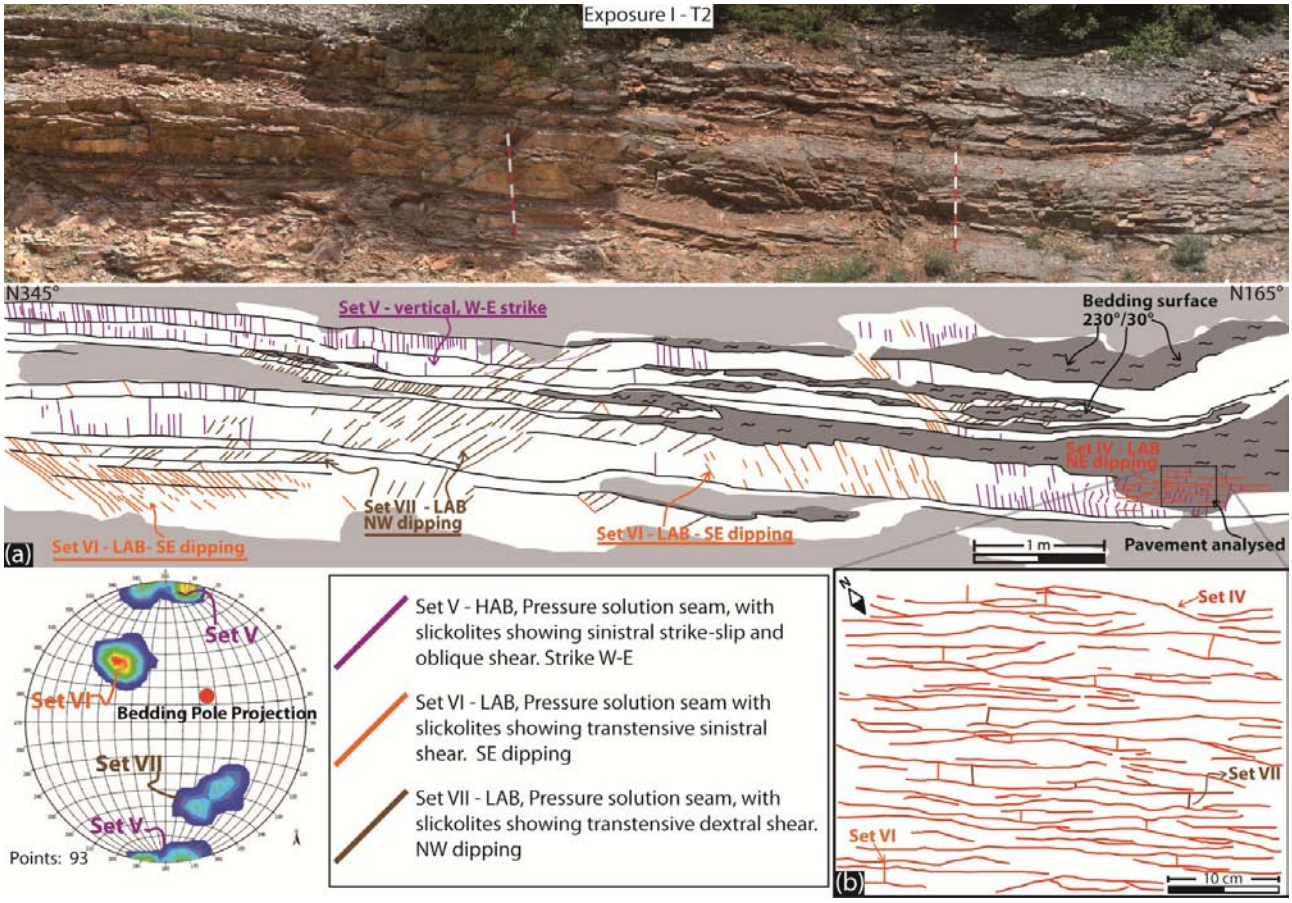

Fig. 4.6: (a) Photomosaic and related line drawings of the T2 outcrop in Exposure 1. Three sets of pressure solution seams (PSSs) are identified (see lower hemisphere equal area projection of PSSs poles and their density contours). (b) Fracture mapping on a small portion of a bed-parallel pavement 30 by 40 cm. Attitude data are expressed in dip azimuth/dip form; HAB: high angle to bedding; LAB: low angle to bedding.

Fracture sets are described below following a temporal criterion (from the oldest to the youngest sets), which was determined by careful observation of their abutting and crosscutting relationships. The affiliation of fractures to specific sets was determined on the basis of fracture attitude (i.e., fracture parallelism; see stereonets in Figs. 4.4 and 4.6) and type. In the T1 outcrop, we recognized four main sets of fractures (Figs. 4.4, 4.5 and 4.7):

Set I: Set I is characterized by HAB (85°-90°) PSSs with toothed surfaces, which are stained with iron oxides and clay residues. Field and thin-section observations show clear evidence of dissolution along these surfaces (Fig. 4.7a-d; see also in supplementary material Fig. S1a-c). The stylolite peaks are generally perpendicular to the PSSs (Fig. 4.7b and d), which are mostly stratabound (Fig. 4.5), and dipping toward N39° with a dip angle of about 72° (see stereonet in Fig. 4.4). PSSs of Set I do not show evidence of shear displacement (Fig. 4.7a and S1a-c) and usually have terminations or nucleation tips right along the bedding surfaces, particularly along the contact between carbonate beds and the thin marly layers.

Set II: Fractures of this set consist of LAB (55°) PSSs (Fig. 4.7e-h and S1d-f), dipping towards N234° with a dip angle of about 84° (see stereonet in Fig. 4.4). Some of these PSSs abut or veer towards those of Set I (Fig. 4.8c), indicating that Set I is older than Set II. Exceptions to this rule are occasionally observed (Fig. 4.8c). Fractures of Set II do not generally show evidence of shear displacement except in a few cases, where some dip-slip reverse (or sub-vertical) offsets were observed (Figs. 4.7f and 4.9).

Set III: This set is formed by LAB (<60°) PSSs, oriented 270°/77°. Some of these surfaces show evidence of younger left-lateral strike-slip offsets (Fig. 4.7i and j). For this reason, some fractures of Set III cut across bedding surfaces and are generally longer than most stratabound fractures forming the background fabric of the T1 outcrop. Fractures of Set III are not as well developed as fractures of other sets occurring in the T1 outcrop.

Set IV: Fractures of this set are the most frequent and pervasive in the T1 outcrop (Figs. 4.4 and 4.5). They consist of LAB (c. 60°) PSSs (Figs. 4.7k, m, n, and S1g-i), which are generally stratabound and dipping towards NE with a dip angle of 40°. Field and thin-section observations show that stylolite peaks are perpendicular to the PSSs surfaces. Occasionally, these fractures show evidence of dip-slip reverse offsets (Fig. 4.7l). Fractures of Set IV normally terminate against or veer towards fractures of Set I, Set II, and Set III (Figs. 4.5a and 4.8).

Although present, fractures of Sets V, VI, and VII (see below) are hard to spot in the T1 outcrop because of their approximately parallel orientation to the outcrop wall (compare stereonet of Fig. 4.6 with orientation of the T1 outcrop reported in Fig. 4.2). For this reason, Sets V, VI, and VII are described in the T2 outcrop, where they are more clearly visible.

The T1 outcrop exposes two reverse, LAB faults that cut through the fractured carbonate beds (see F1 and F2 in Figs. 4.4 and 4.5b). The F1 and F2 faults are roughly parallel to Set IV, and characterized by an offset of between 10 and 20 cm. Slickenlines along these faults show dip-slip kinematics nearly parallel to the outcrop and indicate, together with other kinematic indicators, a reverse sense of motion. The inner structure of the F1 and F2 faults is characterized by the absence of a well-defined fault core containing finely comminuted rock, at least when observed at the mesoscale (i.e., the gouge zone along faults in carbonates can even be, in fact, submillimetric in thickness; e.g., Smith et al., 2011). The two fault zones consist of a segmented slip surface surrounded by a damage zone as thick as 10 cm, containing fractures and, in places, coarse breccias. The traces of F1 and F2 faults are sinuous and, in places, they coincide with or intercept bedding and fracture surfaces (Figs. 4.4 and 4.5b). To understand the nucleation and growth of the largest one of these two faults (see in supplementary material F1

in Fig. S2), we mapped the fault by indicating with different color codes the segments where the fault propagated using pre-existing surfaces (bedding surfaces and fractures of Set IV) and segments where the fault propagated generating new through-going surfaces. Fault mapping (Fig. S2) was carried out in the field by measuring the attitude of each segment of the fault surface and then comparing these orientations with attitudes of the surrounding fracture sets. We also paid attention to the kinematic indicators present over the individual slip surface to assess whether these surfaces were originally PSSs or shear surfaces.

Small, subvertical, LAB faults further deform the rock volume between the F1 and F2 faults. These minor faults strike parallel to fractures of Set II, and are characterized by offsets smaller than 5 cm.

In the T2 outcrop, we recognized three main sets of fractures (Fig. 4.6):

Set V: This set is formed by stratabound, subvertical, HAB, E-W striking PSSs (Fig. 4.10a). Only a few of these PSSs cut through the bedding. Fractures of Set V show slightly toothed surfaces, with iron oxide stains and clay residues. Some of these surfaces (the ones that are non-stratabound) are characterized by left-lateral oblique- to strike-slip small offsets (Fig. 4.10b).

Sets VI and VII: These sets consist of LAB PSSs oriented respectively 145°/45° and 328°/54°, hence nearly perpendicular to the fold axis (see stereonet in Fig. 4.6). These PSSs are stratabound and generally characterized by wrinkled surfaces and clay residues (Fig. 4.10c and e). Sets VI and VII show frequent evidence of transtensional kinematics (Fig. 4.10d and f).

We analyzed a small bedding-parallel pavement located at the base of the T2 outcrop (Fig. 4.6) to document the abutting relationships between fracture sets. This pavement shows that fractures of Sets VI and VII are confined by the longer fractures of Set IV, which is, therefore, older than Sets VI and VII (Fig. 4.6b).

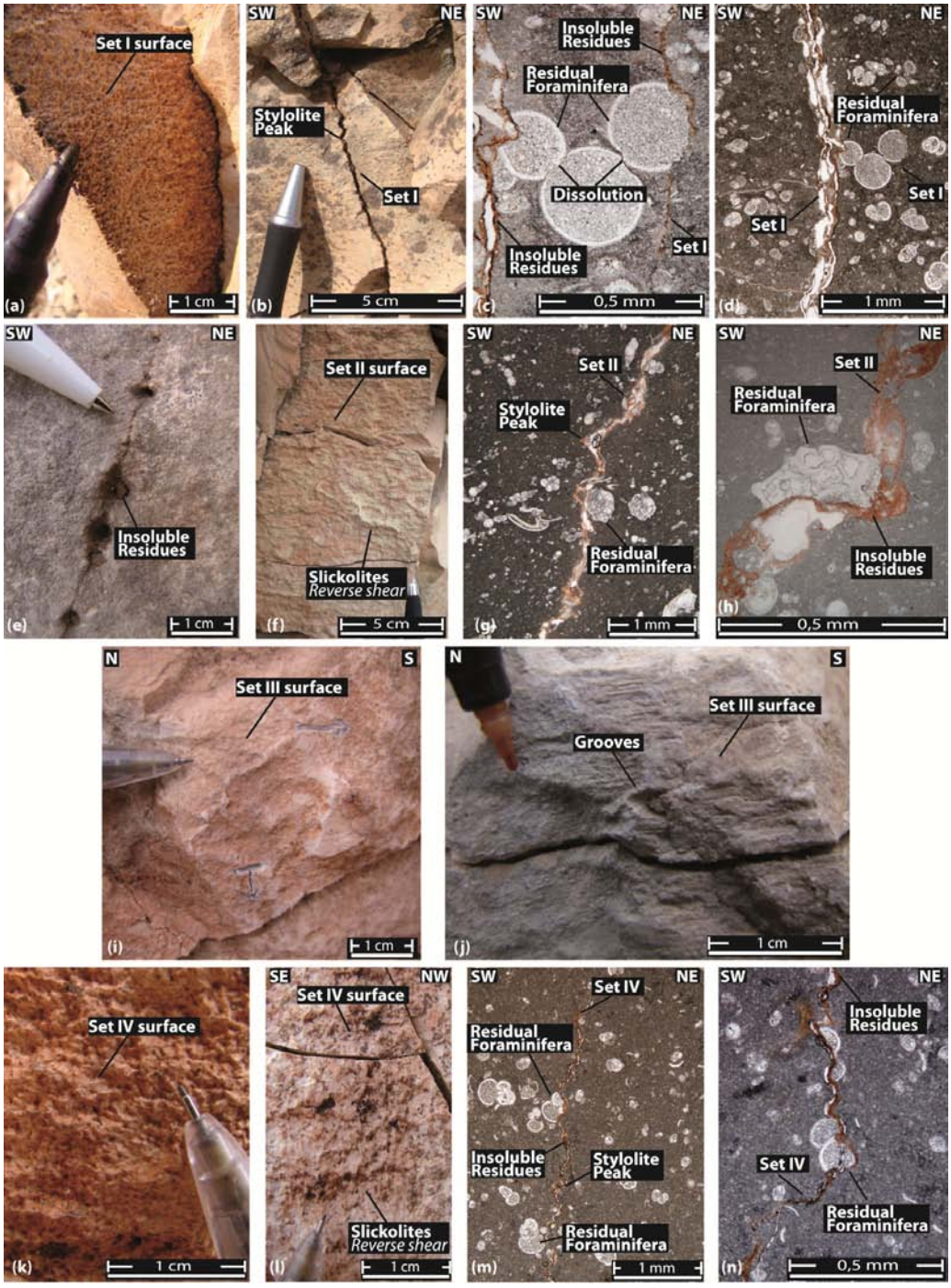

Figure 4.7: Microscopic and mesoscopic photographs of PSSs from Set I, Set II, Set III, and Set IV. (a) Pressure solution seam (PSS) surface of Set I. Set I surfaces are usually characterized by clay residues and by peaks normal to the pressure solution plane. (b) Set I PSS profile showing stylolite peaks. (c) and (d) Set I PSSs (thin-sections) accompanied by partially dissolved shells belonging to planktonic foraminifera. (e) Set II PSS profile accompanied by insoluble residues. (f) Set II PSS surface characterized by slickolites consistent with a reverse dip-slip displacement. (g) and (h) Set II PSSs (thin-sections) with partially dissolved shells belonging to planktonic Foraminifera. (i) and (j) Set III surfaces. This set is generally characterized by PSSs with smooth peaks and, more often, with slickolites and grooves showing a left-lateral strike-slip offset. (k) Set IV PSS surface. Set IV surfaces are usually characterized by clay residues and by perpendicular stylolite peaks. (l) Set II PSS surface characterized by slickolites consistent with a reverse dip-slip offset. (m) and (n) Set II PSSs (thin-sections) accompanied by partially dissolved shells belonging to planktonic Foraminifera.

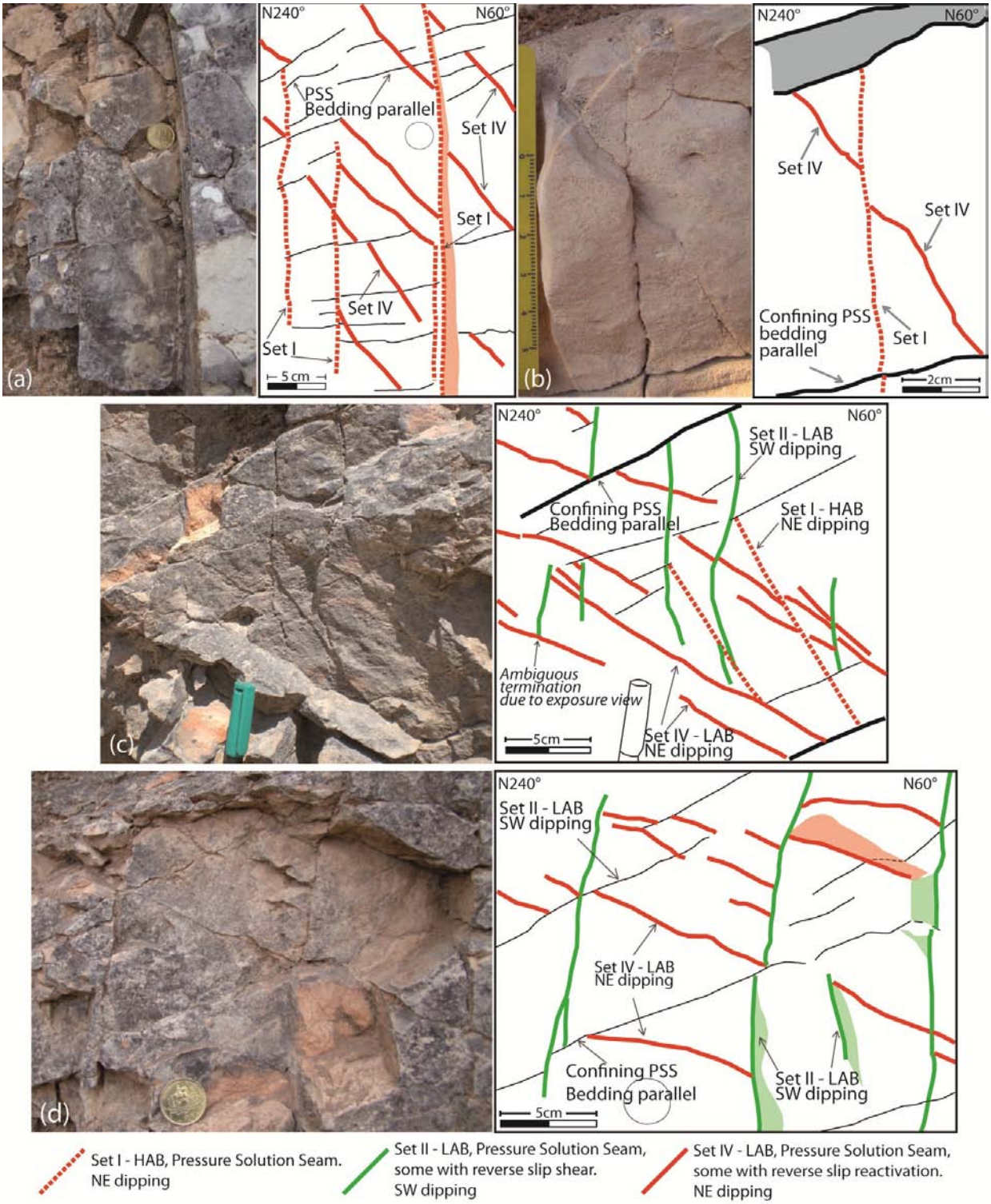

Fig. 4.8: Photographs and related line drawings showing crosscutting and abutting relationships among the most pervasive pressure solution seams (PSSs) of the T1 outcrop in Exposure 1. (a) and (b) PSSs of Set IV terminating against PSSs of Set I. (c) PSSs of Set IV terminating against PSSs of Set I and Set II. Note also that two PSSs of Set II terminate against PSSs of Set I. (d) PSSs of Set IV terminating against PSSs of Set II. HAB: high angle to bedding; LAB: low angle to bedding.

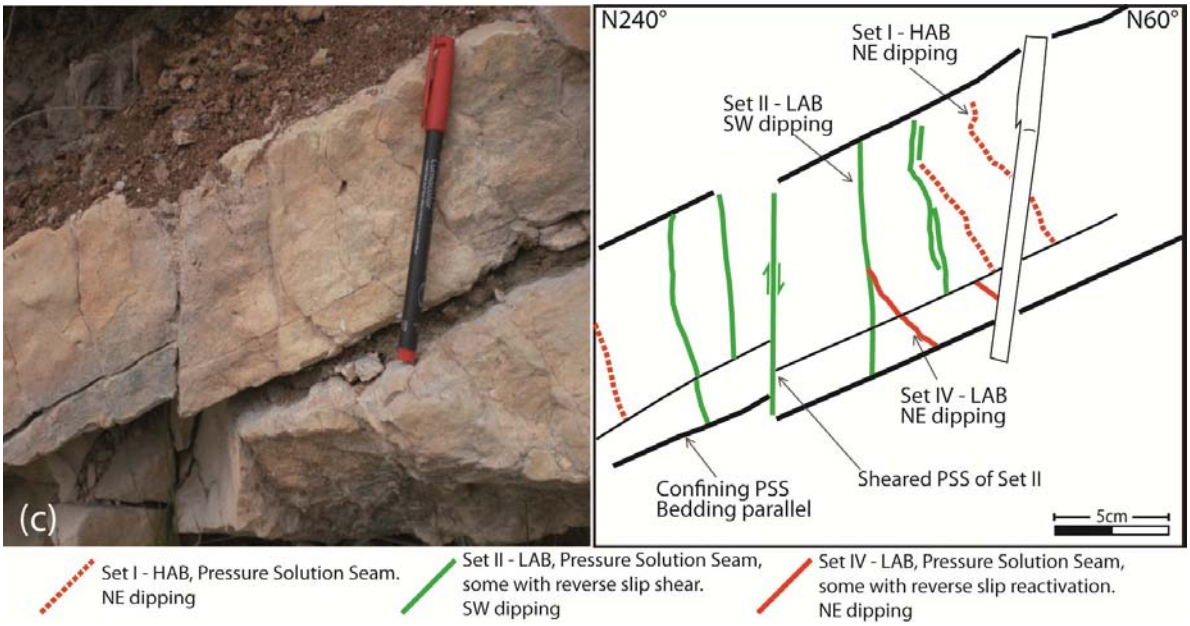

Figure 4.9: Photograph and related line drawing showing the termination of Set IV PSSs against Set II PSSs. Note that Set II PSSs are characterized by subvertical reverse offset. HAB: high angle to bedding; LAB: low angle to bedding.

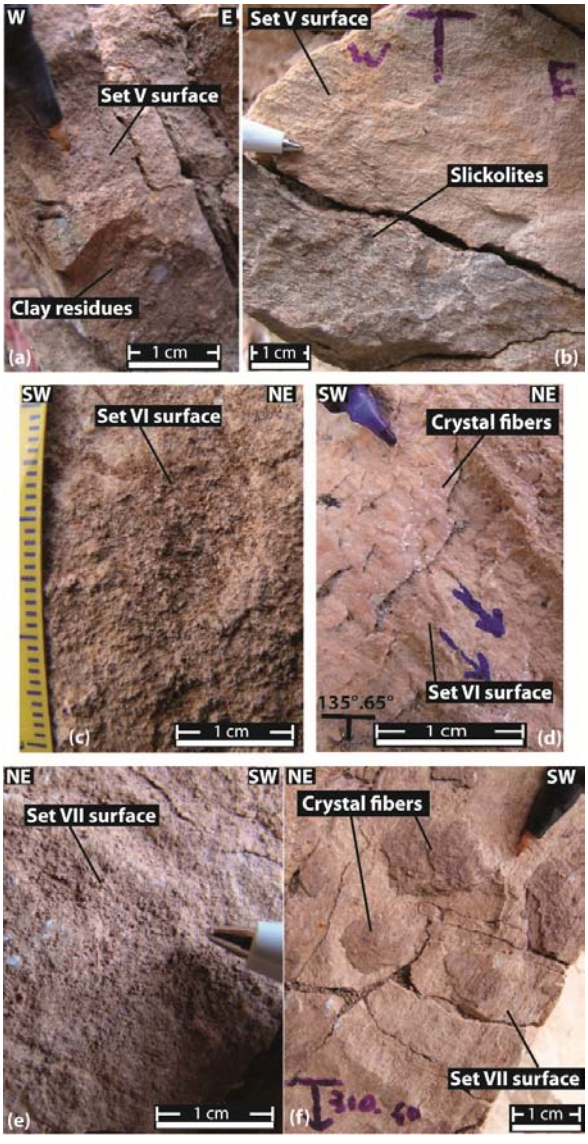

Figure 4.10: Mesoscopic photographs at different scales of fractures from Sets V, VI, and VII. (a) Pressure solution seam (PSS) from Set V. Set V surfaces are usually characterized by clay residues and by smooth perpendicular stylolite peaks. (b) PSS surface from Set V showing slickolites consistent with transtensive offset. (c) PSS surface from Set VI. (d) Surface from Set VI characterized by crystal (calcite) fibers consistent with a left-lateral transtensive offset. (e) PSS surface from Set VII. (d) Surface from Set VII characterized by crystal (calcite) fibers and grooves consistent with a right-lateral transtensive offset.

4.3.2 Exposure 2

The T3 outcrop in Exposure 2 exposes the *Scaglia Rossa* Fm. (Figs. 4.1, 4.2 and 4.11), which is here characterized by a smaller amount of clay with respect to the previously presented T1 and T2 outcrops. The T3 outcrop includes beds 0.1 to 1 m-thick. Marly interlayers are absent; the bedding surfaces usually coincide with PSSs associated with thin and nodular remnants of dissolved limestones. Similarly to the T1 and T2 outcrops, the bedding orientation measured in the T3 outcrop is 230°/30°, which is approximately parallel (the bedding strike) to the *Cingoli* anticline axis (compare stereonet in Fig. 4.11 with the anticline axis in Fig. 4.1). As mentioned above, slickenlines and other kinematic markers present over several bedding surfaces show that bedding underwent flexural slip along the NE-SW trend.

Fractures visible in the T3 outcrop pertain to Sets I, II, III, and IV (Fig. 4.11). Fractures of Sets V, VI, and VII are also present, but poorly exposed, because of their orientation parallel to the T3 outcrop. In general, the T3 outcrop is intensely deformed by closely-spaced PSSs of Set IV, whereas PSSs of Sets I, II, and III are less common. PSSs of Set IV are stratabound, LAB, and usually confined by PSSs of Sets I, II, and III. PSSs of Set I and II are rare in the T3 outcrop. It is interesting to note, however, that some PSSs of Set II are not stratabound, longer than most fractures observed in the outcrop, and characterized by evidence of dip-slip shear offset. Similarly to what happens for Set II, also PSSs of Set III are poorly developed in the T3 outcrop and they are often characterized by evidence of dip-slip shear offset (Fig. 4.11).

On the northeastern side of the T3 outcrop, a 220°/88° oriented sub-vertical fault occurs (see F3 in Figs. 4.11 and 4.12). Slickenlines are dip-slip (pitch angle is about 90°) along the fault plane and kinematic indicators indicate a sub-vertical reverse offset of about 12 cm. The F3 fault surface is rather continuous (except in the upper portion) and it is characterized by the absence of a fault core. A very thin (<1 cm) and discontinuous layer of clay gouge or fine breccia flanks the fault surface in its central and lower portions. Sparry calcite fillings occur along some portions of the slip surface, which is surrounded by a thin (<20 cm) and irregular damage zone containing fractures and pockets of breccias with clasts of variable size (Fig. 4.12d-f, see also in supplementary material Fig. S3). The fault surface is mainly parallel to fractures of Set II and cuts through both bedding surfaces and PSSs of other sets present in the T3 outcrop, particularly PSSs of Set IV. In the lower portion of the fault, a set of SW-dipping joints is documented (Fig. 4.12a and g). It is important to emphasize that the individual exposed fault zone components are characterized by different colors (Figs. 4.11 and 4.12). In particular, we

note that the breccia pockets are significantly lighter (in color) than the surrounding carbonate rocks probably due to the bleaching of iron oxides.

In order to understand the nucleation and growth of the F3 fault (see Fig. S3) we documented the inner fault structure and surrounding fractures with a method similar to that previously explained for the F1 fault (Fig. S2). Unlike the F1 fault, the F3 fault is straight and continuous at the outcrop scale (compare Figs. S2 and S3). Unfortunately, it was not possible to ascertain whether portions of the F3 fault surface coincide with (i.e., takes advantage of) pre-existing fracture surfaces. We only noted that this fault is sub-parallel to the fractures of Set II. This evidence suggests that Set II fractures may have acted as original nuclei for the F3 development.

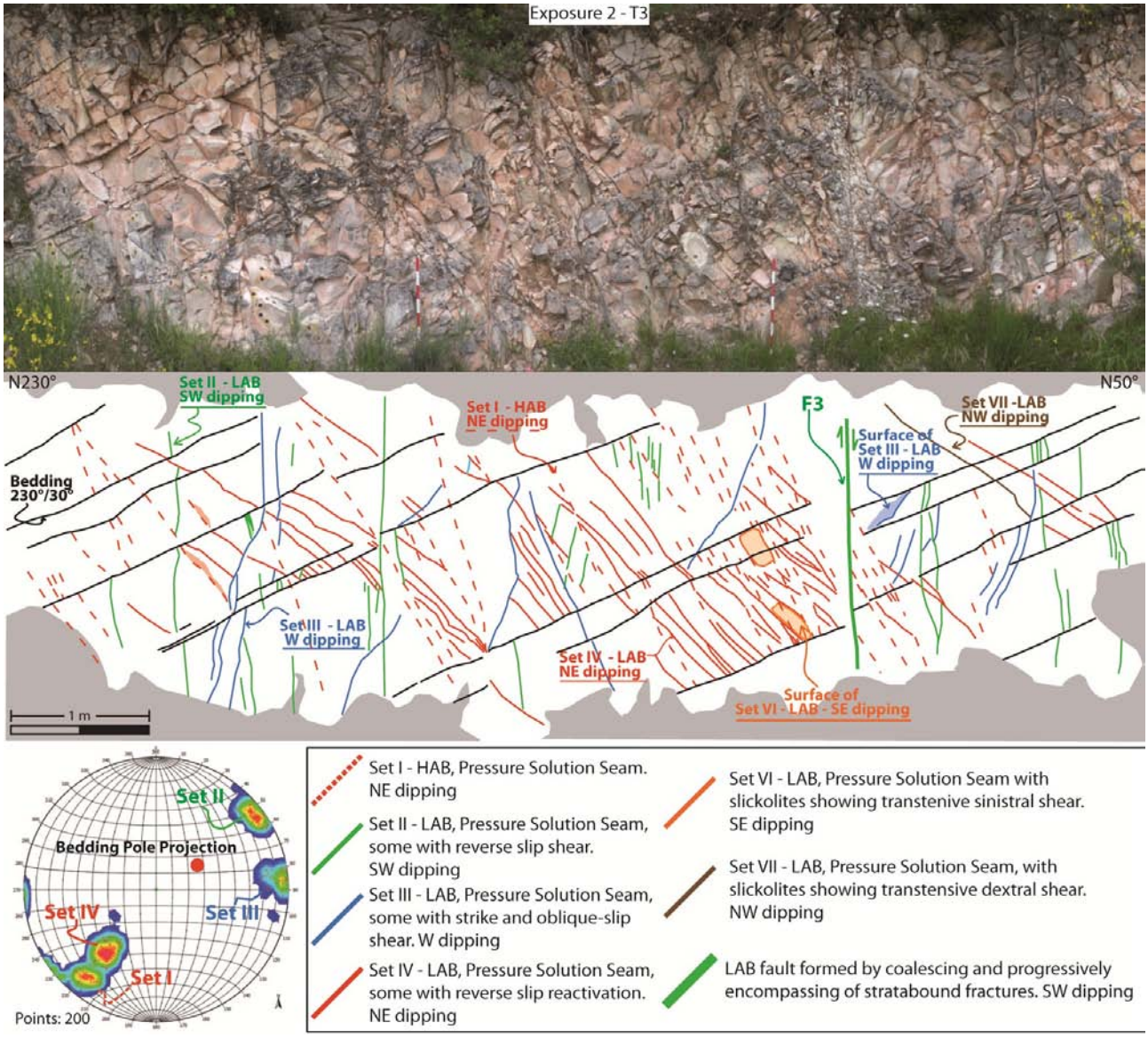

Figure 4.11: Photomosaic and related line drawing of the T3 outcrop in Exposure 2. On the outcrop, fractures of Sets I, II, III, and IV have been mapped (see lower hemisphere equal area projection of PSSs poles and related density contours). Note, on the right side, the presence of a sub-vertical fault (F3) cutting through the fractured carbonate strata. Attitude data are expressed in dip azimuth/dip form; HAB: high angle to bedding; LAB: low angle to bedding.

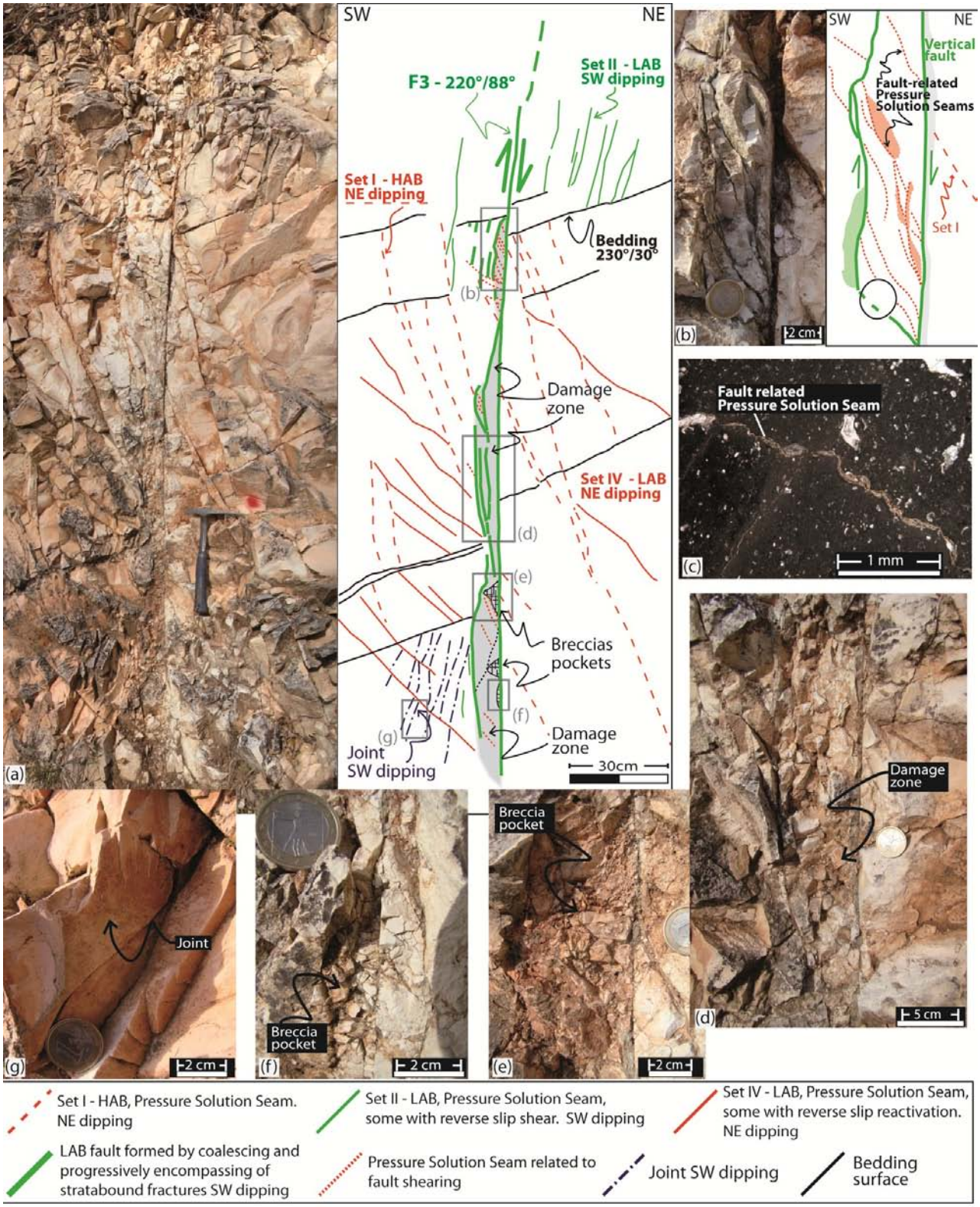

Figure 4.12: (a) Photograph and related line drawings showing the sub-vertical fault (F3) exposed in the T3 outcrop (Fig. 4.11). This fault is mostly parallel to pressure solution seams (PSSs) of Set II. Note the damage zone around the fault surface and pockets of coarse breccia within this damage zone. The fault core is absent or in a very infant stage (i.e., very thin and discontinuous). (b) Photograph and related line drawing showing pressure solution seams probably connected with the shear deformation occurring along two boundary fault strands. (c) Microscopic photograph of one of the pressure solution seams shown in the previous figure (Fig. 4.12b). (d) Photograph of a portion of the damage zone surrounding the F3 fault. (e) and (f) Photographs of breccia pockets within the damage zone surrounding the F3 fault. (g) Photograph of a joint surface next to the F3 fault. Attitude data are expressed in dip azimuth/dip form; HAB: high angle to bedding; LAB: low angle to bedding

4.4 DISCUSSION

The Cingoli carbonate anticline provides the opportunity to study potential fluid conductive structures at a scale below seismic resolution within pelagic carbonates similar to those exploited for hydrocarbons in the nearby Po Plain and Adriatic foreland. With this in mind, at least two main observations are relevant: (1) the study exposures are intensely deformed by a background fabric formed by several sets of closely-spaced, both HAB and LAB, stratabound pressure solution seams (PSSs); (2) this fabric is, in places, overprinted by small-offset faults that enhance interconnection through carbonate strata between PSSs, bedding surfaces, and newly-developed fault segments.

4.4.1 Background Fabric

In Exposures 1 and 2, we recognized seven main sets of fractures deforming carbonate strata of the *Scaglia Rossa* Fm. It is interesting to note that all sets consist of PSSs, indicating that the studied exposures were seemingly deformed under a large mean compressional stress. Note that in these two exposures neither joints (except a few joints adjacent to the faults; Fig. 4.12a) nor veins have been observed (see Chapter 3). Fig. 4.13 shows a possible evolutionary model of PSSs formation mainly based on observations of abutting and crosscutting relationships. In the model, limb rotation is speculative as we have no data to properly constrain the anticline development and related limb rotation. After the formation of bed-parallel PSSs (Fig. 4.13a), the oldest observed set (Set I) in Exposures 1 and 2 is characterized by PSSs lying almost perpendicular to bedding. PSSs of Sets II, III, and IV abut against PSSs of Set I. Given their attitude relative to bedding and anticline axis orientation, we interpret the PSSs of Set I as developed under a layer-parallel-shortening regime at the onset of anticline development (Fig. 4.13b). In our model, the successive feature is Set II, whose PSSs terminate or veer on PSSs of Set I (Fig. 4.8c). Given their attitude, we interpret PSSs of Set II as formed due to a top-to-the-crest (NE) layer parallel shear, which possibly occurred during the very early stages of folding (Fig. 4.13c). PSSs of Set III abut against PSSs of Set I and are, hence, younger than Set I. We could not observe any unambiguous evidence related to the timing of Set II and Set III. We can only say that, due to their attitude, the two sets formed under a top-to-the-foreland layer parallel shear either normal or oblique to the fold axis (e.g., Fischer and Jackson, 1999; Tavani et al., 2011) (Fig. 4.13c). PSSs of Set IV are the most pervasive structures in Exposures 1 and 2.

These structures abut or veer onto the PSSs of Sets I, II, and III and are, therefore, younger than these three sets. We interpret PSSs of set IV as forming due to top-to-the-hinterland (SW) layer-parallel shear during folding (e.g., Erickson et al., 2001) (Fig. 4.13d).

PSSs of Sets VI, and VII abut against PSSs of Set IV, and are therefore all younger than this latter set. We did not observe unambiguous relationships to constrain the relative timing between Set V and all the other sets. The interpretation within the folding process of these sets is rather complicated, because they imply pressure solution processes with compression axis almost normal or oblique to (and not parallel to) the direction of the main tectonic transport (Fig. 4.13e). Further data or a better theoretical understanding are necessary to fully interpret the development of these fracture sets during the folding process.

4.4.2 Small-Offset Faults

In Exposures 1 and 2, we recognized three main low-offset (≤ 20 cm) faults (F1, F2, and F3 in Figs. 4.4 and 4.11). In addition to these three faults, some of the PSSs show evidence of reactivation by shear (e.g., Figs. 4.7f, 4.7l, and 4.9). The F1 and F2 faults are formed by individual strands that are linked together forming the current fault traces. In particular, the traces of these faults include strands of bedding and PSSs (Set IV) surfaces linked together by newly generated fault segments (Fig. S2). This latter architecture suggests that the faults probably nucleated due to initial shearing on pre-existing bedding and PSSs (Set IV) and then formed new shear surfaces (Fig. S2) to connect the pre-existing ones. The evidence that the bedding surfaces, which were activated in shear along these faults, are those with marly and soft interlayers (Figs. 4.4 and S2) supports our hypothesis of fault generation along weak bedding surfaces. We also observe, however, that this is not the only fault nucleation process in the studied exposures. The F3 fault, in fact, cuts through bedding with an angle of about 60° and portions of bedding surfaces are not included in the main fault surface (Fig. S3). The parallelism and closeness between the F3 fault and several PSSs of Set II suggest that the fault nucleated by using surfaces of this latter set. The F3 fault surface is rather continuous through the outcrop and it is therefore difficult to identify its primary nucleation strands. To support our hypothesis of a fault (F3) nucleation along pre-existing PSSs of Set II, we point out that, throughout the studied exposures, several surfaces of this set are reactivated in shear and show small offsets (Figs. 4.7f and 4.9) consistent with the subvertical displacement measured along the F3 fault.

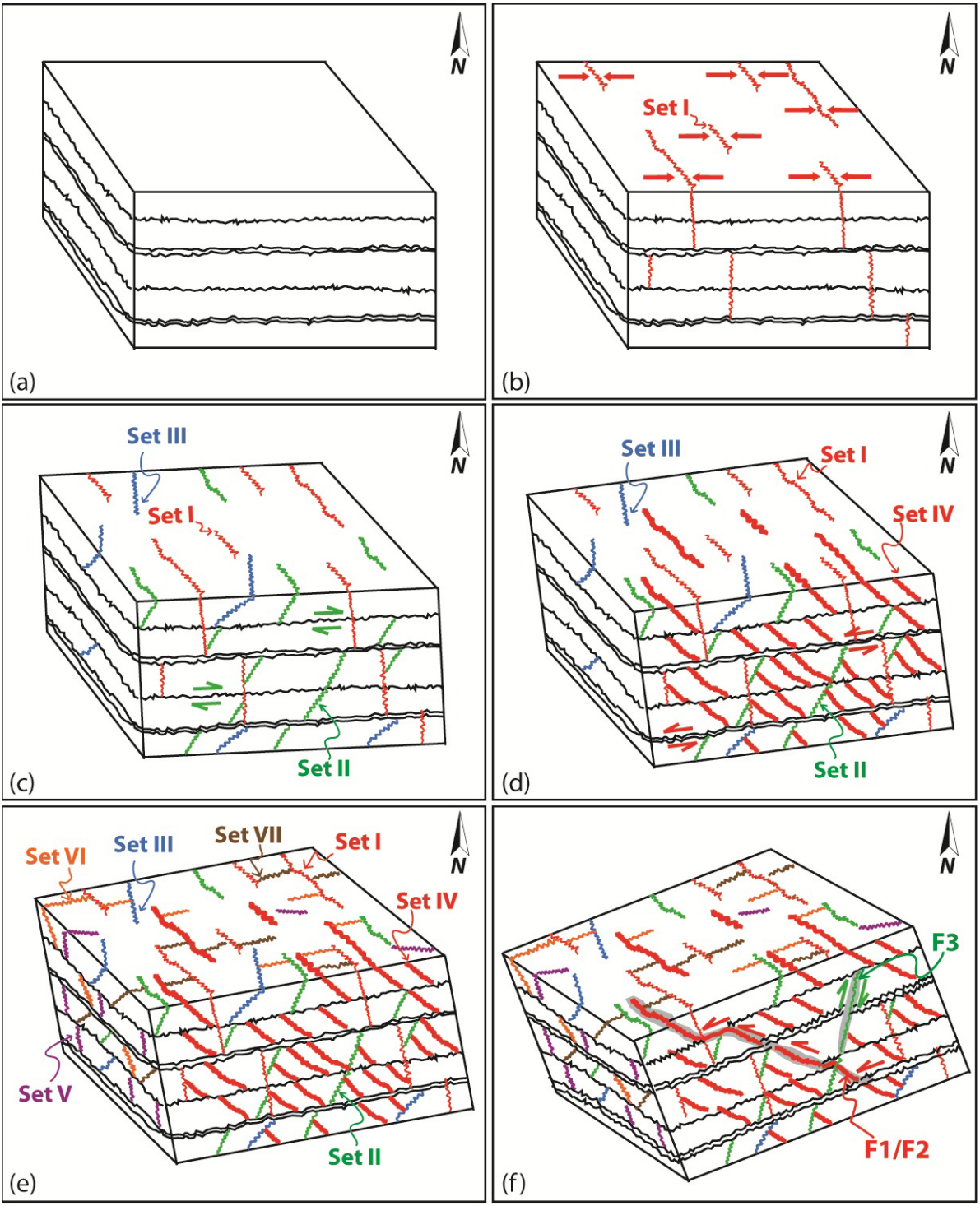

Figure 4.13: Progressive development of pressure solution seams and faults through carbonate strata. Progressive limb rotation is purely indicative.

General insights into the hydrologic behavior of the studied faults may be drawn from the following observations. The architecture of the F1, F2, and F3 faults consists of a narrow (< 20 cm) damage zone that includes interconnected fractures and zones of coarse breccia, which together form a rather tabular, through-going zone of brittle deformation contrasting with the background fabric of stratabound and poorly-connected PSSs (Figs. 4.4 and 4.12). Along portions of the F3 fault, we also observe a very thin gouge zone (< 1 cm thick; Fig. 4.12d) that is not present along the F1 and F2 faults.

Even without porosity and permeability data to quantitatively define the influence of the faults and fractures that we described on fluid flow, our field observations highlight the contrasting structural architecture between the background fabric and the late-stage small-displacement faults. The through-going faults provide a physical connection between rock matrix, pre-existing PSSs, and bedding surfaces for a length of at least a few meters. Instead, the background structural fabric is mostly composed of stratabound and poorly connected PSSs that are likely closed at reservoir conditions, except those fractures that are parallel or nearly parallel to σ_{hmax} in conditions of low mean stress or are kept open by shear (Zoback, 2007; Agosta et al., 2010).

We propose that some of the conductive fractures (or fracture swarms; e.g., Lonergan et al., 2007; Ozkaya et al., 2007; Wennberg et al., 2007; Akbar and Montaron, 2008; Singh et al., 2008; Questiaux et al., 2010; Souque et al., 2011) detected in fractured carbonate reservoirs may be structures similar to the small-displacement faults studied in this paper. In particular, the occurrence (or the lack) of a fault-parallel gouge zone will influence the subsurface fluid flow. The absence of gouge (F1 and F2 faults) would allow fluid flow both normal and parallel to the fault, with flow parallel to the fault favored by fault-parallel elongate fractures (Fig. S2). On the contrary, the presence of gouge would allow fluid flow mainly parallel to the fault (F3 fault; Fig. S3). Field evidence of preferential fluid circulation is shown by the lighter color of some breccia pockets interpreted as bleaching of iron oxides (Fig. S3).

In an effort to evaluate if our results may be generalized to a wider set of situations within similar rock types and tectonic settings we compare our results with previous studies.

Tavani et al. (2008) studied the Mt. Catria anticline (central Italy), characterized by the same sedimentary sequence as the Cingoli anticline, and found reverse faults associated to late-stage folds both in the backlimb and forelimb of the anticline. These faults are parallel to PSSs oblique to bedding in the forelimb, and nearly parallel to other sets of pre-existing PSSs in the backlimb. Graham Wall et al. (2006) found similar structures in carbonate sequences of the Albanides

fold-and-thrust-belt. In this instance, late-stage reverse faults cut through carbonate anticlines reactivating pre-existing PSSs (oblique to bedding) and coalesced to form fault zones with breccias cutting through bedding surfaces. Late-stage syn-folding strike-slip faults were found in the carbonate Añisclo anticline (Pyrenees) by Tavani et al. (2006), in the carbonate Majella anticline (central Apennines) by Antonellini et al. (2008), and in carbonate anticlines of the northern Apennines by Marshak et al. (1982). In the last two cases, the late-stage strike-slip faults were interpreted as originating from pre-existing PSSs. In the case of the Majella anticline, rare late-stage reverse faults were observed reactivating earlier PSSs in the anticline forelimb.

4.5 Conclusions

(1) Exposures of the *Scaglia Rossa* Fm. studied in the backlimb of the Cingoli anticline are affected by a background fabric of closely-spaced stratabound pressure solution seams (PSSs) overprinted in places by small-offset faults that cut through bedding and the background fabric.

(2) Fault nucleation and growth occurred in the previously-fractured, well-layered carbonates by shearing of the pre-existing mechanical weaknesses (pre-existing bedding and PSSs surfaces) and by forming new shear surfaces as fault growth progressed.

(3) Due to their contrasting structural architecture and connectivity, we propose that the background structural fabric would be hydraulically poorly-conductive, but in contrast the late-stage faults would enhance fault-parallel (and maybe the fault-orthogonal) fluid flow.

(4) The occurrence of late-stage faults formed by reactivating early PSSs in carbonate folds other than the Cingoli anticline indicates that the discussed model for fault nucleation and growth in pelagic micrites may be common in other carbonate anticlines with similar rock types.

4.6 Supplementary Material

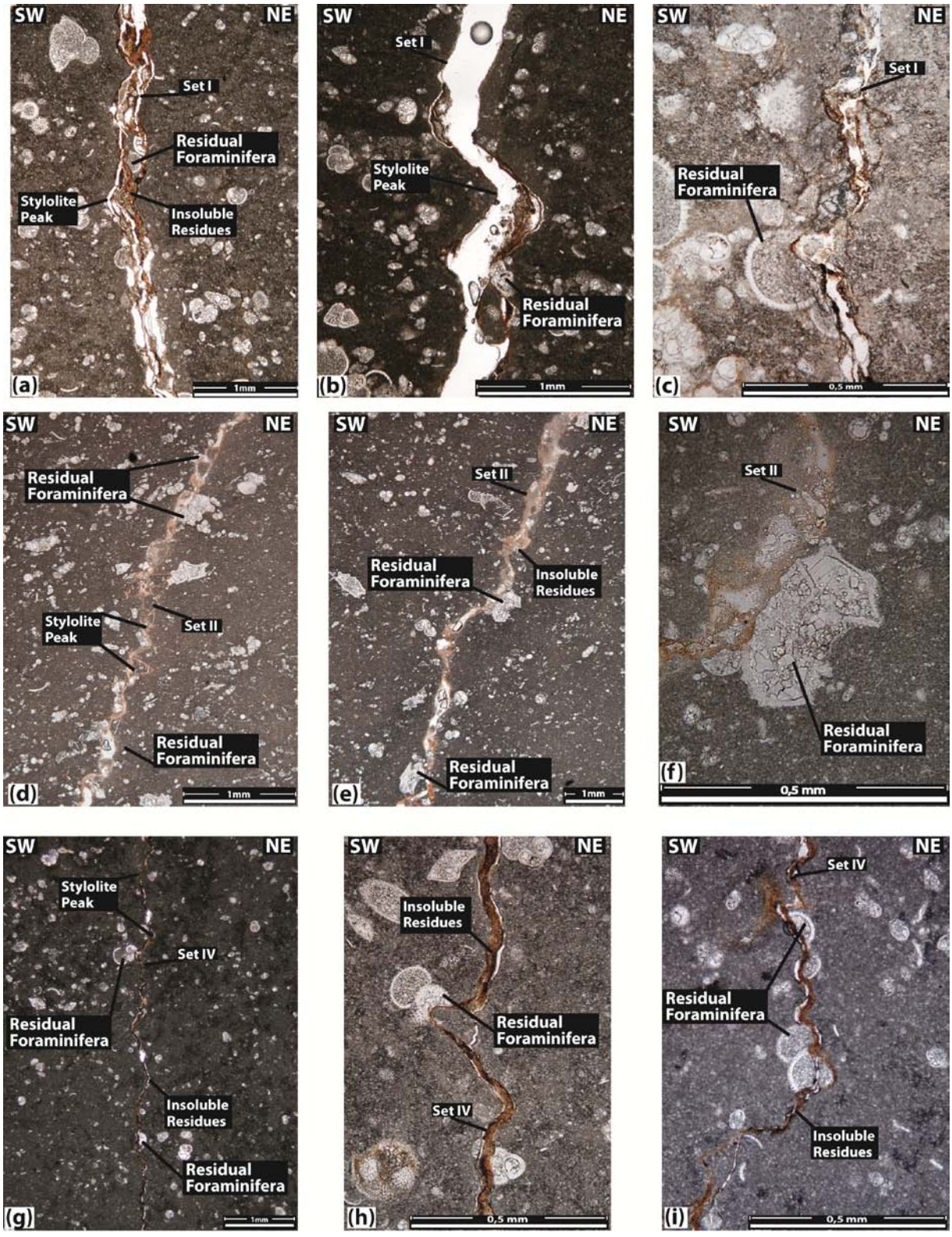

Fig. S1. Microscopic photographs showing evidence of pressure solution along the fractures observed in this study. Note in all photographs stylolite peaks, insoluble residues (reddish material), and partially dissolved fossils along the seams. (a), (b), and (c) PSSs of Set I. (d), (e), and (f) PSSs of Set II. (g), (h), and (i) PSSs of Set IV.

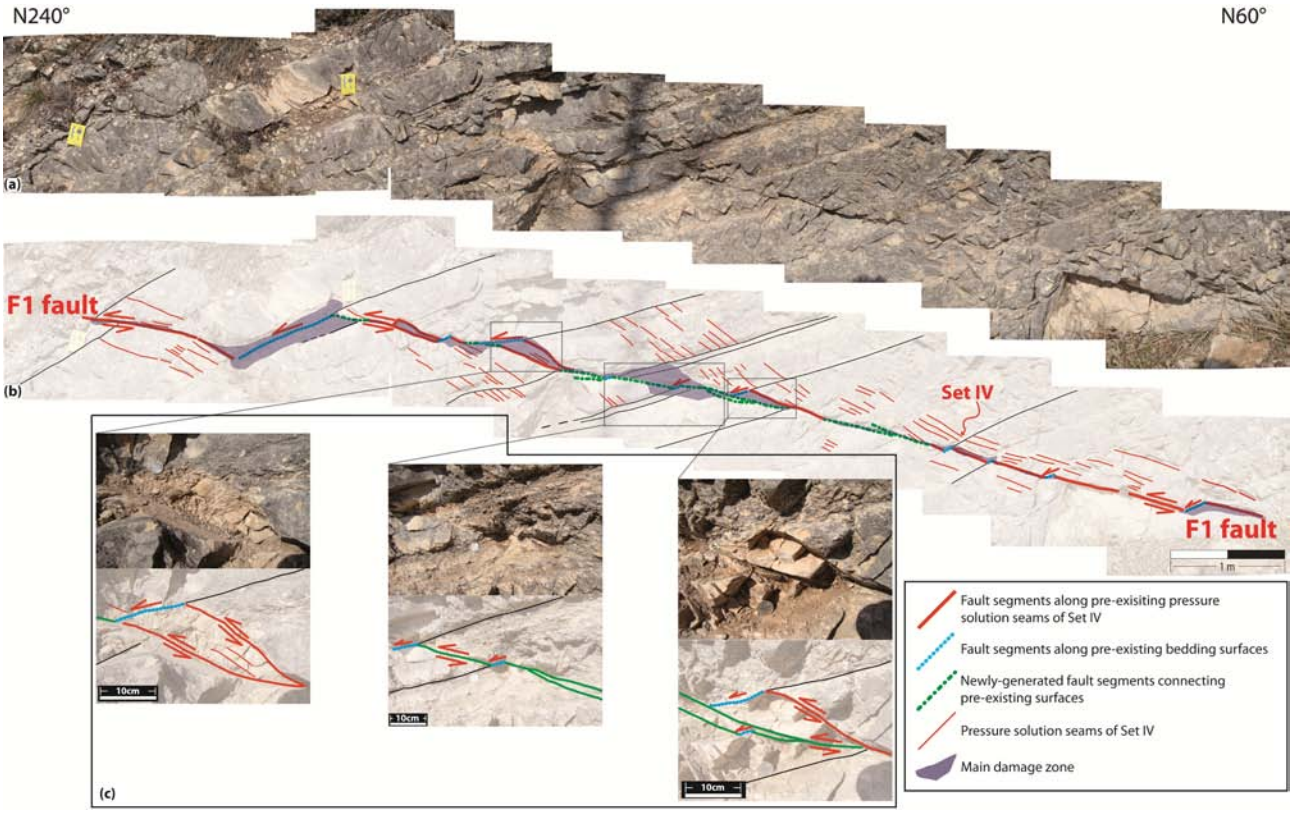

Fig. S2. (a) Photomosaic of the F1 fault in the T1 outcrop. (b) Interpretation (with color codes) of the F1 fault growth along pre-existing surfaces (bedding and PSSs) or along newly-generated shear surfaces connecting the pre-existing ones. See text for further explanations on the method employed. (c) Enlargements (photographs and related line drawings) of the F1 fault segments.

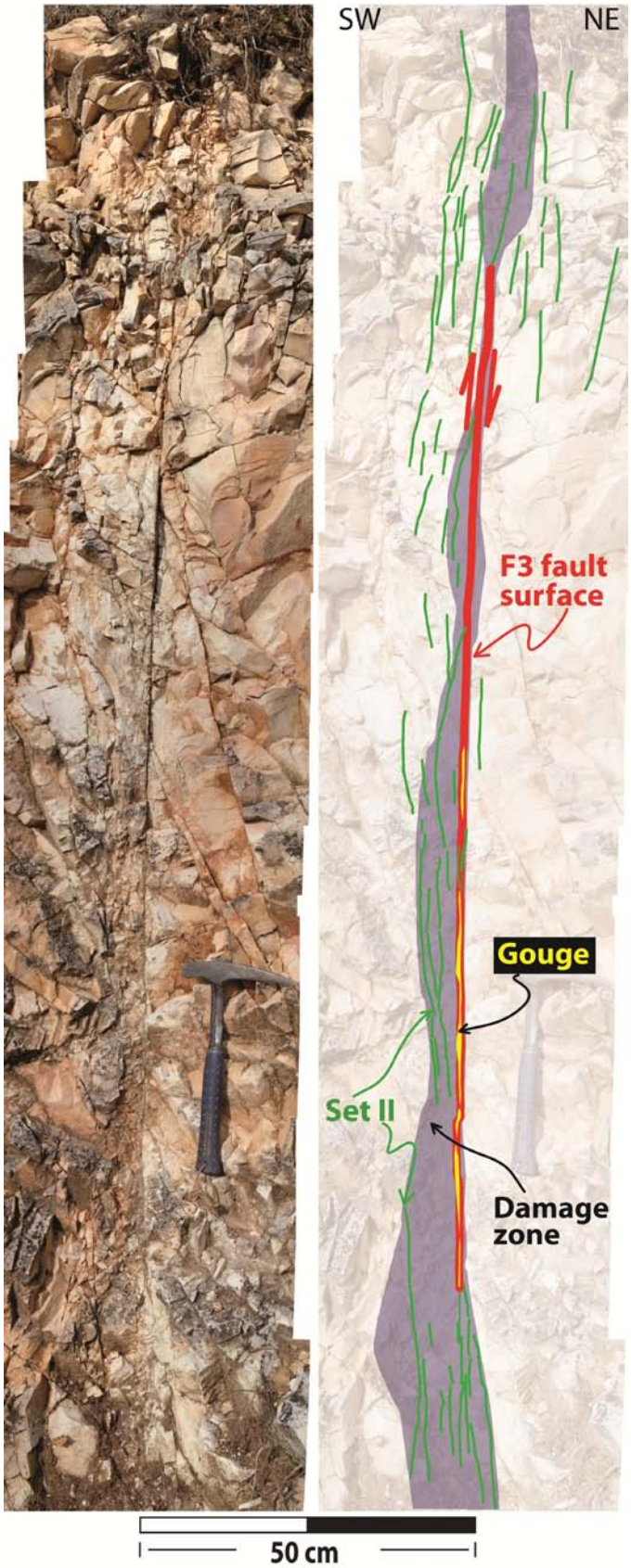

Fig. S3. Photomosaic of the F3 fault in the T3 outcrop and interpretation with color codes of its growth.

REFERENCES

Agosta, F., Prasad, M., Aydin, A., 2007. Physical properties of carbonate fault rocks, Fucino basin (Central Italy): implications for fault seal in platform carbonates. Geofluids 7, 19-32.

Agosta, F., Alessandroni, M., Tondi, E., Aydin, A., 2009. Oblique-slip normal faulting along the northern edge of the Majella anticline: inferences on hydrocarbon migration and accumulation. Journal of Structural Geology 31, 690-774.

Agosta, F. Alessandroni, M., Antonellini, M., Tondi., E., Giorgioni, M., 2010. From fracture to flow: a field-based quantitative analysis of an outcropping carbonate reservoir. Tectonophysics 490, 197-213.

Akbar, M., Montaron, B., 2008. Mapping fracture corridors in naturally fractured carbonate reservoirs in the Middle East. Saudi Arabia Oil & Gas 7, 36-41.

Antonellini, M., Aydin, A., 1994. Effect of faulting on fluid flow in porous sandstones: petrophysical properties. American Association of Petroleum Geologists Bulletin 78, 355-377.

Antonellini, M., Mollema, P.N., 2000. A natural analog for a fractured and faulted reservoir in dolomite: Triassic Sella Group, northern Italy. American Association of Petroleum Geologists Bulletin 84, 314-344.

Antonellini, M., Tondi, E., Agosta, F., Aydin, A., Cello, G., 2008. Failure modes in basin carbonates and their impact on fault development, Majella Mountain, central Italy. Marine and Petroleum Geology 25, 1074-1096.

Aydin, A., 2000. Fractures, faults, and hydrocarbon entrapment, migration and flow. Marine and Petroleum Geology 17, 797-814.

Aydin, A., Antonellini, M., Tondi, E., Agosta, F., 2010. Deformation along the leading edge of the Majella thrust sheet in central Italy. Journal of Structural Geology 32, 1291-1304.

Bally, A.W., Burbi, L., Cooper, C., Ghelardoni, R., 1986. Balanced sections and seismic reflection profiles across the Central Apennines. Memorie della Società Geologica Italiana 35, 257-310.

Barchi, R., Minelli, G., Pialli, G., 1998. The CROP 03 profile: a synthesis of results on deep structures of the northern Apennines. Memorie della Società Geologica Italiana 52, 383-400.

Bellahsen, N., Fiore, P.E., Pollard, D.D., 2006a. From spatial variation of fracture patterns to fold kinematics: A geomechanical approach. Geophysical Research Letters 33, L02301, DOI:10.1029/2005GL024189.

Bellahsen, N., Fiore, P.E., Pollard, D.D., 2006b. The role of fractures in the structural interpretation of Sheep Mountain Anticline, Wyoming. Journal of Structural Geology 28, 850-867.

Billi, A., Salvini, F., 2001. Fault-related solution cleavage in exposed carbonate reservoir rocks in the Southern Apennines, Italy. Journal of Petroleum Geology 24, 147-169.

Billi, A., Salvini, F., 2003. Development of systematic joints in response to flexure-related fibre stress in flexed foreland plates: the Apulian forebulge case history, Italy. Journal of Geodynamics 36, 523-536.

Billi, A., Salvini, F., Storti, F., 2003. The damage zone-fault core transition in carbonate rocks: implications for fault growth, structure, and permeability. Journal of Structural Geology 25, 1779-1794.

Billi, A., 2005. Attributes and influence on fluid flow of fractures in foreland carbonates of southern Italy. Journal of Structural Geology 27, 1630-1643.

Billi, A., Porreca, M., Faccenna, C., Mattei, M., 2006. Magnetic and structural constraints for the non-cylindrical evolution of a continental forebulge (Hyblea, Italy).Tectonics 25, TC3011, doi: 10.1029/2005TC001800.

Billi, A., Primavera, P., Soligo, M., Tuccimei, P., 2008. Minimal mass transfer across dolomitic granular fault cores. Geochemistry, Geophysics, Geosystems 9, Q01001, doi:10.1029/2007GC001752.

Brusseau, M.L., 1994. Transport of reactive contaminants in heterogeneous porous media. Reviews of Geophysics 32, 285-313.

Calamita, F., Deiana, G., 1986. Geodinamica dell'Appennino umbro-marchigiano. Memorie della Società Geologica Italiana 35, 311-316.

Calamita, F., Cello, G., Invernizzi, C., Paltrinieri, W., 1990. Stile strutturale e cronologia della deformazione lungo la traversa M. S. Vicino – Polverigi (Appennino marchigiano esterno). Studi Geologici Camerti, Volume Speciale 1, 69-86.

Calamita, F., Coltorti, M., Pieruccini, P., Pizzi, A., 1999. Evoluzione strutturale e morfogenesi plio-quaternaria dell'Appennino umbro-marchigiano tra il preappennino umbro e la costa adriatica. Bollettino della Società Geologica Italiana 118, 125-139.

Caine, J.S., Evans, J.P., Forster, C.B., 1996. Fault zone architecture and permeability structure. Geology 24, 1025-1028.

Caine, J.S., Tomusiak, S.R.A., 2003. Brittle structures and their role in controlling porosity and permeability in a complex Precambrian crystalline-rock aquifer system in the Colorado Rocky Mountain Front Range. Geological Society of American Bulletin 115, 1410-1424.

Carloni, G.C., 1964. La Geologia dei dintorni di Cingoli (Appennino Marchigiano). Giornale di Geologia 32, 365-401.

Casero, P., 2004. Structural setting of petroleum exploration plays in Italy. In: Crescenti, V., D'Offizi, S., Merlino, S., Sacchi, L. (Eds), Special Volume of the Italian Geological Society for the IGC 32, Florence+0, 189-199.

Centamore, E., Chiocchini, D., Deiana, G., Micarelli, A., Pieruccini, U., 1971. Contributo alla conoscenza del Giurassico dell'Appennino umbro-marchegiano. Studi Geologici Camerti 1, 7-89.

Colacicchi, R., Passeri, L., Pialli, G., 1970. Nuovi dati sul Giurese umbro-marchigiano ed ipotesi per un suo inquadramento regionale. Memorie della Società Geologica Italiana 9, 839-874.

Cooper, M., 1992. The analysis of fracture systems in subsurface thrust structures from the foothill of the Canadian Rockies. In: McClay, K.R. (Ed.), Thrust Tectonics. Chapman and Hall, London, 391-405.

Coward, M.P., De Donatis, M., Mazzoli, S., Paltrinieri, W., Wezel, F.C., 1999. Frontal part of the northern Apennines fold and thrust belt in the Romagna-Marche area (Italy): Shallow and deep structural styles. Tectonics 18, 559-574.

Deiana, G., Cello, G., Chiocchini, M., Galdenzi, S., Mazzoli, S., Pistolesi, E., Potetti, M., Romano, A., Turco, E., Principi, M., 2002. Tectonic evolution of the external zones of the Umbria-Marche Apennines in the Monte San Vicino-Cingoli area. Bollettino della Società Geologica Italiana, Volume Speciale 1, 229-238.

Di Francesco, L., Fabbi, S., Santantonio, M., Bigi, S., Poblet, J., 2010. Contribution of different kinematic models and a complex Jurassic stratigraphy in the construction of a forward model for the Montagna dei Fiori fault-related fold (Central Apennines, Italy). Geological Journal 45, 489-505.

Engelder, T., Scholz, C., 1981. Fluid flow along very smooth joints at effective pressure up to 200 megapascals. In: Carter, N.L. (Ed.), Mechanical Behaviour of Crustal Rock. AGU Geophysical Monograph Series 24, 147-152.

Erickson, S.G., Strayer, L.M., Suppe, J., 2001. Initiation and reactivation of faults during movement over a thrust-fault ramp: numerical mechanical models. Journal of Structural Geology 23, 11-23.

Fischer, M.P., Jackson, P.B., 1999. Stratigraphic controls on deformation patterns in fault-related folds: a detachment fold example from the Sierra Madre Oriental, northeast Mexico. Journal of Structural Geology 21, 613-633.

Fischer, M.P., Higuera-Diaz, I.C., Evans, M.A., Perry, E.C., Lefticariu, L., 2009. Fracture-controlled paleohydrology in a map-scale detachment fold: Insights from the analysis of fluid inclusions in calcite and quartz veins. Journal of Structural Geology 31, 1490-1510.

Galdenzi, S., 1986. Rapporti laterali tra diverse sequenze giurassiche nella dorsale marchigiana fra la Gola della Rossa e Monte Canfaito. Memorie della Società Geologica Italiana 35, 49-55.

Graham Wall, B.R., Antonellini, M., Aydin, A., 2003. Formation and growth of normal faults in carbonates within a compressive environment. Geology 31, 11-14.

Graham Wall, B.R., Girbacea, R., Mesonjesi, A., Aydin, A., 2006. Evolution of fractures and fault-controlled fluid pathways in carbonates of the Albanides fold-thrust belt. American Association of Petroleum Geologists Bulletin 90, 1227-1249.

Gudmundsson, A., 2000. Fracture dimensions, displacements and fluid transport. Journal of Structural Geology 22, 1221-1231.

Guerriero, V., Vitale, S., Ciarcia, S., Mazzoli, S. 2011. Improved statistical multi-scale analysis of fractured reservoir analogues. Tectonophysics 504, 14–24

Lonergan, L., Jolly, R.H.J., Rawnsley, K., Sanderson, D.J., 2007. Fractured Reservoirs. Geological Society, London, Special Publications 270, pp. 279.

Marchegiani, L., Bertotti, G., Cello, G., Deiana, G., Mazzoli, S., Tondi, E., 1999. Pre-orogenic tectonics in the Umbria-Marche sector of the Afro-Adriatic continental margin. Tectonophysics 315, 123-143.

Marshak, S., Geiser, P.A., Alvarez., W., Engelder, T., 1982. Mesoscopic fault array of the northern Umbrian Apennine fold belt, Italy: Geometry of conjugate shear by pressure-solution slip. Geological Society of America Bulletin 93, 1013-1022.

Mattavelli, L., Pieri, M., Groppi, G., 1993. Petroleum exploration in Italy: a review. Marine and Petroleum Geology 10, 410-425.

Mazzoli, S., Deiana, G., Galdenzi, S., Cello, G., 2002. Miocene fault-controlled sedimentation and thrust propagation in the previously faulted external zones of the Umbria-Marche Apennines, Italy. EGU Stephan Mueller Special Publication Series 1, 195-209.

Mazzoli, S., Di Bucci, D., 2003. Critical displacement for normal fault nucleation from en-échelon vein arrays in limestones: a case study from the southern Apennines (Italy). Journal of Structural Geology 25, 1011-1020.

Menichetti, M., 1991. La sezione geologica Cingoli-M. Maggio-Tevere nell'Appennino umbro-marchigiano: analisi cinematica e strutturale. Studi Geologici Camerti, Volume Speciale 1, 315-328.

Micarelli, L., Benedicto, A., Wibberley, C.A.J., 2006. Structural evolution and permeability of normal fault zones in highly porous carbonate rocks. Journal of Structural Geology 28, 1214-1227.

Mollema, P.N., Antonellini, M., 1999. Development of strike-slip faults in the dolomites of the Sella Group, northern Italy. Journal of Structural Geology 21, 271-292.

Morley, C.K., 2007. Development of crestal normal faults associated with deepwater fold growth. Journal of Structural Geology 29, 1148-1163.

Nelson, R.A., 2001. Geologic Analysis of Naturally Fractured Reservoir, 2nd edition, Gulf Professional Publishing, Houston.

Odling, N.E., Gillespie, P.A., Bourgine, B., Castaing, C., Chiles, J.P., Christensen, N.P., Fillion, E., Genter, A., Olsen, C., Thrane, L., Trice, R., Aareth, E., Walsh, J., Watterson, J.J., 1999. Variations in fracture system geometry and their implication for fluid flow in fractured hydrocarbon reservoirs. Petroleum Geosciences 5, 373-384.

Ozkaya, S.I., Lewandoswki, H.J., Coskun, S.B., 2007. Fracture study of a horizontal well in a tight reservoir. Journal of Petroleum Science and Engineering 55, 6-17.

Ozkaya, S.I., Minton, K.R., 2007. Flow potential of fractured corridors and large conductive fractures in a clastic reservoir, Oman. In Lonergan, L., Jolly, R.H.J., Rawnsley, K., Sanderson, D.J., (Eds.), Fractured Reservoirs. Geological Society, London, Special Publications 270, 245-263.

Peacock, D.C.P., Sanderson, D.J., 1995. Pull-apart, shear fractures, and pressure solution. Tectonophysics 241, 1-13.

Pieri, M., Mattavelli, L., 1986. Geologic framework of Italian petroleum resources. American Association of Petroleum Geologists Bulletin 70, 103-130.

Pollard, D.D., Aydin, A., 1988. Progress in understanding jointing over the past century. Geological Society of American Bulletin 100, 1181-1204.

Questiaux, J.-M., Couples, G.D., Ruby, N., 2010. Fractured reservoirs with fracture corridors. Geophysical Prospecting 58, 279-295.

Quintà, A., Tavani, S., 2012. The foreland deformation in the south-western Basque-Cantabrian Belt (Spain). Tectonophysics, DOI: 10.1016/j.tecto.2012.02.015.

Salvini, F., Billi, A, Wise, D.U., 1999. Strike-slip fault-propagation cleavage in carbonate rocks: the Mattinata fault zone. Journal of Structural Geology 21, 1731-1749.

Salvini, F., Storti, F., 2001. The distribution of deformation in parallel fault-related folds with migrating axial surfaces: comparison between fault-propagation and fault-bend folding. Journal of Structural Geology 23, 25-32.

Santantonio, M., 1993. Facies association and evolution of pelagic carbonate platform/basin systems: example from the italian Jurassic. Sedimentology 40, 1039-1067.

Santantonio, M., 1994. Pelagic carbonate platforms in the geologic record: their classification, and sedimentary and paleotectonic evolution. American Association of Petroleum Geologists Bullettin 78, 122-141.

Servizio Geologica d'Italia, 2003. Tolentino. Servizio Geologico d'Italia, Carta Geologica d'Italia 1:50,000, sheet 302, Rome.

Sibson, R.H., 1996. Structural permeability of fluid-driven fault-fractures meshes. Journal of Structural Geology 18, 1031-1042.

Singh, S.K., Abu-Habbiel, H., Khan, B., Akbar, M., Etchecopar, A., Montaron, B., 2008. Mapping fracture corridors in naturally fractured reservoirs: an example from Middle East carbonates. First Break 26, 109-113.

Smith, S.A.F., Billi, A., Di Toro, G., Spiess, R., 2011. Principal slip zones in limestone: microstructural characterization and implications for the seismic cycle (Tre Monti fault, central Apennines, Italy). Pure and Applied Geophysics 168, 2365-2393.

Tavani, S., Storti, F., Fernànedz, O., Muñoz, J.A., Salvini, F., 2006. 3-D deformation pattern analysis and evolution of the Añisclo anticline, southern Pyrenees. Journal of Structural Geology 28, 695-712.

Tavani, S., Storti, F., Salvini, F., Toscano, C., 2008. Stratigraphic versus structural control on the deformation pattern associated with the evolution of the Mt. Catria anticline, Italy. Journal of Structural Geology 30, 664-681.

Tavani, S., Storti, F., Muñoz, J.A., 2010. Scaling relationships between stratabound pressure solution cleavage spacing and layer thickness in a folded carbonate multilayer of the Northern Apennines (Italy). Journal of Structural Geology 32, 278-287.

Tavani, S., Mencos, J., Bausà, J., Muñoz, J.A., 2011. The fracture pattern of the Sant Corneli Bóixols oblique inversion anticline (Spanish Pyrenees). Journal of Structural Geology 33, 1662-1680, doi:10.1016/j.jsg.2011.08.007.

Tondi, E., Antonellini, M., Aydin, A., Marchegiani, L., Cello, G., 2006. The roles of deformation bands and pressure solution seams in fault development in carbonate grainstone of the Majella Mountain, Italy. Journal of Structural Geology 28, 376-391.

Vitale, S., Dati, F., Mazzoli, S., Ciarcia, S., Guerriero, V., Iannace, A., 2012. Modes and timing of fracture network development in poly-deformed carbonate reservoir analogues, Mt. Chianello, southern Italy. Journal of Structural Geology, DOI: 10.1016/j.jsg.2012.01.005.

Wennberg, O.P., Azizzadeh, M., Aqrawi, A.A.M., Blanc, E., Brockbanc, P., Lyslo, K.B., Pickard, N., Salem, L.D., Svånå, T., 2007. The Khaviz anticline: an outcrop analogue to giant fractured Asmari Formation reservoirs in SW Iran. In: Lonergan, L., Jolly, R.J.H., Rawnsley, K., Sanderson, D.J. (Eds.), Fractured Reservoirs, Geological Society, London, Special Publications 270, 23-42.

Willemse, E.J.M., Peacock, D.C.P., Aydin, A., 1997. Nucleation and growth of strike-slip faults in limestones from Somerset, U.K. Journal of Structural Geology 19, 1461-1477.

Zhao, M., Jacobi, R.D., 1997. Formation of regional cross-fold joints in the northern Appalachian Plateau. Journal of Structural Geology 19, 817-834.

Zoback, M.D., 2007. Reservoir geomechanics: earth stress and rock mechanics applied to exploration, production, and wellbore stability. Cambridge University Press, pp. 449.

5. Synthesis

5.1 A conceptual model for fold-related fractures formation

A field survey of the fracture system characterizing the Cingoli anticline has been done in order to study and analyse the formation and evolution of fracture system in a carbonate multilayer.
It has been showed how the structural position (e.g. forelimb, backlimb and hinge zone) and the mechanical stratigraphy are important factors affecting the patterns of the fracture system.
The scheme proposed in literature and the strain distribution model (Price, 1966; Stearns, 1964 and 1968; Stearns and Friedman, 1972; Price and Cosgrove, 1990, Hudleston and Lan, 1993; Evans and Fischer, 2012) schematize well the geometrical orientation of most of the set of fractures observed in the Cingoli anticline. On the other hand, the present work suggests the relevance of the mechanical stratigraphy in particular controlling the type of fractures formed (e.g. pressure solution seams, joints or shear fractures) and their subsequent evolution.
Through a multi-scale analysis, and on the basis of the temporal relationship between fracture sets and their orientation respect layering (e.g. LAB, HAB), it is possible to suggest the evolution of the fracture system during the folding process.
In order to schematize and to propose a conceptual model for the fracture system evolution, I have divided the whole process in 4 main temporal phases:

- **I Phase: Early stage of folding process – layer-parallel shortening**

After the formation of layer-parallel pressure solution seams (PSSs) due to overburden compaction, the studied sequence appears characterized by three units of thinly bedded limestones with different mechanical stratigraphy: limestones and marly limestones with marly interlayers, limestones with chert layers and limestones without chert and marly layers. At this stage the rock sequence should not be considered as a perfectly planar sub-horizontal surface but, on the contrary, it is reasonable to figure out local anisotropies. Small depressions, small positive morphological structures and other patterns formed for structural or sedimentary processes can characterize the sequence stratigraphy.

With the onset of the orogenetic process, after the deposition of the evaporitic sediments of the Laga. Fms (Messinian age), the rock sequence experiences layer parallel shortening. In this first stage the effects of the mechanical stratigraphy are evident. In those sequences characterized by limestones, with or without marly layers, the deformation is accommodate by PSSs orthogonal to the principal regional stress (i.e. SW-NE) and at high-angle to bedding (HAB). Due to local anisotropies, such as curvature of layers surfaces, the stress field can locally change

leading to the formation of HAB PSSs oblique to fold axes. Hence, as the studied limestones are prone to pressure solution, the evidence of pressure solution seams might in some cases be the effect of local, small, tectonic loads. On the other hand, the sequences characterized by limestone with chert layers do not show HAB PSSs. As explain in chapter 3, these sequences act as composite materials and the chert laminae inhibit the formation of PSSs. The sequences characterized by chert laminae are characterized by two sets of HAB joints, perpendicular and parallel to the fold axes. The perpendicular to fold axes joints are considered to develop, during the first stage of folding process, due to the layer parallel shortening (e.g. Fischer and Jackson, 1999; Tavani et al., 2006; Tavani et al., 2008; Tavani et al., 2011). Whereas, the parallel to fold axes joints observed in the limbs, and considered coeval with the perpendicular to fold axes joints, could derive from local anisotropies (e.g. local flexure of layers). As the outcrops in those sites are almost vertical, it is possible that the observation made is misleading.

- **II Phase: Fold formation - Flexural slip top-to-the-crest**

When the fold starts to develop and the limbs rotate, the anticline deforms through the flexural slip process with a sense of motion top-to-the-crest. This process leads to the nucleation of PSSs at an oblique angle to bedding. These LAB PSSs dip toward the hinterland in the western limb and toward the foreland in the eastern limb. LAB PSSs are considered as tail fractures forming in the contractional quadrants relative to shearing along the surfaces experiencing flexural slip. Note that where the flexural slip is weak, such as in those outcrops where the marly levels are absent, these LAB PSSs are not so well developed and the deformation occurs through shearing of pre-existing fractures (e.g. HAB PSSs).

- **III Phase: Fold formation - Flexural slip top-to-the-hinterland**

Several features suggest a change, or a continuous alternation, in the sense of motion of the flexural-slip process. Numerous outcrops show back-thrust (hanginwall-to-the-hinterland) and late-stage LAB PSSs, which in the western limb dip toward the hinge. These structures are incompatible with the PSSs of the phase II (i.e. PSSs dipping toward the hinterland in the western limb). The back-thrust and the late-stage PSSs suggest a kinematic change during the folding process probably due to the increasing of the frictional resistance and the subsequent change in the accommodation process. This process does not mean that the fold change its verging trend, but it is possible to envision an alternation of the kinematic process through time.

Some LAB PSSs sets oblique to the fold axes have been recognized in the field. These fractures imply a direction of the principal stress almost oblique to the main tectonic transport. It is reasonable to consider that the shear due to flexural slip involves only part of the sheet at a time, transferring subsequently the shear on other patches of the layers. Hence, even if the general movement of the flexural slip is oriented SW-NE, in localised patches of the limb, for instance those characterized by anomalies in curvature or by pre-existing structures, the flexural slip could act oblique or even longitudinal to the main shear direction.

- **IV Phase: Late stage fault development**

At the end of Phase III, the Cingoli anticline is characterized by a background fabric of closely-spaced stratabound PSSs, both at HAB and LAB, and, only in those sequences characterized by chert layers, by two sets of joints. With the ongoing of the deformation process, late-stage faults start to form by shearing of the pre-existing structures (e.g. stratabound PSSs, joints) and by forming new shear surfaces as fault growth progressed. The process of shear along the fault surfaces lead to the formation of other small and localized fractures, mainly joints.

REFERENCES

Evans, M.A., Fischer, M.P., On the distribution of fluids in folds: A review of controlling factors and processes, Journal of Structural Geology (2012), http://dx.doi.org/10.1016/j.jsg.2012.08.003.

Fischer, M.P., Jackson, P.B., 1999. Stratigraphic controls on deformation patterns in fault-related folds: a detachment fold example from the Sierra Madre Oriental, northeast Mexico. Journal of Structural Geology 21, 613-633.

Hudleston, P.J., Lan, L., 1993. Information from fold shapes. Journal of Structural Geology 15, 253-264.

Price, N.J., 1966. Fault and joint development in brittle and semi-brittle rocks. Pergamon, Oxford,176 pp.

Price, N.J., Cosgrove, J.W., 1990. Analysis of geological structures. Cambridge University Press, Cambridge, 502 pp.

Stearns, D.W., 1964. Macrofracture patterns on Teton Anticline, N.W. Montana (Eos). Trans A.G.U., 45, 107

Stearns, D.W., 1968. Certain aspects of fractures in naturally deformed rocks. Rock mechanics seminar. R.E. Riecker, 97-118. Terr. Sci. Lab., Bedford, Mass.

Tavani, S., Storti, F., Fernànedz, O., Muñoz, J.A., Salvini, F., 2006. 3-D deformation pattern analysis and evolution of the Añisclo anticline, southern Pyrenees. Journal of Structural Geology 28, 695-712.

Tavani, S., Storti, F., Salvini, F., Toscano, C., 2008. Stratigraphic versus structural control on the deformation pattern associated with the evolution of the Mt. Catria anticline, Italy. Journal of Structural Geology 30, 664-681.

Tavani, S., Mencos, J., Bausà, J., Muñoz, J.A., 2011. The fracture pattern of the Sant Corneli Bóixols oblique inversion anticline (Spanish Pyrenees). Journal of Structural Geology 33, 1662-1680, doi:10.1016/j.jsg.2011.08.007.

Acknowledgements

Acknowledgements

Please reader, consider that this “thank you” is not simply an obligation. In these two words there is much more. There are laughs and happiness. There are friendships and life. There are days spent together. There is snow and the hot sun of the summer. There are travels. There is sharing. There are people that you have never met before and suddenly became your friends or fundamental advisors. There are people that you have met when the project was already going on and you know, they will be with you for all your life. There are people that you know since you were born and every day you would like to say to them “thank you”. There are people who have trusted you and you hope to have gone some way towards repaying this faith.

This and much more is within “Thank you”.

First I want to thank you my supervisors; much of the vision for the project has developed within our discussions. Marco Antonellini, thank you for welcoming and accepting me and for becoming my supervisor. Your help has been invaluable. Thank you for all the time you spent with me in the field. Snow, rain and heat never stopped us. Your suggestions and your approach to the geosciences and to structural geology helped me to solve any intriguing problems. Davide Scrocca, after five years working together you still believe in me and in my capacity…or you are reckless or I am an excellent liar. Davide, thank you for your support both in term of all the time that we have discussed scientific problems together and the financial support that you have offered me. This PhD project has been funded totally by your personal funds. Andrea Billi, thank you for the time spent with me in front of your PC, helping me to find the best way to elaborate part of this project. You have always helped me to think outside the box. But Andrea, please turn down your music!

I want to thank the University of Bologna and the Earth Sciences department. The PhD coordinators, Prof. William Cavazza and Roberto Barbieri and all the professors and researchers of the department, especially Prof. Vincenzo Picotti.

Prof. Fabrizio Agosta and Prof. Riccardo Caputo are kindly acknowledged for the review of this work. I gratefully acknowledge Independent Resources plc for its financial support; in particular, Roberto Bencini and Independent Resources plc’s technical staff are thanked for productive discussions.

I am also grateful to Prof. Massimo Santantonio and to Dott. Marco Brandano for their insights into the Mesozoic stratigraphy and field discussions. The Servizio Ambiente e Paesaggio

- P.F. Informazioni Territoriali ed Ambientali e Beni Paesaggistici of Marche Region and Chiara D'Ambrogi of the ISPRA Agency provided useful geological data. Midland Valley is acknowledged for providing 2DMove and 3DMove software useful for geological cross section construction. F. Agosta, N. Bellahsen, S. Smith, and S. Tavani are warmly thanked for the revision of the manuscript and for the constructive comments.

I want to thank all the people that I met in Cingoli. I will never forget Stefania and Sergio. They are my field family. Thank you to the owner of the quarry, Giacomo Menghi, who allowed me to move freely within the quarry. Roberto and all the workers in the quarry, you are all unforgettable people.

Michele, Barbara, Checco, Francesco, Filippo, Francesca, Mauro, Salomon, Mauro B....thank you! Fabio and Margherita, my personal hotel in Bologna, thank you for your hospitality. Valeria Venturi, we have spent many times together. We have been in U.K. and after we met again in Ravenna. Maybe, I was not physically with you in that special moment, but you will always have my friendship.

Vincent, Sora Paola e Riccia..my new family..what great fun!

And now, I want to thank YOU. You, that person that I met when this PhD was already started. You do not need words. You know, I know..that's it!

And finally my family. Mom, Dad, Fra e Sara, you have always be present and you will be forever!

Thank you.

P.S. Thush..thank you for your help and for the Guild of student in Brum!